



HAL
open science

Microstructure and texture evolution during annealing of plane strain compressed fcc metals

Magdalena Maria Miszczyk

► **To cite this version:**

Magdalena Maria Miszczyk. Microstructure and texture evolution during annealing of plane strain compressed fcc metals. Other. Ecole Nationale Supérieure des Mines de Saint-Etienne, 2013. English. NNT : 2013EMSE0695 . tel-00904405

HAL Id: tel-00904405

<https://theses.hal.science/tel-00904405>

Submitted on 14 Nov 2013

HAL is a multi-disciplinary open access archive for the deposit and dissemination of scientific research documents, whether they are published or not. The documents may come from teaching and research institutions in France or abroad, or from public or private research centers.

L'archive ouverte pluridisciplinaire **HAL**, est destinée au dépôt et à la diffusion de documents scientifiques de niveau recherche, publiés ou non, émanant des établissements d'enseignement et de recherche français ou étrangers, des laboratoires publics ou privés.

NNT : 2013 EMSE 0695

THÈSE

présentée par

Magdalena MISZCZYK

pour obtenir le grade de

**Docteur de l'École Nationale Supérieure des Mines de Saint-Étienne
en cotutelle avec l'Institut de Métallurgie et de Science des Matériaux
de la Académie Polonaise des Sciences**

Spécialité : Sciences et Génie des Matériaux

MICROSTRUCTURE AND TEXTURE EVOLUTION DURING ANNEALING OF PLANE STRAIN COMPRESSED FCC METALS

soutenue à Cracovie, le 14 juin 2013

Membres du jury

Président :	Marek BLICHARSKI	Professeur, UST, Cracovie
Rapporteurs /	Stanisław DYMEK	Professeur, UST, Cracovie
Examineurs Externes :	Dorte Juul JENSEN	Professeur, UTD, Denmark
	Jarosław MIZERA	Professeur, WUT, Varsovie
Autres Examineur(s) :	Marek BLICHARSKI	Professeur, UST, Cracovie
	Romain QUEY	Dr, ENSM-SE, Saint-Etienne
Directeur(s) de thèse :	Julian DRIVER	Professeur, ENSM-SE, Saint-Etienne
	Henryk PAUL	Professeur, IMMS-PAS, Cracovie
Co-directeur de thèse :	Claire MAURICE	Dr, ENSM-SE, Saint-Etienne

The work was carried out in 2007-2011 in the framework of the **Environmental Ph.D. Studies of Materials Science** held at the **Institute of Metallurgy and Materials Science of the Polish Academy of Sciences** in Kraków, and the **Faculty of Physics, Astronomy and Applied Computer Science and the Faculty of Chemistry of the Jagiellonian University**. In 2008-2010 years the work was carried out under the '*co-tutelle*' system at the **École Nationale Supérieure des Mines de Saint-Étienne** in the **Centre Sciences des Matériaux et des Structures**, France.

ACKNOWLEDGMENTS:

I would like to express my heartfelt gratitude to **the Directors of the Institute of Metallurgy and Materials Science** in Kraków and **the École Nationale Supérieure des Mines de Saint-Étienne**, in particular, **the Centre Sciences des Matériaux et des Structures (SMS)** in France for enabling the implementation of this PhD dissertation.

Individual thanks:

- to supervisors: **Prof. Henryk Paul** and **Prof. Julian H. Driver** for the scientific management and comprehensive help during the PhD thesis,
- to **Dr Claire Maurice** for her commitment and valuable leads in carrying out research and learning on the scanning electron microscope,
- to **Prof. Adam Morawiec** for Kikuchi diffraction pattern solutions and providing the numerical program to statistically analyze the distribution of disorientation axes,
- to **Dr Andrzej Piatkowski** for great help in carrying out research, numerous leads and discussions,
- also, I would like to grateful all my **colleagues** from **the Institute of Metallurgy and Materials Science** and **the SMS centre** (Saint-Étienne) for all their kindness, co-operation and help,
- I am sincerely grateful to my **family** and **friends** for their support,
- I thank **the Région Rhône-Alpes** for received a scholarship.

Author

Microstructure and texture evolution during annealing of plane strain compressed fcc metals

Speciality: Material Science

Keywords: nucleation and recrystallization, microstructure, texture, single crystals, plane state of strain, orientation mapping

Abstract

In the case of flat semi-products made of face-centered cubic (fcc) metals and alloys, one of the important parameters affecting the anisotropic material properties is its crystallographic texture. This parameter describes the suitability of sheets for plastic shaping during deep drawing. Despite much experimental research performed to explain the mechanisms controlling the transformation of as-deformed state texture components into recrystallized ones this process still remains unclear. The present research program is a renewed attempt at explaining the transformation mechanisms.

The following series of experimental investigations has focused on a model analysis of transformations which occur in single crystals, with stable orientations, i.e. Goss{110}<001> and brass{110}<112>, of several fcc metals with different stacking fault energies. The deformation is carried out by channel-die compression to simulate the rolling process of thin sheets. This approach to analyzing the problem makes its description simpler and clearer since the stability of the orientation during deformation enables one to precisely define the orientation relationship which appears when the 'primary nucleus' is formed. Another important aspect is that the deformation of stable orientation crystallites (up to large deformations) practically does not lead to the appearance of many high-angle boundaries; even if they appear it is in limited numbers. In the absence of high-angle boundaries, the conventional mechanism of primary nucleation, based on the presence of pre-existing nuclei in the deformed structure, cannot be accepted as valid for explaining texture change during recrystallization. The research program carried out in this study aims at not only defining preferences in the selection of new grain orientations and the determination of disorientation relationship dominating between recrystallized and deformed phases, but also 'associating' this relation to possible dislocation mechanisms (thermally induced dislocation motion). The interest in the above topic originated in the fact that current theories to describe the processes of texture transformation are inconsistent. The most conspicuous case regards the 'classical' disorientation relation of 40° <111> type across the migrating recrystallization front.

The present work is mostly based on local orientation measurement by means of high-resolution scanning electron microscopy, together with some complementary measurements performed by means of transmission electron microscopy.

The recrystallization process is closely related to the preceding straining process during which numerous crystal defects are generated. Thermally activated displacement of dislocations inside the dislocation cells and the migration of dislocation small-angle boundaries imply a change of orientation of the area where these processes occur. The classical orientation relation for fcc metals between the deformed matrix and the recrystallized grain, described as $40^\circ\langle 111 \rangle$, was only rarely found.

A detailed analysis of all the disorientations in different directions across the recrystallization front clearly shows the occurrence of $\alpha\langle uvw \rangle$ orientation relation. In the case of high SFE metals, the decisive role is played by axes close to the poles of the most active $\{111\}$ planes during deformation. The disorientation axes lie close to the normal of (111) plane but only rarely coincide with them. In medium-low SFE metals, growth occurs by both boundary migration and twinning (from the initial nucleus orientation) on different $\{111\}$ twinning planes followed by growth of the twinned areas. In most cases the normal of the twinning plane lies very close to the rotation axis.

Regardless of the initial crystal orientation, there is a strong relation of the as-deformed orientations with the orientations of new grains at the initial stages of recrystallization. For the metals studied here and both initial orientations at the initial stages of recrystallization, the appearance of a specific number of new orientation groups of new grains was demonstrated. The orientation relation across the recrystallization front 'defines' the final rotation by angles in the range $25\text{-}45^\circ$ around axes mostly grouped about the $\langle 122 \rangle$, $\langle 012 \rangle$, $\langle 112 \rangle$ and $\langle 111 \rangle$ directions. In the case of high SFE metals, the decisive role is played by axes close to the poles of the most active $\{111\}$ planes during deformation. In the case of metals with medium and low SFE (i.e. undergoing twinning in recrystallized grains) these were the axes grouped around the normals of all four $\{111\}$ planes. But also in this case, one clearly observes a preferential grouping of disorientation axes around the poles of the most active planes during deformation. (Although the rotation axes approach the normal vector of the active slip planes during deformation, they only rarely coincide with the exact location of the $\langle 111 \rangle$ direction.)

A large fraction of new grains, regardless of the metal, are characterised by a strongly elongated shape. It probably results from the thermally activated movement of selected dislocation families, travelling in pairs on one of the most active during deformation planes.

Modifications de la microstructure et de la texture pendant le recuit des métaux déformés de structure c.f.c

Domaine : Génie des Matériaux

Mots clés : nucléation et recristallisation, microstructure, texture, monocristaux, état de déformations planes, cartes d'orientation

Résumé :

La possibilité de prévoir les modifications de texture lors du recuit fait l'objet des recherches intensives, menées par les nombreux centres de recherche de par le monde. Dans le cas des (semi) produits plats réalisés en métaux et alliages, dont la structure cristalline est cubique à faces centrées, la texture cristallographique constitue un des paramètres les plus importants, ayant une influence sur les propriétés anisotropes du matériau. Ce paramètre décrit l'utilité des tôles à être formées dans des processus d'étirage profond. Cependant le processus de la transformation de la texture de l'état déformé en texture de l'état recristallisé continue d'être très peu connu.

Le présent programme de recherche constitue une tentative d'expliquer les mécanismes de transformation contrôlant la transformation de la texture qui a lieu lors des opérations technologiques du recuit. Les expériences ont été conduites sur les échantillons monocristallins dont les orientations étaient dites « stables » : Goss{110}<001> et 'brass' {110}<112>, déformées jusqu'à la plage des degrés importants de déformation lors de l'essai de compression encastrée modélisant le processus de laminage. Ensuite les échantillons ont été soumis au recuit à des températures situées dans le domaine de recristallisation primaire. L'analyse des transformations cristallographiques a été menée sur des métaux représentant un large spectre d'énergie du défaut d'empilement : petite - Cu-2% Al, moyenne - Cu et Ni grande - Al et Al-1%Mn. Lors du travail on a analysé les mécanismes de contrôle des phases initiales de recristallisation et, notamment : les mécanismes responsables de la formation de l'orientation du germe initial et leur rapport avec les systèmes de glissement actifs lors du processus de déformation, le rôle des limites du petit angle pendant ce processus, le processus de la formation des macles, etc.

L'explication des questions ci-dessus s'appuyait principalement sur les mesures des orientations locales au moyen du microscope électronique à balayage et du microscope électronique en transmission. L'analyse détaillée de la désorientation à travers le front de recristallisation a montré clairement que les orientations initiales des grains n'étaient pas dues au hasard. Les axes de désorientation dans la relation à travers le front de recristallisation se

trouvaient près des normales aux plans $\{111\}$, mais ne se recouvraient que sporadiquement avec la direction $\langle 111 \rangle$. Les axes situés près des normales aux plans fortement privilégiés pendant la déformation étaient tout particulièrement représentés. La distribution de l'angle de rotation en relation à travers le front de recristallisation présentait les préférences à la formation de deux maxima : près des valeurs 30° et $45-55^\circ$. Dans les métaux à l'énergie de fautes d'empilement moyenne et petite on a expliqué le rôle du mécanisme formation des macles pendant la formation de la texture de recristallisation. Dans la plupart des cas analysés, la normale au plan de formation des macles se trouvait à proximité de l'axe de désorientation 'définissant' l'axe de rotation dans la relation d'orientation entre l'état déformé et recristallisé.

Zmiany mikrostruktury i tekstury podczas wyżarzania odkształconych metali o sieci rsc

Dyscyplina: Inżynieria Materiałowa

Słowa kluczowe: zarodkowanie i rekrytalizacja, mikrostruktura, tekstura, monokryształy, płaski stan odkształcenia, mapy orientacji

Streszczenie:

Możliwość przewidywania zmian teksturowych podczas wyżarzania jest przedmiotem intensywnych badań prowadzonych przez wiele ośrodków badawczych na całym świecie. W przypadku (pół)wyrobów płaskich wykonanych z metali i stopów o strukturze sieci regularnie ściennie centrowanej, tekstura krystalograficzna jest jednym z najważniejszych parametrów wpływających na anizotropowe właściwości materiału. Parametr ten opisuje przydatność blach do kształtowania w procesach głębokiego tłoczenia. Jednakże proces przemiany tekstury stanu zdeformowanego w teksturę stanu zrekrystalizowanego nadal jest zagadnieniem silnie nierozpoznanym.

Niniejszy program badawczy jest próbą wyjaśnienia mechanizmów transformacyjnych kontrolujących przemianę tekstury, jaka dokonuje się w technologicznych operacjach wyżarzania. Badania doświadczalne przeprowadzono na próbkach monokrystalicznych, o tzw. orientacjach stabilnych, tj. Goss $\{110\}\langle 001\rangle$ i 'brass' $\{110\}\langle 112\rangle$, deformowanych do zakresu dużych stopni odkształcenia w próbie nieswobodnego ściskania, modelującej proces walcowania. Następnie próbki poddawano procesowi wyżarzania w zakresie rekrytalizacji pierwotnej. Analizę zmian krystalograficznych prowadzono na metalach reprezentujących szerokie spektrum energii błędu ułożenia (EBU): małej - Cu-2% Al, średniej - Cu i Ni oraz dużej - Al i Al-1%Mn. W pracy analizowano mechanizmy kontrolujące początkowe stadia rekrytalizacji, a zwłaszcza: mechanizmy odpowiedzialne za uformowanie się orientacji początkowego zarodka oraz ich związek z aktywnymi w procesie odkształcenia systemami poślizgu, rolę granic małego kąta w tym procesie, proces bliźniakowania rekrytalizującego, etc.

Wyjaśnienie powyższych problemów opierało się głównie na pomiarach orientacji lokalnych w skaningowym i transmisyjnym mikroskopie elektronowym. Szczegółowa analiza dezorientacji poprzez front rekrytalizacji wyraźnie pokazała, że orientacje początkowych ziaren nie są przypadkowe. Osie dezorientacji w relacji orientacji poprzez front rekrytalizacji leżały w pobliżu normalnych do płaszczyzn $\{111\}$, lecz jedynie sporadycznie pokrywały się z kierunkiem $\langle 111\rangle$. Szczególnie silnie reprezentowane były osie położone w pobliżu normalnych do płaszczyzn silnie uprzywilejowanych w procesie odkształcenia. Dystrybucja

kąta obrotu w relacji orientacji poprzez front rekrytalizacji wykazywała preferencje do formowania dwu maksimów: w pobliżu wartości 30° i $45-55^\circ$. W metalach o średniej i małej EBU, wyjaśniono rolę mechanizmu bliźniakowania w formowaniu się tektury rekrytalizacji. W większości analizowanych przypadków, normalna do płaszczyzny zbliźniaczenia leżała w pobliżu osi dezorientacji 'definiującej' oś obrotu w relacji orientacji pomiędzy stanem zdeformowanym a zrekrystalizowanym.

TABLE OF CONTENTS:

Symbols.....17

Abbreviations.....18

1. INTRODUCTION.....19

2. STATE OF THE ART.....22

2.1. Structural events occurring during annealing – definitions.....22

2.2. Texture transformations. Nucleation and growth mechanisms in the recrystallization process.....25

2.2.1. The theory of oriented nucleation and oriented growth - half a century of discussion.....25

2.2.2. Nucleation - the beginning of recrystallization.....28

2.2.2.1. Nucleation by the migration of high-angle grain boundaries existing in the deformed structure.....29

2.2.2.2. Nucleation through the migration of low-angle boundary.....29

2.2.2.3. Nucleation through the coalescence of subgrains.....30

2.2.3. Occurrence of the three nucleation mechanisms – discussion.....30

2.3. Crystallographic aspect of nucleation of recrystallization.....32

2.4. Recrystallized grain growth and grain re-orientation. The role of recrystallization twinning.....36

2.5. Summary of the bibliography.....39

3. SCIENTIFIC PURPOSE AND DISSERTATION THESIS.....45

3.1. Objectives.....45

3.2. Thesis.....45

4. MATERIAL AND RESEARCH METHODOLOGY.....47

4.1. Material.....47

4.1.1. Ideal Goss (110)[00-1] orientation.....49

4.1.2. <i>Ideal 'brass' (110)[1-1-2] orientation</i>	52
4.2. Experimental procedure	54
4.2.1. <i>Plane strain compression (channel-die) test</i>	54
4.2.2. <i>Recrystallization</i>	55
4.2.3. <i>Determining the crystal orientations and analysis of texture evolution</i>	56
4.2.3.1. <i>Global textures measurements by X-ray diffraction</i>	56
4.2.3.2. <i>Local orientation measurements</i>	60
4.2.3.3. <i>Structural observations at optical microscopy scale</i>	62
5. RESULTS AND DISCUSSION	64
5.1. The description of the deformed state	64
5.1.1. <i>Goss{110}<001> orientation</i>	65
5.1.1.1. <i>Microstructure characterization based on SEMFEG/EBSD local orientation measurements</i>	65
5.1.1.2. <i>Dislocation structure</i>	71
5.1.2. <i>Brass {110}<112> orientation</i>	74
5.1.2.1. <i>SEM/EBSD microstructure and texture</i>	78
5.1.2.2. <i>TEM microstructure</i>	81
5.1.3. <i>Crystal lattice rotation during deformation - the rotation axes identification</i>	84
5.1.3.1. <i>Accuracy of disorientation determination</i>	84
5.1.3.2. <i>Crystal lattice rotation. The rotation axes identification</i>	84
5.1.3.3. <i>Microband structure development</i>	90
6. PARTIALLY RECRYSTALLIZED STATE	92
6.1. Early stages of recrystallization in metals of high SFE	92
6.1.1. <i>General description of the recrystallization process - large area analysis based on SEM/EBSD orientation maps</i>	98

6.1.2. <i>Disorientation angle and disorientation axes distribution</i>	99
6.1.3. <i>Statistical analysis of the distribution of disorientation angles and axes</i>	101
6.1.4. <i>The directionality of grain growth</i>	107
6.1.5. <i>Analysis of particular cases of new orientation formation during recrystallization</i>	115
6.1.6. <i>In-situ recrystallization in TEM. Microstructure and texture changes analyzed by TEM-based local orientation measurements</i>	116
6.1.7. <i>Recrystallization twinning in high SFE metals</i>	127
6.2. Early stages of recrystallization in medium and low SFE fcc metals	130
6.2.1. <i>Large area analysis</i>	130
6.2.2. <i>Statistical analysis of the disorientation angle and axis distributions in medium- low SFE metals</i>	138
6.2.3. <i>Single grain of uniform orientation and first recrystallization twins</i>	144
6.2.4. <i>The crystallography of the recrystallization growth</i>	153
7. SUMMARY AND CONCLUSIONS	157
8. ANNEXE 1	161
9. ANNEXE 2	163
10. REFERENCES	185

SYMBOLS:

\bar{d}_a - factor describing the ratio of the average size of grains with a particular orientation

\bar{d}_r - factor describing the ratio of the average size of grains of a random orientation

T_d - deformation temperature

T_m - homologous temperature

α - factor separating oriented growth and oriented nucleation

α_d - factor describing the fraction (number) of grains with a given orientation

α_r - factor describing the fraction (number) of grains with random orientation

β^3 - factor describing oriented growth

γ_{SFE} - stacking fault energy

ABBREVIATIONS:

CBED - convergent beam-electron diffraction

CRSS - critical resolved shear stress

EBS - Electron Backscatter Diffraction

ED - Extension Direction

fcc - face-centered cubic

HAGB - high-angle grain boundaries

IPF - Inverse Pole Figure

LAGB - low angle grain boundaries

ND - Normal Direction

ODF - Orientation Distribution Function

OG - oriented growth

ON - oriented nucleation

PSC - plane strain compression

RF - recrystallization front

SAD - selected area diffraction

SEM - Scanning Electron Microscopy

SFE - stacking fault energy

TEM - Transmission Electron Microscopy

TD - Transverse Direction

TKP - Transmitted Kikuchi Patterns

1. INTRODUCTION

For several decades the possibility of predicting textural transformations during annealing has been the subject of intensive research by numerous research centres all over the world. This is so because the subject is a crucial part of important technological processes for shaping flat bars, sheets or tapes, by stamping or rolling. In particular, during deep drawing of metals, the associated problem of anisotropic plastic flow is of key importance for both the quality of the fabricated final product and the 'economics' of the process itself.

In the case of flat semi-products made of face-centered cubic (fcc) metals and alloys, one of the important parameters affecting the anisotropic material properties is its crystallographic texture. This parameter describes the suitability of sheets for plastic shaping during deep drawing. The finishing stages of sheet manufacturing are completed mainly by means of cold rolling, usually up to large deformations. These processes lead to a high strengthening of the metal accompanied by significant structural changes and the formation of new sharp texture components of the deformed state. Subsequent heat treatment (annealing) leads to a complete transformation of the texture components (Fig. 1.1).

Despite much experimental research performed to explain the mechanisms controlling the transformation of as-deformed state texture components into recrystallized ones (i.e. the transformation that takes place during technological annealing processes), this process still remains unclear.

The present research program is a renewed attempt at explaining the transformation mechanisms. Most earlier work on this subject has been based on experiments with polycrystalline materials. In the author's view such an approach to analyzing the mechanisms of texture transformation is very difficult due to multiple factors influencing the process.

In order to clarify this problem, it is advisable to perform experimental research under conditions where the number of free parameters affecting this transformation is minimized. Therefore, the following series of experimental investigations has focused on a model analysis of transformations which occur in single crystals, with stable orientations, of several fcc metals with different stacking fault energies (SFE). The deformation is carried out by plane strain compression (channel-die compression) to simulate the rolling process of thin sheets. This approach to analyzing the problem makes its description simpler and clearer since the stability of the orientation during deformation enables one to precisely define the orientation

relationship which appears when the 'primary nucleus' is formed. Another important aspect is that the deformation of stable orientation crystallites (up to large deformations) practically does not lead to the appearance of many high-angle boundaries; even if they appear it is in limited numbers. This is of paramount importance for the discussion of mechanisms controlling textural transformations during recrystallization. In the absence of high-angle boundaries, the conventional mechanism of primary nucleation, based on the presence of pre-existing nuclei in the deformed structure, cannot be accepted as valid for explaining texture change during recrystallization. It is then justified to ask the following important question: *what is the general mechanism controlling recrystallization nucleation, and what is the role of low-angle boundaries?*

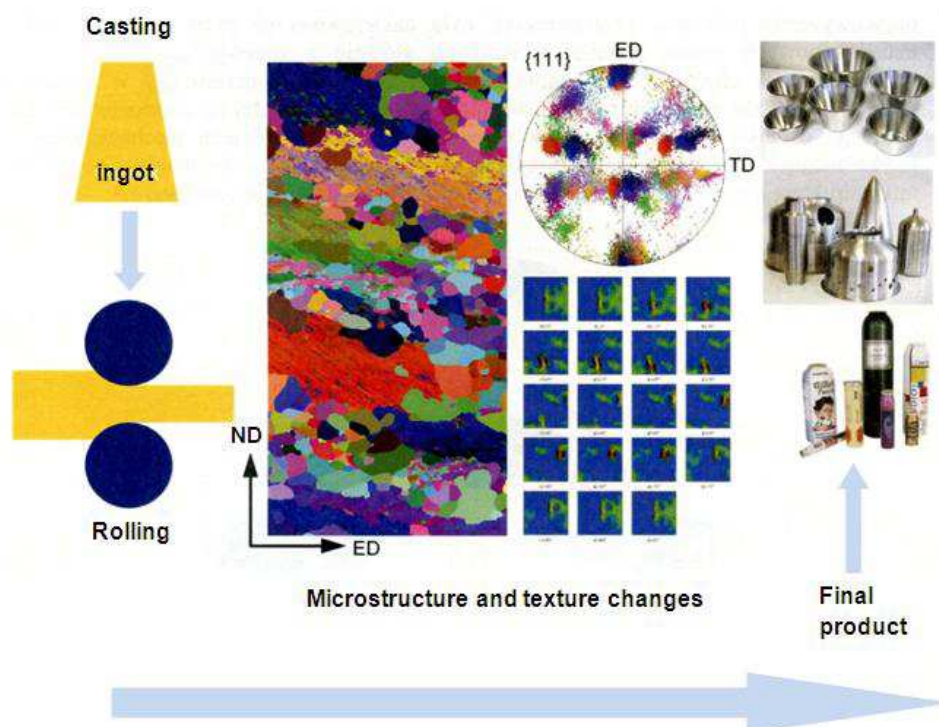


Fig. 1.1. Schematic presentation of microstructure and texture changes during thermo-mechanical processing of flat semi-products [Paul (2009)].

Since recrystallized regions show dislocation densities of the order of 10^6 - 10^8 cm^{-2} (i.e. much lower than those of the deformed state - 10^{12} cm^{-2}), it is justified to put another question: *is it possible to link dislocation removal from a given region (nucleus) with its change of orientation, with respect to the orientation of the deformed state?*

Previous research shows that the orientations of single nuclei of homogenous orientation (i.e. without recrystallization twins) are quite different from those of the deformed state orientations. They are considerably 'scattered' but it can certainly be stated that they are not accidental [Paul (2002b), Albou *et al.* (2010b)]. These studies also showed that a given 'image' of the as-deformed texture provide a limited number of variants of orientation families of new grains [Paul (A2002a, 2002c)].

The research program carried out in this study aims at *not only defining preferences in the selection of new grain orientations and the determination of disorientation relationship dominating between recrystallized and deformed phases, but also 'associating' this relation to possible dislocation mechanisms (thermally induced dislocation motion).*

A very clear correlation between microtexture and microstructure is enabled by the recent development of transmission and scanning electron microscopy techniques of local orientation measurement at the level of single dislocation cells [Steeds and Morniroli (1992), Morniroli (1998), Zaefferer (2000), Fundenberger *et al.* (2002), Humphreys and Hatherly (2004a)].

The present work is mostly based on local orientation measurement by means of high-resolution scanning electron microscopy (SEM), together with some complementary measurements performed by means of transmission electron microscopy (TEM). By describing the crystallographic relation between the 'deformed phase' and the new recrystallized grains ('recrystallized phase'), the present work provides new experimental data for the microstructural and microtextural conditions of primary recrystallization in fcc metals. Systematic orientation measurements, with a strictly defined step size, enable the orientation determination of given structural elements and the calculation of their mutual crystallographic relations (disorientations). This provides a basis for describing the mechanisms leading to their formation.

A major part of the research program related to local orientation measurements presented in this work was performed in France (2008-2010) during the author's stay at the Materials Research Centre (Centre Sciences des Matériaux et des Structures) in École Nationale Supérieure des Mines de Saint-Étienne, financed by a grant from the Région Rhône-Alpes.

2. STATE OF THE ART

2.1. Structural events occurring during annealing - *definitions*

Plastic shaping of metals has been used to produce final metal products since the Bronze age. Consequently, a number of transformations occurring during deformation and annealing have been long known. However, systematic research on the issues of structural recovery by annealing was initiated only in the early 20-ties of the 20th century. From a technological viewpoint, the aim of annealing is to restore plasticity and material softening, as well as to refine and homogenize the grain size in the previously strained material. During annealing the strength decrease is accompanied by an increase in the capacity for plastic flow.

In the literature it is widely accepted that *the recrystallization process* defines the formation of new grains in the deformed metals through the formation and migration high-angle boundaries, while the driving force of this process is the release of plastic deformation stored energy. Usually *high-angle grain boundaries* (HAGB) are characterized as those whose disorientation is greater than $10-15^\circ$ between the adjacent areas. Accordingly, *low angle grain boundaries* (LAGB) are described by disorientations lower than $10-15^\circ$. Plastic strain energy stored during the deformation (mainly in form of dislocations) may be released in three major processes, i.e. *recovery*, *recrystallization* and *grain growth* [e.g. Doherty *et al.* (1997b), Humphreys and Hatherly (2004a)]. *Recovery* includes all the processes that result in decreasing the stored energy, which do not require the migration of high-angle boundaries. The effect of this process is the rearrangement of dislocations into low energy structures, e.g. through the formation of low-angle boundaries between the subgrains. *Recrystallization* consists in the formation of high-angle boundaries and their migration, and its driving force is the structure's tendency to release the plastic strain stored energy. This process is preceded by the appearance of the primary nucleus capable of further growth.

According to classical definitions, *nucleation* is the formation of small regions, practically free of any structural defects, which, at least partly, include a high-angle boundary with regard to the deformed state of the surrounding regions [Cahn (1950), Doherty *et al.* (1997b), Humphreys and Hatherly (2004a)]. After complete recrystallization *grain growth* is defined as their average size growth, and its driving force is the tendency of the system to minimize the active surface of grain boundaries. This final stage of transformation occurring during annealing may take the form of either '*normal grain growth* ', which decreases the fraction of

small size grains, or '*abnormal grain growth*', which is the phenomenon of strong growth of particular grains, attaining a size well above the average size. Earlier research, however, shows that it is extremely difficult to precisely separate these two processes, i.e. the nucleation and the growth of grains.

The literature on the subject also devotes a lot of space to two alternative types of this particular transformation. On the one hand, we may deal with a two-stage mechanism, originating in the appearance of 'primary nucleus' and their growth. In this type of process, the initial stage of transformation is linked to the appearance of 'small regions', surrounded by a distinctive boundary, and at the same time 'structurally' and 'orientation' different from the adjacent surroundings [Humphreys and Hatherly (2004a)]. This mechanism is described in the literature as *discontinuous recrystallisation*. On the other hand, *continuous* or '*in-situ*' recrystallisation may take place in some cases; the system evolves slowly and homogeneously, by a gradual decrease in the dislocation density during annealing without a discernable moment for the appearance of new grains. This process is associated with a noticeable structure 'thickening' [Jazaeri and Humphreys (2004a, 2004b)].

However, it was noticed quite early on that the separation between recovery and recrystallization (and in particular its form described as 'continuous or *in-situ* recrystallization') is not clearly defined. Hornbogen [Hornbogen and Köster (1978)], while analyzing the behavior of Al alloys containing fine second phase particles, observed that the recrystallization of these metals is very difficult. Despite this, the recovery processes rapidly lead to intensive softening of the alloy (so-called '*extended recovery*' process). In reference books these two phenomena were not distinguished for a long time. Only Humphreys and Chan (1996a) offered their separation and 'border line' between these stages was established based on the analysis of changes in the ratio of low- to and high- angle boundaries.

During the development of a new grain microstructure, a crucial step is the formation of primary nuclei, i.e. dislocation-free regions in the deformed matrix which are capable of further growth. From a thermodynamic point of view nucleation may be defined as the activation of recrystallization sources, while dislocation-free and stress-free nuclei may subsequently 'consume' the deformed state 'phase'. From a structural point of view, this process is linked to the formation of a high-angle boundary called *the recrystallization front* (RF) and then its migration.

The nucleus needs to have 'sufficient size' (usually assumed $>1\mu\text{m}$) to be capable of further growth [e.g. Rios and Sandim (2005)]. In the literature it is accepted that the new grain orientations are different to those described by the texture components of the deformed state. However, *there is no consensus for the 'route' by which the transition occurs from the as-deformed orientation to the primary nuclei orientation* and the resulting formation of the final texture of the fully recrystallized material; consequently *there is no adequate description of mechanisms controlling this transformation.*

The growth stage occurs through the migration of high-angle boundary ('generated' between recrystallized or recovered phase and the deformed phase) into the deformed structure. As a consequence of the growth, due to high-angle boundary migration, a completely new texture is created. Recrystallization processes at this stage are relatively easy to examine, e.g. by means of microscopic analyses at various scales (optical microscopy, SEM and TEM). These methods most often include investigating the correlation of growth rate with disorientation (boundary type) and driving force [Engler *et al.* (1996), Molodov *et al.* (1995), Winning *et al.* (2002)]. Nevertheless, relatively little attention on growth kinetics is paid to the mechanisms behind the rearrangement of atoms on both sides of the recrystallization front. In the author's opinion this is a key problem in analyzing the phenomena connected to textural transformations. It is beyond doubt that the observed rearrangements (of dislocations and low-angle boundaries) lead to a situation where, on both sides of the recrystallization front, the crystal structure is retained, i.e. the nucleus has the same crystal structure as the matrix into which it is growing. However, it is the orientation of the forming nucleus that undergoes a change (with respect to orientations detected in the deformed matrix). It is then justified to ask the following question:

What mechanisms causes the orientations of new grains to be different from those of the surrounding as-deformed regions and are these mechanisms linked to atomic diffusion processes or dislocation motion?

The latter aspect, i.e. the attempt to relate the orientation change with thermally induced dislocation motion has been present for several years. It will also be a major subject for the present research program.

2.2. Texture transformations. Nucleation and growth mechanisms in the recrystallization process

Two groups of interconnected issues are particularly important for the current analysis. On the one hand, the description of the mechanisms of structural (morphological) changes that take place in the cold-deformed metal during annealing is already debatable, on the other hand, the description of mechanism in charge of texture changes is even more controversial.

2.2.1. *The theory of oriented nucleation and oriented growth - half a century of discussion*

The title of this chapter was taken from the textbook '*Thermo-Mechanical Processing of Metallic Materials*' by Verlinden *et al.* (2007) and nicely reflects the controversies over textural transformation in annealing. The reasons for the formation of 'sharp' recrystallization texture in metals subjected to plastic deformation have been a controversial issue for over 60 years. This results from the fact that, in many cases, recrystallization of metals, following a moderate deformation, leads to a highly scattered 'image' of the texture. This behaviour is fundamentally different from that observed in (some) heavily deformed metals, where annealing often causes the formation of strong textural components. A classical example is the appearance of a strong 'cube', i.e. $\{100\}\langle 001\rangle$ component in some (but not all) highly deformed fcc metals (e.g. during rolling) and subsequently annealed; another example concerns the formation a strong $\{100\}\langle 011\rangle$ - type texture in silicon steels.

Despite the fact that at present there is no full description of the transformation mechanism, it is accepted that the orientations of recrystallized grains 'originate from the orientations' of the deformed matrix regions from which they grow. This obvious fact led some authors [Burgers *et al.* (1931)] to claim that new grains should be characterized by orientations similar to the orientation of the deformed state. If we make the additional assumption that a given deformed state region 'produces' the same number of nuclei and that all nuclei 'grow in the same way' inside the deformed state structure, then we can expect 'a replica of the texture' of the deformed state in the recrystallized phase [Verlinden *et al.* (2007)]. *However, such a mechanism is not observed in practice.*

In an attempt to bypass the inconvenience in this reasoning, it was assumed that higher nucleation frequencies occur in deformed crystallites with 'certain' orientations and/or with

higher growth potential and consequently influence the 'image' of the texture to a greater degree. Such a description underlies two fundamental and opposing groups of theories attempting to describe the mechanism of texture change: oriented nucleation (ON) and oriented growth (OG).

In agreement with the classical description, the ON model is based on the hypothesis that grains with orientations which constitute the texture of the fully recrystallized material nucleate with higher frequency from grains with other orientations. On the contrary, the OG model assumes that grains of a given orientation grow much bigger than the average diameter of the recrystallized grains and thus determine the 'shape' of the final texture. The basis of the OG model is the observation of high mobility of boundaries characterized by certain distinctive disorientations.

The theory of oriented nucleation was formulated in 1931 by Burgers and Louwse [Burgers and Louwse (1931)]. They assumed that the distribution of orientations recognized in the deformed state determines the exceptional capabilities of 'the growth of orientation' dominating the recrystallization texture. Analyzing the locations of preferred nucleation in deformed and recrystallized single- and poly- crystals of aluminium, they established the occurrence of rotations around $\langle 112 \rangle$ directions across the migrating recrystallization front (in the direction of preferred growth) as the dominant relation during the formation of new grains. The theory assumes that all the potential nuclei are activated without any preferences. However, those with very mobile boundaries (rapid growth) will grow faster and will have a strong effect on the final texture of the recrystallized state.

*The theory of oriented growth was formulated by Barrett in 1940 [Barrett (1940)] and is based on the observations in a series of single crystals of fcc metals that the preferred growth relations possess disorientations of $45^\circ \langle 111 \rangle$ -type. It was established that the recrystallization texture is determined by the nuclei which are capable of the fastest growth within the deformed matrix. The preferred grains are those which possess the most advantageous orientation relationship (disorientation) through the migrating recrystallization front as compared to the deformed regions. However, it is still *an open issue to define the most advantageous orientation relationship, favourable to rapid growth.**

The original ON model is indeed a hypothesis that grains with orientations dominant in the fully recrystallized material nucleate with higher frequency as compared to grains with random orientations [Doherty *et al.* (1997b)]. This proposal is based on the observation that

some volumes in the deformed material structure are preferred for the appearance of nuclei. Examples are band-like strain inhomogeneities such as shear bands or transition bands [Blicharski and Gorkzyca (1978), Akef and Driver (1991), Liu *et al.* (1995), Driver *et al.* (2000), Goodfrey *et al.* (2001), Paul (2002), Paul *et al.* (2002c), Glez and Driver (2003), Dymek and Wróbel (2003), Afrin *et al.* (2011)], or heavily deformed zones around large second-phase particles [Humphreys (1977), Ardakani and Humphreys (1994), Ferry *et al.* (1996), Engler *et al.* (1997, 2001)], etc.

Doherty *et al.* (1997b) give a general condition for heavily oriented nucleation, which can be expressed as a number derived from the relation:

$$\alpha = \alpha_d / \alpha_r \gg 1$$

where: α_d - describes the fraction (number) of grains with the given orientation (e.g. 'distanced' of 10-15° from the ideal position), whereas α_r - describes the fraction (number) of grains with random orientation.

To meet the condition for oriented nucleation, the frequency of grains possessing a given orientation must be significantly higher than the frequency of grains with a random orientation (i.e. any other orientation). In this context, the factor describing oriented growth (β^3) can be derived from the ratio of the average size of grains with a particular orientation (\bar{d}_d) to the average size of the rest of the grains (\bar{d}_r). A strong effect of oriented growth occurs when:

$$\beta^3 = (\bar{d}_d / \bar{d}_r)^3 \gg 1$$

Therefore, Doherty [Doherty *et al.* (1997b)] defined these models as the effect of the frequency of grains with a given orientation (for ON) and the effect of the average grain size (for OG). Assuming spherical shape for the recrystallized grains, the factor of grain size predominance is most often described to the third power. It is easily observable that a strong recrystallization texture will occur when both α and β^3 are higher than 1. Employing these two parameters allows quantifying the recrystallization, *but it still omits altogether the crystallographic aspect of orientation transformation which takes place during the recrystallization.*

2.2.2. *Nucleation - the beginning of recrystallization*

In the literature the most controversial problem is the description of mechanisms leading to the formation of the primary nucleus capable of further growth. The kinetic model of recrystallization predicts that completely new grains are formed during recrystallization due to skipping 'atom upon atom' similarly to other phase transformations. Nevertheless, the analysis performed by Doherty *et al.* (1997b) shows that such a process, due to energy issues, is difficult to realize. Rios and Sandim (2005) additionally prove that, apart from little driving force stimulating the occurrence of recrystallization, the *interfacial energy* between non-recrystallized and recrystallized zone (across a high-angle boundary) is very large. As a result very large nuclei appear with a diameter of $\sim 1\mu\text{m}$ (or 10^{10} atoms), e.g. [Rios and Sandim (2005)], which, in turn, indicates that it is impossible to imagine the process as a consequence of thermal fluctuation of such a large group of atoms.

Other issues also arise. Compared to 'classical' solid state reactions, recrystallization results in the appearance of relatively small number of nuclei per unit volume. Rios and Sandim (2005) notice that '*... from each million of 'embryos' (deformation cells or subgrains) only one of them transforms into a nucleus ...*'. Moreover, the growth rate of the primary nucleus, in most cases, decreases during further recrystallization. This can often be explained by the presence of orientation gradients (affecting the change of orientation relationship through the recrystallization front) in the deformed state structure.

Current classical recrystallization theory attempts to omit this difficulty. Following Cahn's idea [Cahn (1949)], it is assumed that the nuclei which transform into 'new recrystallized grains' are not formed during annealing but already exist in the deformed state [Doherty (1978), Humphreys and Hatherly (2004a)].

The appearance of a recrystallization nucleus with lower dislocation density surrounded by at least one high-angle boundary with high mobility, capable of quick migration into the deformed or recovered structure [Rios and Sandim (2005)] causes its rapid transformation into a completely new grain with an orientation different from the deformed surroundings. Since annealing is closely associated with a reduction of the dislocation density and/or their rearrangement, this idea may be used to explain the mechanism of texture change. In the literature, three models describing nucleation may be found based respectively on: high-angle boundary migration, low-angle boundary migration (between subgrains) and subgrains coalescence.

2.2.2.1. *Nucleation by the migration of high-angle grain boundaries existing in the deformed structure*

This model was originally suggested by Beck and Sperry [Beck and Sperry (1950)]. It is based on optical microscopy observations and later by means of TEM [Bailey (1963)] on deformed copper, nickel, gold, silver and aluminium. These materials were subjected to relatively small strain (below 40%), annealed and analyzed in terms of the migration of boundaries existing in the material. The proposed mechanism assumes the existence in the deformed state structure of high-angle grain boundaries, which are capable of migrating inside heavily deformed regions. The condition for this process to happen is derived from the balance between energy reduction by lowering the density of crystal structure defects incorporated in the moving boundary, and the increase in the overall surface of the boundary. This model is frequently used to explain the observed *bulging effect* of high-angle boundaries separating complementarily oriented deformed regions.

2.2.2.2. *Nucleation through the migration of low-angle boundaries*

This model was proposed independently by Beck and Sperry (1950) and Cahn (1949) and later completed by Cottrell and Mould (1976). The model is based on the phenomenon of *polygonization* in which the regions of low dislocation density are surrounded by subgrain boundaries (low-angle boundaries, i.e. $<10-15^\circ$) and requires the thermally activated migration of boundaries. This boundary motion leads to reducing the stored energy by removing part of the structural defects (*annihilation*) or the 'rearrangement' of the boundaries into low-energy structures (*polygonal systems*). This model also includes the possibility of interacting with other low-angle boundaries. The absorption of dislocations into the low-angle boundary causes an increase in the orientation difference through the migrating boundary which leads to raising its energy and mobility. This process continues until the low-angle boundary transforms into a high-angle boundary. Experimental proofs of the occurrence of this process were presented by many authors, e.g. Sandström *et al.* (1978), Varma and Willitis (1984), Walter and Koch (1963) and Blum *et al.* (1995), etc.

2.2.2.3. *Nucleation through the coalescence of subgrains*

Originally, this model was formulated in 1948 by C. S. Smith (1947/1948); the author based on the investigations carried out by Hu (1962 and 1963) on single crystals of Fe-3%Si alloy. However, literature reports analyzing this concept reveal a lot of controversy. At an early stage of research on recrystallization phenomenon, Li (1962), who was analyzing the thermodynamic conditions of nucleation, concluded that '*the nucleation by coalescence cannot to be dominant*'. But the work done by Doherty and Szpunar (1984) strongly confirms the concept of nucleation by coalescence. They prove that coalescence of subgrains at temperatures below $0.65T_m$ (where: T_m - melting point of metals) is a significant mechanism of recrystallization. Experimental proofs based on TEM observations were earlier presented by Sandström *et al.* (1978), Jones *et al.* (1979a) and Jones (1980).

Subgrain coalescence is a mechanism that causes a reduction of the stored energy by the disappearance of boundaries between the subgrains via the rotation of the crystal lattice of one of the regions. From the point of view of changes in microstructure coalescence is the process by which two or more neighboring, slightly disoriented subgrains merge to form a single, larger grain. The decrease of the total free energy due to the disappearance of boundaries between the subgrains causes a rise in the orientation difference and energy of the remaining boundary fragments. The last aspect, linked to the misorientation increase is particularly significant for considering the change of 'a selected' region's orientation as compared to orientations identified in the deformed state. The increase of the orientation difference resulting from the lattice rotation of an area leads to the appearance of a high-angle boundary of high mobility, that is, to the formation of a nucleus capable of further growth. Rios and Sandim (2005) based on TEM results concluded that nucleation rooted in coalescence outweighs the mechanism of boundary migration between subgrains in the lower range of annealing temperatures.

2.2.3. *Occurrence of the three nucleation mechanisms - discussion*

Nucleation can be seen as a dislocation rearrangement resulting in the development of regions of low dislocation density bounded by high-angle boundaries capable of fast migration into the deformed matrix. In severely deformed polycrystalline samples, the fraction of high-angle

boundaries is generally very large, and these boundaries play a role in the nucleation of new grains. However, nucleation by migration of deformation-induced high-angle boundaries cannot be seen as unique or universal. For instance, in the case of fcc crystallites with stable orientations in plane strain compression ($\{110\}\langle 112\rangle$ or $\{110\}\langle 001\rangle$), high-angle boundaries are not present or are only very rare, but nucleation still occurs. Therefore, in deformed materials where the fraction of low-angle boundaries is still large, the two remaining mechanisms, both based on migration of low-angle boundaries, are also needed for the early stages of recrystallization.

Ferry and Humphreys (1996) have described discontinuous subgrain growth in deformed (channel-die) and annealed $\{110\}\langle 001\rangle$ -oriented aluminium single crystals. After deformation the microstructure showed neither large orientation gradients nor heterogeneities, making the material resistant to recrystallization. The authors attributed the discontinuous subgrain growth to orientation differences between the subgrains formed during deformation. However, the existence in the deformed microstructure of strain inhomogeneities seems not to be a necessary condition for preferred recrystallization. An analysis of recrystallization behaviour of aluminium bicrystalline samples of different stable/unstable orientation combinations led Paul and Driver [Paul and Driver (2005)] and Blicharski et al [Blicharski *et al.* (1995)] to the conclusion that recrystallization is observed more easily and more frequently in the crystallites of stable ($\{110\}\langle 001\rangle$) orientation with respect to unstable ones of $\{100\}\langle 001\rangle$.

The largest controversy in the literature is associated with the occurrence of subgrain coalescence and the migration of low angle boundaries (sub-boundaries). Based on much literature data *the subgrain migration mechanism* seems to be associated with high strains (Ray *et al.* (1975)), a large spread in the subgrain size (Kreisler and Doherty (1978)), relatively high annealing temperatures [Varma and Willitis (1984) and Walter and Koch (1963)] and occurs preferentially in low-SFE metals [McQueen and Jonas (1975)]. The mechanism of *subgrain coalescence* in turn, seems to be associated with transition bands [Kreisler and Doherty (1978)], a large spread in the distribution of subgrain angles [McQueen and Jonas (1975), Doherty (1978)], moderate strains, regions adjacent to grain boundaries [Ray *et al.* (1975)], relatively low annealing temperatures [Walter and Koch (1978), Varma and Willitis (1984)] and metals with medium-high SFE [McQueen and Jonas (1975)].

2.3. Crystallographic aspect of nucleation of recrystallization

The crystallographic aspects of new orientation generation have been the subject of discussion for several years. They concern both the description of mechanisms 'controlling' the texture transformation as well as the relations between the 'texture images' of the deformed and recrystallized states.

In its 'pure form', OG theory assumes that the growth potential of a given nucleus depends on the orientation difference at the migrating recrystallization front [Barrett (1940)]. Intuitively, it is obvious that the fastest growing nuclei contribute to the final shaping of the recrystallization texture. This statement suggests a relation between the rate of recrystallization front migration and the disorientation between regions of the deformed state. Research to document this interrelation has been undertaken many times in the last decades, e.g. [Liebman *et al.* (1956), Gottstein and Shvindlerman (1992), Molodov *et al.* (1995), Winning *et al.* (2002)]. Results on polycrystalline materials led Lücke (1974), to formulate the so-called *compromise theory*. According to this concept, following an earlier idea by Beck (1953), the development of nuclei with orientations such that they can simultaneously consume more texture components is preferred. Sztwiertnia and Haessner (1995) assumed, that a compromise orientation is such a that new grain orientation can not only grow at the expense of a large part of the strained matrix but also the probability of its growth being blocked by unfavourably oriented fragments of deformed matrix is the smallest. However, these approaches are strictly statistical, and therefore conclusions about the mechanisms controlling the recrystallization process are very tentative.

A variant of the above idea is the concept '*of pinned orientations*' (*orientation pinning*) proposed by Juul Jensen (1995). It was observed that a grain growing in the deformed structure comes across regions with different orientations. This results in differences of the rate of recrystallization front migration. In the particular case when a low-angle boundary is formed (when the orientation of nucleus and the surrounding strained matrix are similar) the nucleus' growth is observed to stop. As a consequence, only those nuclei grow which have a 'favourable' orientation relationship with the surrounding matrix. This idea, however, has some inconveniences since it assumes that the nucleus orientations are random. Additionally, their crystallographic interrelation to the deformed matrix is unclear.

It also ignores some observations of the nucleation process in fcc metals, where only a few families of new nuclei orientations were identified. Additionally, they displayed a certain

correlation with the arrangement of the predominant slip systems of the deformation process [Driver *et al.* (2000), Paul *et al.* (2002a), Paul and Driver (2002b), Wróbel *et al.* (2003)]. Recent research performed on single crystals represents an alternative method of analysis to investigations of polycrystals. *The possibility of systematically measuring the orientation changes, with the active slip systems allows a deeper understanding of the mechanisms responsible for recrystallization texture changes.*

However, even in the case of experiments on single crystals there is no general agreement about their interpretation. The results of Parthasarathi and Beck (1961) on aluminium single crystals indicate the development of recrystallization texture components after rolling resulting from rotations around the $\langle 111 \rangle$ direction close to the normal direction. These results are clearly in contrast to earlier work by Liu and Hibbard (1955) who claimed that in deformed single crystals of copper and aluminium, the only recrystallization components that develop were obtained by a rotation around the $\langle 111 \rangle$ lying close to the rolling direction. Additionally, it was pointed out that these axes were linked to the normals of the slip planes of the most active systems during the deformation.

The above idea was revisited a few years ago by Paul *et al.* (2002c). In a series of experiments on fcc metals single crystals of different SFE, and based on SEM and TEM techniques of local orientation measurements, a relation was found between the nuclei orientation and the predominant slip systems during deformation, e.g. [Paul *et al.* (2002a)]. These results partly confirm the concept suggested by Ibe and Lücke (1966) and later developed by Duggan *et al.* (1990) in their micro-growth selection model. According to this concept, the formation of a nucleus with an orientation with large growth potential results from the selection among a series of nuclei appearing in the deformed matrix. According to this theory, the greatest growth potential is displayed by those nuclei which form a boundary of $40^\circ \langle 111 \rangle$ with the deformed matrix [Dugan *et al.* (1990 and 1993)].

The OG model, which highlights the relation between boundary mobility and disorientation (through the migrating recrystallization front) [Barrett (1940)] has been strongly promoted for a few decades by authors associated with universities in Aachen and Göttingen. Studies by Liebmann *et al.* (1956) and lately by Molodov *et al.* (1995) show that recrystallization front disorientations of $40^\circ \langle 111 \rangle$ (close to the special $\Sigma 7$ boundary, i.e. $38.2^\circ \langle 111 \rangle$) are connected with the maximum of the growing grain's mobility for most fcc metals and alloys. However,

as classical investigations by Lücke (1974) show, the highest mobility is observed for boundaries with $\langle 111 \rangle$ rotation axis but with the angles $>40^\circ$.

Already during the early stages of research on texture changes in recrystallization, a group of studies can be found whose authors investigate the issue of explaining the appearance of $\langle 111 \rangle$ disorientation axes and try to associate the formation of primary nuclei with dislocation mechanisms. This problem may also stimulate further discussion. Analyzing texture changes during recrystallization of cold-rolled pure metals Al, Cu, Ag and Cu-Zn alloy, Liu and Hibbard (1955) proved that the $\langle 111 \rangle$ disorientation axes in orientation relationship between nucleus orientations and its deformed neighbourhood were strongly connected to the $\{111\}$ planes active during deformation.

On the one hand, one can consider the movement of two dislocation systems including screw components, leading to the formation of a twist boundary with the rotation axis parallel to $\langle 111 \rangle$ direction. On the other hand the $\{111\}$ pole figures depicting the nuclei orientation and those of the nearest deformed region, indicate a rotation of the crystal lattice by $\langle 112 \rangle$ direction 'distanced' by 19.5° from the common $\langle 111 \rangle$ pole [Paul *et al.* (2002c)]. Such a rotational tendency may result from the co-ordinated movement of dislocations with an edge component, towards the recrystallization front on one of $\{111\}$ planes in the $\langle 110 \rangle$ direction. In this context the results are similar to those of the Burgers and Louweres study from 1931.

Classical recrystallization theory assumes that successful nuclei possess the $\alpha\langle 111 \rangle$ orientation relationship with respect to the deformed matrix (with α close to 40°). A lot of effort has been put into giving physical reasons for this orientation relationship. Based on crystallography, Ridha and Hutchinson (1984) explained its occurrence by a coordinated movement of two families of pure-screw dislocations with orthogonal Burgers vectors. A similar idea was used by Inoko and Kashihara (1993), Inoko *et al.* (2010) in their interpretation of the growth mechanisms of recrystallized grains (after tensile deformation) due to boundary migration by absorbing piled-up edge dislocations. Good agreement between a variant of the $\langle 111 \rangle$ rotation axes and the normal to highly active slip planes, with which dislocation boundaries align, was also noticed in rolled and channel-die compressed aluminium samples [Inoko *et al.* (2010)]. However, already in [Inoko and Kashihara (1993)], the occurrence of other axes was indicated. The $\langle 111 \rangle$ direction is only one of a few observed disorientation axes; the other most frequent are $\langle 112 \rangle$, $\langle 100 \rangle$, $\langle 012 \rangle$, $\langle 221 \rangle$ or $\langle 110 \rangle$, as noticed, e.g. by Paul (2003), Sabin *et al.* (2003), Paul *et al.* (2012), etc.

After partial recrystallisation of polycrystalline metals, the fraction of boundaries characterized by $\langle 111 \rangle$ rotation axes is usually large. On the one hand, this is due to the presence of nearly complementarily oriented deformed areas. On the other hand, disorientations between fully recrystallized grains are usually characterized by rotations around $\langle 111 \rangle$ axes; analysis of the SEM orientation maps performed at various stages of recrystallization indicates that $\langle 111 \rangle$ -type rotations are more frequent at later stages of recrystallization, when the fraction of boundaries between recrystallized grains significantly increases. The disorientation angles successively approach 40° , and – generally - the disorientation angle distribution approaches the Mackenzie distribution (1964). It is also worth mentioning that with random disorientation distribution, the distribution of disorientation axes has a maximum near the $\langle 111 \rangle$ pole [Mackenzie and Thomson (1957)].

In the description of the nucleation mechanism, proposed by Paul *et al.* (2012) the critical role in the formation of the recrystallization nucleus is played by changes in the density of low-angle boundaries, their thermally activated migration and their ability to accumulate dislocations. The thermally activated climb and cross slip of dislocation loops influence the subgrain orientations and favour the elimination of boundaries between them, as initially proposed by Li (1962) and discussed many times by, e.g. Doherty and Szpunar (1984), Doherty *et al.* (1997b), Ferry and Humphreys (1996) and Rios and Sandim (2005). The process ultimately leads to the formation of dislocation-free larger subgrains with new orientations. Consequently, thermally activated migration of the dislocations stored inside cells and/or low-angle boundaries, leads (in some places) to dislocation ‘accumulation’ and formation of boundaries with growing disorientation and rising mobility. It is accepted that a moving low-angle boundary absorbs dislocations, and with growing orientation difference, increases its energy and mobility.

A particular role in the formation of new grains can also be ascribed to the coalescence process. Coalescence is a local process. If it occurs near a pre-existing high-angle boundary, local equilibrium conditions are changed, initiating boundary migration. It is often observed that the coalescence of subgrains on one side of a high-angle boundary yielded a subgrain large enough to grow rapidly into the adjacent grain (by positive curvature of high-angle boundary).

2.4. Recrystallized grain growth and grain re-orientation. The role of recrystallization twinning

The texture of the fully recrystallized material is formed both by grain growth and twinning. However, after recrystallization nucleation in materials with medium-low SFE, the formation of annealing twins plays an essential role in the final texture; there is in fact no other way to obtain from the nucleus orientations all the new orientations present in the recrystallized microstructure [Berger *et al.* (1988)]. Wilbrandt and Haasen (1980) have shown that multiple twinning can lead to an almost ‘grey’ texture after six generations if the twinning systems operated at random. However, in most observed cases twins are only observed up to the third generation [Paul *et al.* (2007)].

The formation of annealing twins on a particular twinning system from a single isolated grain orientation does not occur at random. This result has major consequences for the annealing texture formation, i.e. non-random twinning limits the number of orientations which can occur in the recrystallized structure. From the point view of the origins of new orientations, the different stages of recrystallization nucleation and growth [Paul *et al.* (2007)] can be described as:

- (i) the formation of single isolated nuclei of uniform orientation,
- (ii) the early stages of grains growth and the first recrystallization twins,
- (iii) the formation of grains with different twinning variants leading to successive twin generations, and
- (iv) the formation of chains of different nuclei by recrystallization twinning.

Physical intuition suggests that the first nuclei start from some components of the as-deformed state. However, most of the previous investigations on deformed fcc metals, e.g. [Berger *et al.* (1988), Duggan *et al.* (1990, 1993), Hjelen *et al.* (1991), Juul Jensen (1995), Doherty *et al.* (1997b), Engler *et al.* (2001), Paul *et al.* (2002a)] clearly show that single, isolated nuclei (small grains) of uniform orientation (i.e. without recrystallization twins) possess different orientations with respect to the adjacent deformed regions.

Earlier studies on low SFE metals [Berger *et al.* (1988), Doherty *et al.* (1997b)] or medium SFE pure metals but deformed at very low temperature, e.g. at 77K [Paul *et al.* (2002c)], have clearly shown the existence of a well-defined crystallographic relation between the local

deformation substructure and the first recrystallized regions of uniform orientation. The first-formed nuclei frequently exhibit near $(25-40^\circ)\langle 111 \rangle - \langle 112 \rangle$ type disorientations. Subsequently, the initial nucleus can change its orientation by twinning [Paul *et al.* (2002c)]. However, it is not yet obvious which of the different possible recrystallization twinning systems will be successful. In this context recrystallization twinning can only be regarded as a secondary mechanism.

The occurrence of different twinning variants (different twinning planes and several generations of recrystallization twins) then obscures the primary orientation relationship. From a crystallographic point of view, recrystallization growth in twinned structures is very similar to that observed in non-twinned metals of unstable orientations [Paul *et al.* (2002c)] in which transition bands were formed (e.g. in rolled $\{100\}\langle 011 \rangle$ -oriented fcc crystals). Also the different orientation relationships between a new grain and the adjacent as-deformed areas are seen to be responsible for quite different growth rates [Paul (2003)].

The fact that only a limited number of possible variants of new nuclei orientation are observed introduces a small modification into the micro-growth selection model originally proposed by Duggan *et al.* (1990). Based on the idea of Ibe and Lücke (1966), it is suggested that the formation of nuclei favourably oriented for growth is the result of growth selection between a variety of nuclei. As an example, a successful cubic nucleus will form in a local orientation with a $30-40^\circ\langle uvw \rangle$ relation to its immediate neighbours. The observed cases of single isolated nuclei of uniform orientation (independently of the scale of observation - SEM or TEM) mostly possess a disorientation relation with respect to the nearest as-deformed neighbours which can be described as $25-40^\circ$ rotation angle and rotation axes close to the $\langle 111 \rangle$ or $\langle 112 \rangle$ directions. This leads to the formation of a non-random distribution of new grain orientations and only a limited quantity of their parents [Paul *et al.* (2002c)].

A twin relationship between the deformed and recrystallized grains (forming compact chains of grains) was found, e.g. by Berger *et al.* (1988) during their detailed local orientation measurements by TEM, and also by Gottstein (1984) where the twin related components were derived from ODFs (Orientation Distribution Function) and pole figures. However, Paul *et al.* (2007) based on SEM/EBSD measurements stated (in opposition to some earlier experimental data) that exact twin relations between isolated, recrystallized grains, of uniform orientation and as-deformed neighbourhood, have never been observed. Multiple twinning can re-orientate (in some cases) the grain into (near to) twin relations with respect to the components

of the as-deformed state. Only occasionally, does twinning within recrystallized grains play a decisive role in cube grain formation, as observed by Paul *et al.* (2007). The near-cube-oriented areas were always twin related to the other parts of the recrystallized grains with the cubic twin $\{122\}\langle 122\rangle$ orientation.

The mechanisms responsible for the texture transformations observed at the very early stages of recrystallization are schematically summarized in Figure 2.1 [Paul *et al.* (2007)]. The most often observed orientation relationship is very close to the above $25\text{-}40^\circ \langle uvw\rangle$ relation.

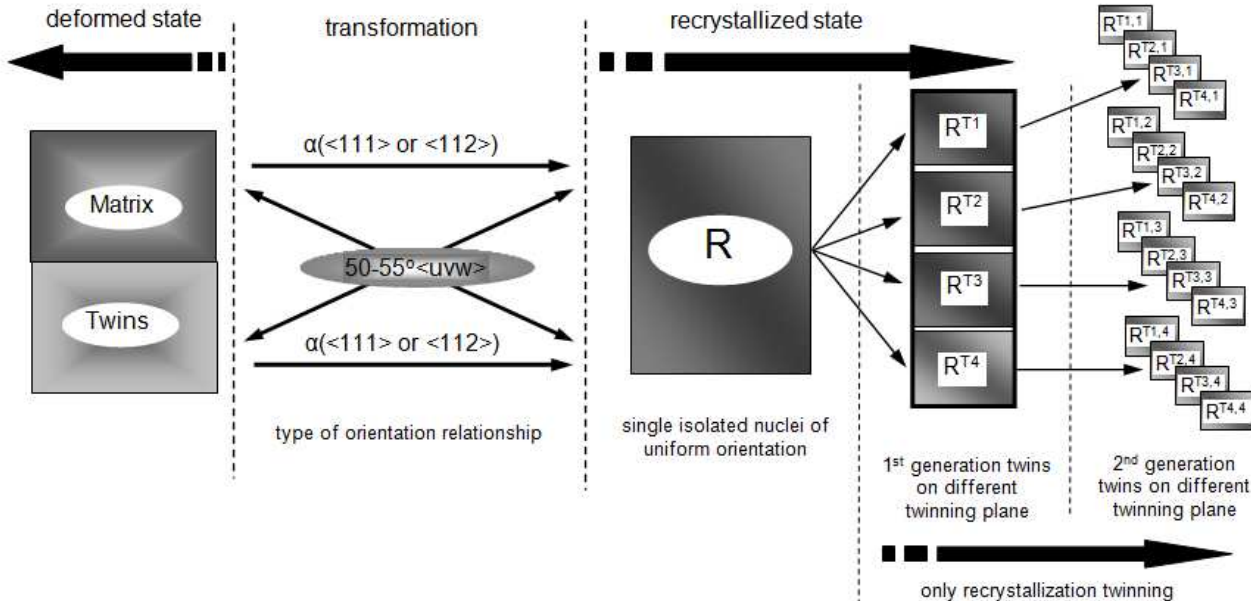


Fig. 2.1. Schematic representation of the orientation changes resulting from primary nucleation and successive recrystallization twinning observed at the early stages of recrystallization [Paul *et al.* (2007)].

2.5. Summary of the bibliography

A solution, even if only approximate, to the problem of texture transformation during annealing is particularly important for modelling the development of recrystallization textures in metals and, at the same time, facilitates the choice of thermo-mechanical processes to obtain semi-products with tailored textures. As shown in the introductory part of the literature review, the controversies around the initial stages of recrystallization texture formation have been long focused on answering the question which of the two competing groups of theories - ON or OG describes the texture transformation better. The main problem in this debate is to establish the effect of the as-deformed orientations on the selection of initial nuclei orientations, determining their role in ‘controlling’ the final texture of the fully recrystallized material, and also determining the transformation mechanisms.

The particular problem of selecting a $\langle 111 \rangle$ direction as the disorientation axis of the migrating recrystallization front may be a subject for discussion. *It is certainly accurate to state that rotation around this axis only rarely takes place at the initial stages of recrystallization.* Earlier work on fcc single crystals, led to the conclusion that the $40^\circ \langle 111 \rangle$ relationship is characteristic of the later stages of recrystallization, i.e. when orientation relationships between neighbouring recrystallized grains begin to dominate.

In the author’s opinion, as in the theory proposed by Beck (1953) and Cahn (1949), the recrystallized grains ‘...do not nucleate in the classical fashion but rather grow from pre-existing sub-grains and cells...’ [Doherty *et al.* (1997b)]. Within this approach, some low-angle boundaries accumulate dislocations and nuclei become increasingly disoriented with respect to their neighbours. This leads to a decrease of stored energy due to the removal and rearrangement of structural defects.

In this context it seems reasonable to reconsider the crystallographic aspects of the appearance of orientations of new grain nuclei during recrystallization, and in particular the orientation relationship between the new grain and its nearest deformed surroundings and to define the observed preferences. The series of investigations carried out in this work aims at *not only defining preferential orientations of new grain nuclei and the predominant orientation relationship between recrystallized and deformed phases, but also its relation to the dislocation mechanisms, i.e. thermally induced dislocation motion.* The above assumption is partly based on the results of earlier analyses published in the literature on the subject [Cahn

(1949), Beck (1953), Bailey (1963), Doherty and Szpunar (1984), Inoko and Kashihara (1993), Paul *et al.* (2002c), Paul *et al.* (2007), Inoko *et al.* (2010)].

The crystallographic aspect of recrystallization was analyzed quite a long time ago in classical studies from the first period of research on texture transformations [Bailey (1963), Doherty and Szpunar (1984)], but later however, completely ignored. Numerous studies presented mainly by authors linked to Aachen University [i.e. Lücke K., Gottstein G., Engler O.] analyzed early stages of recrystallization in terms of its thermodynamic aspect, totally omitting its crystallographic background. In the author's opinion it is necessary to consider both these aspects. This results from the obvious fact that the nucleus forming within the structure of the deformed state must fulfil the condition of thermodynamic stability and represent a lower energy 'system' comparing to its nearest surroundings. Humphreys and Hatherly (2004a) claimed, based on Cahn's idea (1950), that '*...new grains cannot nucleate as totally new ones but they are formed from the regions which always exist in the deformed matrix*'. Therefore, one of the intuitive consequences of the above statement may be the thesis that a starting point of new orientations are the components found in the deformed state. It means that the orientation of each new grain originates from a 'family' of orientations indentified in the deformed state. However, a clearly observable change in nuclei orientation with respect to the as-deformed orientations suggests dislocation removal from a given region. The following questions then need answering:

- *what causes new grains to grow from small recovered regions of (sub)grains or dislocation cells, and*
- *what mechanism is responsible for the appearance of new orientations different from those observed in the deformed material?*

The literature on recrystallization pays a lot of attention to the role of high-angle boundaries and the conditions of their migration. Such an approach combines the final, macroscopic, texture of recrystallized material with the thermodynamic aspects of the process. Nevertheless, it is unable to provide a comprehensive answer to the question about the mechanisms controlling the formation of a new grain inside the deformed structure and especially to explain its different orientation with respect to the deformed surroundings from which it grows. In the author's view it results *from an omission of the role of low-angle boundaries*. Their thermally activated migration combined with thermally activated movement of dislocation stored inside (sub)grains and/or the diffusion of vacancies [Rios and

Sandim (2005), Paul *et al.* (2012)] may play a key role in the orientation change of a 'chosen area' with respect to the deformed matrix, and in the formation of high-angle boundaries (in fact the 'transformation' of low-angle boundaries into high-angle ones). Still, the nature of this process is not clear enough for the time being. In particular, it is not documented:

- *if this dislocation motion occurs in single or complex systems,*
- *what the relation of the moving dislocation systems is with regard to the major active systems during straining.*

These are problems, whose examination is proposed in the series of analyses in the present study. Such an approach has already been proposed in the literature. For example, Haessner (1978) analyzing results from early investigations on the issues of textural changes during recrystallisation found that a drop in the stored energy may result from:

- the influence of point defects, which leads to their partial disappearance,*
- annihilation of opposite sign dislocations and shrinking of dislocation loops,*
- re-arrangement of dislocations into arrays of lower energy, e.g. through the formation of low-angle boundaries,*
- the formation of high-angle boundaries,*
- the absorption of point defects and dislocations through the migrating high-angle boundaries, and*
- reducing the surface of grain boundaries.*

The effects in points (a)-(d) can be ascribed to the recovery stage, whereas in points (e) and (f) they are associated with recrystallisation and grain growth. In most cases, the distribution of defects in the structure of the deformed state is more or less non-uniform, so the 'routes' along which the transformations of various regions occur during annealing can differ strongly from each other. This is one of the main reasons why the present study analyzes the behaviour during recrystallization of deformed crystallites with stable orientations.

It is assumed that, for the clarity of the current analysis, it is necessary to determine parameters connected to the orientation of the deformed matrix. Such an approach allows analyzing the change in orientation of new grains with 'reference' to the same orientation of the deformed state. Since recrystallization is an irreversible, thermally activated transformation which takes place through the nucleation and growth (of nuclei) and is

inherently associated with plastic deformation, the present study attempts to answer the question:

is it possible to connect the events occurring during the deformation with the observed transformation of the texture in annealing?

The brief analysis made in section 2.2.3 leads to the conclusion that the decisive role at the initial stages of recrystallization is played by low-angle boundaries and the dislocations accumulated inside the deformed (sub)grains. In fact, the mechanisms describing the nucleation through the migration of low-angle boundaries and coalescence share many common features. On their ‘basis’ a highly disputed mechanism of nucleation through the migration of strain-induced high-angle boundaries can also be explained. This process, often observable in annealed crystallites of unstable orientations, may indeed be based on a coalescence mechanism on one side of a high-angle boundary formed during deformation. If it occurs near the pre-existing high angle boundary, local equilibrium conditions are changed. This initiates the boundary migration. It has often been observed that the coalescence of subgrains on one side of a high-angle boundary yielded a (sub)grain large enough to grow rapidly into the adjacent grain (by positive curvature of high-angle boundary). This leads to the growth of the region with a reduced dislocation density and an increase in the disorientation of the surrounding boundary [Paul *et al.* (2012)]. This increases the driving force of the process and at the same time increases the mobility of high-angle boundary segment, Fig. 2.2.

The mechanisms of nucleation by coalescence and low-angle boundary migration explain two significant issues. Firstly, the phenomenon of nucleus orientation change with respect to the surrounding matrix as a consequence of dislocation movement inside a given region, and secondly the increased disorientation across the boundaries (by dislocation accumulation) which results in their increased mobility.

The proposed series of investigations will in fact concern the analysis of the disorientation relationship appearing between a new grain and the deformed region. The basic research technique will be the techniques of local orientation measurements based on both SEM and TEM.

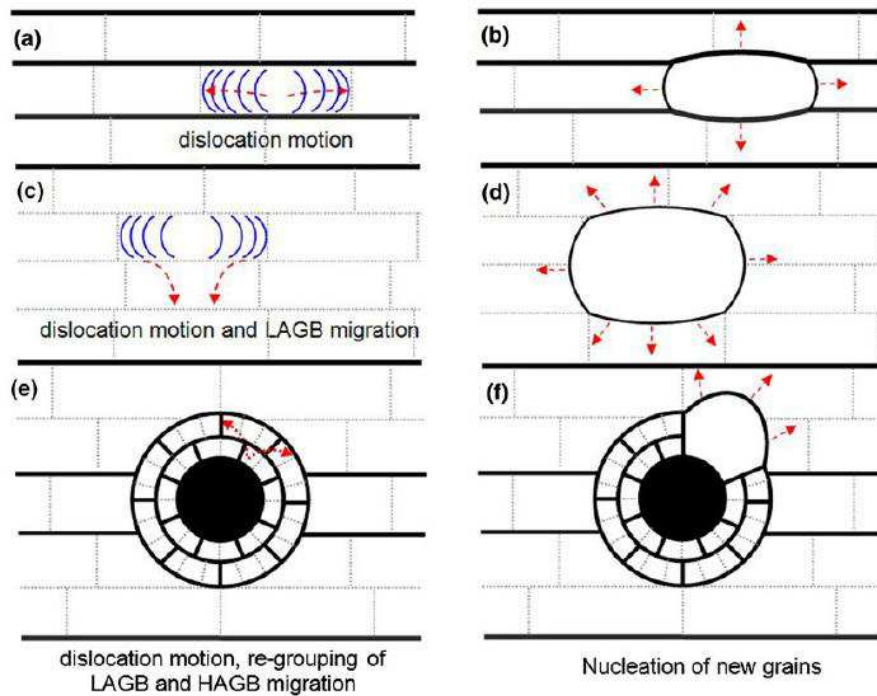


Fig. 2.2. Schematic presentation of formation of new grains inside lamellar structures of different thicknesses and around large second phase particles. (a), (c) and (e) Initial structures after deformation; (b), (d) and (f) corresponding changes observed after short annealing leading to nuclei formation. Thicker lines represent larger disorientations. Dashed arrows show directions of boundary migration [H. Paul *et al.* (2012)].

In the literature dealing with the texture changes phenomenological descriptions tend to prevail. The above mentioned theories have both advocates and opponents, however, in the author's view they only describe the later stages of the recrystallization process. These descriptions fail to explain the fundamental question about the mechanism of forming recrystallization textures, in particular at the initial stages of transformation from the deformed to recrystallized state.

There is a lack of studies concerning the considered relationship (Fig. 2.3) and therefore the following question remains unanswered: *how do the as-deformed orientations influence the selection of recrystallized grain orientations?* Since so far the nature of the process of texture transformation has been not well understood, this general question motivates this work.

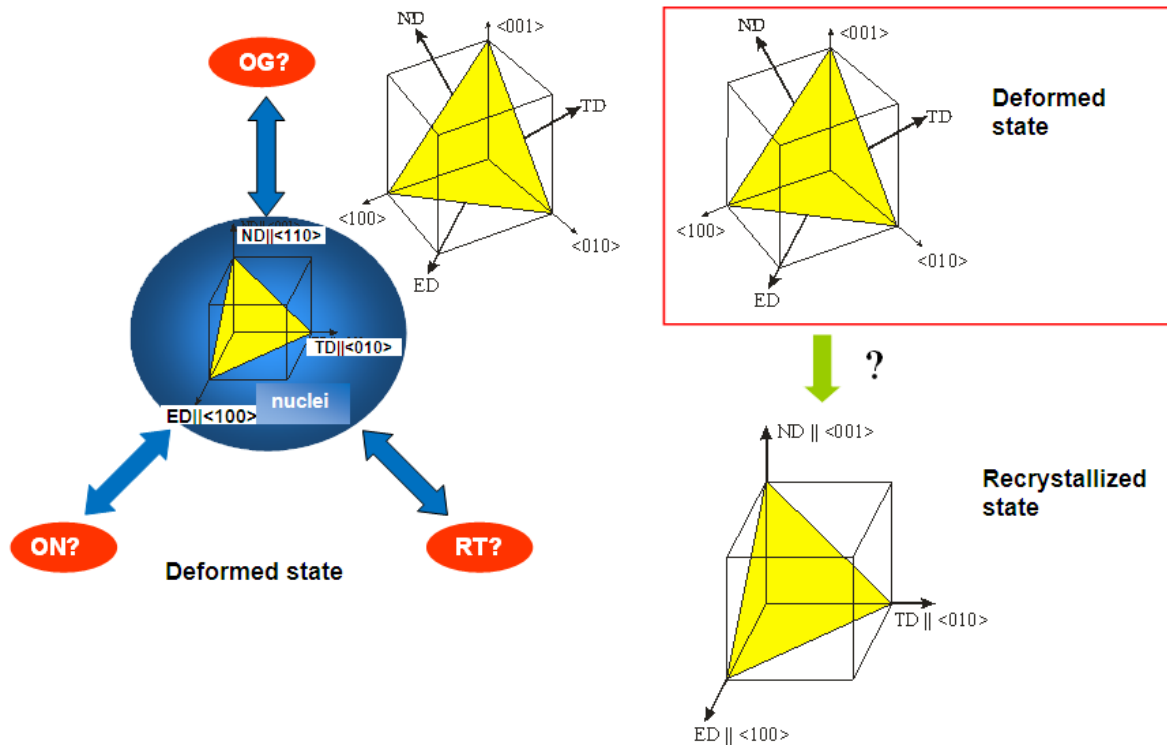


Fig. 2.3. Schematic presentation of controversies of the recrystallization texture formation in homogeneous structure of the deformed state. Case of medium to high stacking fault energy metals.

3. SCIENTIFIC PURPOSE AND DISSERTATION THESIS

3.1. Objectives

The objective of this research program is to identify and 'crystallographically' describe the relations between deformed and recrystallized states occurring during the early stages of recrystallization of low, medium and high SFE fcc metals. Analysis of the results should then provide an explanation of the mechanism by which the as-deformed orientations influence the selection of single individual grains and thereby contribute to the formation of a given disorientation across the recrystallization front.

In particular, analysis of the experimental data should provide a correlation between the mechanisms responsible for the deformation behaviour and those dominating during the rearrangement of dislocation at the initial stages of recrystallization. This set of issues includes the description of mechanisms responsible for the appearance of the primary nucleus orientation and their growth into the deformed structure, the determination of the effect of active slip systems on primary nucleus orientation selection, and an explanation of the role of recrystallization twinning. In the case of metals with medium and low SFEs, we shall examine the role of recrystallization twinning in the formation of preferred growth orientations and, in particular, explain which of the possible twinning systems may succeed in growing during recrystallization. The explanation of the above issues was mainly based on local orientation measurements in SEM and TEM.

3.2. Thesis

In this research program the assumed thesis was as follows:

there is a relationship between the orientation of nuclei of new grains appearing at the early stages of recrystallisation and the deformed regions from which new grains grow, and that the transformation of the texture's 'image' can be linked to the predominant slip systems during deformation.

In order to verify this thesis, it was decided to investigate crystallographic correlations appearing at the early stages of recrystallization between the deformed and recrystallized

regions in single crystals of fcc metals, with stable orientations (deformed in plane strain compression) and representing a wide spectrum of SFE.

4. MATERIAL AND RESEARCH METHODOLOGY

Earlier research results on crystallographic aspects of nucleation in single crystals of unstable orientation, e.g. [Paul *et al.* (2002c, 2007), Bijak (2008)] indicated the difficulties of analysing heterogeneous deformation structures. The present research program aims to avoid this problem by using single crystalline specimens of stable (in PSC) orientations, i.e. that do not form band-like strain inhomogeneities of deformation. This thereby enables a clear comparison of the orientation of a new grain nucleus to the (relatively stable) orientation of the surrounding deformed matrix. The mechanisms of texture transformation at the early stages of recrystallization are studied by analysing the changes that occur inside a deformed structure with relatively small disturbances of the crystal lattice.

4.1. Material

The early stages of recrystallization were analyzed on single crystals of fcc metals of stable (in PSC) orientations, i.e. brass $\{110\}\langle 112\rangle$ and Goss $\{110\}\langle 001\rangle$. The samples were deformed in channel-die; it is widely accepted that channel-die compression physically simulates the rolling of thin plates. Both orientations show no tendency to form band-like strain inhomogeneities in PSC up to the later stages of deformation. The materials possess a wide range of SFE values: from high - Al and Al- 1% wt.Mn, through medium - Ni and Cu to low - Cu-2% wt.Al (Table 4.1). The choice of single crystals of stable orientations simplified the current microstructural and texture analyses and improved its clarity (good structural and textural 'stability' during deformation, no grain boundaries, no or very few high-angle boundaries after deformation, etc.).

In the case of metals with 'high' SFE, the analysis of nucleation seems to be quite a simple issue, mainly due to the absence of twins both in the deformed and recrystallized states. Whereas in the case of metals with 'medium' and 'low' SFE the issue becomes more complex because of the possibility of the recrystallization twinning. Twins facilitate the growth of the recrystallized grains and the appearance of new orientations (usually contributing to rapid growth).

Recrystallization twinning complicates the interpretation of the observed orientation relationship between the deformed and recrystallized phases. However, it also provides an opportunity to analyse the reasons for the occurrence of recrystallization twinning. In this context, *it will be particularly important to recognize the mechanism responsible for the*

selection of twinning variants in the recrystallized phase, and in particular to discuss which of the four possible variants can successfully grow and thereby decisively influence the 'shape' of the final texture of the recrystallized material.

Metal	Crystallographic orientations	Deformation conditions	Deformation	Stacking fault energy (SFE)*
Al	{110}<001> and {110}<112>	T _d =293K	ε=0.51 and ε=0.92	γ _{SFE} >170 mJm ⁻²
Al-1%wt.Mn	{110}<001> and {110}<112>	T _d =293K	ε=0.51 and ε=0.92	γ _{SFE} =166mJm ⁻²
Ni	{110}<001> and {110}<112>	T _d =293K	ε=0.51 and ε=0.92	γ _{SFE} =128 mJm ⁻²
Cu	{110}<001> and {110}<112>	T _d =293K	ε=0.51 and ε=0.92	γ _{SFE} =78 mJm ⁻²
Cu-2%wt.Al	{110}<001> and {110}<112>	T _d =293K	ε=0.51 and ε=0.92	γ _{SFE} <10 mJm ⁻²

Tab. 4.1. The materials analyzed in this work and deformation conditions. SFE values were taken from Murr (1975).

The single crystals of all metals were prepared by Bridgman's method in graphite moulds from high purity materials.

- Aluminium (99.998%) and Al-1%wt.Mn alloy single crystals were prepared at the Materials Science Centre (Centre Sciences des Matériaux et des Structures) in École Nationale Supérieure des Mines de Saint-Étienne) in France using modified (horizontal) Bridgman's method.
- The single crystals of copper (99.99%) and Cu-2%wt.Al alloy were produced at the Department of Structure and Mechanics of Solids at the Faculty of Non-Ferrous Metals of AGH University of Science and Technology in Krakow.
- Ni (99.98%) single crystals were made at the Institute of Nuclear Technology in Świerk. In that case the samples were cut out from massive blocks with a diameter of about 100mm by means of a wire saw.

The chemical compositions of the research material were determined at the Institute of Metallurgy and Materials Science of Polish Academy of Sciences in Krakow by means of a Jobin Yvon 10000RF glow discharge optical emission spectrometer. The examination used

the volumetric analysis method for homogeneous solid materials with a diameter of 4mm and chemical composition analysis up to 15mm into the material.

From these single crystalline ingots of the following dimensions: 25x10x80mm, 20x15x85mm (Al, Al-1%wt.Mn), 10.5x10.5x80mm (Cu, Cu-2%wt.Al) and 24x10.5x70 mm (Ni), samples were cut out using a wire saw (model Unipress WS22 - tungsten wire of 0.06 μm thickness).

The next step was the preparation of cube shaped samples with the final size of 10x10x10mm³ to perform PSC tests. Before deformation the samples were polished using abrasive papers with decreasing grade and subsequently, to eliminate stresses, they were also polished with Struers 3 μm and 1 μm diamond paste.

From the crystallographic point of view, the orientations show different configuration of active slip systems. They are defined by two pairs of single systems (brass {110}<112> orientation) or two pairs of symmetrically located co-planar systems (Goss {110}<001> orientation). The chosen orientations strongly restrict (and practically eliminate) the occurrence of deformation twinning, even in low SFE Cu-2%Al alloy. This simplifies the current analysis and makes it even clearer.

4.1.1. Ideal Goss (110)[00-1] orientation

The preferred slip systems for crystals with the 'ideal' Goss (110)[00-1] orientation (Euler angles: $\varphi_1=90^\circ$, $\Phi=90^\circ$, $\varphi_2=45^\circ$) are defined as (111)([01-1]+[-101]) and (-1-11)([0-1-1]+[101]); they are shown in Fig. 4.1. Each of the preferred slip systems is characterized by an identical value of Schmid factor of 0.82, calculated according to Tucker (1961), on the assumption of ideal plane state of strain. These slip systems are situated symmetrically with respect to the plane perpendicular to ED. The (111) and (-1-11) planes are inclined by $\pm 35^\circ$ to the compression plane. The traces of the active slip system operating on three mutually perpendicular sections, i.e. ED-TD, ND-ED and ND-TD are shown in Fig. 4.2.

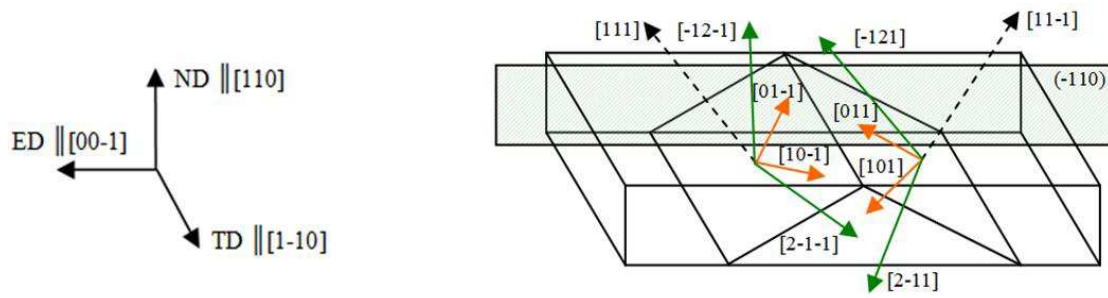


Fig. 4.1. Schematic presentation of preferred slip systems in the ideal (110)[00-1] orientation.

GOSS ORIENTATION (110)[00-1]

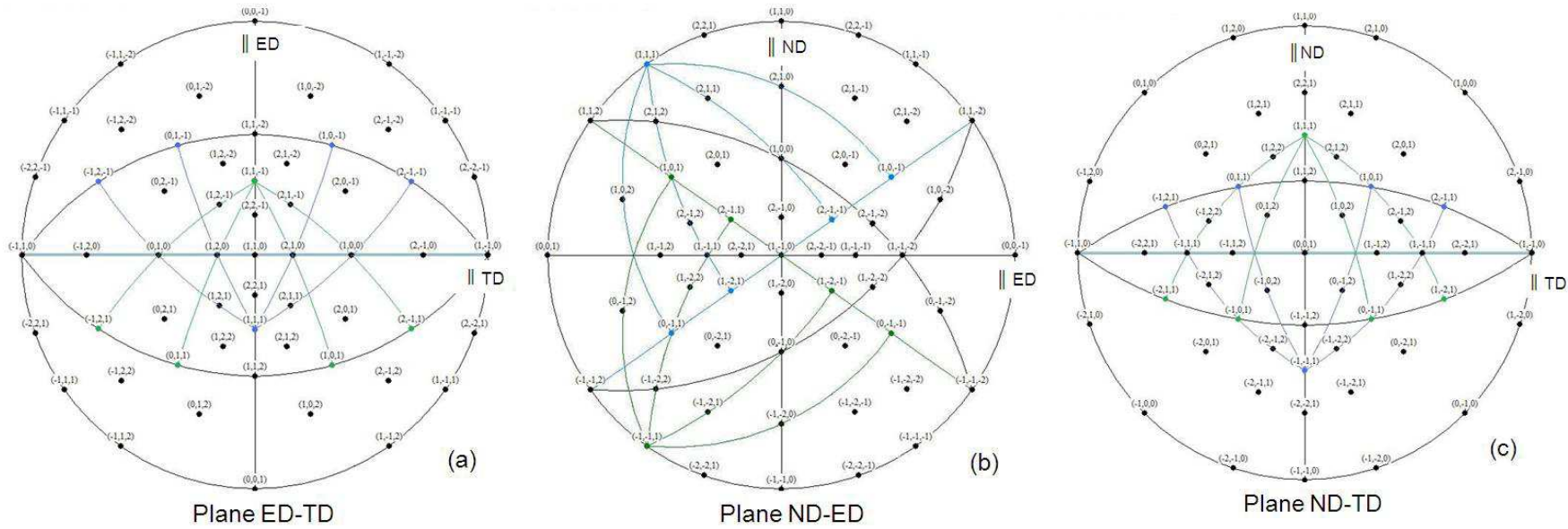


Fig. 4.2. Stereographic projections showing configuration of the most active slip systems in the ideal (110)[00-1] orientation.

Plane of presentation: (a) (110), (b) (1-10), and (c) (00-1).

4.1.2. Ideal 'brass' (110)[1-1-2] orientation

A different configuration of active slip systems can be found in the case of the second of the analysed orientations, i.e. brass orientation, Fig. 4.3, described here by (110)[1-1-2] (Euler angles: $\varphi_1=235^\circ$, $\Phi=90^\circ$, $\varphi_2=45^\circ$). The Schmid factors indicate the occurrence of symmetrically situated slip systems, operating on (111) and (-1-11) planes. Two of the systems, i.e. (111)[-101] and (-1-11)[0-1-1] have Schmid factor values of 0.82 whereas the other two, i.e. (111)[01-1] and (-1-11)[101] have the value of Schmid factor of 0.54. Figure 4.4. shows stereographic projections corresponding to three mutually perpendicular sections, i.e. ED-TD, ND-ED and ND-TD with marked traces of planes where the most preferred slip systems operates.

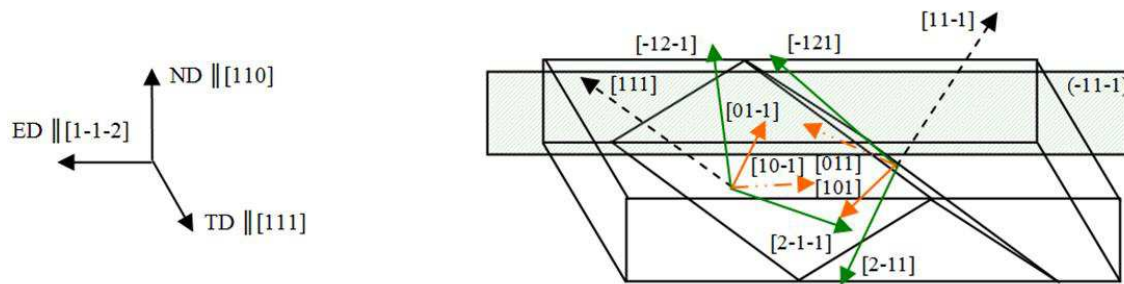


Fig. 4.3. Schematic presentation of preferred slip systems in ideal (110)[1-1-2] orientation.

BRASS ORIENTATION (110)[1-1-2]

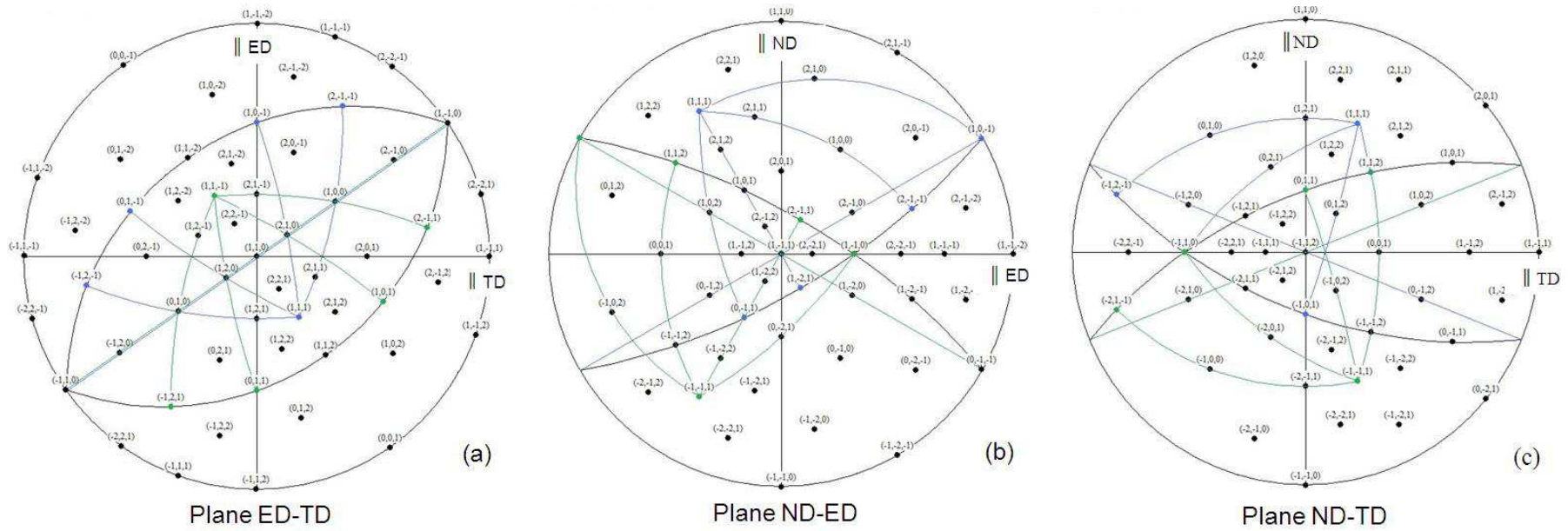


Fig. 4.4. Stereographic projections showing configuration of the most active slip systems in ideal (110)[1-1-2] orientation.

Plane of presentation: (a) (110), (b) (1-11), and (c) (1-1-2).

4.2. Experimental procedure

4.2.1. Plane strain compression (channel-die) test

The prepared samples were deformed by lubricated channel-die. This method is commonly considered to be a model approximation of plane strain. An INSTRON 3382 tensile testing machine (electromechanical type) with a 100kN load cell was used for the tests, Fig. 4.5. The samples were deformed at ambient temperature (293K), to one of two deformations, i.e. 40% and 60% compression, corresponding to logarithmic strains ($\epsilon = \ln(h_0/h)$, where: h_0 and h initial and final sample high, respectively) of 0.51 and 0.92, using multistage tests. In order to minimize friction between the sample, the punch and the walls of the channel-die, each sample was wrapped in 0.2mm thick Teflon™ tape BISAN P.T.F.E. At each strain intervals of about 0.2, the Teflon™ ribbon was changed, so that friction was very low. Additionally, after every pass the free ends of the samples were rectified (using wire saw cutting) to restore the original sample height to length ratio of 1. All of the samples were deformed at the same crosshead velocity of 0.2mm/s (this gives the initial strain rate of $0.02s^{-1}$).

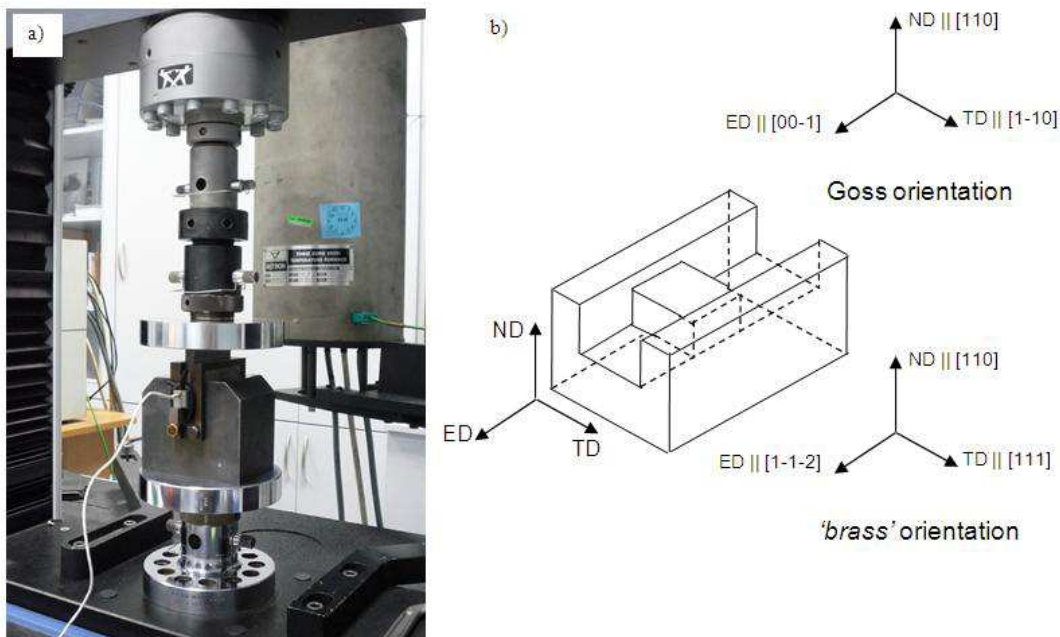


Fig. 4.5. Plane strain deformation by channel-die compression. (a) Testing machine and (b) schematic presentation of external directions for Goss (110)[00-1] and brass (110)[1-1-2] orientations.

4.2.2. Recrystallization

The recrystallization behaviour was investigated by two kinds of experiments. Firstly, the deformed bulk samples were annealed and then analyzed by means of a SEM equipped with a high resolution EBSD system. Secondly, by *in-situ* recrystallization experiments (for the case of the Al-1%wt.Mn alloy); thin foils taken from the as-deformed samples, were heated in a TEM to a temperature of ~300°C using a 'heating holder'. Annealing times ranged between 60 and 120s. This relatively high temperature of recrystallization was selected to ensure sufficiently rapid recrystallization in the thin foils.

In the case of the bulk (ex-situ) experiments, the deformed samples were cut perpendicular to the transverse direction into smaller, ~2.5-3.0mm thick sheets by means of a wire saw, then mechanically and electrologically polished. (Generally, the transverse direction was parallel to the following crystallographic directions: [1-10] for Goss single crystals and [1-11] for brass (110)[1-1-2] crystals).

Sample descriptions		Recrystallization conditions			
Single crystals with Goss (110)[00-1] orientations					
Metal	Deformation		Temperature		Time
	[%]	[log]	[°C]	[K]	[sec]
Al	40	0.51	345	618	25
	60	0.92	330	603	20
Al-1wt.%Mn	40	0.51	413	686	25
	60	0.92	403	676	20
Ni	40	0.51	590	863	25
	60	0.92	550	823	25
Cu	40	0.51	335	608	40
	60	0.92	335	608	25
Cu-2wt.%Al	40	0.51	570	843	30
	40	0.92	490	763	30

Table 4.2. Recrystallization conditions for Goss (110)[00-1] orientation.

Recrystallization was performed using a Nabertherm furnace without protective atmosphere. Prior to proper annealing, preliminary tests were run to establish optimal recrystallization settings (recrystallization limited to initial stages). Tests were carried out for all materials, orientations and strains. The recrystallization settings (temperature and annealing time) analysed in this work for all materials, both orientations and both deformations are provided in Tables 4.2. and 4.3.

Sample descriptions		Recrystallization conditions			
Single crystals with brass (110)[1-1-2] orientations					
Metal	Deformation		Temperature		Time
	[%]	[log]	[°C]	[K]	[sec]
Al	40	0.51	423	696	25
	60	0.92	403	676	25
Al-1wt.%Mn	40	0.51	423	696	30
	60	0.92	385	658	30
Ni	40	0.51	640	913	30
	60	0.92	560	833	30
Cu	40	0.51	335	608	70
	60	0.92	335	608	25
Cu-2wt.%Al	40	0.51	570	843	45
	40	0.92	470	743	60

Table 4.3. Recrystallization conditions for brass (110)[1-1-2] orientation.

4.2.3. Determining the crystal orientations analysis of texture evolution

4.2.3.1. Global textures measurements by X-ray diffraction

The initial single crystal orientations and texture measurements after deformation on the sample scale were performed using a PHILIPS X-ray diffractometer X-Pert PW 1830, equipped with textural goniometer ATC-3 set up with a K_{α} -series radiation filter for Co anode (Fig. 4.6). Using the reflection method, three incomplete pole figure were measured, i.e. {111}, {110} and {001}. The α angle ranged from 0 to 85°. The measurements were recorded within a 5°x5° mesh and the beam intensity at 1 second intervals. The results of global texture

measurements are presented in the form of complete $\{111\}$ pole figures by means of LaboTex 3.0 software (Annexe 1).

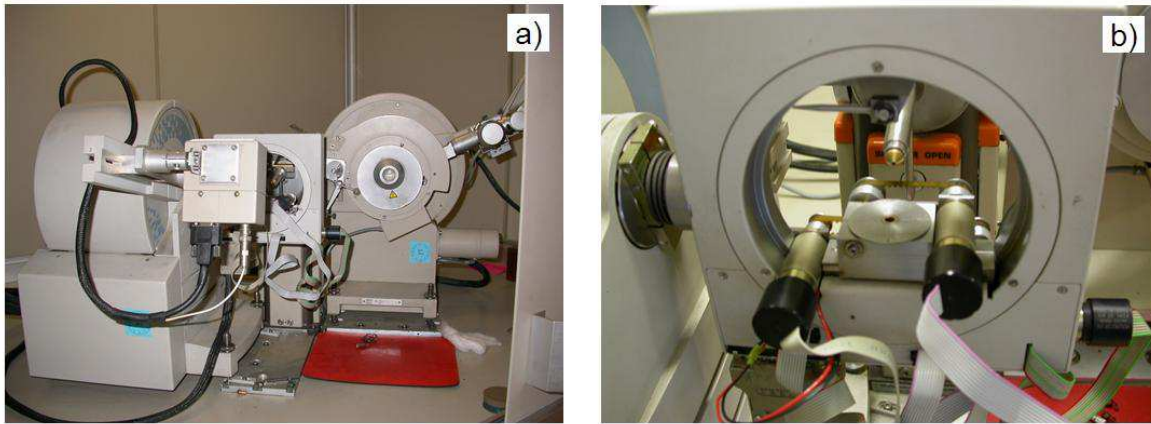


Fig. 4.6. Global texture measurements. PHILIPS X-ray diffractometer (X Pert PW 1830) equipped with ATC-3 goniometer.

During sample preparation we aimed for the output orientations not to deviate over 5° from the 'ideal' orientation. The degree of the deviation of each sample from the ideal arrangement is shown in Tables 4.4 and 4.5. Sample scale measurements of textures were also carried out after every stage of deformation and also after subsequent annealing.

Single crystals with (110)[00-1] orientation								
Metal	No.	Ideal orientation $\varphi_1, \Phi, \varphi_2$	Initial orientation $\varphi_1, \Phi, \varphi_2$	Deviation initial orientation from ideal orientation $\alpha <uvw>$ $\varphi_1, \Phi, \varphi_2$	Deviation initial orientation from ideal orientation (external directions)			Deformation [%]
					ND*	ED*	TD*	
Al	1.	90°, 90°, 45°	90°, 90°, 45°	0°	-	-	-	40%
	2.	90°, 90°, 45°	90°, 90°, 45°	0°	-	-	-	60%
Al-1%Mn	3.	90°, 90°, 45°	90°, 90°, 40°	5° <0 0 1> 5°, 0°, 0°	-	+5	-	40%
	4.	90°, 90°, 45°	90°, 90°, 40°	5° <0 0 1> 5°, 0°, 0°	-	+5	-	60%
Ni	5.	90°, 90°, 45°	89°, 90°, 45°	1° <-0.7 -0.7 0> 45°, 1°, 315°	-1	-	-	40%
	6.	90°, 90°, 45°	89°, 89°, 45°	1° <0.9 0> 0°, 1.4°, 0°	-1	-1	-	60%
Cu	7.	90°, 90°, 45°	90°, 90°, 45°	0°	-	-	-	40%
	8.	90°, 90°, 45°	90°, 91°, 44°	1.4° <-0.5 0.5 0.7> 134.9°, 1°, 226.2°	-1	+1	-1	60%
Cu-2%Al	9.	90°, 90°, 45°	88.5°, 90°, 45°	1.5° <0.7 0.7 0> 45°, 1.5°, 315°	-1.5	-	-	60%
	10.	90°, 90°, 45°	87°, 90°, 45°	3° <0.7 0.7 0> 45°, 3°, 315°	-3	-	-	40%

*Adopted + direction in accordance with clockwise while – direction counterclockwise

Tab. 4.4. The {111} pole figures showing initial orientation of samples - case of (110)[00-1] orientation. Global texture measurements by X-ray diffraction.

Single crystals with (110)[1-1-2] orientation								
Metal	No.	Ideal orientation $\varphi_1, \Phi, \varphi_2$	Initial orientation $\varphi_1, \Phi, \varphi_2$	Deviation initial orientation from ideal orientation $\alpha <uvw>$ $\varphi_1, \Phi, \varphi_2$	Deviation initial orientation from ideal orientation (external directions)			Deformation [%]
					ND*	ED*	TD*	
Al	1.	234.7°, 90°, 45°	234.7°, 90°, 45°	0°	-	-	-	40%
	2.	234.7°, 90°, 45°	234.7°, 90°, 45°	0°	-	-	-	60%
Al-1%Mn	3.	234.7°, 90°, 45°	231.7°, 90°, 45°	3° <0.7 0.7 0> 45°, 3°, 315°	-3	-	-	60%
	4.	234.7°, 90°, 45°	234.7°, 88°, 42.1°	3.5° <0.4 -0.4 0.8> 317.9°, 2°, 45°	-	-2	+2.9	40%
Ni	5.	234.7°, 90°, 45°	231.7°, 90°, 45°	3° <0.7 0.7 0> 45°, 3°, 315°	-3	-	-	60%
	6.	234.7°, 90°, 45°	229.7°, 90°, 45°	5° <0.7 0.7 0> 45°, 5°, 315°	-5	-	-	40%
Cu	7.	234.7°, 90°, 45°	239.7°, 90°, 45°	5° <-0.7 -0.7 0> 225°, 5°, 135°	+5	-	-	40%
	8.	234.7°, 90°, 45°	237.7°, 90°, 45°	3° <-0.7 -0.7 0> 225°, 3°, 135°	+3	-	-	60%
Cu-2%Al	9.	234.7°, 90°, 45°	238.8°, 89.6°, 40.5°	6° <-0.4 -0.6 0.7> 234.5°, 4.1°, 130°	+4.1	-0.4	+4.5	60%
	10.	234.7°, 90°, 45°	239.7°, 90°, 45°	5° <-0.7 0.7 0> 225°, 5.04°, 135°	+5	-	-	40%

*Adopted + direction in accordance with clockwise while – direction counterclockwise
 Tab. 4.5. The {111} pole figures showing initial orientation of samples - case of (110)[1-1-2] orientation.
 Global texture measurements by X-ray diffraction.

4.2.3.2. Local orientation measurements

Most of the research program was based on local orientation measurements by means of SEM and TEM. Using a high resolution SEM equipped with EBSD facility was of paramount significance. These investigations were aimed at describing the nucleation mechanisms and at explaining the recrystallization twinning mechanisms in fcc metals with a wide range of SFE values.

SEM local orientation measurements. Structure observations at the light microscopy scale allowed selecting regions for a detailed analysis of structural and textural changes by means of local orientation measurement in the SEM. Samples prepared beforehand for structural observations by light microscopy were re-polished in order to remove the anodized layer (Al and Al-1%wt.Mn) or to level the surface after 'deep etching' (Cu and Cu-2%wt.Al) and subsequently electropolished; polishing settings are given in Table 4.6. (Sample preparation for optical microscopy analysis and local orientation measurements reduces sample thickness to about 1.2-1.5mm, with respect to the sample thickness after recrystallisation. This indicates that the SEM/EBSD analyses were performed close to the middle of the thickness of recrystallized samples).

	Single crystals with Goss (110)[00-1] and brass (110)[1-1-2] orientation			
Electrolyte and conditions of electropolishing	Al and Al-1%wt.Mn	Cu	Cu-2%wt.Al	Ni
		A2, in 18°C and 18V, 12 sec	D2, in 22°C and 20V, 10 sec	D2, in 22°C and 20V, 10 sec

Table 4.6. Electropolishing conditions for samples preparation - SEM/EBSD measurements.

Structural and textural changes were analysed along longitudinal section (ND-ED) using the EBSD technique in a FEG-SEM JEOL 6500F or Zeiss Supra 55VP. The local orientation measurements were performed at the Materials Science Center of the École Nationale Supérieure des Mines de Saint-Étienne (France). The applied step size varied between 0.1 and 1.0µm. The maximum rate of measurement was up to 0.02s/pixel (for Jeol 6500F). Through a suitable preparation of samples and proper choice of measurement parameters, the number of

correctly indexed measurement points (even for large areas) was always above 95% (within reasonable time). The measurements were taken at a 15-20kV electron beam accelerating voltage, beam current of 16–19nA, sample inclination of 70° and working distance - 18.6mm (JEOL 6500F) and 15mm (Zeiss Supra 55VP). In both types of microscopes, diffraction pattern acquisition and orientation calculation was done with the Channel 5 software by HKL Technology.

TEM local orientation measurements and microstructural observations. The evolution of the dislocation structure and corresponding texture changes during deformation and annealing were analyzed by bright field imaging and orientation mapping in a TEM. The TEM thin foils were prepared from the plates of 0.16mm thickness. They were cut out by a wire saw from bulk samples previously analysed at the macro- (OM) and meso- (SEM) scales. The sheets were thinned up to about 0.1mm on abrasive paper P1200, keeping the edge parallel to ND or ED. After thinning, 3mm diameter discs were cut out from the plates, and were later thinned electrolytically. Polishing values for all the materials, crystallographic orientations and the degrees of deformation are given in Table 4.7.

	Single crystals with Goss (110)[00-1] and brass (110)[1-1-2] orientation			
Electrolyte and conditions of electropolishing	Al and Al-1%wt.Mn	Cu	Cu-2%wt.Al	Ni
		A2, in 5°C and 20V	D2, in 5°C and 4V	D2, in 5°C and 4V

Table 4.7. Electropolishing conditions for TEM thin foil preparation.

The TEM thin foils were analysed with respect to changes occurring in the dislocation structure, and for selected cases, texture changes by means of local orientation measurement using TEM. The semi-automatic system was based on the detection and analysis of the Kikuchi diffraction patterns.

In the case of orientation mapping a step size of 20nm and spot size between 5nm and 10nm were used. Specimens for microscopic investigations were cut from the middle layers of the deformed samples. The TEM thin foils were prepared by the twin-jet technique using TenuPol-5. In each case, very large thin areas of hundreds μm^2 were transparent for the

electron beam. The foil thicknesses of areas suitable for microscopic observation ranged between 100nm and 400nm. Orientations were measured using a CM20 PHILIPS microscope operating at the nominal voltage of 200kV, equipped with an in-house automatic mapping system based on Kikuchi patterns. The orientation maps were created by scanning selected areas of the thin foils. The patterns were registered and then indexed using the software described in [Morawiec (1997), Fundenberger *et al.* (2003)]. Post-processing analysis of the orientation maps was performed using the Channel 5 software by HKL Technology. The analyses of dislocation structures after deformation and short annealing were performed at IMMS PAS with using a CM20 TEM (Philips) at an accelerating voltage of 200kV.

4.2.3.3. *Structural observations at the optical microscopy scale*

Macroscopic observations of samples deformed to intermediate and final deformations were made by standard optical microscopy. The samples were pre-polished using abrasive papers - P1000 and P1200, and then polished with diamond pastes of decreasing grain grade SiC: 3 μ m, 1 μ m and $\frac{1}{4}$ μ m. In the case of pure Al and the Al-1%wt.Mn alloy the samples were anodized at 20V in a HBF₄-based solution. The method allows identifying regions with variable orientation. In the case of pure Cu, Cu-2%wt.Al and the Ni alloy, in order to identify the deformed and recrystallized structures a solution composed of CrO₃-10g, NH₄Cl-1.875g, HNO₃-12.5ml, H₂SO₄-12.5ml, H₂O-225ml was used. Structural observations were performed in polarized light using NEOPHOT 2 and Leica optical microscopes (at IMMS PAS and EMSE).

After optical microscopy of the deformed single crystals, the same samples were annealed and then immersed in LamPlan Resine 605, re-polished on abrasive papers (finally on P4000 grade abrasive paper) and with diamond pastes. During mechanical polishing of the partially recrystallized samples a layer of 0.5-0.8mm thickness was removed. The final stage of sample preparation was electropolishing using TenuPol 5. Electropolishing settings are given in Table 4.6.

To identify new, recrystallized grains, the pure Al and Al-1%wt.Mn alloy samples were anodized (20V) in the same HBF₄ solution, for 180s. In the case of the Cu and Cu-2%wt.Al alloy samples, a solution based on analytically pure 65% nitric acid 63.01g/mol was used for

3s (Cu) and 4.5s (Cu-2%wt.Al). In the case of Ni a solution of 20cm³ hydrochloric acid (1,18), 18g of iron chloride, and 30cm³ of 96% ethyl alcohol was applied for 90s at room temperature.

5. RESULTS AND DISCUSSION

In order to explain the mechanisms controlling new grain orientation formation during the initial stages of recrystallization, it is of key importance to show the correlations that occur (or not) between the disorientation axes identified in the deformed state and those that define the disorientation through the recrystallization front. (The appearance of specific disorientation axes between particular pixels of the orientation maps generated for the deformed structure is determined by the activity of specific slip systems). Therefore, before analyzing the mechanisms controlling the formation of new grain orientations during recrystallization, a thorough characterization of the deformed state will be performed.

5.1. The description of the deformed state

The structural changes of the deformed state are analyzed below based on the orientation maps presented as a ‘function’ of image quality factor or by the application of an IPF colour code. The traces of the active slip systems observed in orientation maps are compared with texture scattering observed in $\{111\}$ pole figures. Therefore, each orientation map also includes the $\{111\}$ pole figure in the co-ordinate system corresponding to the orientation map. These meso- scale microstructures are compared with the nano-/micro- scale ones observed in TEM.

The description of the possible 12 slip systems using the Bishop and Hill notation is given in Table 5.1. The principal slip systems expected to operate can be determined by a classical relaxed Taylor model for plane strain (channel-die) compression of $\{110\}\langle 001\rangle$ and $\{110\}\langle 112\rangle$ crystals, e.g. [Skalli *et al.* (1983), Godfrey *et al.* (2001)] on the assumption of homogeneous deformation and equal critical resolved shear stress (CRSS); they are listed in Table 5.2. In the brass orientation, slip is expected (in equal quantities) on the $+a_2$ and $-b_1$ systems. In the Goss orientation, slip occurs on the same two planes ($-a_1, +a_2, -b_1, -b_1, +b_2$) but each slip (equally preferred) occurs in two directions (co-planar or CP slip).

In the case of the Goss orientation, two symmetrically situated pairs of co-planar slip systems (with respect to the plane perpendicular to TD) operate in planes inclined at 35° to ED and ensure the stability of the sample orientation up to large strains. For the brass orientation, slip on the same two planes occurs but with single slip along each plane, and thence the orientation's strong stability in plane strain compression.

Slip plane	111			-1-11			-111			-11-1		
Slip direction	01-1	-101	1-10	0-1-1	101	-110	0-11	101	-1-10	0-1-1	-101	110
Bishop & Hill notation	a ₁	a ₂	a ₃	b ₁	b ₂	b ₃	c ₁	c ₂	c ₃	d ₁	d ₂	d ₃

Table 5.1. Description of the 12 slip systems in Bishop and Hill (1951) notation.

Crystal orientation	Active slip systems (Bishop & Hill notation)
Goss (110)[00-1]	a ₁ , -a ₂ , -b ₁ , +b ₂
Brass (110)[1-1-2]	-a ₂ , +b ₁

Tab. 5.2. Active slip systems operating in (110)[00-1] and (110)[1-1-2] orientations (classical relaxed Taylor model for channel-die compression).

5.1.1. Goss {110}<001> orientation

5.1.1.1. Microstructure characterization based on SEMFEG/EBSD local orientation measurements

The orientation maps for all five metals of the Goss-oriented samples were recorded at strains of 0.51 and 0.92 are presented in Figs. 5.1. and 5.2. One of the most important conclusions that results from the SEM/EBSD analysis of the deformed state is that the microstructure appears finer at lower SFE, i.e. the microband width becomes smaller.

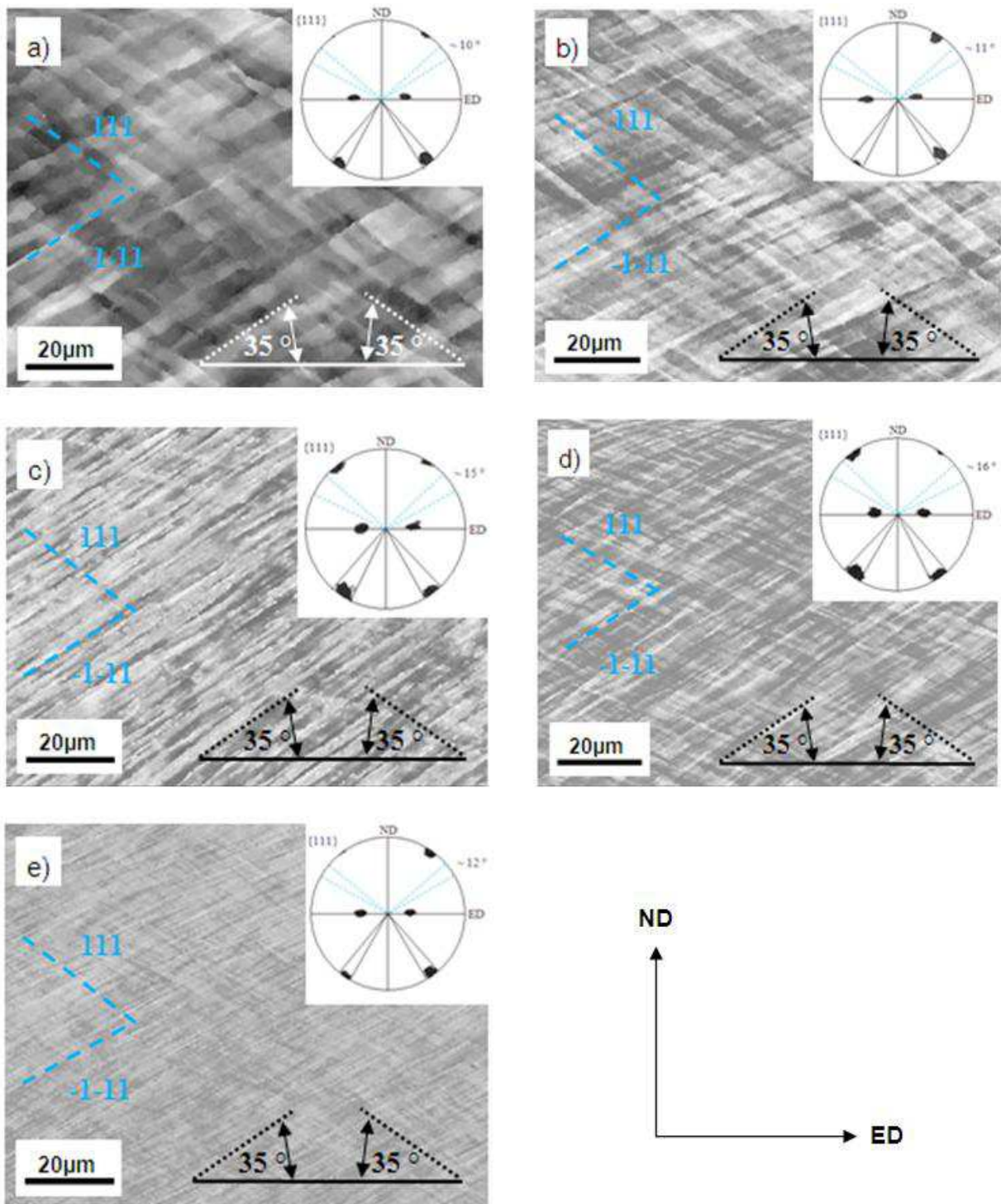


Fig. 5.1. Microstructures observed in (110)[00-1] oriented single crystals, deformed up to logarithmic strains of 0.51 and corresponding {111} pole figures: (a) Al , (b) Al-1%Mn, (c) Ni, (d) Cu, (e) Cu-2%Al. SEM/EBSD local orientation measurements in ND-ED section with step size of 100nm. Orientation maps presented as 'function' of Schmid factor. Blue, dashed lines marked traces of the most active slip systems.

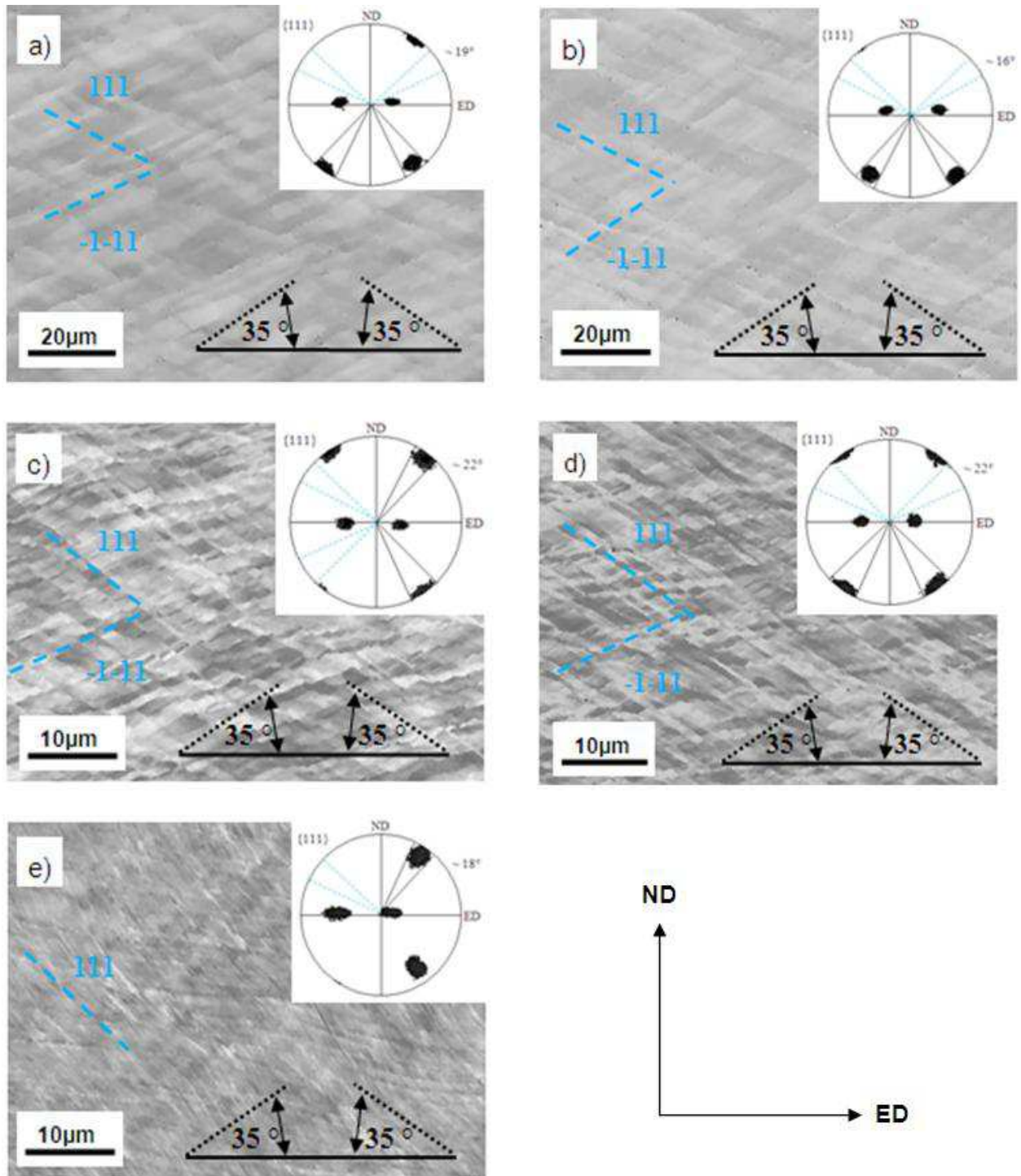


Fig. 5.2. Microstructures observed in (110)[00-1] oriented single crystals, deformed up to logarithmic strains of 0.92 and corresponding {111} pole figures: (a) Al, (b) Al-1%Mn, (c) Ni, (d) Cu, (e) Cu-2%Al. SEM/EBSD local orientation measurements in ND-ED section with step size of 100nm. Orientation maps presented as 'function' of Schmid factor. Blue, dashed lines marked traces of the most active slip systems.

In accordance with previous investigations, the PSC single crystals of the ideal Goss orientation remained stable up to strains of unity, as shown by the $\{111\}$ pole figures of the mapped areas, and did not reveal the formation of band-like strain inhomogeneities. Only a uniform dislocation cell substructure is formed (Fig. 5.1. a)), as observed earlier, e.g. by Bauer (1977), Wróbel *et al.* (1995 and 1996), Ferry and Humphreys (1996), Borbély *et al.* (2007) and Paul *et al.* (2010) on similarly oriented Cu crystals. (But at strains of 2 they form bands through the crystal thickness). Up to logarithmic strains of ~ 1.0 , the microstructures consist of two complementary sets of elongated bands, initially inclined at $\pm 35^\circ$ to ED. The angle φ related to the observed boundaries changed with the deformation (the inclination angle of microband boundaries mainly aligned along the two symmetrical directions $\pm\varphi$ to ED). Each set of dislocation band occupied nearly the same volume of the crystal, but in some cases one set of the walls was more pronounced locally, as observed earlier for example by Ferry and Humphreys (1996) and Borbély *et al.* (2007), Paul *et al.* (2008b)].

Both sets of dislocation walls marking the bands were inclined very close to the expected traces of the active $\{111\}$ slip planes. (They were always within the scatter limit of normals to the $\{111\}$ planes; this is clearly visible in the pole figures of Figs. 5.3 and 5.4). As a result of their intersection, rectangular cells with dimensions of 1-2 μm were formed. For higher strains the microstructure appeared to be progressively ‘wavier’ and the traces of the active slip systems were not as regular as those observed at lower deformations, as presented earlier by Borbély *et al.* (2007) and Paul *et al.* (2010).

The orientations of areas corresponding to the above microstructures confirm the stability of the initial orientation at low deformations (Fig. 5.1) with clearly visible scatterings of the $\langle 111 \rangle$ poles around ND and ED at higher deformations (Fig. 5.2). The beginning of abnormal subgrain growth during recrystallization in copper single crystals of Goss $\{110\}\langle 001 \rangle$ orientation was studied, e.g. by Ferry and Humphreys (2006). They observed an overall orientation spread in the as-deformed crystal of $\sim \pm 10^\circ$ about ND. This effect was strongly connected with orientation groups cyclically deviated $\pm 5^\circ$ from the ideal Goss $\{110\}\langle 001 \rangle$ orientation, i.e. in the neighbouring areas of microbands ND rotated $\pm 5^\circ$ through the thickness.

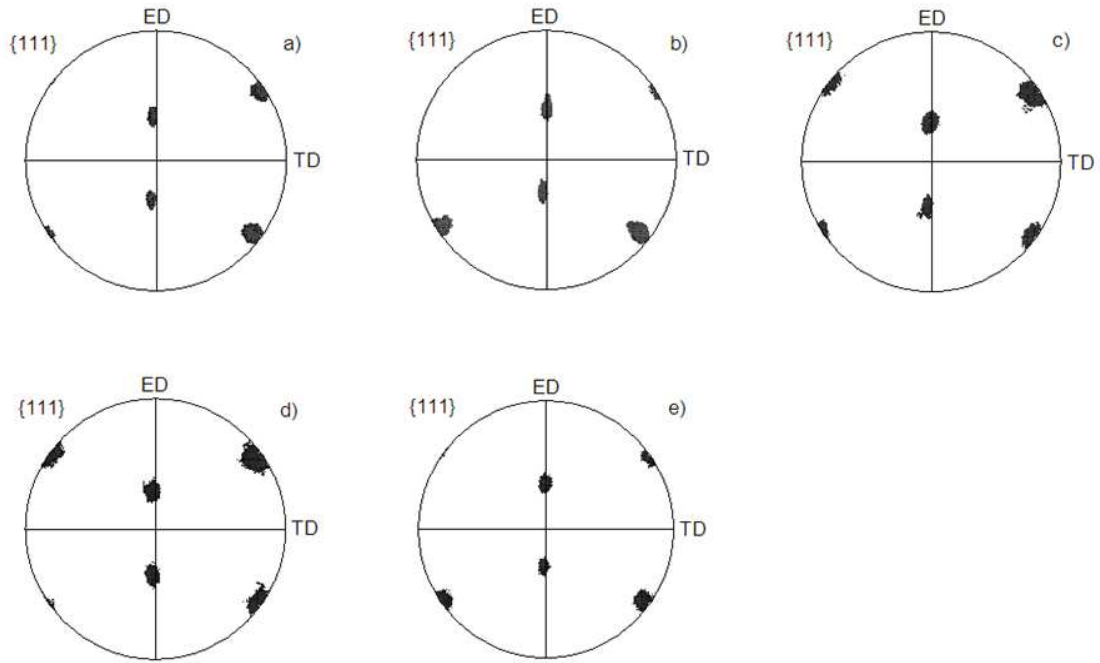


Fig. 5.3. The {111} pole figures of (110)[00-1]-oriented single crystals deformed up to 0.51: (a) Al, (b) Al-1%wt.Mn, (c) Ni, (d) Cu and (e) Cu-2%Al. SEM/EBSD local orientation measurements in ND-ED plane. Step size of 100nm.

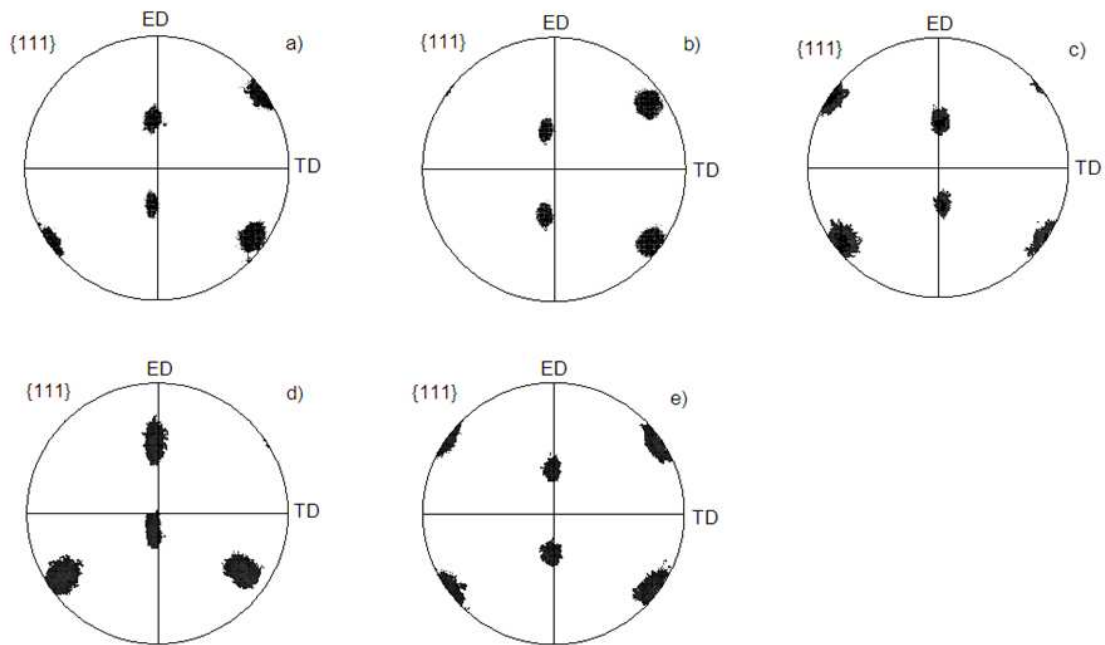


Fig. 5.4. The {111} pole figures of (110)[00-1]-oriented single crystals deformed up to 0.92: (a) Al, (b) Al-1%wt.Mn, (c) Ni, (d) Cu and (e) Cu-2%Al. SEM/EBSD local orientation measurements in ND-ED plane. Step size of 100nm.

The samples which were slightly deviated from the ideal Goss orientation, deformed to the strain of 0.51, reveal a homogeneous distribution of slips without any significant tendency to strain localization. In the case of single crystals, more heavily deviated from the ideal position, usually only one set of microbands predominates, as shown clearly, e.g. for Al (60%) and Al-1%Mn (60%) in Figs. 5.2. a) and b). In these cases, in the areas located close to both top corners of the sample, a well-marked tendency to non-homogeneous flow was also observed. This effect coincides with significant spatial variations of the dislocation wall inclinations and a strong scattering of the $\langle 111 \rangle$ poles. Both sets of dislocation walls marking the bands were inclined very close to the expected traces of the active $\{111\}$ slip planes. However, at higher deformations further spatial variations of both sets of microbands, or even the disappearance of one of them, were also clearly observed (Fig. 5.2. e).

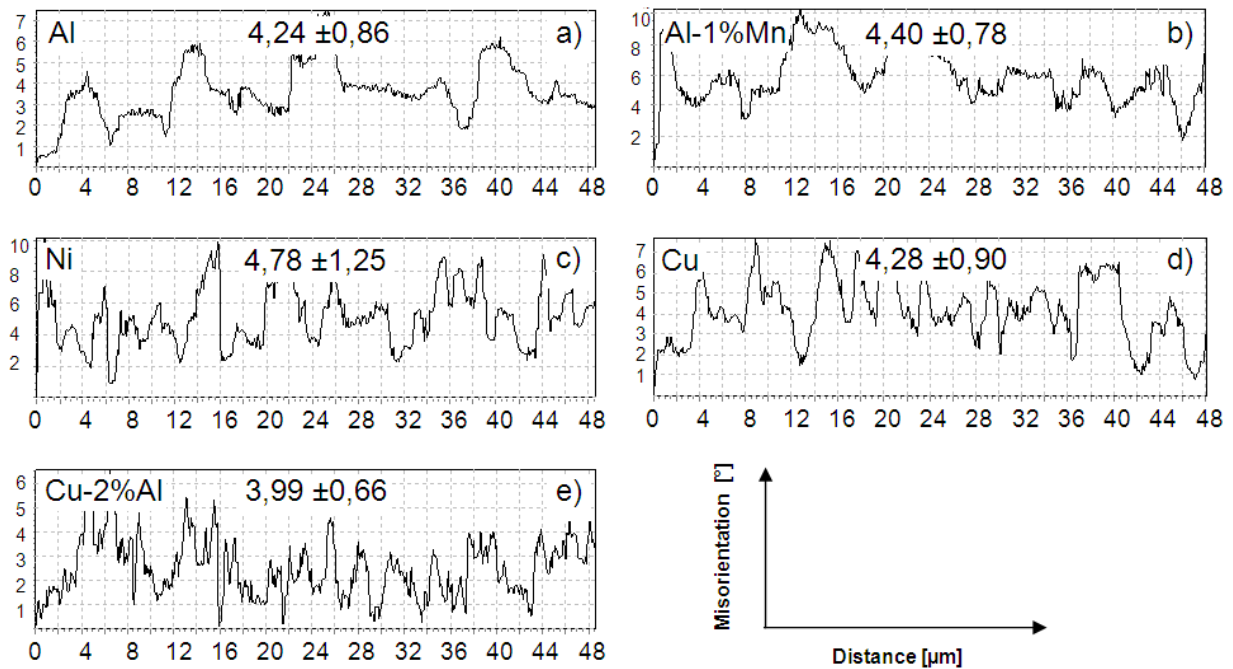


Fig. 5.5. Disorientation 'line scans' along ED measured in ND-ED section of $(110)[00-1]$ oriented samples: a) Al, b) Al-1%Mn, c) Ni, d) Cu and e) Cu-2%Al. Samples deformed up to logarithmic strains of 0.51.

Figures 5.5-5.6 compare typical disorientation line scans for the 5 metals of different SFE after strains of 0.51 and 0.92. All the Goss-oriented samples revealed a relatively small orientation spread. After strains of 0.51 the disorientation angles were significantly below 10° (Fig. 5.5) and the disorientation axes were situated close to TD (for more details see section 5.1.3). In samples deformed to strains of 0.92, disorientation line scans along ED showed a small increase of the orientation spread, occasionally up to $\sim 12^\circ$ (Fig. 5.6). For both deformations the disorientation distribution is rather homogeneous and the adjacent cells displayed opposite rotation senses, as reported earlier, e.g. by Ferry and Humphreys (1996), Borbély *et al.* (2007), and Paul *et al.* (2010a, 2010b).

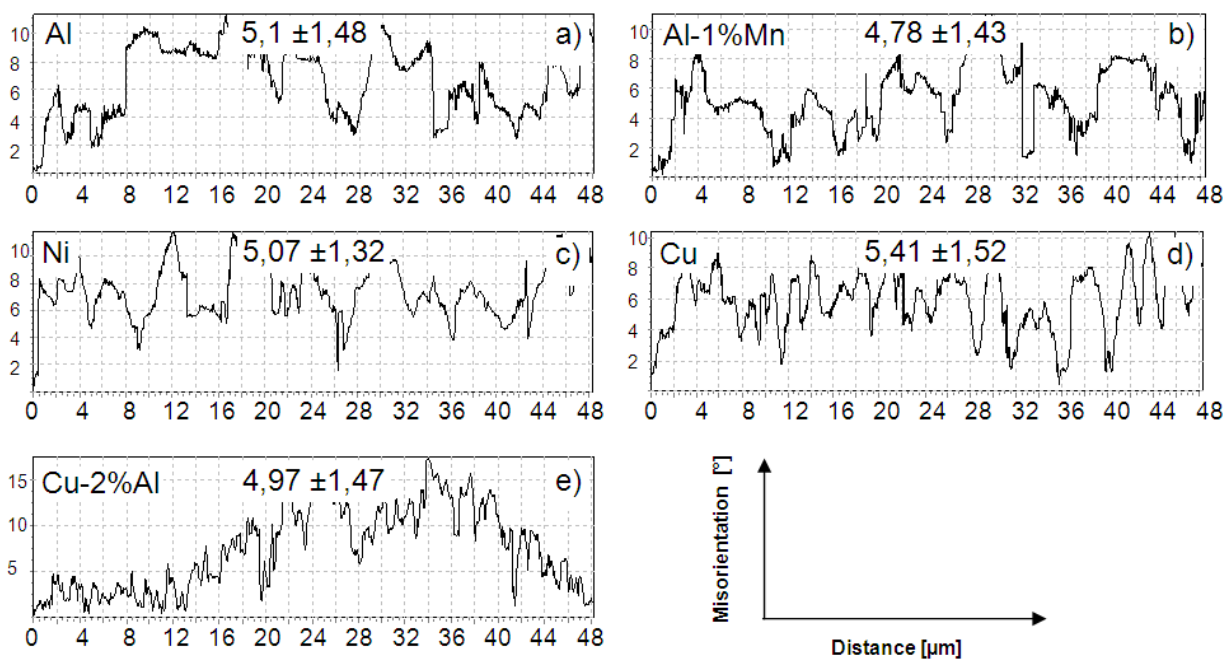


Fig. 5.6. Disorientation ‘line scans’ along ED measured in ND-ED section of (110)[00-1] oriented samples for: a) Al, b) Al-1%Mn, c) Ni, d) Cu and e) Cu-2%Al. Samples deformed up to logarithmic strains of 0.92.

5.1.1.2. Dislocation structures

The microband structures observed by TEM were very similar to the dislocation microstructures analysed at the meso- scale by FEG-SEM/EBSD. The TEM observations and

local orientation measurements of the deformed samples were carried out on longitudinal sections at both deformations, i.e. 0.51 and 0.92.

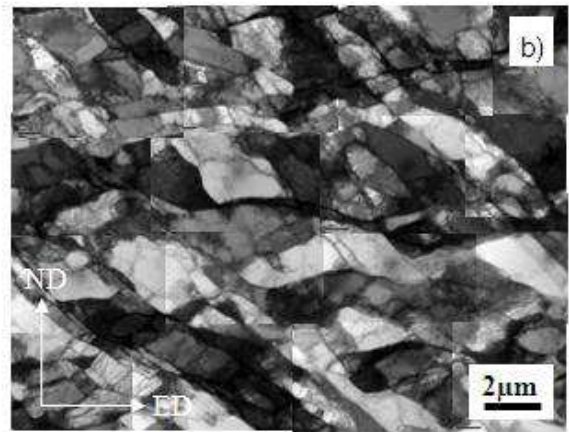
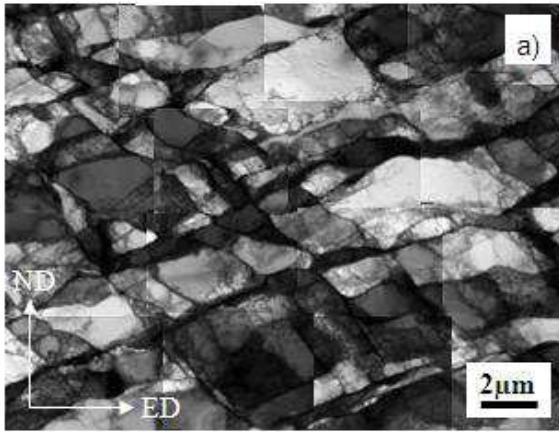
In accordance with previous results, the homogeneously deformed crystals of Goss orientation remain stable up to large strains and generally do not reveal the formation of band-like strain inhomogeneities even at the TEM scale; only a uniform dislocation cell substructure was formed (Figs. 5.7), as observed earlier for example by Bauer (1977), Wróbel *et al.* (1995, 1996), Paul *et al.* (2010) on similarly oriented Cu crystals and Godfrey *et al.* (2001) on Al single crystal. Each set of dislocation bands occupied nearly the same volume of the crystal, but usually one set of the walls was more pronounced locally.

For lower deformations, the disoriented dislocation walls coincide well with the traces of the {111} planes on the longitudinal plane. At this stage of deformation, as a result of microband intersections, rectangular cells with dimensions of 0.2-2 μm , were formed. (The dimensions of the cells depend on the SFE, decreasing at lower SFE. For Al, the width of the elongated cells is an order of magnitude greater than that observed for the Cu-2%Al alloy). At higher deformations the traces of the active slip systems were not as regular as those observed at lower deformations, indicating significant cross-slip at this stage of deformation. (Fig. 5.7 b) and j)). The orientations of areas corresponding to the above microstructures were analysed for selected cases by TEM orientation imaging. They confirm the stability of the initial orientation at low deformations and clearly visible scattering of the $\langle 111 \rangle$ poles around ND and ED at higher deformations.

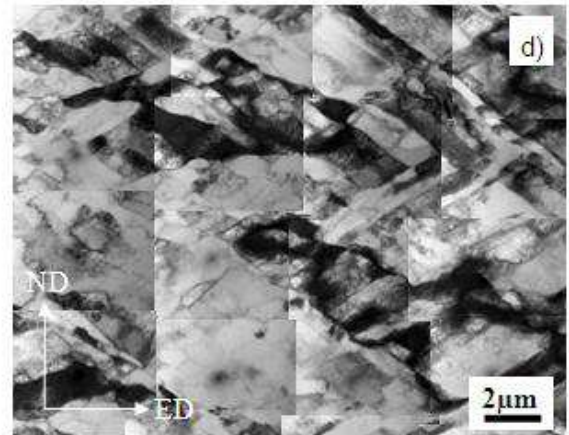
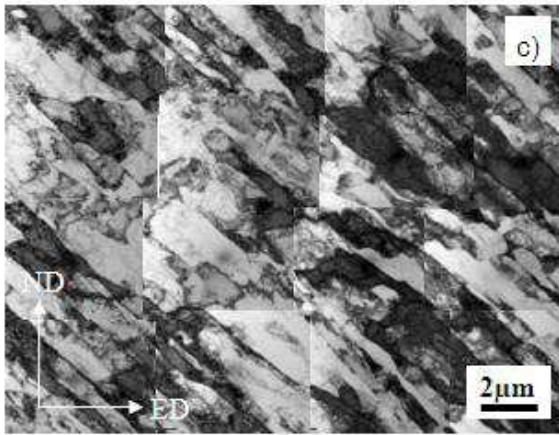
$\epsilon=0.51$

$\epsilon=0.92$

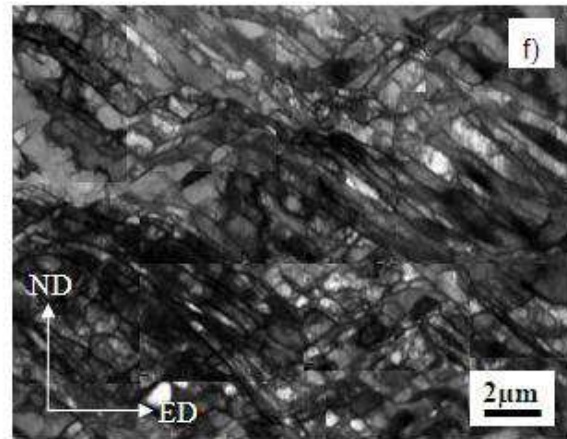
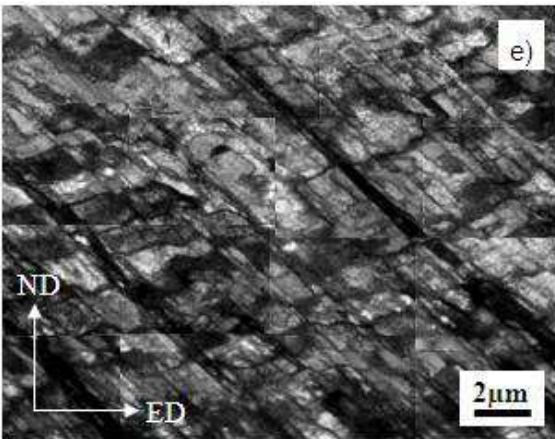
Al



Al-1%Mn



Ni



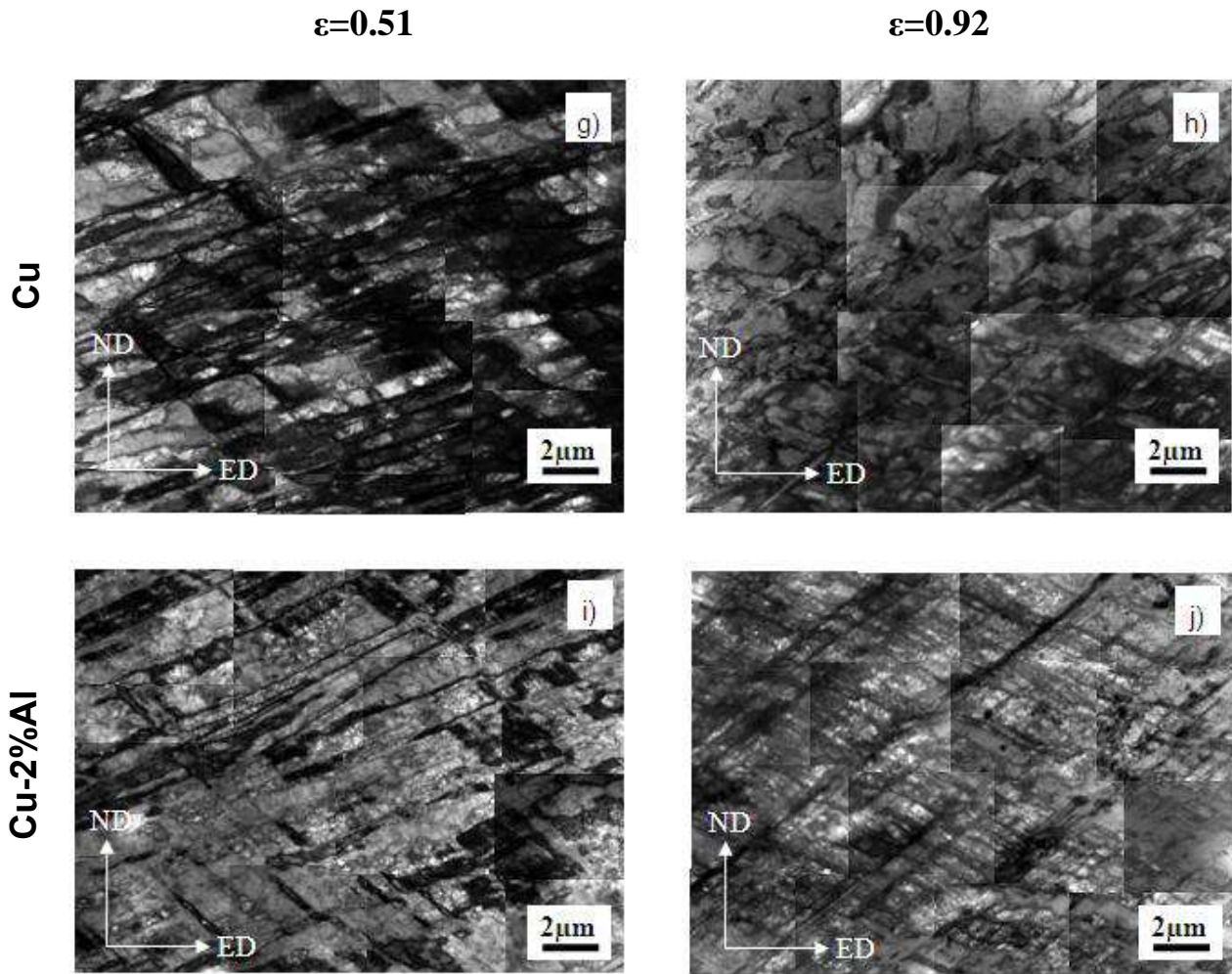


Fig. 5.7. Bright field images showing TEM microstructures observed in ND-ED section; (a) and (b) - Al, (c) and (d) - Al-1%Mn, (e) and (f) - Ni, (g) and (h) - Cu, (i) and (j) - Cu-2%Al. 1st and 2nd column's showing samples deformed up to logarithmic strains of 0.51 and 0.92, respectively. Single crystals of (110)[00-1] orientation.

5.1.2. Brass {110}<112> orientation

The ideal brass orientation is also stable in plane strain compression up to very high deformations [Skalli *et al.* (1983), Wróbel *et al.* (1996), Doherty (1997a), Godfrey *et al.* (2001), Paul *et al.* (2008b), Albou *et al.* (2010a)]. Two major slip systems, operating in planes initially inclined at $\pm 30^\circ$ to the extension direction (ED) and intersecting the compression

plane at 35° with respect to transverse direction (TD) are activated from the earliest stages of deformation (Fig. 5.8 and 5.9).

In fact, the initial crystal orientations used here were ‘non-ideal’ and usually shifted by some degree from the exact position. Crystal plasticity calculations performed using either the full or relaxed Taylor conditions lead to the conclusion that the ideal brass $\{110\}\langle 112\rangle$ orientation should be stable. However, only a small deviation from this ideal position by rotation around certain axes can lead to more or less noticeable instability. Godfrey et al (2001) showed that the deformation of samples with orientations deviating 3° from ED, after the strain of 0.55 and 1.5, led to the rotations of orientations up to 6° and 12° away from the ideal one, respectively.

As expected, the samples undergo a macroscopic shear in the compression plane along the extension direction ($\varepsilon_{ED/ND}$), typical of plane strain compressed *brass*-oriented crystals. Standard crystal plasticity predicts this shear as a consequence of slip on the (111)[10-1] and (-1-11)[0-1-1] (-a2 and b1) systems (Figs. 4.3-4.4 and Tables. 5.1-5.2). For the ideal brass orientation, these two systems have equal amplitudes and their lattice rotations balance out to zero rotation up to large strains. For the brass orientation rotated by a few degrees, slip occurs on the same systems but usually one of them is favoured compared with the other one, so that non-zero lattice rotation develops. For example, in the case of the sample initially rotated by a few degrees around ED, $\varepsilon_{ED/ND}$ and $\varepsilon_{ED/TD}$ shear occurs in the longitudinal plane and along the extension direction due to the off-ideal orientation.

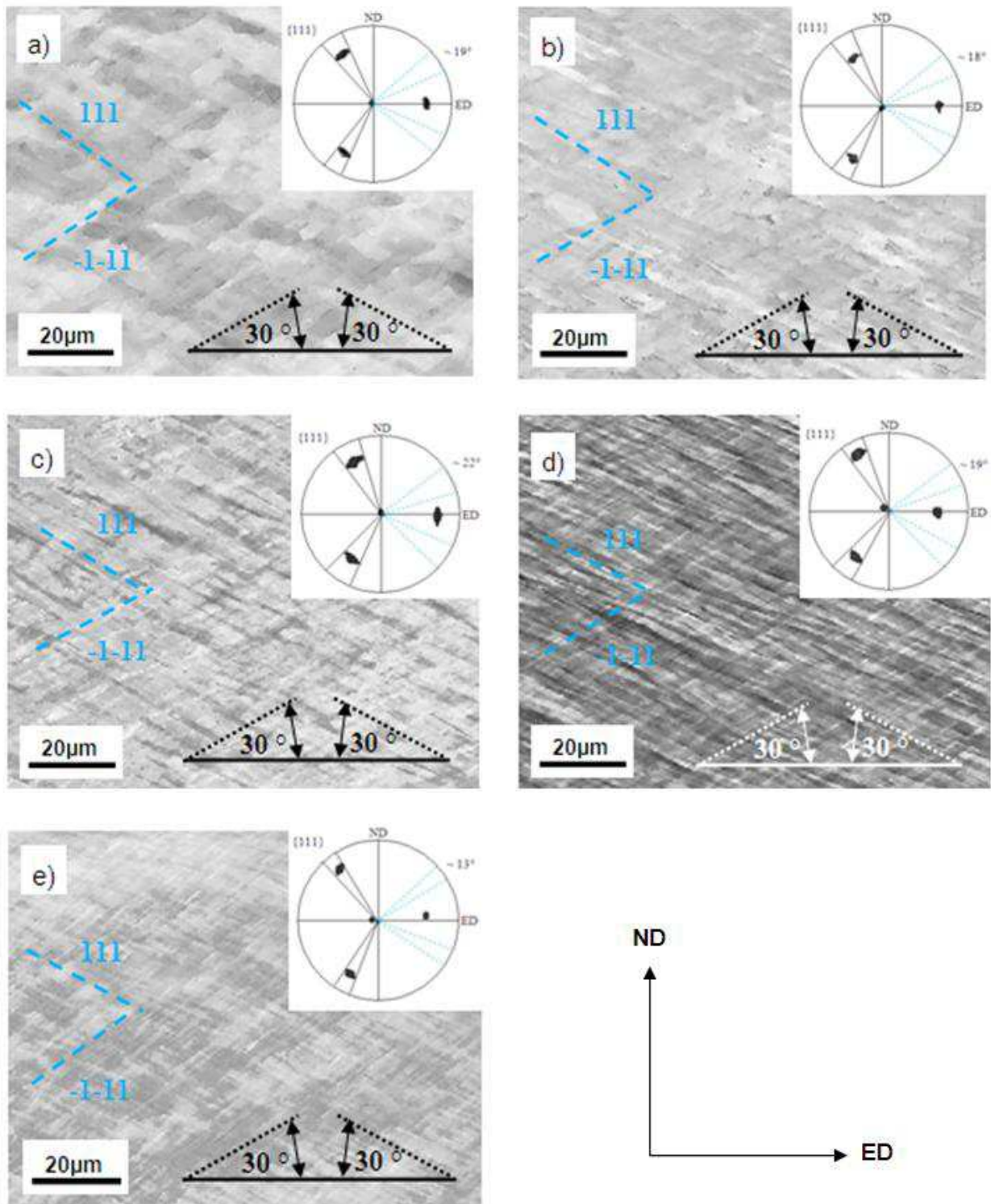


Fig. 5.8. Microstructures observed in $(110)[1-1-2]$ oriented single crystals, deformed up to logarithmic strains of 0.51 and corresponding $\{111\}$ pole figures: (a) Al, (b) Al-1%Mn, (c) Ni, (d) Cu, (e) Cu-2%Al. SEM/EBSD local orientation measurements in ND-ED section with step size of 100nm. Orientation maps presented as 'function' of Schmid factor. Blue, dashed lines marked traces of the most active slip systems.

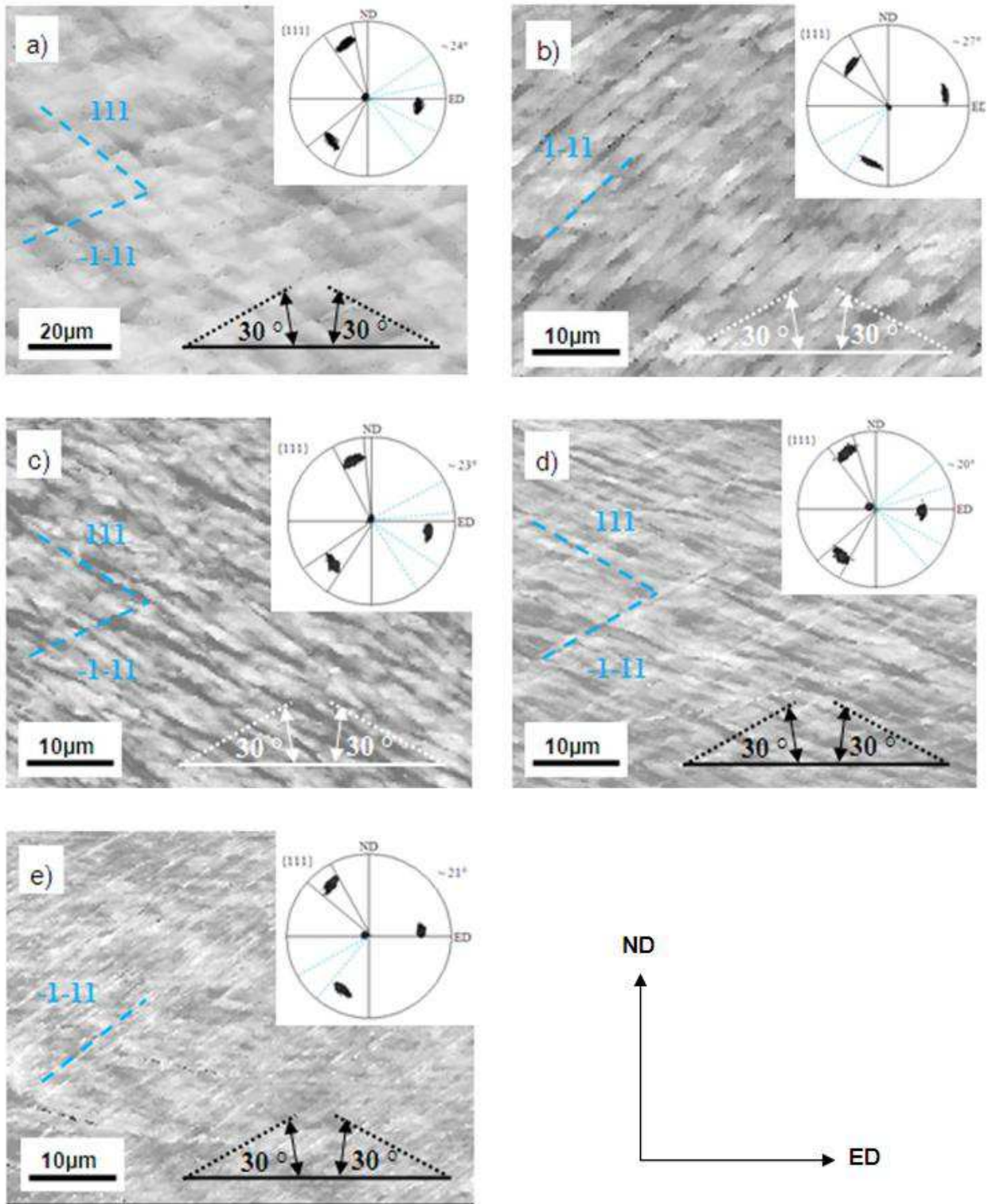


Fig. 5.9. Microstructures observed in $(110)[1-1-2]$ oriented single crystals, deformed up to logarithmic strains of 0.92 and corresponding $\{111\}$ pole figures: (a) Al, (b) Al-1%Mn, (c) Ni, (d) Cu, (e) Cu-2%Al. SEM/EBSD local orientation measurements in ND-ED section with step size of 100nm. Orientation maps presented as 'function' of Schmid factor. Blue, dashed lines marked traces of the most active slip systems.

5.1.2.1. SEM/EBSD microstructures and textures

Local orientation measurements at low deformations (0.51) showed two, well-marked families of low angle boundaries. These families of dislocation walls observed in longitudinal sections were inclined at $\sim(\pm)30^\circ$ with respect to ED (Fig. 5.8). Similarly as in the case of Goss-oriented samples, the general observation is that the microband width decreases as the SFE decreases. In this way a coarser structure is observed in the case of pure Al and a finer one for the Cu-2%Al alloy (Fig. 5.9). The $\{111\}$ pole figures of Figs 5.10-5.11, corresponding to the orientation maps made on the ND-ED plane, showed little scattering of the initial orientation. The deformed microstructures observed in crystals of brass orientation were very sensitive to the exact initial orientation. If the initial orientation was deviated from the ideal position only one set of microbands was clearly visible. This was especially noticeable after deformations corresponding to 0.92 logarithmic strains. (Fig. 5.9).

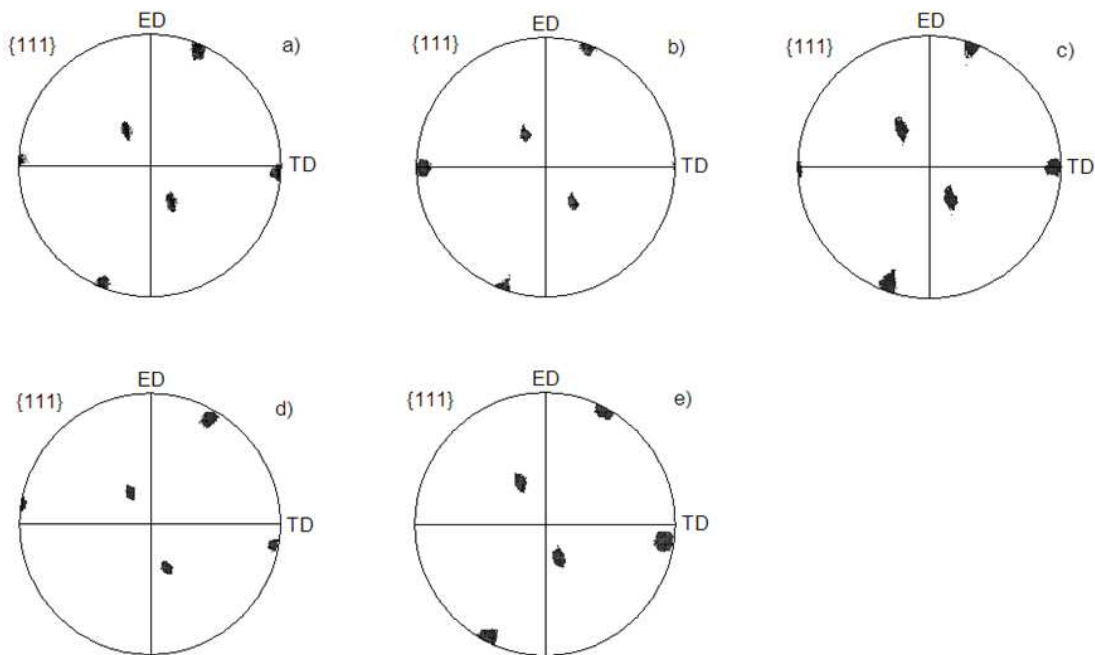


Fig. 5.10. The $\{111\}$ pole figures of $(110)[1-1-2]$ -oriented single crystals deformed up to 0.51: (a) Al, (b) Al-1%wt.Mn, (c) Ni, (d) Cu and (e) Cu-2%Al. SEM/EBSD local orientation measurements in ND-ED plane. Step size of 100nm.

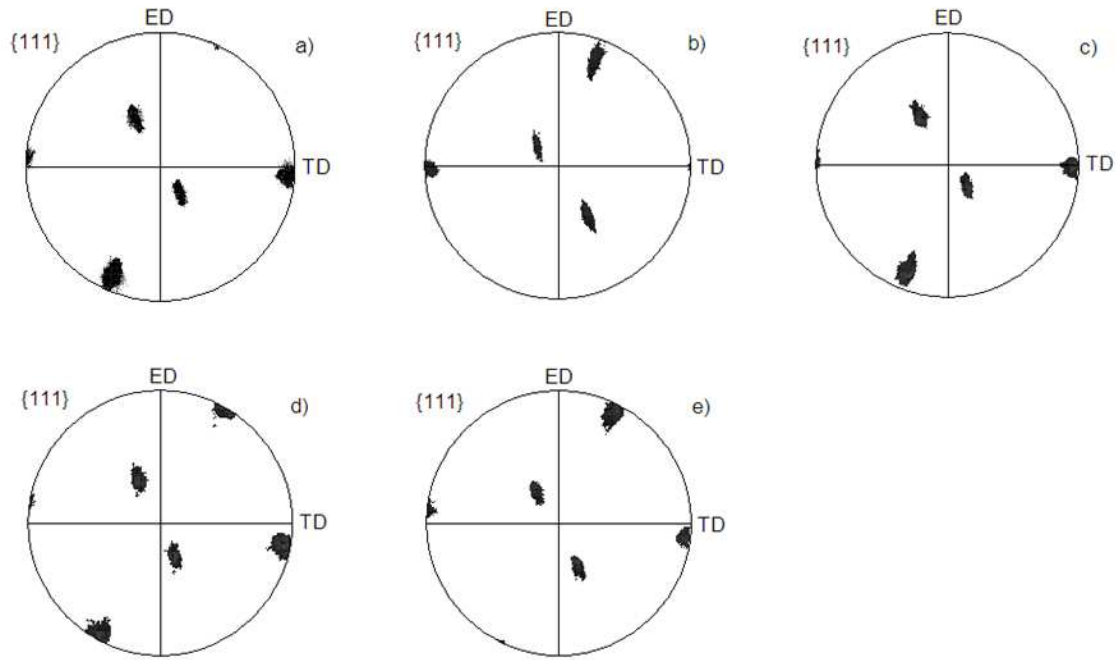


Fig. 5.11. The $\{111\}$ pole figures of $(110)[1-1-2]$ -oriented single crystals deformed up to 0.92: (a) Al, (b) Al-1%wt.Mn, (c) Ni, (d) Cu and (e) Cu-2%Al. SEM/EBSD local orientation measurements in ND-ED plane. Step size of 100nm.

Disorientation line scans were also calculated between individual elongated cells and along particular directions. At a low deformation, all analyzed points had an orientation close to the initial one; disorientation angles rarely exceeded a few degrees. At a higher deformation, the scatter of the disorientation line scans increased significantly and a near-periodic variation of the disorientation angle was clearly observed on Fig. 5.12-5.13. In this case, the amplitude reached $\sim 10^\circ$, for the lines scan along ED. The orientation changes were not random and showed a regular cyclic pattern with varying amplitudes and wavelength of $5-8^\circ$ and $2-10\mu\text{m}$, respectively. The amplitude and wavelength were strongly correlated with SFE. A close inspection of the orientation distribution showed that dominant, short-range fluctuations, reached the scale of the repeated intersections of the microbands aligned at 30° to ED. These fluctuations very often induced a general rotation of the crystal lattice towards the $\{112\}\langle 110\rangle$ orientation, as presented earlier by Paul *et al.* (2010b), Albou *et al.* (2010a), Miszczyk *et al.* (2011).

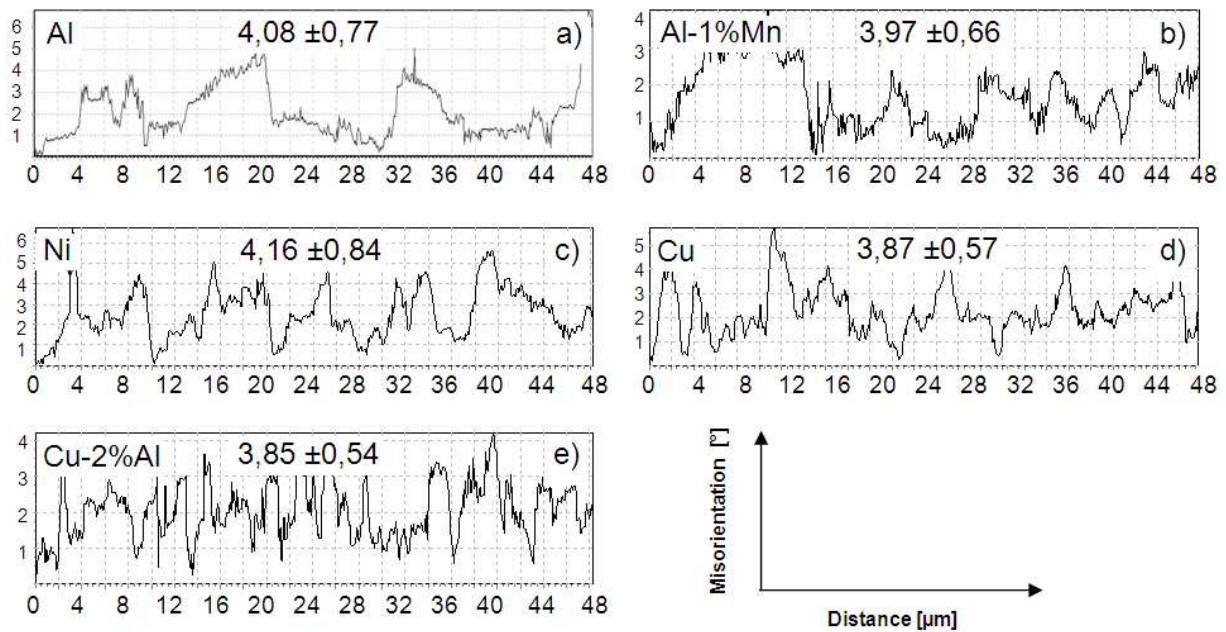


Fig. 5.12. Disorientation ‘line scans’ along ED measured in ND-ED section of (110)[1-1-2]-oriented samples: a) Al, b) Al-1%Mn, c) Ni, d) Cu and e) Cu-2%Al. Samples deformed up to logarithmic strains of 0.51.

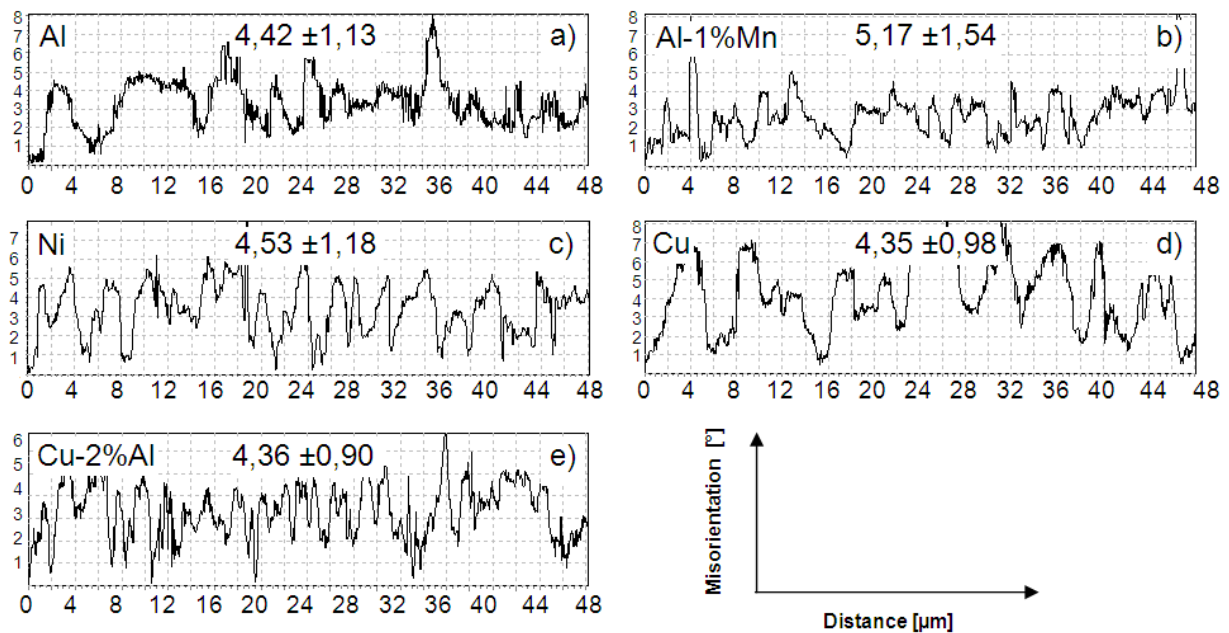


Fig. 5.13. Disorientation ‘line scans’ along ED measured in ND-ED section of (110)[1-1-2]-oriented samples: a) Al, b) Al-1%Mn, c) Ni, d) Cu and e) Cu-2%Al. Samples deformed up to logarithmic strains of 0.92.

5.1.2.2. TEM microstructure

The microband structures observed at the meso-scale by SEM/EBSD were very similar to the dislocation microstructures observed by TEM. At low deformations the microstructures consisted of two complementary sets of elongated bands, initially inclined at $\pm 30^\circ$ to ED (Fig. 5.14 a), c), e), g), i)). Both sets of dislocation walls marking the bands were closely inclined to the expected traces of active $\{111\}$ slip planes. For higher strains, very often one set of dislocation walls was the most preferred dislocation substructure observed on the ND-ED plane. Additionally, with increasing strain, the microstructure appeared to be progressively 'wavier' and the traces of active slip systems were not as regular as those observed at lower deformations (Fig. 5.14 b), d), f), h), j)). This is in accordance with the results obtained by Godfrey *et al.* (2001) who reported that some of the dislocations within boundaries arose from unpredicted slips. Since TEM observations are generally restricted to small areas, usually $\sim 100\mu\text{m}^2$, variations in microband alignment over large distances is very difficult to characterize by this technique.

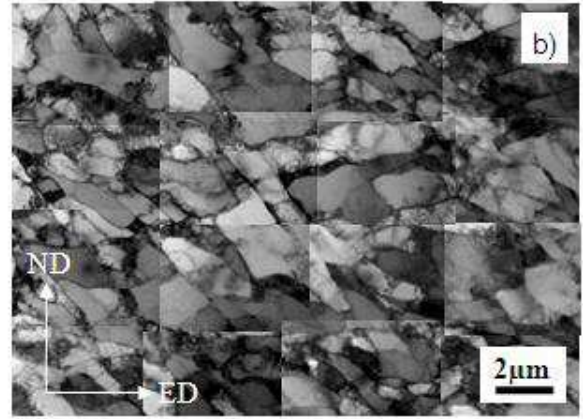
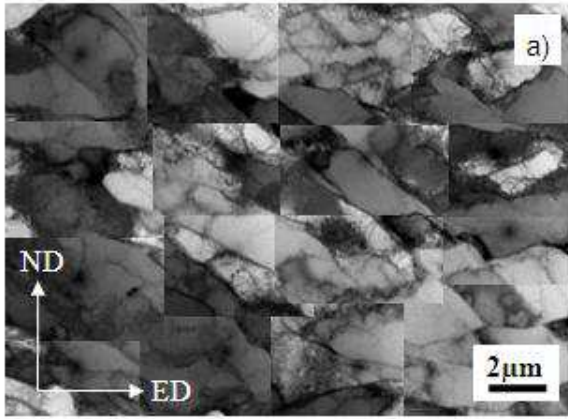
Some extremely thin twins were occasionally found (Fig. 5.15) but the overall density of twins was very low. The presence of twins was confirmed by means of Selected Area Diffraction patterns and bright/dark field images. These thin deformation twins were observed in pure copper and Cu-2%Al alloy (low SFE metals) of both orientations, i.e. $\{110\}\langle 001\rangle$ and $\{110\}\langle 112\rangle$.

Similar thin twins were observed in copper single crystals of $\{110\}\langle 011\rangle$ orientation by Wróbel *et al.* [Wróbel *et al.* (1996)] after changing the deformation path. They justified the occurrence of twinning by the fact that in the second deformation the critical resolved shear stress for slip may be comparable to the twinning stress. However, in the present work this effect may result from the low temperature (-35°C) thin foil deformation that occurs during thin foil preparation.

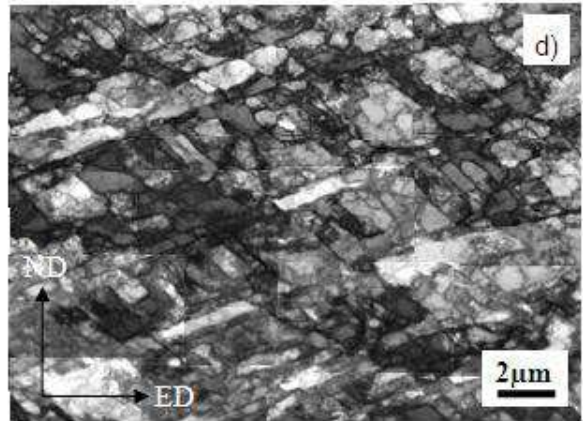
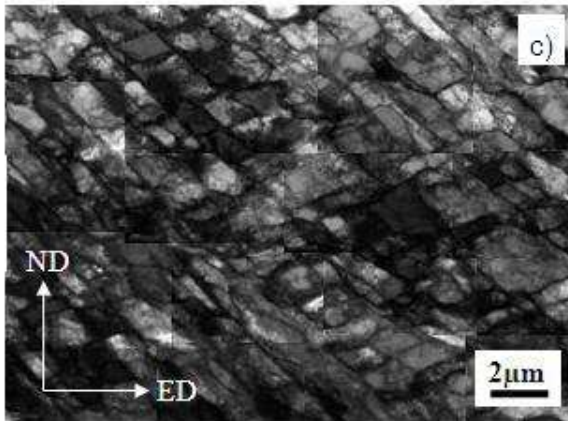
$\epsilon=0.51$

$\epsilon=0.92$

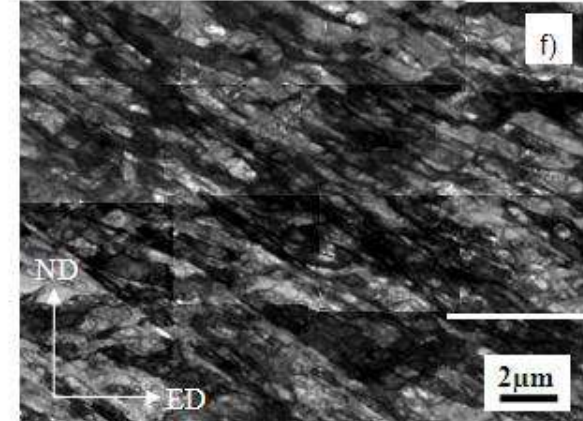
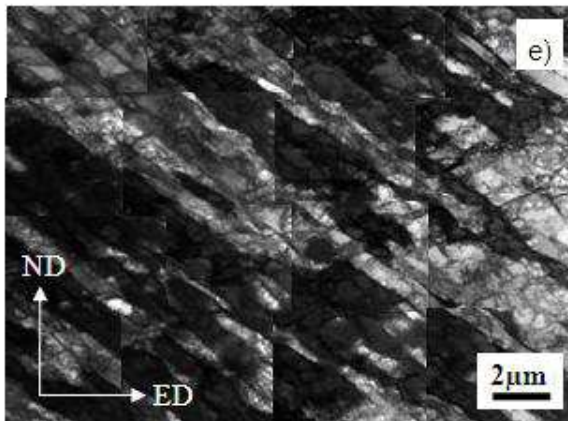
Al



Al-1%Mn



Ni



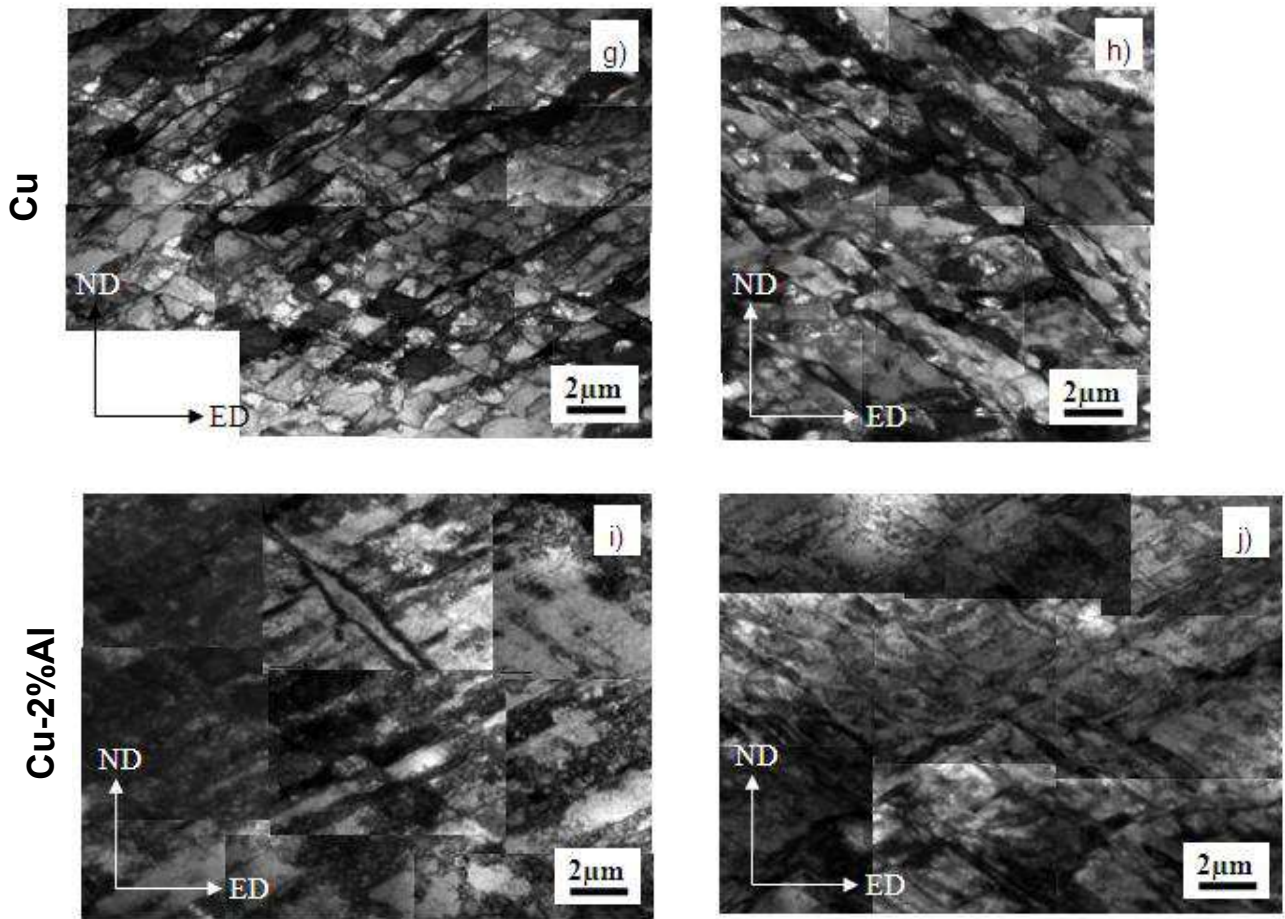


Fig. 5.14. Bright field images showing TEM microstructures observed in ND-ED section; (a) and (b) - Al, (c) and (d) - Al-1%Mn, (e) and (f) - Ni, (g) and (h) - Cu, (i) and (j) - Cu-2%Al. 1st and 2nd column's showing samples deformed up to logarithmic strains of 0.51 and 0.92, respectively. Single crystals of (110)[1-1-2] orientation.

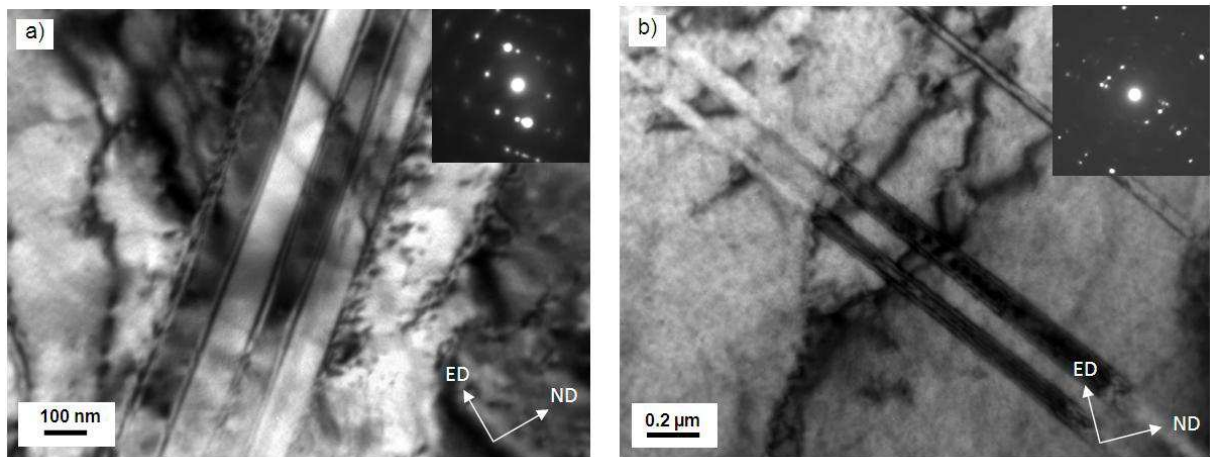


Fig. 5.15. TEM bright field images showing formation of deformation twins in copper. Initial sample orientation: (a) - (110)[00-1] and (b) - (110)[1-1-2], deformed up to logarithmic strains of 0.51.

5.1.3. Crystal lattice rotation during deformation - the rotation axes identification

5.1.3.1. Accuracy of disorientation determination

Determining the disorientation axes for orientation relations between adjacent regions of the deformed state enables one to identify the active slip systems. Prior to a detailed analysis of the disorientation axes distribution, a test was carried out to assess the value of the disorientation angle which can provide a reliable determination of the disorientation axis. Literature reports often give the value of 0.5° as the angular resolution accuracy of standard SEM/EBSD and this directly impacts the accuracy of the disorientation axes.

The spread of random errors should be modelled by a suitable distribution of the group of rotations (e.g., the von Mises-Fisher distribution [Morawiec (2004)]). Since the orientation spreads are small, all our rotations are close to identity. In the parameterization by the rotation vector $(\omega_x, \omega_y, \omega_z) = \omega_n$, the metric of the rotation space in the neighbourhood of the identity is nearly Cartesian. Therefore, it is reasonable to approximate the proper distribution by trivariant normal (Gaussian) distributions of rotations parameterized by $(\omega_x, \omega_y, \omega_z)$. Such distributions of random errors will be assumed here, and the precision quantified by standard deviations.

To estimate the accuracy of disorientations in maps, one needs to refer experimental results to true disorientations. As a convenient experimental reference, the well-known orientation relations between adjoining pixels located on opposite sides of twinning boundaries (recrystallization twins) for a partly recrystallized state were analysed.

Coherent recrystallization twins are easily discernible in maps of fcc metals with an exact $\Sigma 3$ disorientation ($60^\circ \langle 111 \rangle$). An example of the distribution of deviations from the ideal $\Sigma 3$ disorientation for fifty measured disorientations between twins is shown in Fig. 5.16. The data originate from Cu, Ag and Cu-2%Al specimens of (112)[11-1] oriented single crystal (after 50% channel-die deformation and then partly recrystallized). Fig. 5.16 illustrates the accuracy in disorientation determination between fcc twins using standard EBSD patterns. The ellipses represent twice the standard deviations. In this case, the deviation of the mean disorientation from the ideal $\Sigma 3$ was 0.5° , while the standard deviation from the mean was $\sim 0.4^\circ$ for each direction. As presented in Figure 5.16 the scattering of the calculated disorientations from the ideal $\Sigma 3$ disorientation is close to $1.5\text{-}2^\circ$. This indicates that the accuracy of the standard FEGSEM/EBSD system for disorientation determination is limited to values of the disorientation angles near $1.5\text{-}2^\circ$. Therefore, in further analysis, only the positions of the

disorientation axes corresponding to disorientation angles equal or larger than 1.5° will be analysed.

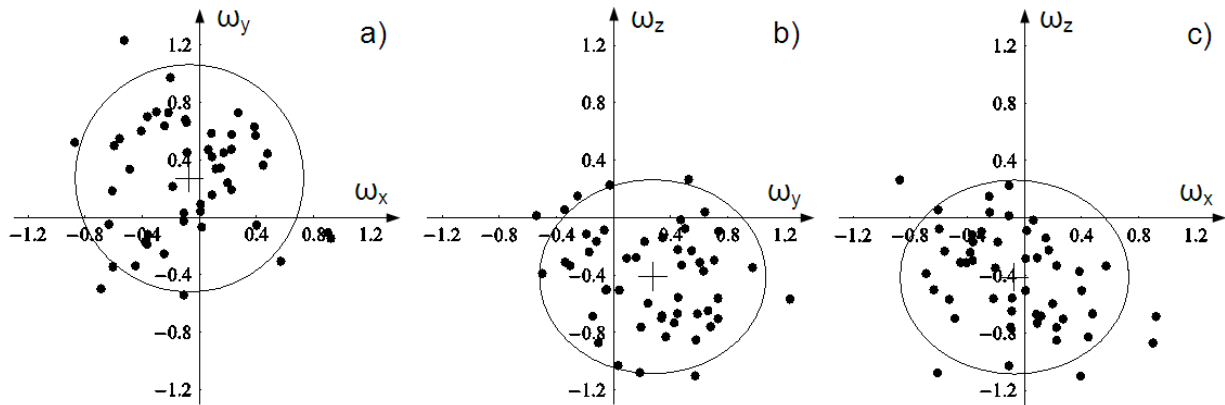


Fig. 5.16. Illustration of accuracy in determination of disorientations between fcc twins using Kikuchi patterns. The ellipses represent twice the standard deviations. The data originate from three maps of specimens recrystallized after deformation of (112)[11-1] oriented single crystals: Cu and Cu-2%wt.Al partly recrystallized (60s/460°C) after 50% channel-die deformation, and Ag recrystallized (30s/265°C) after 67% deformation.

5.1.3.2. Crystal lattice rotation. The rotation axes identification

Figures 5.17-5.18 give the positions of the $\langle 112 \rangle$ and $\langle 110 \rangle$ axes in the sample coordinates corresponding to the ideal Goss (110)[00-1] and brass (110)[1-1-2] orientations. *In the case of Goss orientation*, the traces of the two slip planes on which the four most active slip systems operate (a_1 , $-a_2$, $-b_1$, $+b_2$) are drawn as dotted lines (Fig. 5.17 a-j)). Four $\langle 112 \rangle$ axes lie close to the TD-direction: $[2-11]$, $[2-1-1]$, $[1-2-1]$ and $[1-21]$. They belong to the respective active slip systems. One direction of $[1-10]$ coincides with TD. *In the case of the brass orientation*, the traces of the two slip planes on which the two most active slip systems operate ($-a_2$, $+b_1$) are also drawn as dotted lines (Fig. 5.18 a-j)). Three $\langle 112 \rangle$ axes lie close to the TD-direction: $[1-21]$, $[2-11]$, and $[1-12]$. The first two belong to $-a_2$ and $+b_1$ slip systems. Three $\langle 110 \rangle$ axes are also in the vicinity of TD and one $[1-10]$ axis corresponds to the intersection of the (111) and (-1-11) slip planes.

The distribution of disorientation axes for deformed single crystals (i.e. the disorientation relationship between adjacent pixels of the orientation map) was analysed based on stereographic projections on the compression plane, i.e. for the ED-TD reference system. Since the disorientation axes result from the activity of certain slip systems, preferences in the distribution of disorientation axes are conditioned by the movement of dislocations in particular slip systems.

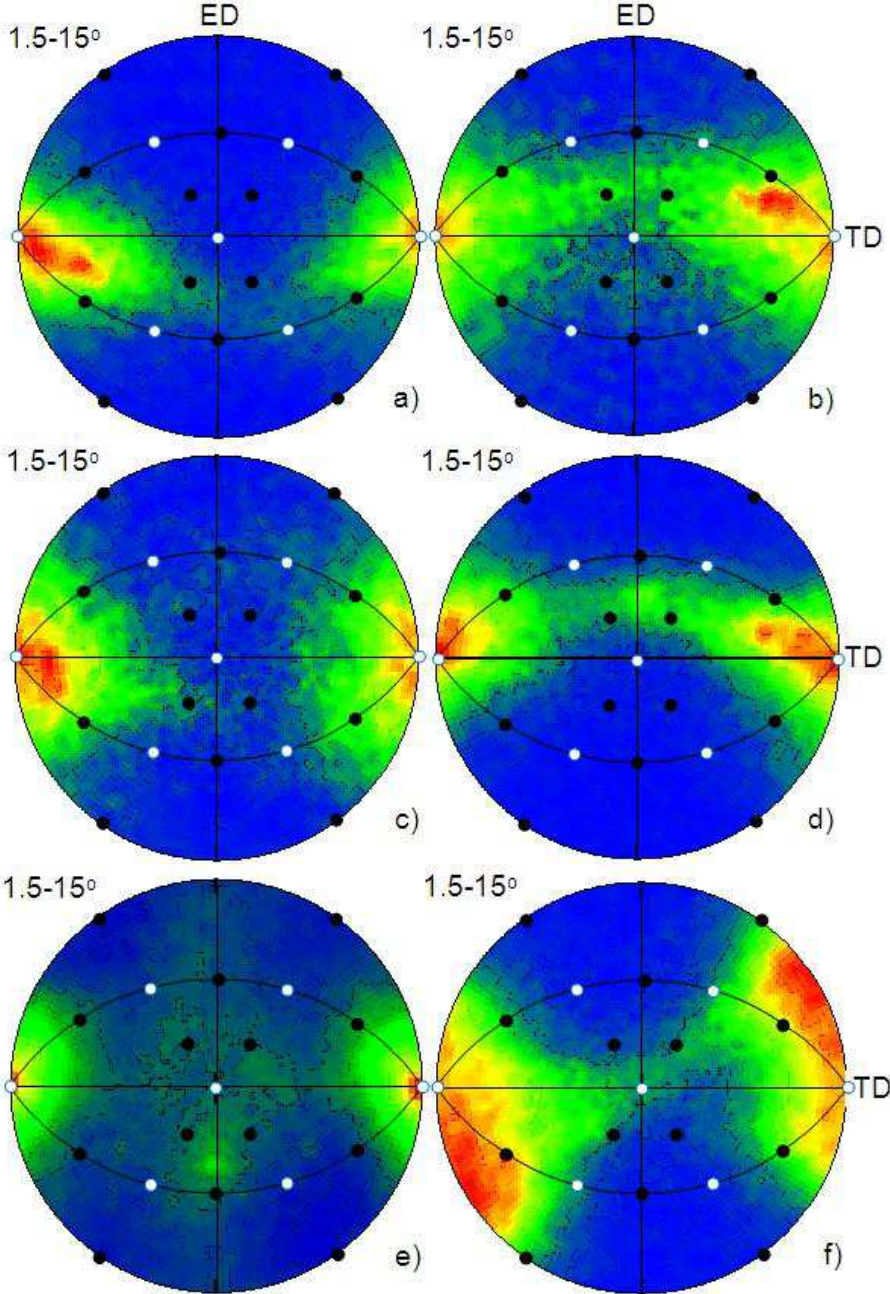
In the case of Goss oriented crystallites, it can be established that in most of the observed cases, the maximum density of disorientation axes occurred in the vicinity of TD (Fig. 5.17). It was, however, quite clear that a precise overlapping of the maximum density with the transverse direction only rarely occurred. The most frequent axes were those near $\langle 012 \rangle$, $\langle 221 \rangle$, $\langle 111 \rangle$ and $\langle 112 \rangle$ (but lying near TD). An additional maximum of densities near ED was sometimes observed - e.g. Al-1%Mn (60%) and ND – Cu (40% and 60%), Ni (60%).

These tendencies were clearly noticeable for Ni crystal deformed 40% (Fig. 5.17 e)), where two maxima of disorientation axes were observed. On the one hand, the distribution of disorientation axes displays a strong scattering with a pronounced inclination to a clear maximum near the $[-120]$ direction. (It is important to remember that the trace of intersection of the active (111) and (11-1) planes coincides with TD). On the other hand, the stretching is sufficiently wide to observe disorientation axes near $[-221]$.

In the case of brass $\{110\}\langle 112 \rangle$ oriented crystallites, the distribution analysis of the disorientation axes displays a 'departure' of the maximum from TD (Fig. 5.18). (It should be emphasized that for brass oriented crystals, the trace of the intersection of the active slip planes, as observed on the compressions plane, is inclined by 35° from TD). In most cases the maximum of disorientation axes are located in the 'range' between TD and the direction set by the intersection trace of the (111) and (11-1) planes, e.g. planes most active during deformation. This was accompanied by a wide spectrum of disorientation axes between $[-11-1]$ (\parallel TD), $[-22-1]$ (location of maximum density), $[-110]$ (intersection trace of slip planes) with a wide 'broadening' to $[-12-1]$ (i.e. scattering towards ND axis).

The observed orientation changes were not accidental. Most of the rotations occur around axes lying close to TD away from, and almost back to, the initial crystal orientation. In samples which were more strongly rotated from the ideal brass position, those cyclic orientation variations correspond to the general unstable behaviour of the crystallite and the crystal lattice rotation towards $\{112\}\langle 110 \rangle$ [Paul *et al.* (2008b)]. Apart from the rotation axes

close to $\langle 112 \rangle$, also disorientation axes close to the $\langle 111 \rangle$ crystallographic directions (\parallel TD) were found. It is suggested that the slip could have occurred on the most stressed slip systems, since an imbalance of slip on those two systems leads to a rotation around the $\langle 111 \rangle$ axis.



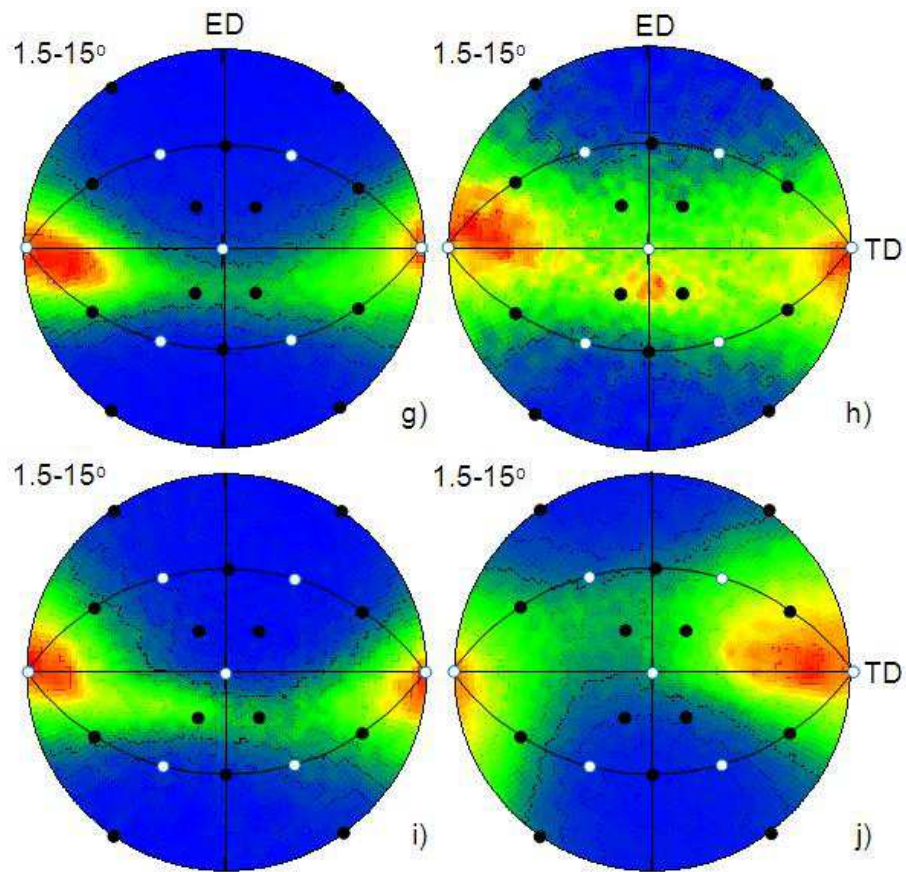
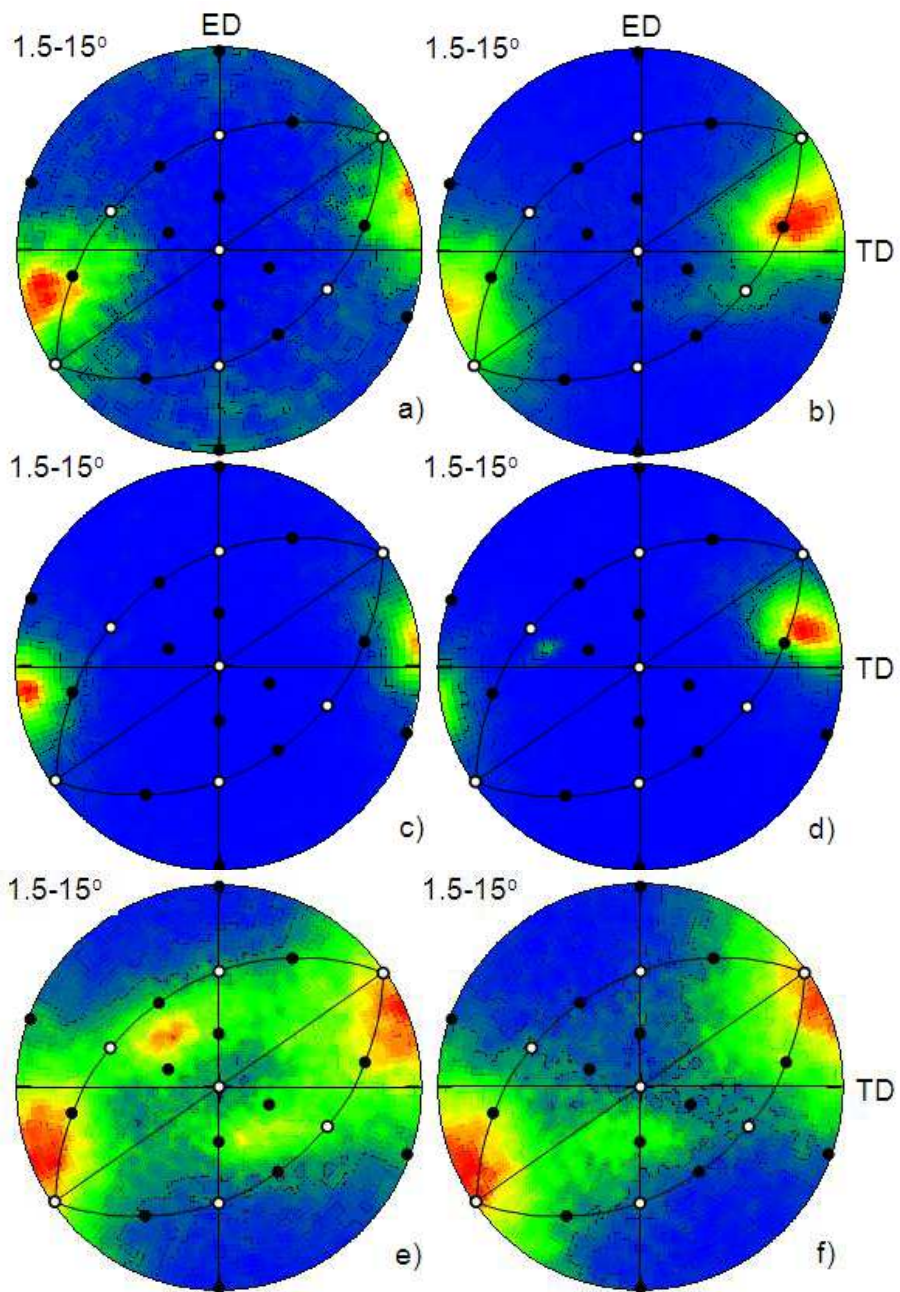


Fig. 5.17. Disorientation axis projections of: (a) and (b) - Al, (c) and (d) - Al-1%Mn, (e) and (f) - Ni, (g) and (h) - Cu, (i) and (j) - Cu-2%Al crystals. 1st and 2nd columns show samples after a strain of 0.51 and 0.92, respectively. Single crystals of (110)[00-1] orientation.



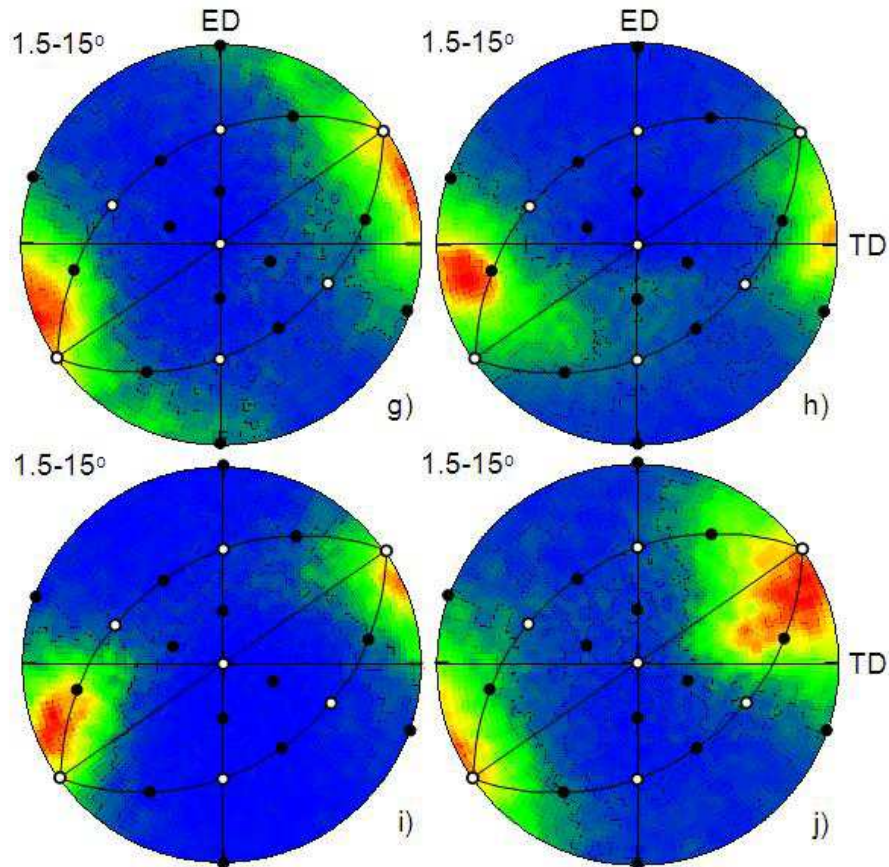


Fig. 5.18. Disorientation axis projections of: (a) and (b) - Al, (c) and (d) - Al-1%Mn, (e) and (f) - Ni, (g) and (h) - Cu, (i) and (j) - Cu-2%Al crystals. 1st and 2nd columns show samples after a strain of 0.51 and 0.92, respectively. Single crystals of (110)[1-1-2] orientation.

5.1.3.3. Microband structure development

For both sample orientations, two sets of dislocation walls make up the preferred dislocation substructure observed in the ND-ED plane (longitudinal sections) after deformations of 0.51 and 0.92. The small differences in the inclination of the dislocation boundaries with respect to ED were due to the orientation of the initial crystal lattices.

The problems of the exact microband alignment, the spatial variations in orientation and the crystallographic character of dislocation slip have been pointed out many times in the past. In both crystal orientations, the traces of the microband boundaries correspond to the preferred

slip systems. Since both crystals show a relatively high orientation stability, the calculated disorientations are very low ($<10^\circ$). Only in some cases do small regions near the corners of the sample show a significantly stronger scattering of the orientations; the spread of the orientations distinguished was $\sim 15^\circ$. However, the majority of the disorientation axes were always lying close to TD. The regions of stronger crystal lattice rotation were the privileged places for the nucleation of new grains after annealing.

Microband alignment is by nature only approximate since the microbands become rapidly broken into segments which make various angles with the (sample) external directions, e.g. ED. For the case of polycrystalline materials, the deformed grains of (nominally) stable orientations are characterized by a relatively wide spread of local orientations, e.g. due to interaction with neighbouring grains, so that the microbands should be correlated with the local parameters rather than their averages [Godfrey *et al.* (1998), Winther *et al.* (2000), Winther (2003), Winther *et al.* (2004), Hurley *et al.* (2003), Bate *et al.* (2005), Humphreys and Bate (2006)]. Lately Albou *et al.* [Albou *et al.* (2010)] have conducted a systematic study of microband alignments in the brass oriented Al crystals and found that in the range of strain used here (0.5-1) the microbands coincide closely with the slip plane traces. This is not necessarily valid for lower or higher strains.

The presented orientation maps confirm the periodic nature of the orientation changes. The observed microstructures revealed periodic orientation changes along line scans at microband boundaries. As a result of the operation of different slip systems within particular microbands, opposite rotations leading to different orientations are observed. Very often neighbouring microbands are disoriented $\sim 8-10^\circ$ by a rotation near TD. Along the line scan, the orientations varied in a characteristic periodic manner, as described earlier for Al-0.3%Mn alloy [Paul *et al.* (2008b), Miszczyk *et al.* (2011)].

6. PARTIALLY RECRYSTALLIZED STATE

To clarify the description of the mechanisms governing the early stages of recrystallization, the different cases of nucleation will be analyzed and discussed separately for the two groups of metals, i.e. the high SFE metals that do not undergo twinning (Al and Al-1%Mn) and those that can twin during recrystallization (Ni, Cu and Cu-2%Al). Special attention will be paid to the occurrence of single isolated grains, i.e. the recrystallized areas without recrystallization twins, surrounded by high angle grain boundaries and their relation with respect to the nearest deformed matrix. Of course the author is aware that microstructures represented by orientation maps are only ‘images’ observed on the section and do not take into consideration events (mainly recrystallization twinning) occurring below the surface. Therefore, *the analysis focuses on the occurrence (during recrystallization) of single isolated grains in non-twinned materials and which is crucial to explain the grain nucleus orientation relation with respect to the orientation of the deformed neighbourhood.*

The reference literature on twinning of high SFE metals is very limited and the dominating view is that recrystallization twins in Al and its alloys do not occur. However, in the present work, some recrystallisation twins were observed in this group of metals. But it is important to note that twinning in the recrystallized phase even if it occurs, plays practically no role in the formation of the texture ‘image’ of fully recrystallized state.

At the beginning of recrystallization the volume fraction of the recrystallized phase was usually small. But the statistics were always sufficient to identify preferred orientation relationship across the recrystallization front. Excluding the cases of copper for both orientations, the number of single grains surrounded by a deformed matrix, was found to be between a few tens and several hundreds.

6.1. Early stages of recrystallization in metals of high SFE

The analyses performed in this part of the thesis concern the behaviour of pure aluminium and Al-1%Mn at the early stages of recrystallization. For both metals and both orientations, the initial stages of recrystallization were analysed for two deformations, i.e. 0.51 and 0.92 (Figs. 6.1-6.4). In most cases (for applied annealing times), single isolated grains of homogeneous

orientation surrounded entirely by deformed regions were observed. Only rarely did they tend to be grouped in compact chains.

For the lower deformation emphasis was placed on statistical analyses, to describe preferences in orientation relation between the recrystallized grains and their adjacent deformed surrounding. Orientation maps, covering large areas (tens of thousands μm^2) in which the first recrystallized grains appeared, were analysed. For the larger deformation, the analysis focused on selected cases of the formation of orientations of 'early' grains, and an attempt was made to explain their relationship with orientation groups recognized in the deformed state.

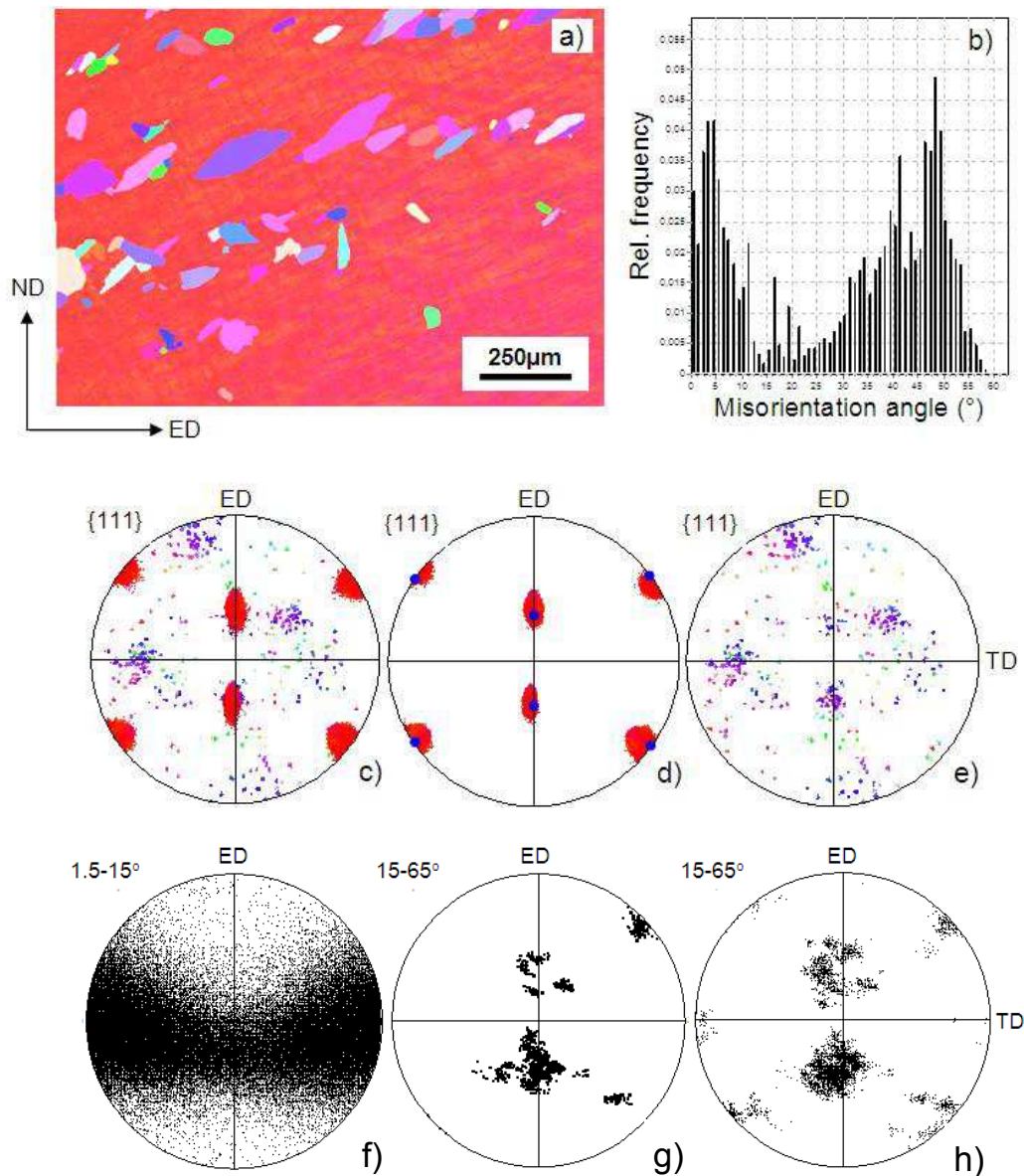


Fig. 6.1. Early stage of recrystallization in Al single crystal of (110)[00-1] orientation. (a) Orientation map, (b) disorientation angles distribution for whole orientation map, (c) - (e) the {111} pole figures showing orientations of (c) whole map, (d) only deformed crystal and (e) only recrystallized grains. (f) - (h) Disorientation axis projections: (f) only between pixels of the deformed state, (g) between recrystallized grain and the deformed state for single isolated grains and (h) between all recrystallized grains and the deformed state. Sample deformed to a strains of 0.51 and then recrystallized at 618K for 25s.

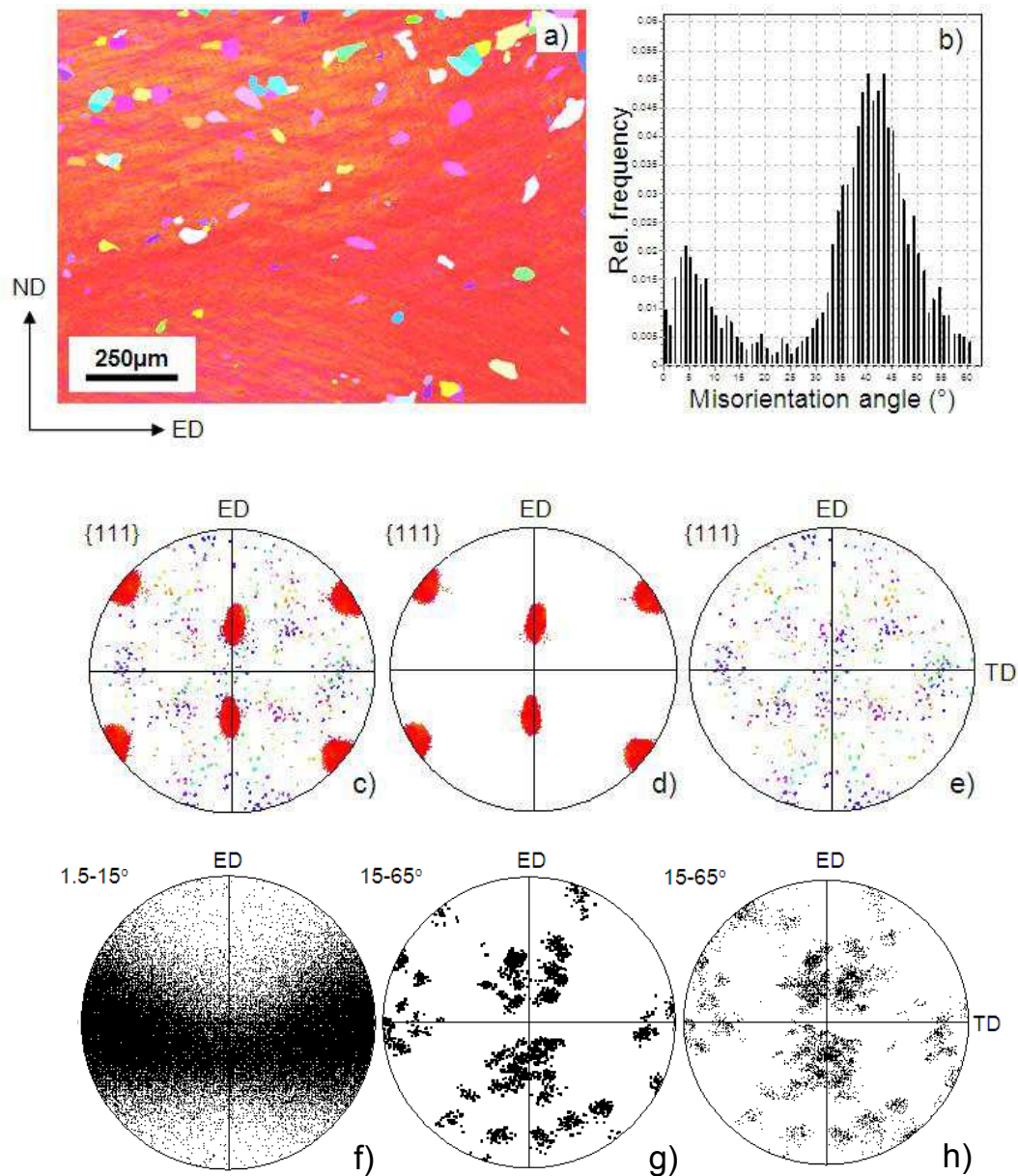


Fig. 6.2. Early stage of recrystallization in Al-1%Mn single crystal of (110)[00-1] orientation. (a) Orientation map, (b) disorientation angles distribution for whole orientation map, (c) - (e) the {111} pole figures showing orientations of (c) whole map, (d) only deformed crystal and (e) only recrystallized grains. (f) - (h) Disorientation axis projections: (f) only between pixels of the deformed state, (g) between recrystallized grain and the deformed state for single isolated grains and (h) between all recrystallized grains and the deformed state. Sample deformed up to a strains of 0.51 and then recrystallized at 686K for 25s.

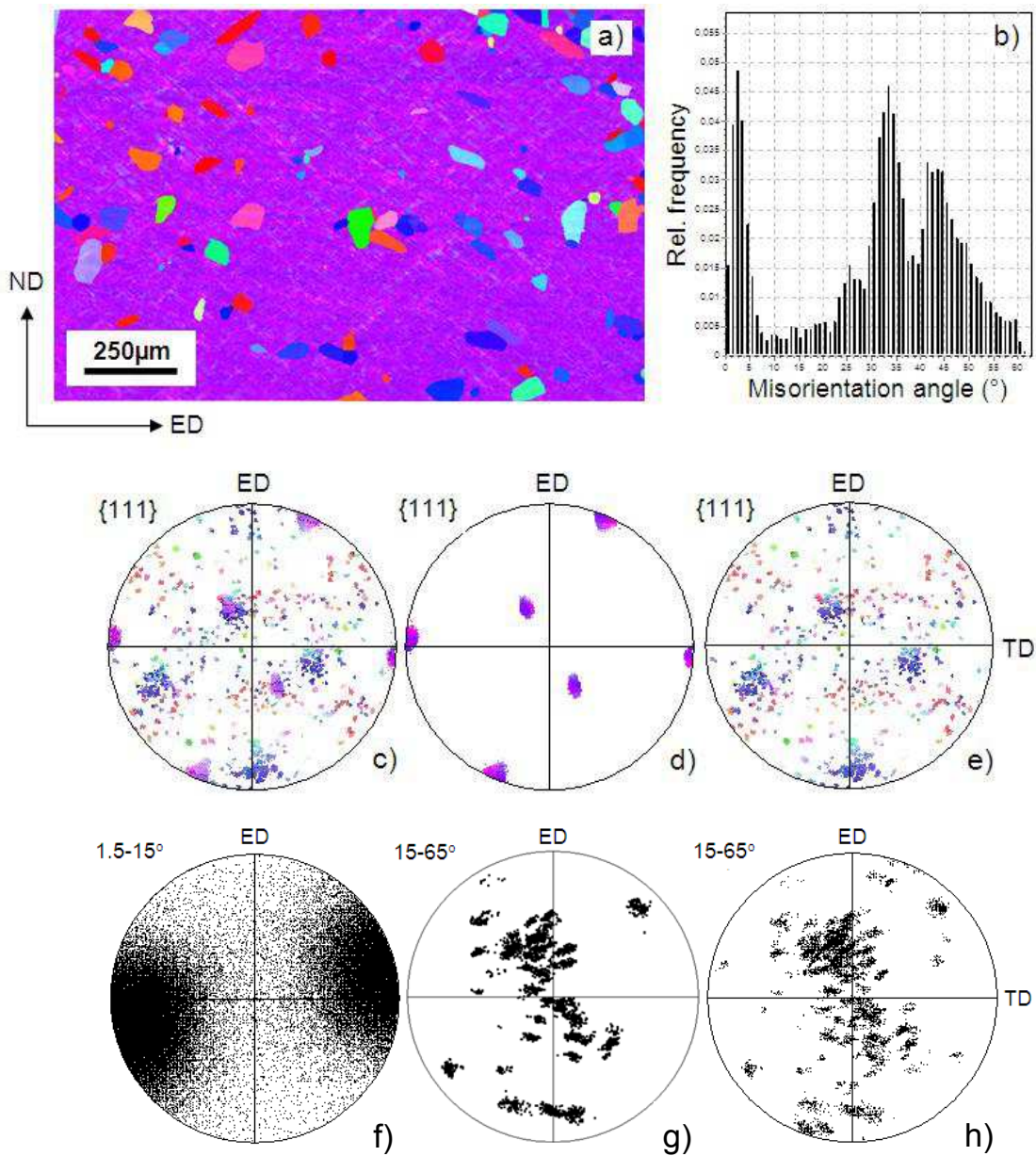


Fig. 6.3. Early stage of recrystallization in Al single crystal of $(110)[1-1-2]$ orientation. (a) Orientation map, (b) disorientation angle distribution for whole orientation map, (c) - (e) the $\{111\}$ pole figures showing orientations of (c) whole map, (d) deformed state and (e) recrystallized state. (f) - (h) Disorientation axis projections: (f) only between pixels of the deformed state, (g) between recrystallized grain and the deformed state for single isolated grains and (h) between all recrystallized grains and the deformed state. Sample deformation 0.51 and then recrystallized at 696K for 25s.

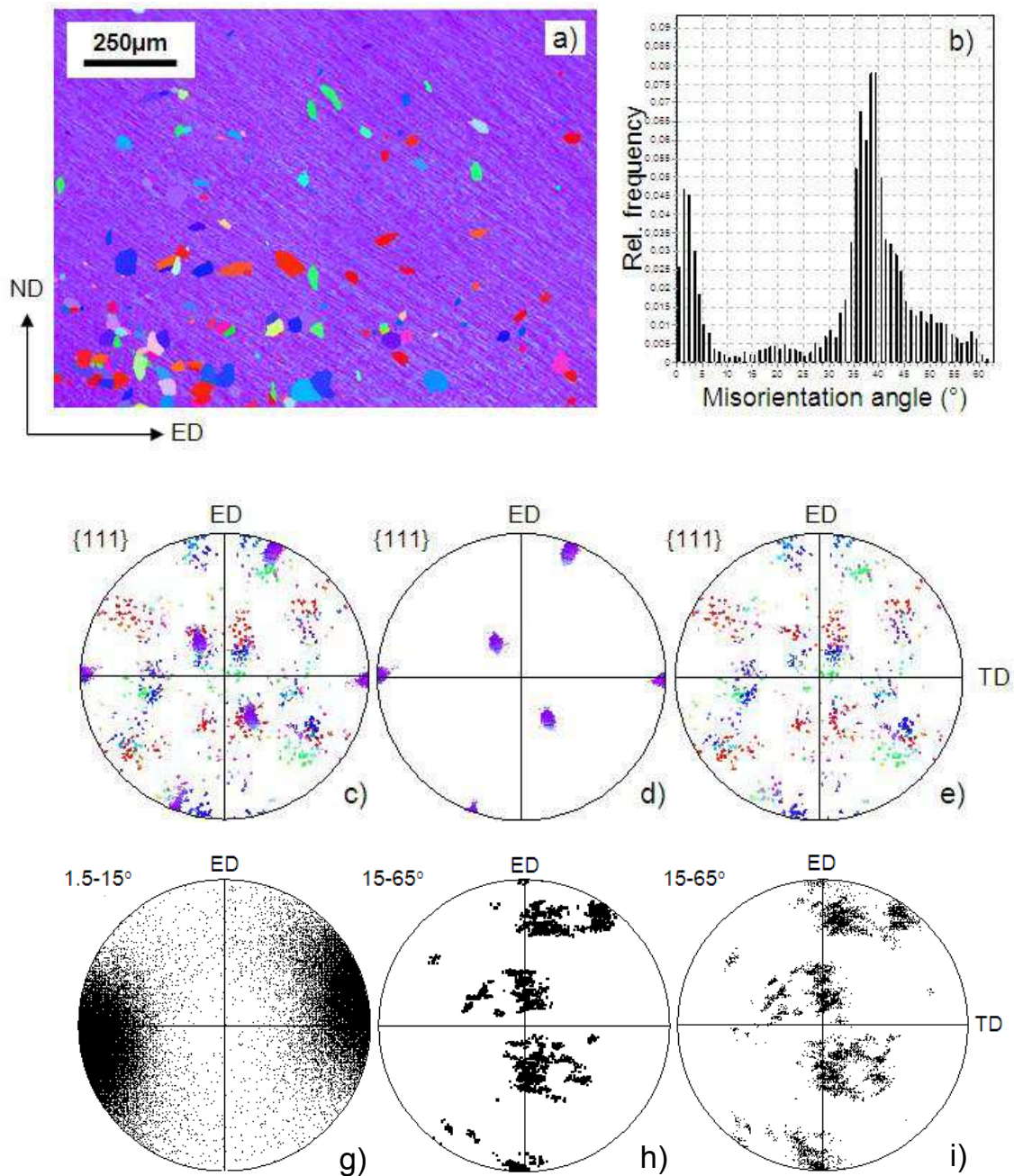


Fig.6.4. Early stage of recrystallization in Al-1%Mn single crystal of (110)[1-1-2] orientation. (a) Orientation map, (b) disorientation angle distribution for whole orientation map, (c) - (e) the {111} pole figures showing orientations of (c) whole map, (d) only deformed state and (e) only recrystallized state. (f) - (h) Disorientation axis projections: (f) only between pixels of the deformed state, (g) between recrystallized grain and the deformed state for single isolated grains and (h) between all recrystallized grains and the deformed state. Sample deformed up to logarithmic strains of 0.51 and then recrystallized at 696K for 30s.

6.1.1. General description of the recrystallization process - large area analysis based on SEM/EBSD orientation maps

After short annealing only discontinuous recrystallization was observed. New grains nucleate preferentially in small areas characterized by relatively large crystal lattice rotation (usually areas situated near the top corners of the sample). The process of new grain formation coincides with a drastic decrease of the dislocation density within the deformed substructures. The dislocation density in the cell walls decreases and isolated dislocations and narrow dislocations dipoles are annealed out of the cell interior. In accordance with the literature [Humphreys and Hatherly (2004a)] no ‘special crystallographic differences’ between deformed and recovered structures were observed. Recrystallization twins occurred only sporadically. Therefore, the process of recrystallization twinning basically does not disturb the analysis of textural transformation in metals of high SFE.

The orientation maps for both metals and both initial orientations deformed up to 0.51 are presented in Figs. 6.1-6.4. Single isolated grains constitute a significant part of the recrystallized fraction. Only in rare cases do these grains show a tendency to form complex chains. Most of the grains are of nearly equiaxed morphology. But in many cases, the recrystallized grains were found to have an elongated morphology, with the longer axes (in longitudinal section) closely parallel to the traces of the {111} planes, on which the most active slip system operates, as is visible in the SEM/EBSD maps in Figs. 6.1 c), 6.2 c), 6.3 c), 6.4 c).

Figures 6.1 a) and 6.3 a) (for Al), Figs. 6.2 a) and 6.4 a) (for Al-1%wt.Mn) show the orientation maps, the {111} pole figures calculated separately for the deformed (Fig. 6.1 f), 6.2 f), 6.3 f), 6.4 f)) and the recrystallized ‘grains’ (Fig. 6.1 g)-h), 6.2 g)-h), 6.3 g)-h), 6.4 g)-h)), as well as the corresponding distribution of the disorientation axes between new grains and the nearest deformed areas (Fig 6.1 b), 6.2 b), 6.3 b), 6.4 b)). All {111} pole figures and the disorientation axis distribution are presented in the ED-TD sample coordinate system.

High-angle boundaries appear only between the deformed state and the recrystallized state. The distribution of disorientation angle values for high-angle boundaries corresponding to orientation maps shows the prevalence of values ranging between 30 and 50° (Fig 6.1 b), 6.2 b), 6.3 b), 6.4 b)).

As expected, the deformed (in fact recovered) textures show a relatively high stability for both orientations (and for both metals) after a strain of 0.51 (see Figs. 6.1 c), 6.2 c), 6.3 c), 6.4 c)). The orientations of the new isolated grains (i.e. completely surrounded by the deformed matrix) are scattered but not random. It is clear that some new grain orientations are more populated than others. This, non-random, 'nucleation' of the new grain orientations leads to preferred disorientation axes and angles in the orientation relationships between the deformed and recrystallized areas.

6.1.2. Disorientation angle and disorientation axes distribution

The disorientation axes between particular pixels of the recovered state were generally similar to those observed in the deformed state. Most of the disorientation axes coincide with $\langle 111 \rangle$ and $\langle 011 \rangle$ directions for the brass and Goss oriented samples, respectively. However, a discernible scattering towards some other axes (also near TD) was also observed, as discussed earlier for the deformed state.

The disorientation axis distribution between neighbouring regions of deformed/recovered crystals and their distribution observed across the recrystallization front differ strongly. Figures 6.1 g)-h), 6.3 g)-h) (for Al) and 6.2 g)-h) also 6.4 g)-h) (for Al-1%wt.Mn) show the disorientation axes distributions in the ED-TD sample coordinate system. The disorientations were calculated separately for the deformed (recovered) areas (between adjacent pixels of the deformed state) and across the recrystallization front (between the new grains and the nearest deformed neighbourhood). The latter orientation relationship was analysed separately for single isolated grains (Fig. 6.1 g), 6.2 g), 6.3 g), 6.4 g)) and the same grains together with the grains involved into the chains (Fig. 6.1 h), 6.2 h), 6.3 h), 6.4 h)). However, as can be seen, the observed differences were very small.

The general conclusion that can be drawn from the comparison of the preferred disorientation axes is that there is a lack of 'correspondence' between the distribution for the deformed crystal and the one identified across the recrystallization front. This leads to the first significant conclusion: the *dislocation mechanisms responsible for crystal lattice rotations during deformation do not exactly 'match' those controlling the formation of the recrystallized grains.*

It is evident that the formation of new grain orientations, which is not random, leads to some preferences in the distribution of the disorientation axes between the deformed and recrystallized areas. This orientation relationship, usually described in the literature by α <111> relations, is in fact very rarely observed. Figure 6.3 g) shows that only a relatively small fraction of the disorientation axes coincide with poles of the {111} planes. The most populated disorientation axes were usually shifted towards the <221>, <012>, <123> or <112>, lying close to selected normals of the {111} slip planes, with which the dislocation boundaries mostly align. The most populated disorientation angles in the disorientation relation between the new grain and the deformed areas varied between 30° and 50°, as visible in Figs. 6.1 b), 6.2 b), 6.3 b), 6.4 b).

The orientation maps of the samples after partial recrystallization were analysed mainly in terms of preferred disorientation distribution axes across the recrystallization front. Therefore, the first step was to divide the orientation maps into fractions of deformed and recrystallized areas. It is well documented that the orientations of recrystallized grains are different from those defining the deformed state. The general rule is that the <111> poles of the deformed crystal do not coincide with the poles of the recrystallized grains. Despite the fact that the recrystallized grain orientations are heavily scattered, it can be claimed with certainty that they are not random. Only a finite number of groups of recrystallized grain orientations were observed. Their formation shows some symmetry characteristics, i.e. the texture image of the first recrystallized grains is quite symmetrical with respect to the external coordinate directions. It was noticed that if the formation of a grain orientation caused by a positive rotation around a certain axis in a given region occurs, grains with the crystal lattice of the negative rotation appear in neighbouring regions. The effect is observable for both of the analysed orientations for grains of uniform orientations (see Annexe 2, e.g.: grains R3 and R4 in the case of figure A2.10 for Al (110)[1-1-2] or grains R2 and R3 in the case of figure A2.12 for Al-1%Mn). However, the effect is observed evidently when recrystallisation twins occur (see, e.g.: Fig. 6.23 for Al (110)[00-1], Fig. 6.34 for Cu (110)[00-1] and Figs. 6.38 and 6.39 for Cu (110)[1-1-2]). In the latter cases the normals of the twinning planes lie close to the rotation axis (between deformed and recrystallized states).

Further analysis of the disorientation axis distribution provides some other interesting information. In Figs. 6.1-6.4f) it can be seen that for the deformed (recovered) crystal the distribution of disorientation axes between adjacent pixels of the orientation map corresponds

to the 'image' obtained for orientation maps of the 'post deformation' state. For the 'brass' orientation the disorientation axes are located between the $\langle 011 \rangle$ direction corresponding to the trace of the intersecting active slip $\{111\}$ planes, and the TD ($\parallel \langle 111 \rangle$) direction. Concurrently, there is a clear extension of the region where disorientation axes occur towards the ND direction (Fig. 6.3f), 6.4f). In the case of the Goss orientation, the disorientation axes between adjacent pixels of the deformed (recovered) crystal are mainly situated near TD. (Fig. 6.1 f), 6.2 f)). However, a strong scattering of the maximum density 'towards' two symmetrical $\langle 221 \rangle$ axes (situated in the compression plane) and additional 'scattering' towards ND (more precisely towards one of the $\langle 012 \rangle$ direction) are observed.

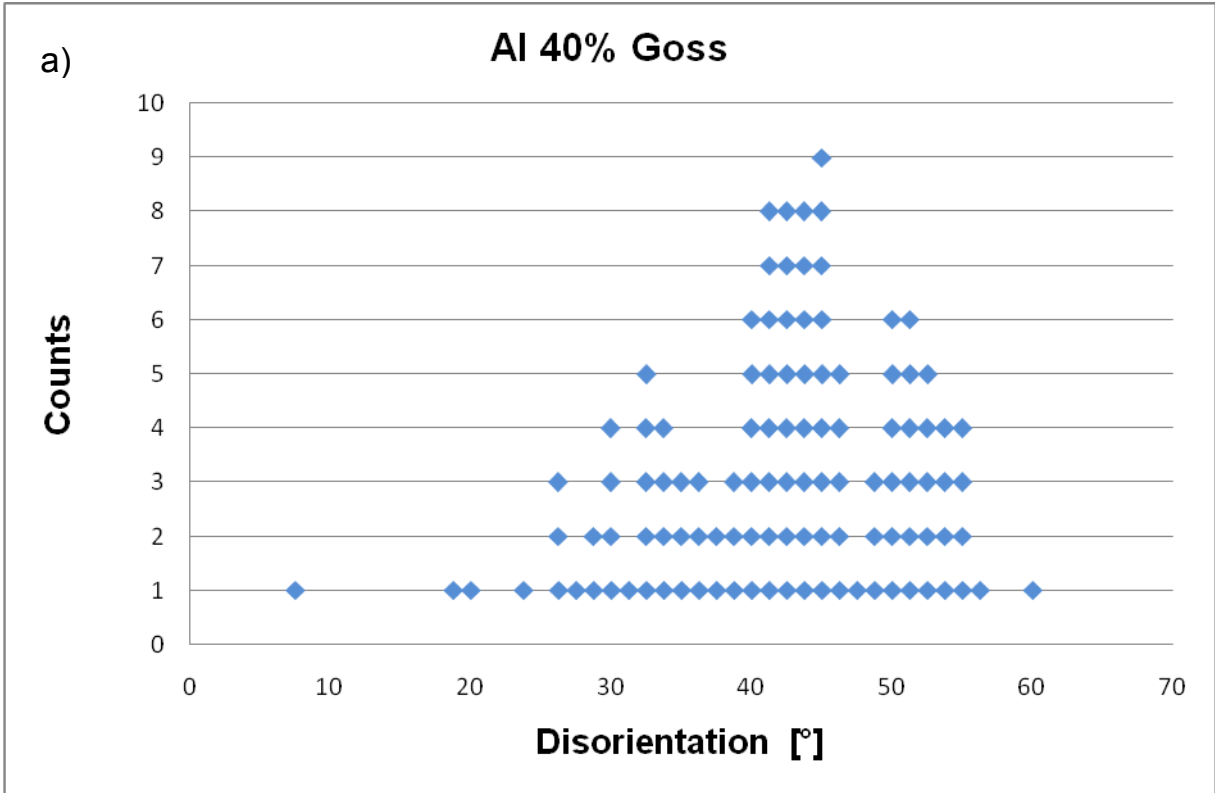
Analysis of the disorientation axes across the recrystallization front also confirms that these axes are not located randomly. For both the Goss and brass orientations (Fig. 6.1-6.4 g)), a definite majority of disorientations axes are located around the poles of the (111) and (1-1-1) planes, i.e. those of the active slip systems during deformation. *Nevertheless, the disorientation axes do not coincide exactly with the poles of these planes.* Most frequently a whole range of axes from the $\langle 111 \rangle$ poles is observed, particularly near the $\langle 012 \rangle$, $\langle 112 \rangle$ and $\langle 221 \rangle$ axes. It should be mentioned that in some rare cases, disorientation axes were found 'quite' distant from the $\{111\}$ plane poles of the active systems (including the vicinity of the two remaining $\langle 111 \rangle$ poles). This can be seen for typical cases of the orientation relations of some isolated single grains of homogeneous orientation in Annexe 2.

6.1.3. Statistical analysis of the distribution of disorientation angles and axes

In the present study, we have tried to 'statistically' describe the measured 'values' of disorientation between recrystallized grains and the surrounding deformed (recovered) areas from which these grains originate. In contrast to the preceding analysis of the individual orientation maps, this part of the study summarizes results obtained for slightly different annealing conditions (separately for the metal and orientation - Tabs. 4.2 and 4.3).

This analysis examines the distribution of disorientation angles and axes in samples deformed to strains of 0.51, for which between several tens and a few thousand disorientations could be measured.

The 'frequencies' of disorientation angles, for the orientation relationships of boundaries between isolated single grains of homogeneous orientation (surrounded by high-angle boundaries) and deformed (recovered) regions are presented in Figs. 6.5-6.6. The range of potential disorientation angles was binned by intervals of 1.25° and the number of disorientations across the recrystallization front corresponding to a given angular range was counted. The analysis proves that the prevalent range of angles across the migrating recrystallization front was between 30 and 55° and was not identical for all cases. As expected, in most cases the maximum frequency of the disorientation angles was between 40 and 45° . Only in the case of Al crystals with 'brass' initial orientation, was the maximum frequency of the disorientation angles closer to 30 - 35° (Fig. 6.6).



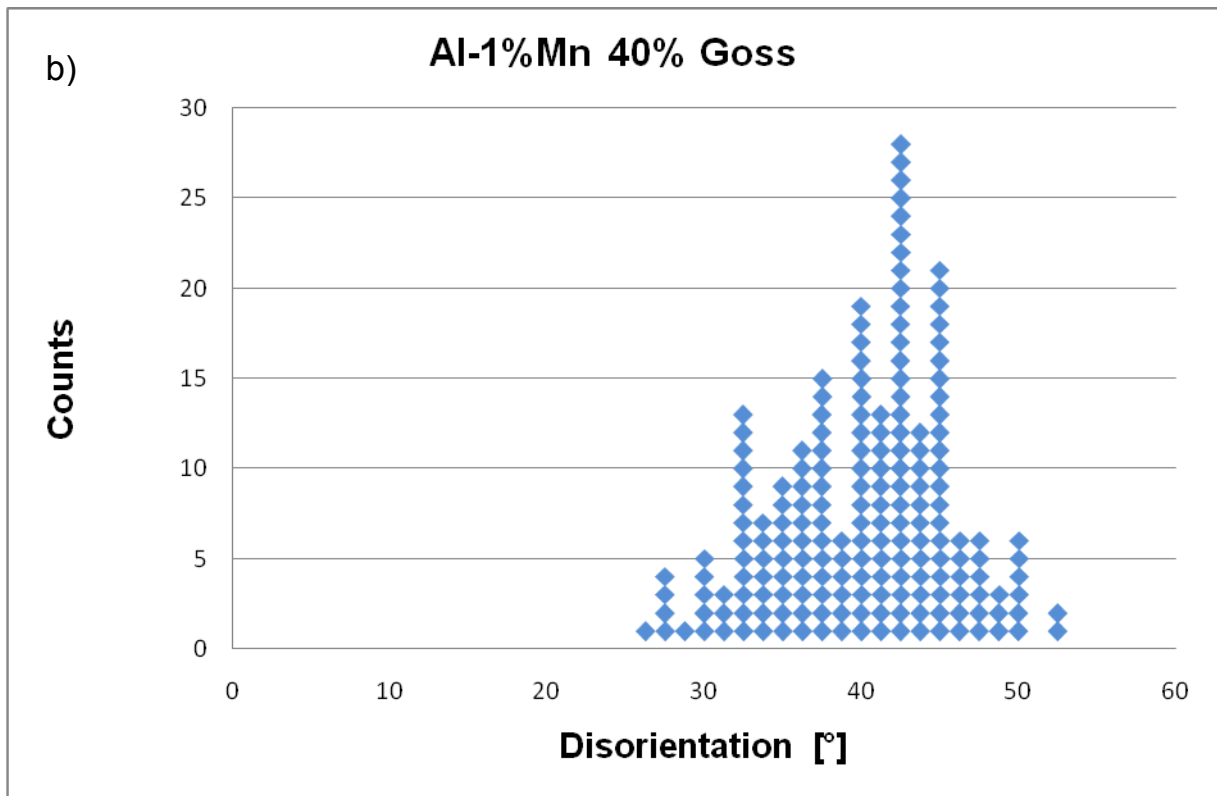
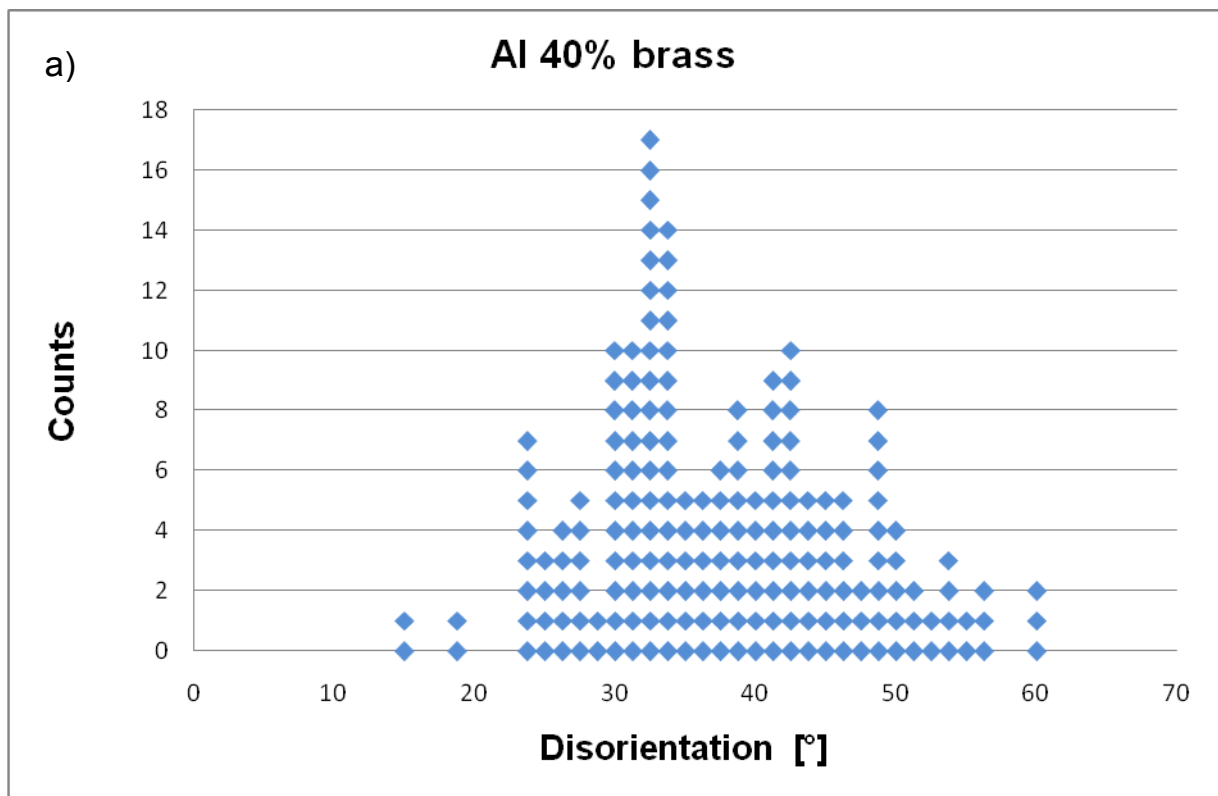


Fig. 6.5. Disorientation angle distribution for (a) Al and (b) Al-1%Mn crystals of (110)[00-1] orientation. The graph corresponds to Fig. 6.1 and Fig. 6.2 for Al and Al-1%Mn, respectively.

Disorientation relations between single isolated grains and its deformed neighborhood.



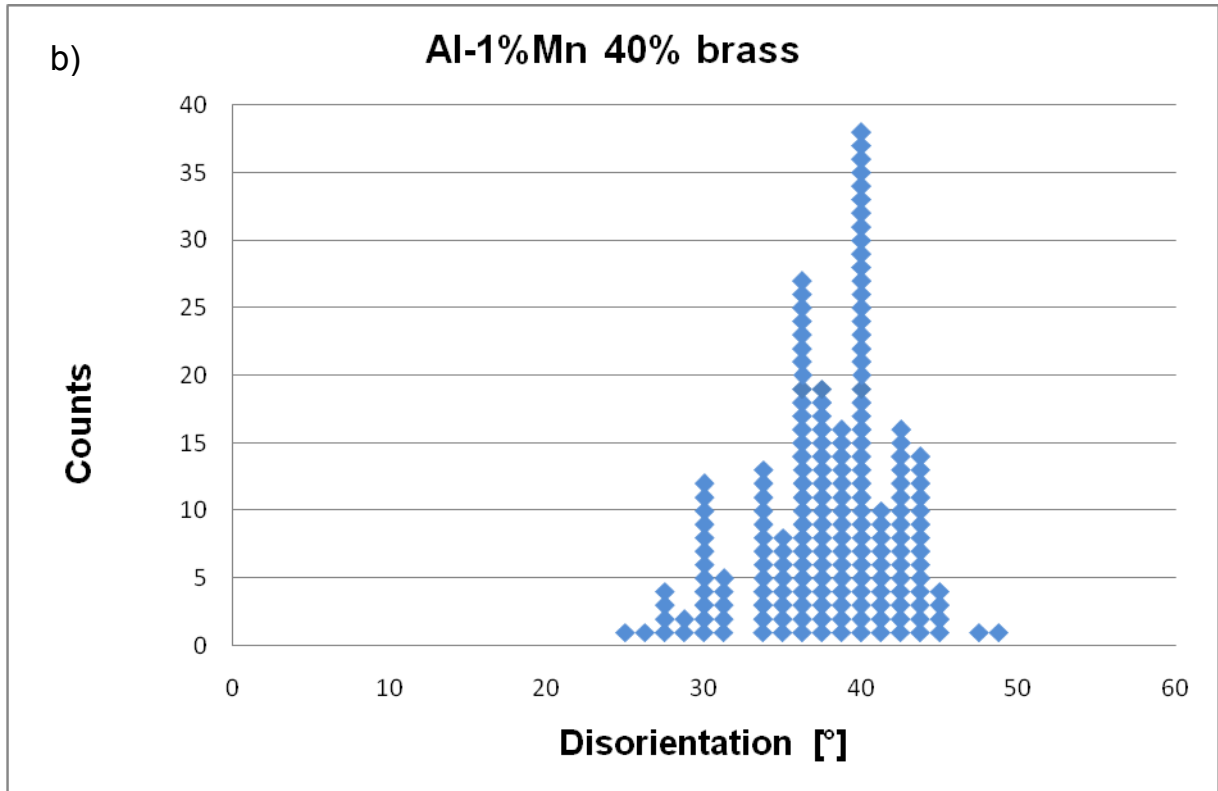


Fig. 6.6. Disorientation angle distribution for (a) Al and (b) Al-1%Mn crystals of (110)[1-1-2] orientation. The graph corresponds to Fig. 6.3 and Fig. 6.4 for Al and Al-1%Mn, respectively.

Disorientation relations between single isolated grains and its deformed neighborhood.

While the presentation of disorientation angle frequencies is relatively simple, the presentation of disorientation axis frequencies causes more serious problems. The distributions of axes depend on two parameters; more precisely, the domain of such distributions is the two-dimensional ‘standard triangle’. The question is: *how can we describe the preferences in the grouping of disorientation axes?*

We have chosen to classify the disorientation axes into 7 groups represented by $\langle 001 \rangle$, $\langle 011 \rangle$, $\langle 012 \rangle$, $\langle 111 \rangle$, $\langle 112 \rangle$, $\langle 122 \rangle$ and $\langle 123 \rangle$ low-index axes. These particular axes frequently appear in analyses of orientation relationships of grains on both sides of the recrystallization front, and are located in various ‘sectors’ of the standard triangle.

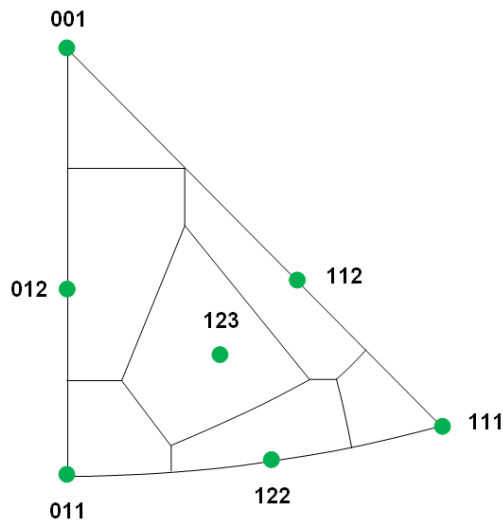


Fig. 6.7. Schematic of the division of the standard triangle into 7 regions containing particular classes of disorientation axes.

Based on these selected axes, the standard triangle is split into 7 regions using Voronoi tessellation: each region consists of all points closer to a given selected axis than to any other. For an experimentally determined disorientation axis, its angular 'distance' to the selected class defining axes was calculated, and the experimental axis was ascribed to the class represented by the selected axis with the smallest angular distance.

In order to compare the experimental axes in these classes, one should allow for the fact that the areas of the regions are not equal, and also, because of crystal symmetry, the equiprobable distribution of disorientation axes is not uniform, i.e., there is a higher or lower concentration of axes in different directions [Mackenzie (1964)]. Both factors have been taken into account in our calculations.

The calculated frequencies are collected in Tabs. 6.1 and 6.2. The columns contain the explicit number of experimental axis in a class, the percentage of axes within the class, and the fractions after accounting for the differences in the areas of regions and the impact of crystal symmetry. It can certainly be concluded that the near- $\langle 111 \rangle$ axes are not always distinguished (taking under consideration the counts of cases of particular axes). Axes belonging to the neighbourhood of $\langle 221 \rangle$ and $\langle 012 \rangle$ directions, and to a lesser degree $\langle 112 \rangle$, are equally (often even more strongly) represented. All these classes of disorientation axes are well represented in the deformed state as well.

Al (110)[00-1]						
Classification of 550 axes						
Classes	Counts	[%]	Rand1 [%]	Rand2[%]	Distrib1	Distrib2
0 0 1	1	0.18	10.0	6.3	0.02	0.03
0 1 1	8	1.45	8.7	10.8	0.17	0.14
0 1 2	13	2.36	25.2	19.5	0.09	0.12
1 1 1	125	22.73	5.0	7.1	4.54	3.22
1 1 2	126	22.91	15.5	15.1	1.48	1.52
1 2 2	188	34.18	11.4	16.3	3.00	2.10
1 2 3	89	16.18	24.2	25.0	0.67	0.65

Al-1%Mn (110)[00-1]						
Classification of 804 axes						
Classes	Counts	[%]	Rand1 [%]	Rand2[%]	Distrib1	Distrib2
0 0 1	21	2.61	10.0	6.3	0.26	0.41
0 1 1	34	4.23	8.7	10.8	0.48	0.39
0 1 2	119	14.80	25.2	19.5	0.59	0.76
1 1 1	35	4.35	5.0	7.1	0.87	0.62
1 1 2	196	24.38	15.5	15.1	1.58	1.62
1 2 2	154	19.15	11.4	16.3	1.68	1.18
1 2 3	245	30.47	24.2	25.0	1.26	1.22

- 1 - in relation to random directions on the unit sphere.
2 - in relation to DISorientation axes of random MISorientations.

Tab. 6.1. Fractions of particular classes of disorientation axes across the recrystallization front calculated for Al and Al-1%Mn single crystals of (110)[00-1] orientation. Samples deformed to strains of 0.51 and then lightly annealed.

Al (110)[1-1-2]						
Classification of 803 axes						
Classes	Counts	[%]	Rand1 [%]	Rand2[%]	Distrib1	Distrib2
0 0 1	7	0.87	10.0	6.3	0.09	0.14
0 1 1	65	8.09	8.7	10.8	0.93	0.75
0 1 2	90	11.21	25.2	19.5	0.45	0.58
1 1 1	113	14.07	5.0	7.1	2.81	1.99
1 1 2	108	13.45	15.5	15.1	0.87	0.89
1 2 2	229	28.52	11.4	16.3	2.50	1.75
1 2 3	191	23.79	24.2	25.0	0.98	0.95

Al-1%Mn (110)[1-1-2]						
Classification of 970 axes						
Classes	Counts	[%]	Rand1 [%]	Rand2[%]	Distrib1	Distrib2
0 0 1	3	0.31	10.0	6.3	0.03	0.05
0 1 1	13	1.34	8.7	10.8	0.15	0.12
0 1 2	63	6.49	25.2	19.5	0.26	0.33
1 1 1	31	3.20	5.0	7.1	0.64	0.45
1 1 2	219	22.58	15.5	15.1	1.46	1.50
1 2 2	287	29.59	11.4	16.3	2.60	1.82
1 2 3	354	36.49	24.2	25.0	1.51	1.46

1 - in relation to random directions on the unit sphere.

2 - in relation to DISorientation axes of random MISorientations.

Tab. 6.2. Fractions of particular classes of disorientation axes across the recrystallization front calculated for Al and Al-1%Mn single crystals of (110)[1-1-2] orientation. Samples deformed to strains of 0.51 and then lightly annealed.

6.1.4. The directionality of grain growth

The orientation maps (on the ND-ED plane) for both initial orientations show that a considerable number of recrystallized grains are of elongated shape. These grains exhibit a well defined lattice rotation with respect to the deformed crystal orientations. An example of the crystal lattice rotation, related to the appearance of heavily elongated grains, was carried out on Al single crystals of $\{110\}\langle 001\rangle$ and $\{110\}\langle 112\rangle$ orientations strained to 0.51 (Figs. 6.8-6.14). To a first approximation, this aspect of nucleation and grain growth leads to the following conclusions:

- the longest grain direction runs along the traces of (111) and (11-1) planes, i.e. the most active planes during strain, and which are symmetrically located to the ND-TD plane.
- The orientations of the elongated grains are related to those of the group of the deformed crystals. The crystal lattice of each of the grain groups is rotated (positively or negatively) around diverse groups of disorientation axes.
- The rotation axes are situated near the poles of (111) and (11-1) planes. This may suggest a mechanism for the formation of a new grain by thermally activation movement of dislocation families, 'travelling' in pairs on one of the above-mentioned planes. Although

the rotation axes approach the normal vector of the preferred slip planes they only rarely coincide with the exact location of the $\langle 111 \rangle$ directions.

- The crystal lattice rotation of elongated grains takes place around axes near the $\langle 111 \rangle$ pole, corresponding to the $\{111\}$ plane across which preferred grain growth occurs. This is shown by stereographic projections of the rotation axis distributions between deformed (recovered) and recrystallized regions. The crystal lattice of the grains elongated along a (111) plane undergoes rotation around axes near the $[111]$ direction. By analogy, the crystal lattice of the grains elongated along the $(11\bar{1})$ plane undergoes a rotation around the near $[11\bar{1}]$ direction.
- An explanation of these results can be based on the thermally activated, coordinated movement of dislocations. If the rotation axis lies close to the $[111]$ direction (normal of the (111) slip plane), it can be assumed that the dislocation movement (of two families) takes place on the $(11\bar{1})$ plane (Fig. 6.10). Then, the rotations by $30\text{-}50^\circ$, resulting from dislocation movement on the $(11\bar{1})$ plane, induce a 'resulting' rotation around the axis near the pole of the (111) plane. By analogy, the movement of two dislocation families on the (111) plane, inducing a rotation around axes close to the $[11\bar{1}]$ pole, may be assumed. The spread of the lattice rotation angles of individual grains for a given category may result from an 'unequal' contribution of the two dislocation families (systems) grouped on one plane. This case is very similar to that which describes twist boundary formation.
- An additional 'contribution' to the lattice rotation of a crystal is possible by the thermally activated movement of dislocations 'stored' in another system, less preferred during deformation, or the movement of a different combination of dislocation families (inactive during deformation). In each of these cases, dislocation motion must lead to slight variations of the disorientation axes. These cases seem to predominate during the transformation of the 'image' of texture at the initial stages of recrystallization.

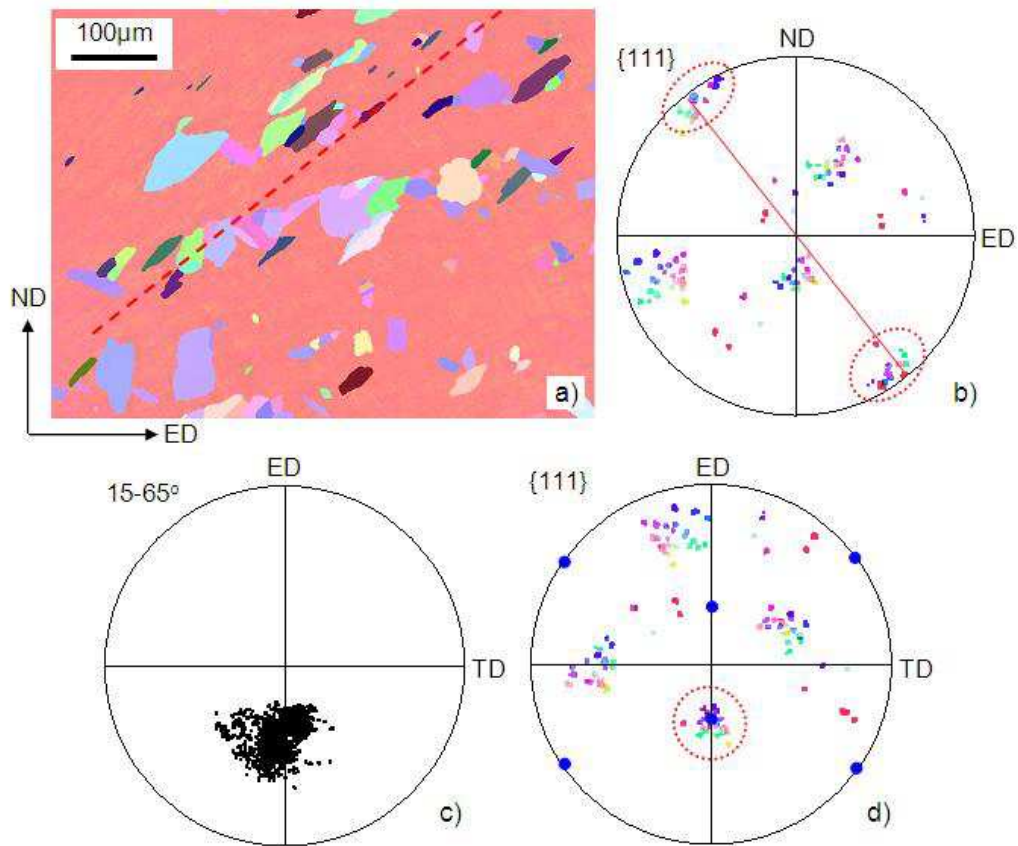


Fig. 6.8. Directionality observed at early stages of recrystallization in Al single crystal of $(110)[00-1]$ initial orientation. Privileged growth along traces of (111) planes. (a) SEM/EBSD orientation map (IPF||X color code was applied), (b) and (d) the $\{111\}$ pole figures presented in ND-ED and ED-TD planes, respectively. (c) Disorientation axes distribution in ED-TD plane. Sample deformed up to strains of 0.51 and then recrystallized at 618K for 25s. SEM/EBSD orientation measurements with step size of $2\mu\text{m}$.

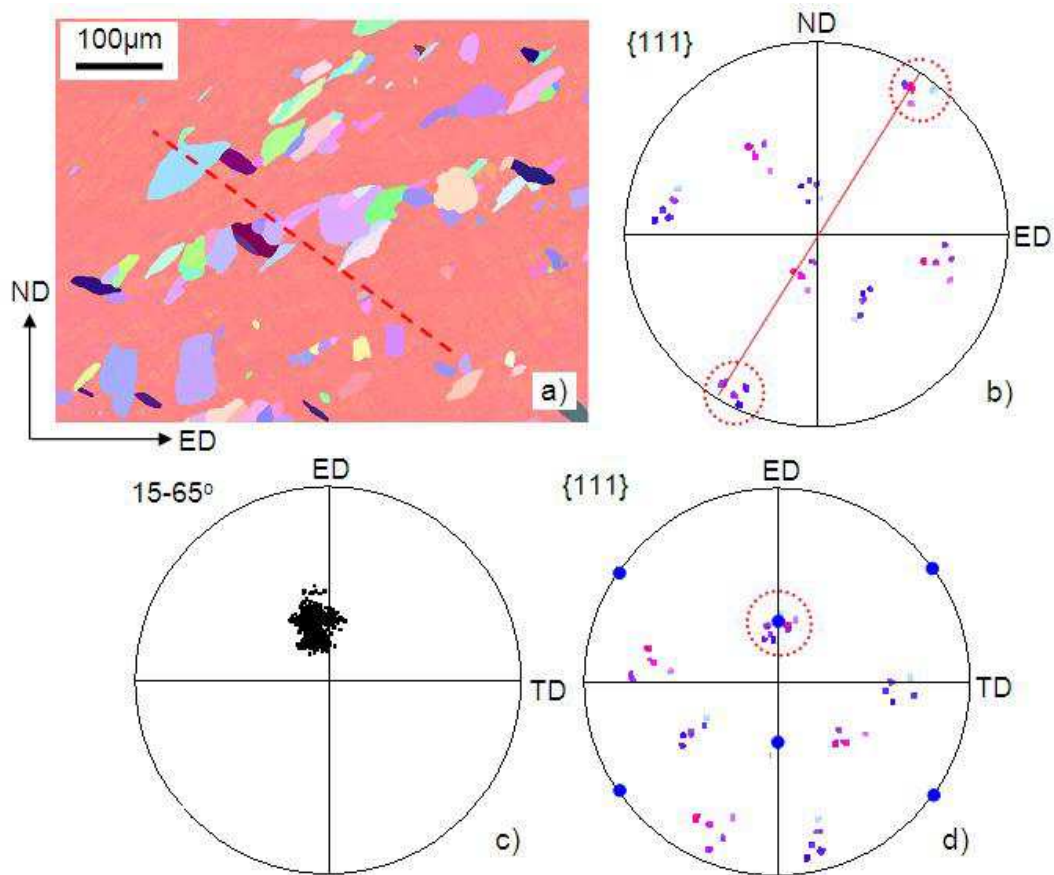


Fig. 6.9. Directionality observed at early stages of recrystallization in Al single crystal of (110)[00-1] initial orientation. Privileged growth along traces of (11-1) planes. (a) SEM/EBSD orientation map (IPF||X color code was applied), (b) and (d) the {111} pole figures presented in ND-ED and ED-TD planes, respectively. (c) Disorientation axes distribution in ED-TD plane. Sample deformed up to strains of 0.51 and then recrystallized at 618K for 25s. SEM/EBSD orientation measurements with step size of 2µm.

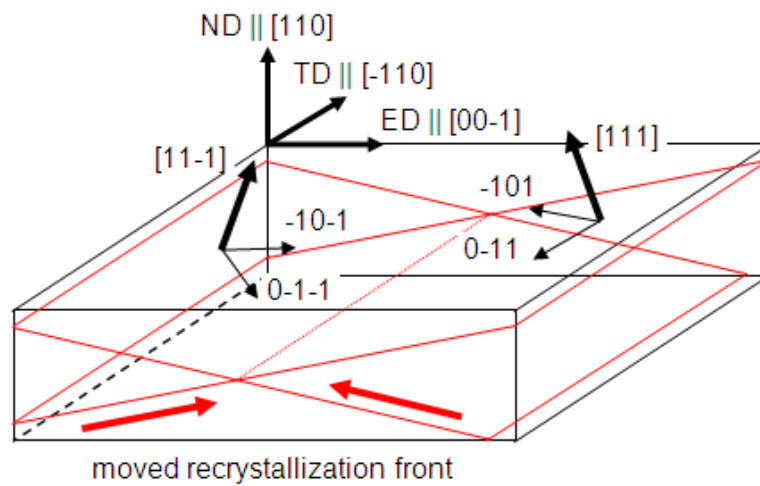


Fig. 6.10. Privileged growth at early stages of recrystallization along the most active slip planes. The traces of the most active slip systems coincide well with the directions of fastest growth in the (110)[00-1] oriented single crystal.

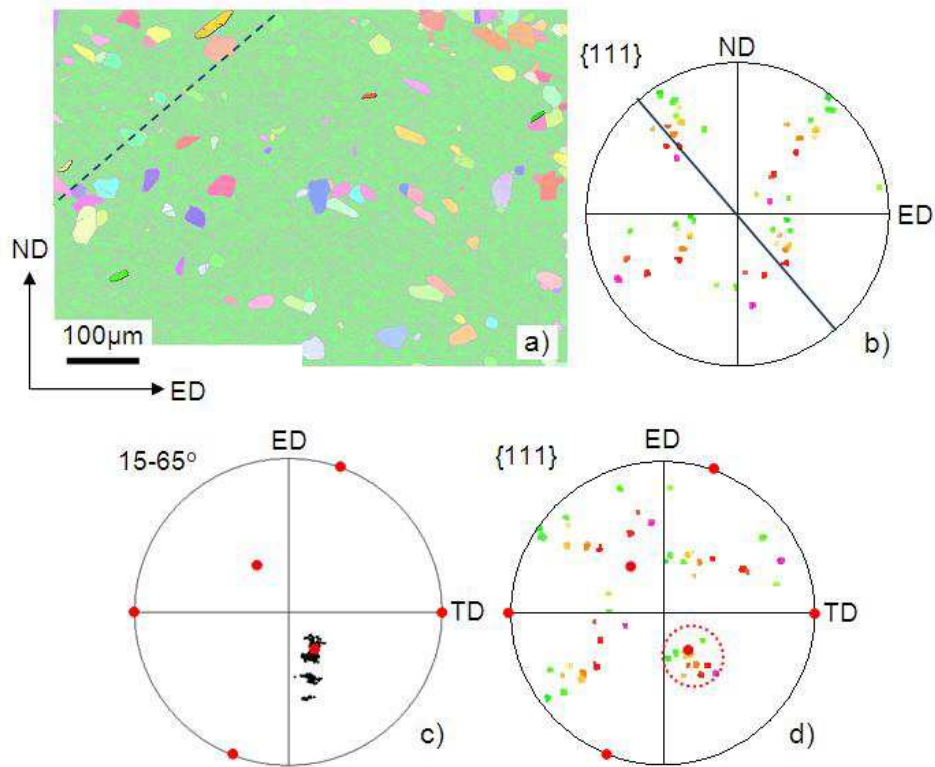


Fig. 6.11. Directionality observed at early stages of recrystallization in Al single crystal of (110)[1-1-2] initial orientation. Privileged growth along traces of (11-1) planes. (a) SEM/EBSD orientation map (IPF||X color code was applied), (b) and (d) the {111} pole figures presented in ND-ED and ED-TD planes, respectively. (c) Disorientation axes distribution in ED-TD plane. Sample deformed up to strains of 0.51 and then recrystallized at 696K for 25s. SEM/EBSD orientation measurements with step size of 2µm.

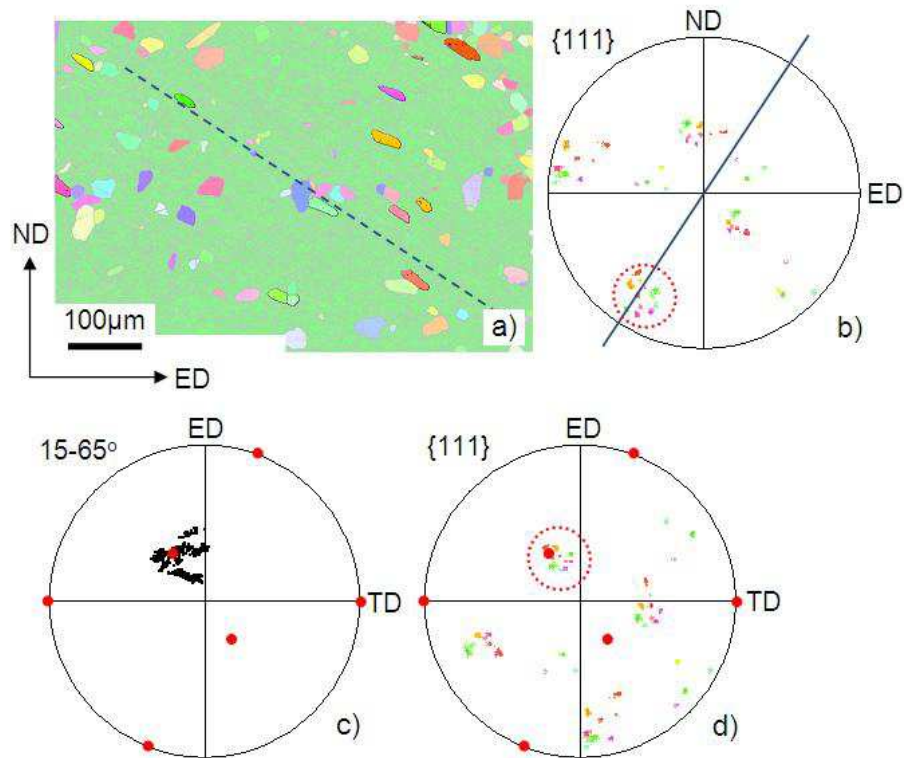


Fig. 6.12. Directionality observed at early stages of recrystallization in Al single crystal of (110)[1-1-2] initial orientation. Privileged growth along traces of (111) planes. (a) SEM/EBSD orientation map (IPF||X color code was applied), (b) and (d) the {111} pole figures presented in ND-ED and ED-TD planes, respectively. (c) Disorientation axes distribution in ED-TD plane. Sample deformation 0.51 and recrystallized at 696K for 25s. SEM/EBSD orientation measurements with step size of 2µm.

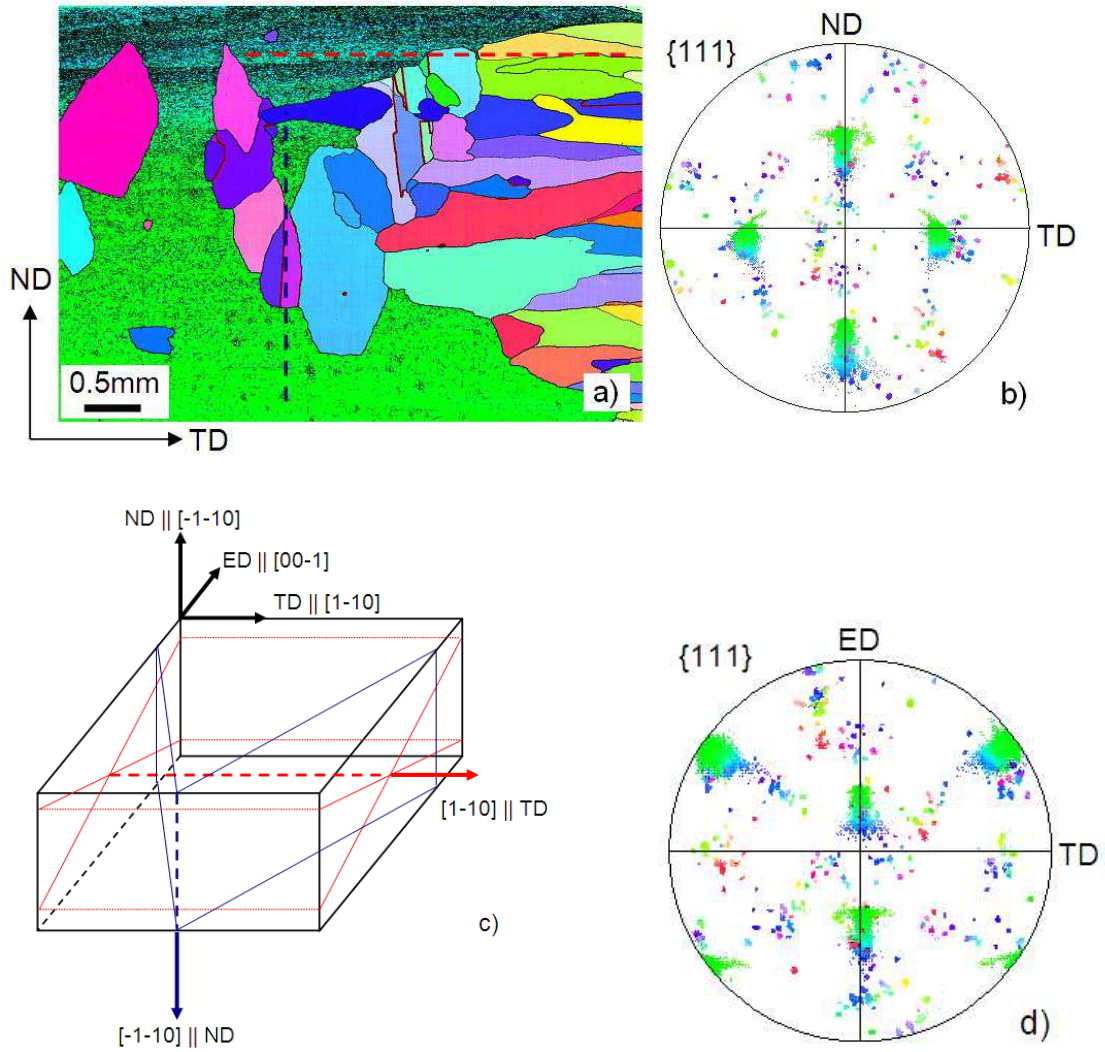


Fig. 6.13. Directionality observed at early stages of recrystallization in Al-1%Mn single crystal of (110)[00-1] initial orientation. (a) SEM/EBSD orientation map (color code - IPF ||Y) on the ND-TD plane and (b) corresponding the {111} pole figure. (c) Spatial situation of the most active slip planes. (d) The {111} pole figure on ED-TD plane. Sample deformed up to strains of 0.51 and then recrystallized at 680K for 70s. SEM/EBSD orientation measurements with step size of 2.8 μ m.

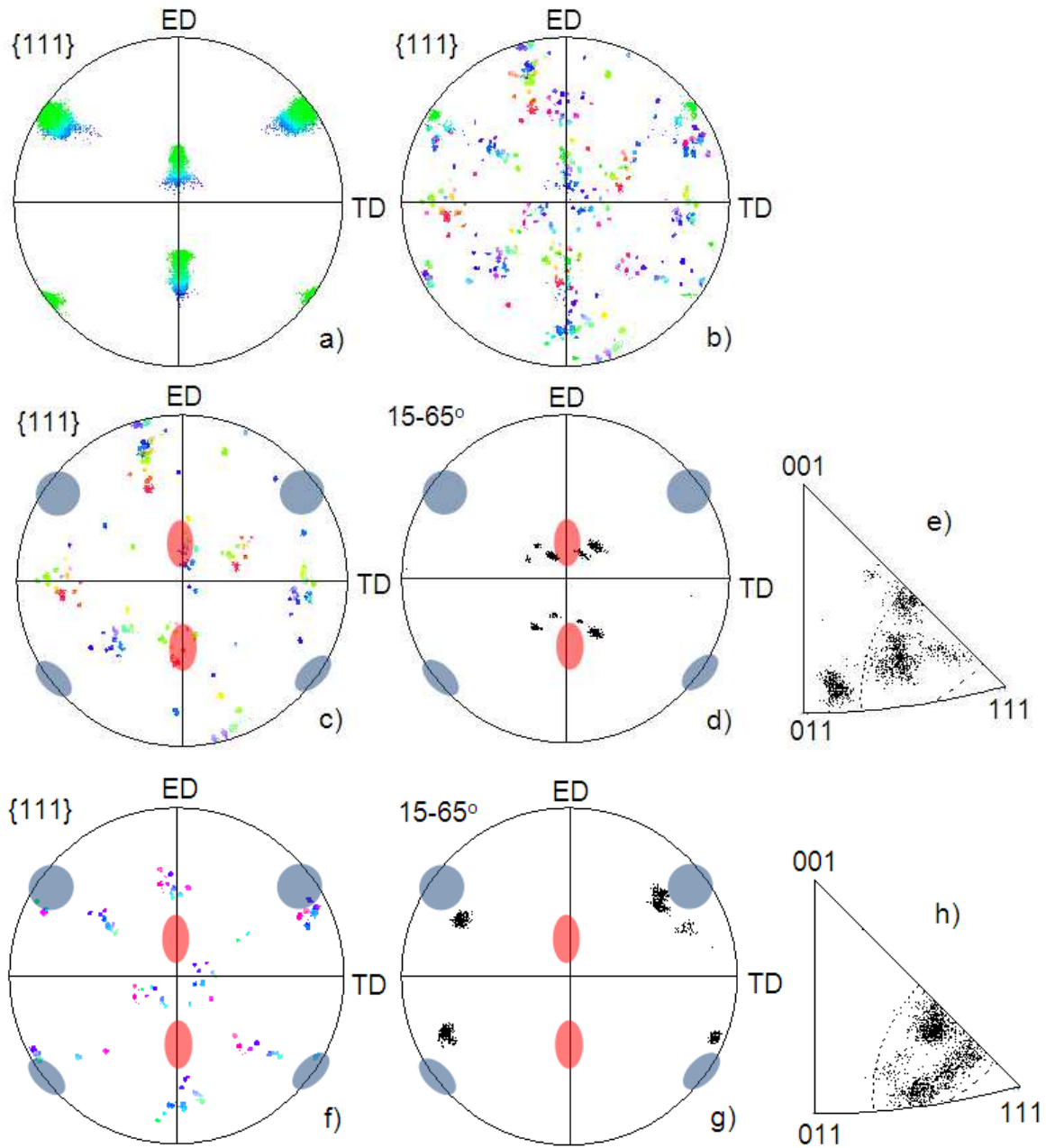


Fig. 6.14. The $\{111\}$ pole figures corresponding orientation map presented in Fig. 6.13a. (a) only deformed and (b) only recrystallized 'regions'. (c) Orientation of grains growing horizontally (disoriented around axes lying near the red circles) and corresponding disorientation axis projections presented in (d) sample and (e) crystal coordinates. (f) Orientation of grains growing vertically (disoriented around axes lying near the blue circles) and corresponding disorientation axes projections presented in (g) sample and (h) crystal coordinates.

6.1.5. Analysis of particular cases of new orientation formation during recrystallization

This part of the analysis was performed based on orientation maps made with a step size of 100nm. Some selected examples, which reflect the diversity of the disorientation relations across the recrystallization front, are presented in Annexe 2. (Figs. A2.1 - A2.21). In most cases, this analysis concerns the orientation relations across the boundaries (recrystallization front) of single isolated grains growing into the deformed structure. Very rarely groups of grains exhibiting a twin relationship between the regions of recrystallized grains were analysed.

Each of the orientation maps was complemented by the corresponding $\{111\}$ pole figure, the disorientation angle distribution between the recrystallized grain and its nearest deformed neighbourhood, as well as the disorientation axis distribution for the above relation presented both in the crystal and sample systems. (The frequency of the disorientation angle for an individual case cannot be compared to other cases. The values are calculated based on an arbitrarily selected number of points through the recrystallization front).

The basic results from this analysis can be summarised as follows:

1. The $\alpha <111>$ type orientation relation between the recrystallized and deformed regions is only occasionally observed. Definitely, it can be claimed that it is not dominant.
2. In the early stages of the process the most common axes for the orientation relation across the recrystallization front are close to the $<012>$, $<221>$, $<111>$ and $<112>$ directions.
3. The observed disorientation axes across the recrystallization front are different from those of the deformed state i.e. between individual pixels of the orientation map of the deformed (recovered) crystal.
4. The spread of the disorientation axes is closely related to the orientation fluctuations in the deformed crystal. This spread enables (in some areas) the recrystallization front to maintain a constant grain orientation during the growth of the recrystallized grain into the deformed crystal.
5. The disorientation angle across the recrystallization front varied between $25-55^\circ$ with a wide maximum between 30° and 45° . Similarly to the disorientation axis distribution,

the special role of near 40° disorientation angle is not confirmed, in contradiction to much previous literature.

6.1.6. *In-situ recrystallization in TEM. Microstructure and texture changes analyzed by TEM-based local orientation measurements*

The microstructure and texture evolution in the deformed and recrystallized states were investigated by TEM-based orientation mapping in a number of samples of the Al-1%Mn alloy. The crystallographic character of microbands was confirmed by orientation measurements¹ based on selected area diffraction (SAD) or Transmitted Kikuchi Patterns (TKP).

The evolution of the dislocation structure and corresponding texture changes during annealing were analyzed by bright field imaging and local orientation measurements in a TEM with a spot size between 5nm and 10nm. Specimens for microscopic investigations were cut from the centre layers of the deformed samples. In each case, very large thin (transparent for electron beam) areas of hundreds μm^2 were obtained. The foil thickness of areas suitable for microscopic observation ranged between 100 and 400nm. Orientations were measured using a CM20 PHILIPS microscope operating at the nominal voltage of 200kV, equipped with an in-house local orientation measurements system based on Kikuchi patterns.

As regards *in-situ* heating experiments in the TEM, it should be noted [Paul *et al.* (2012)] that the recrystallization dynamics depend on the specimen thickness. This causes difficulties in any direct comparison of in-situ recrystallization with that observed in bulk samples. The problem was first discussed by Fujita *et al.* [Fujita *et al.* (1967)], and an explanation of the slower growth in foils was given by Roberts and Lehtinen [Roberts and Lehtinen (1974)]; they conclude that the recrystallization front at a given temperature can only move forward if the combination of stored energy and foil thickness is ‘sufficiently large’. Hutchinson and

¹ For the particular case of plane strain compression, the slip pattern distribution and local lattice re-orientations measured by either equipped with TEM and SEM EBSD facilities on the ND-ED plane are only capable of giving an unequivocal description of the active slip systems when their slip planes contain the TD. In any other case, it is difficult to define precisely the spatial distribution of the active slip systems using only one section, e.g. the longitudinal section containing the ND and ED directions. This is particularly important in the debate whether the slip patterns are oriented along crystallographic planes or are primarily a function of the deformation mode [Winther (2003), Albou *et al.* (2010a)].

Ray [Hutchinson and Ray (1973)] showed that the minimum foil thickness for recrystallization experiments was determined not only by the amount of stored energy but also by the size of the cell structure itself. In specimens with cellular microstructures, the specimen thickness should be at least equal to the thickness of the cells. Thus, with 200kV electron beam penetrating ~ 400nm thick Al-1%Mn foils, it is possible to apply a standard analytical TEM for *in-situ* recrystallization experiments of strongly deformed samples with 200-400nm cells.

The bright field image observed in the ND-ED section and the corresponding {111} pole figure showing the orientations of the deformed structure are presented in Figures 6.15-6.22, respectively. The bright field image demonstrates that the deformed areas are composed of slightly elongated cells grouped into clusters of similar orientations with most boundaries parallel to highly active slip planes. The orientations of neighbouring cells differ only slightly. The thickness of elongated cells ranges between 200 and 300nm whereas their length attains 1-2 μ m. The disorientation angles between cells do not exceed a few degrees. The structural observations confirm the development of a microband structure. For single crystals more deviated from the ideal initial orientation, one microband family predominates as shown in Fig. 6.15 a). The {111} pole figure showing the measured orientations of this region is presented Fig. 6.15 b) on the ND-ED plane. However, in most cases a structure composed of two families of microbands was observed (Fig. 6.16-6.17).

The textural and structural 'stability' of these microstructures was analysed during *in-situ* recrystallization in the TEM. For deformed samples of the Al-1%Mn alloy the standard process cannot be seen (at the TEM scale) as the classical sequence of recovery, recrystallization and growth with a clearly marked moment for the emergence of nuclei. Recrystallization does not generally occur by the growth of isolated nuclei into the surrounding deformed matrix but by a progressive decrease of dislocation density. Accordingly, in our TEM recrystallization experiments, it was frequently observed that the microstructure evolved rather uniformly by the mechanism of continuous recrystallization. This continuous recrystallization was observed in thinner areas, where new grains with clearly outlined recrystallization fronts started to grow into thicker areas of thin foils (>300nm) during the later stages of annealing.

The combination of thin foil heating and TEM-based orientation mapping made it possible to correlate microstructural changes with the evolution of orientations inside small dislocation-

free areas that appeared at very early stages of recrystallization. Figures 6.18 a) and b) show a TEM bright field image and the corresponding $\{111\}$ pole figures giving the orientations of new, recrystallized grains and those identified within the deformed (recovered) structure. The microstructure of recovered areas resembles the one observed in the deformed state. Although the cell interiors are free of dislocations, the elongated cell shapes are still clearly visible. Cell coarsening is also observed. The distribution of disorientation angles inside the recovered areas is similar to that observed in deformed areas. The disorientation axes are grouped around crystallographic directions located near TD.

The formation of the new grain orientations points to the same mechanism previously observed at the meso- scale by means of SEM/EBSD. Despite several attempts we failed to record the initial formation stage of a recrystallization nucleus, and its subsequent growth into the deformed structure. In practice the analysed cases concern the later stages of recrystallization. The observed migrating recrystallization front was part of the boundary of a large recrystallized grain, growing out of the 'thicker' areas of the thin foil. When progressing towards the electron transparent areas the dynamics of the process rapidly decreased. Migration was often seen to stop in the areas where the foil thickness was very small. In many cases, further annealing (under the same thermal conditions) was unable to move the recrystallization front inside the deformed (strongly recovered) structure.

All these cases of disorientation across recrystallization front belonged to the same group as those observed at the meso- scale by SEM/EBSD. Thus, all the orientation relations of the recrystallization front seen in thin foils are the same as those found in bulk samples. Since the grain orientation during growth does not change, it follows that the general mechanism of generating initial nuclei orientation in bulk samples and in thin foils (by *in-situ* recrystallization TEM experiments) is the same. In other words, the crystallographic aspects of the nucleation of a new grain remain the same. This is not changed by the drag effect of the surface, in very thin regions of foil, on the mobility of the recrystallization front.

The mechanism of incorporating the deformed structure into the growing grain through the migrating recrystallization front is particularly difficult to observe. To a great extent, this results from a rapidity of the process. When the recrystallization front stopped, under given thermal conditions in thin areas of foil, and the annealing temperature was raised to provoke its motion, a transition to the next 'stationary state' occurred abruptly.

In the dislocation cell area, immediately before the recrystallization front, a large decrease in the dislocation density was noticed. In most cases, dislocations preceding the recrystallization front were grouped in small-angle boundaries, i.e. the boundaries separating the cells. Further from the recrystallization front, the dislocations inside the dislocation cells tended to gather in low energy systems or rearrange by climbing. In some cases, the migration of small-angle boundaries and/or coalescences led to the formation of larger regions of homogeneous orientation before the recrystallization front.

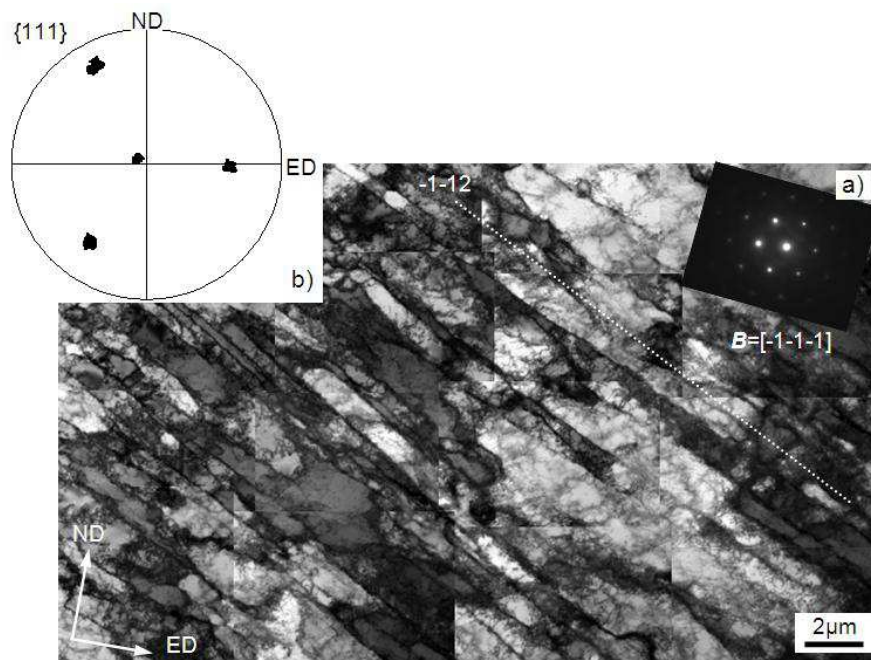


Fig. 6.15. (a) TEM bright field image showing one family of microbands. Al-1%Mn crystal with (110)[1-1-2] orientation, deformed to a strain of 0.51 and (b) the corresponding {111} pole figure, presented in the co-ordinate system of the bright field image.

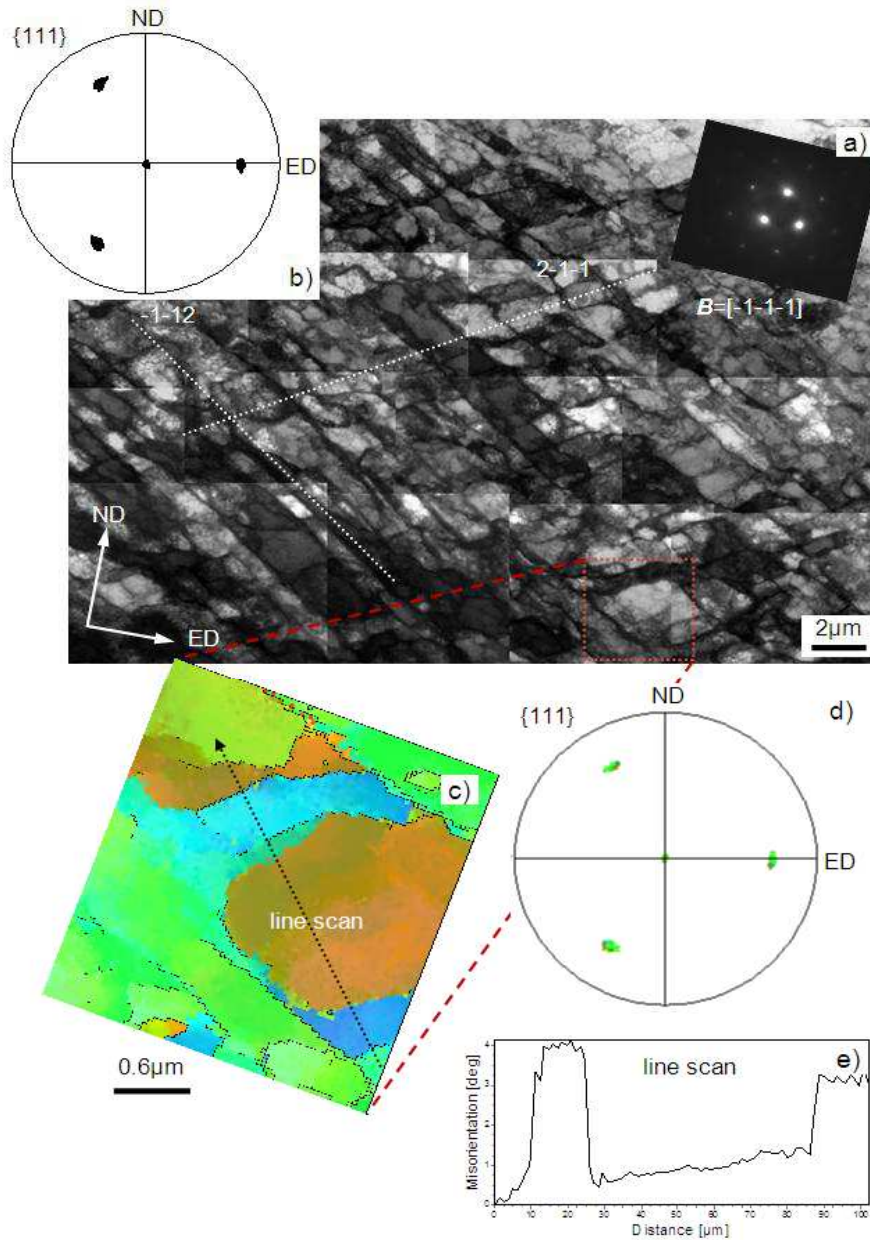


Fig. 6.16. (a) TEM bright field image showing two families of microbands. Al-1%Mn crystal with (110)[1-1-2] orientation, deformed to a strain of 0.51; (b) the {111} pole figure in the same co-ordinate system, i.e. ND-ED; (c)TEM orientation map made from the area marked in (a) and (d)corresponding line scan marked in (c). Step size of 20nm.

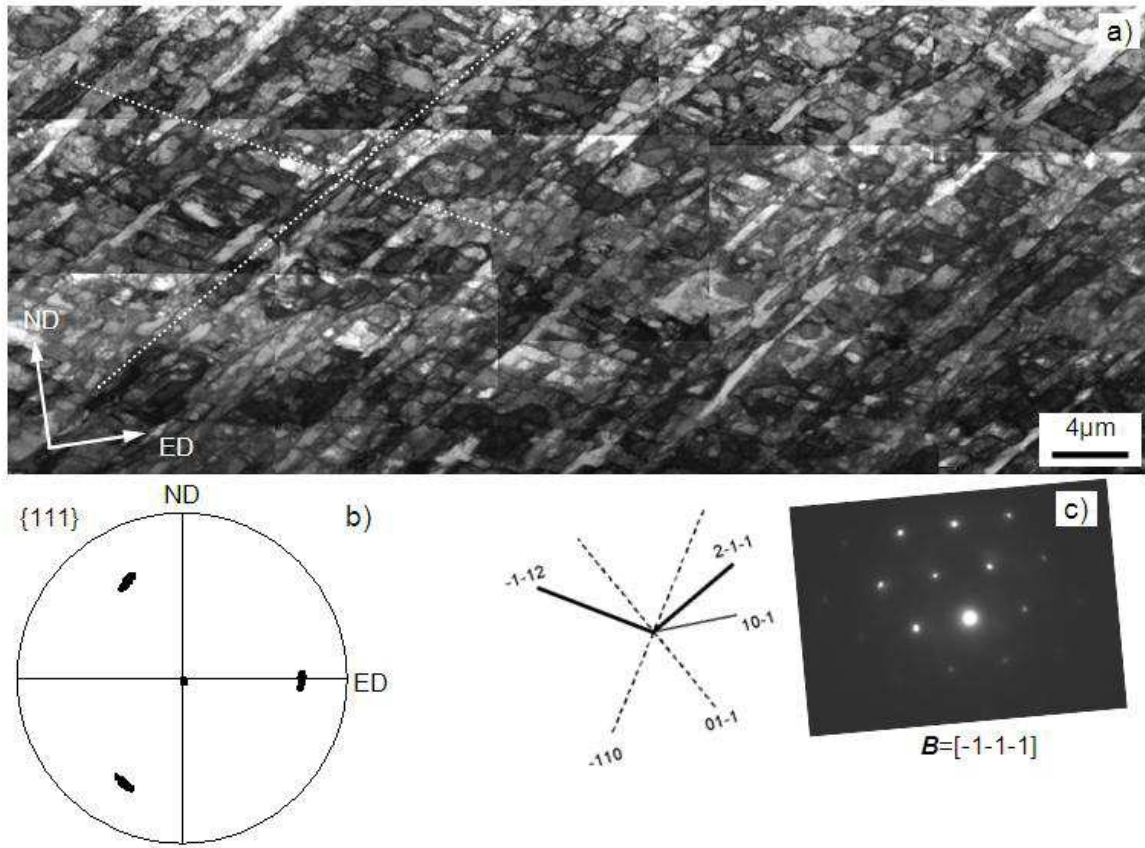


Fig. 6.17. (a) TEM bright field image showing one family of microbands. Al-1%Mn crystal with (110)[1-1-2] orientation, deformed to a strain of 0.92 and (b) the corresponding {111} pole figure in the co-ordinate system of the bright field image.

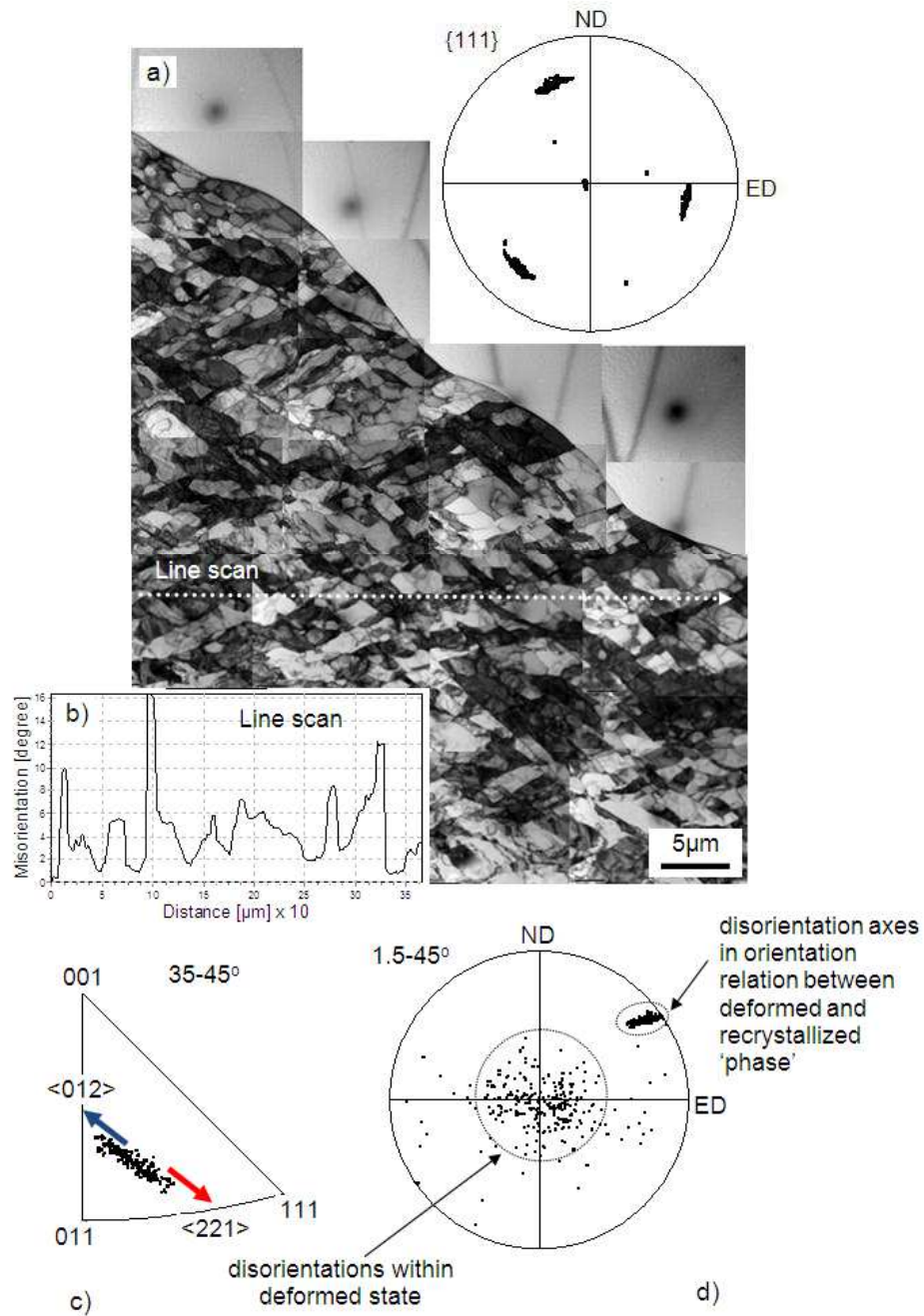


Fig. 6.18. Recrystallization grain growth during in-situ recrystallization in TEM (case 1). (a) TEM microstructure observed in the ND-TD section of Al-1%Mn sample with (110)[1-1-2] orientation and the corresponding {111} pole figure. (b) Line scan showing cumulative disorientation along dashed line marked in (a). (c) Standard triangle showing disorientation axes distribution across recrystallization front (within the range of 35-45°). (d) Disorientation axes projection showing all of the disorientation axes between neighbouring measured points.

Sample deformation 0.51.

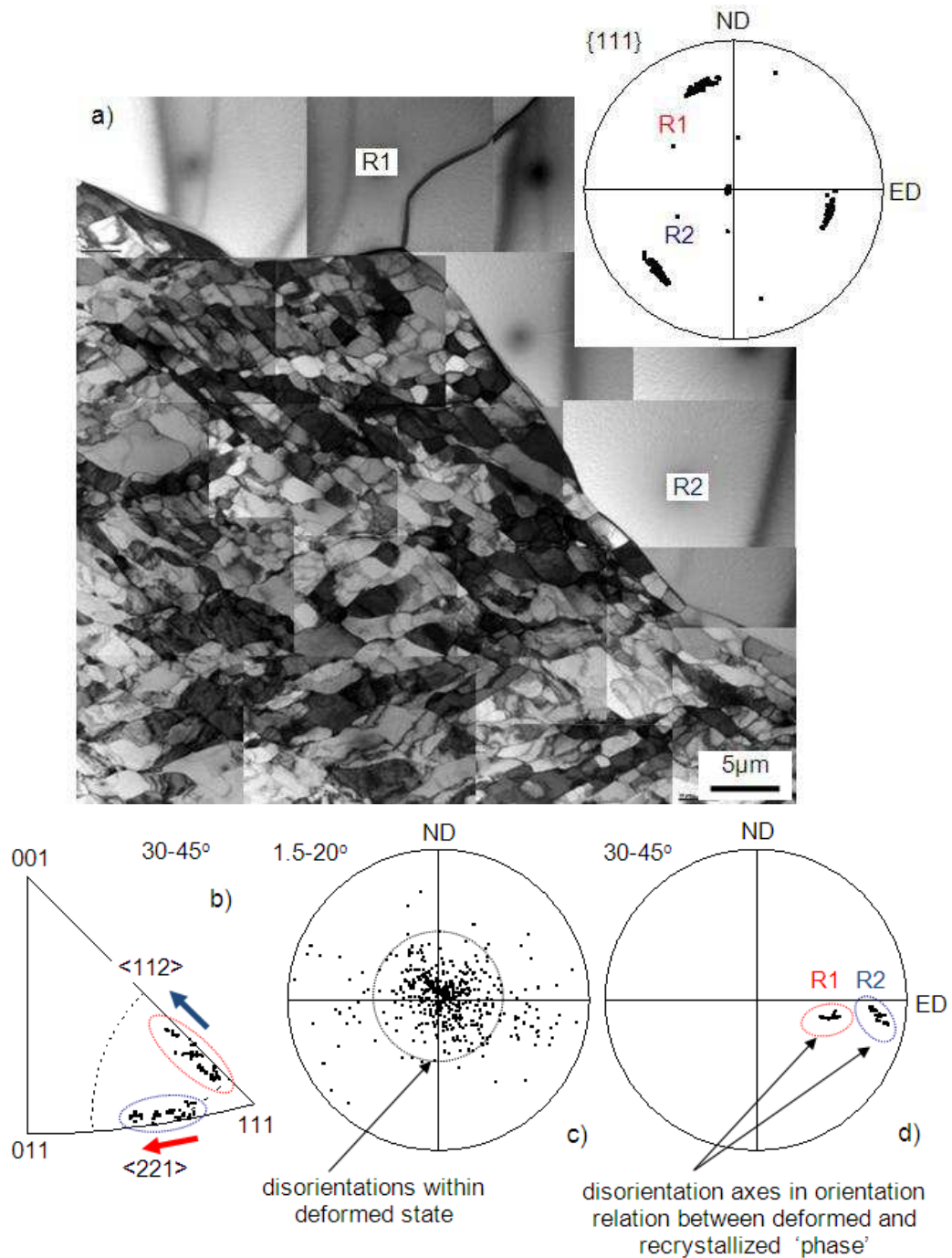


Fig. 6.19. Recrystallization grain growth during in-situ recrystallization in TEM (case 2). (a) TEM microstructure observed in the ND-TD section of Al-1%Mn sample with (110)[1-1-2] orientation and corresponding the {111} pole figure. (b) Standard triangle showing disorientation axes distribution in relation across recrystallization front (within the angles range of 35-45°). Disorientation axes projections showing the disorientation axes distribution between neighbouring points of (c) the deformed state and (d) across recrystallization front. Sample deformation 0.51.

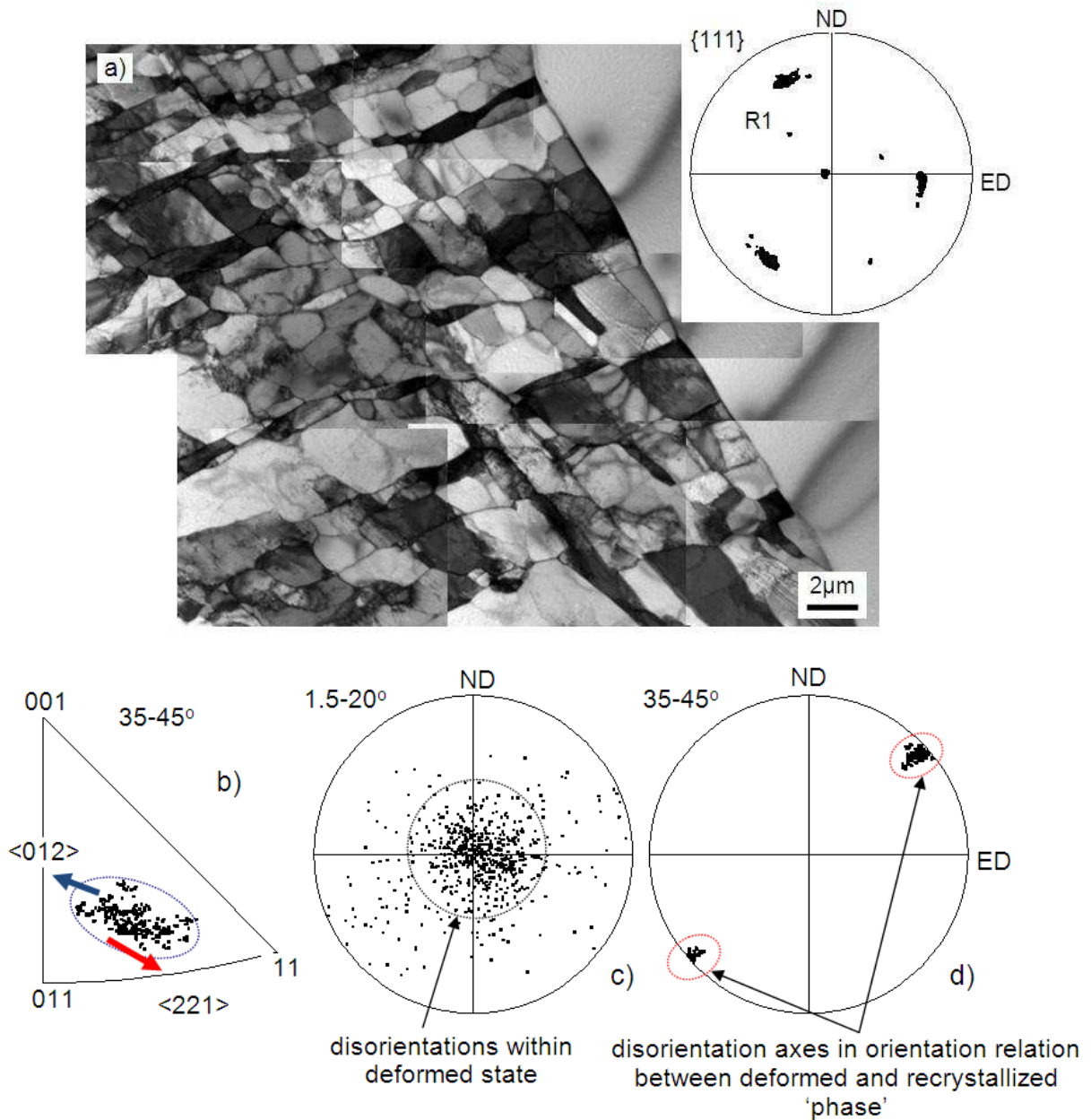


Fig. 6.20. Recrystallization grain growth during in-situ recrystallization in TEM (case 3). (a) TEM microstructure observed in the ND-TD section of Al-1%Mn sample with $(110)[1-1-2]$ orientation and corresponding the $\{111\}$ pole figure. (b) Standard triangle showing disorientation axes distribution in relation across recrystallization front (within the angles range of $35-45^\circ$). Disorientation axes projections showing the disorientation axes distribution between neighbouring points of (c) the deformed state and (d) across recrystallization front. Sample deformation 0.51.

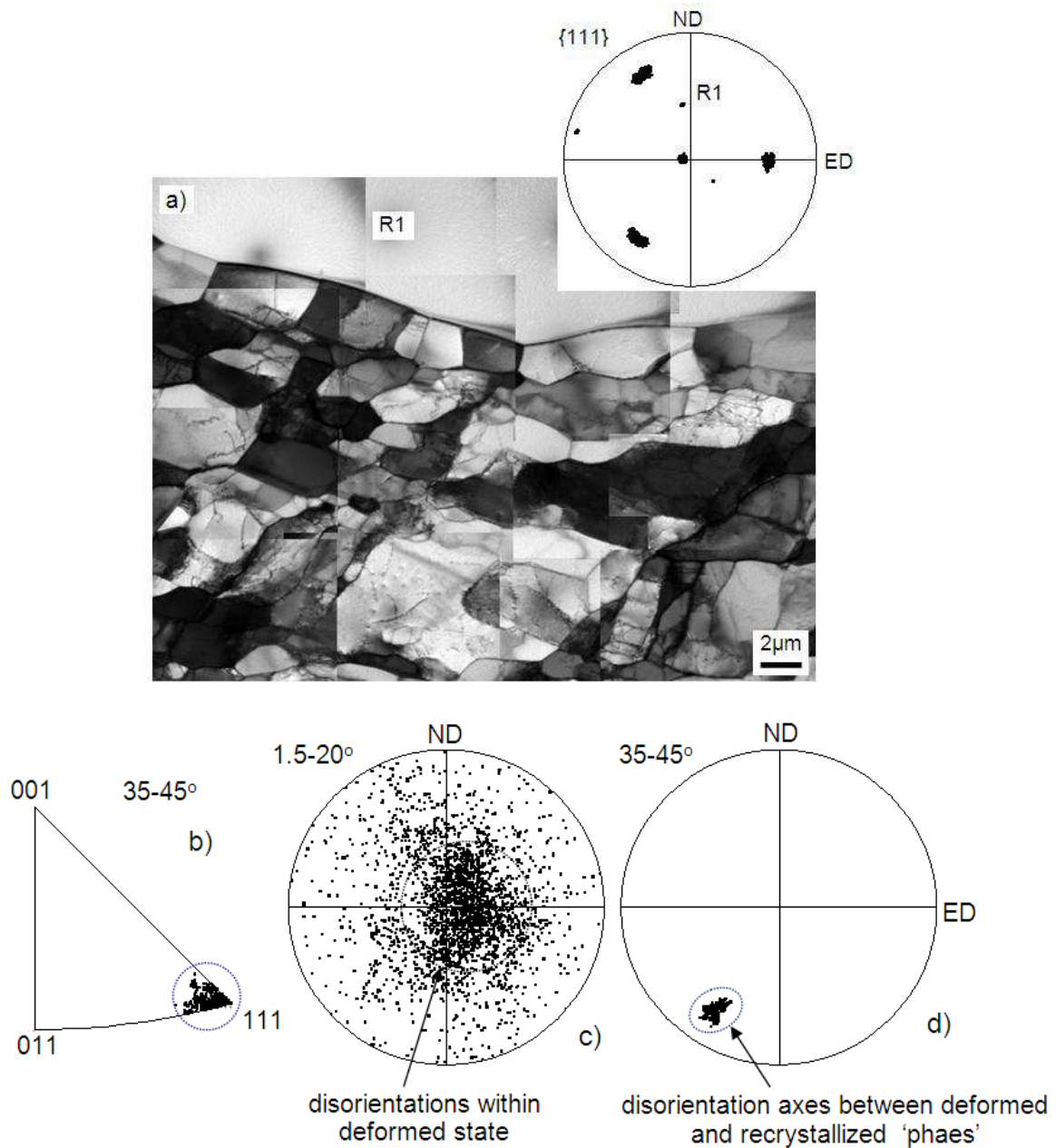


Fig. 6.21. Recrystallization grain growth during in-situ recrystallization in TEM (case 4). (a) TEM microstructure observed in the ND-TD section of Al-1%Mn sample with (110) [1-1-2] orientation and corresponding the {111} pole figure. (b) Standard triangle showing disorientation axes distribution in relation across recrystallization front (within the angle range of 35-45°). Disorientation axes projections showing the disorientation axes distribution between neighbouring points of (c) the deformed state and (d) across recrystallization front. Sample deformation 0.51.

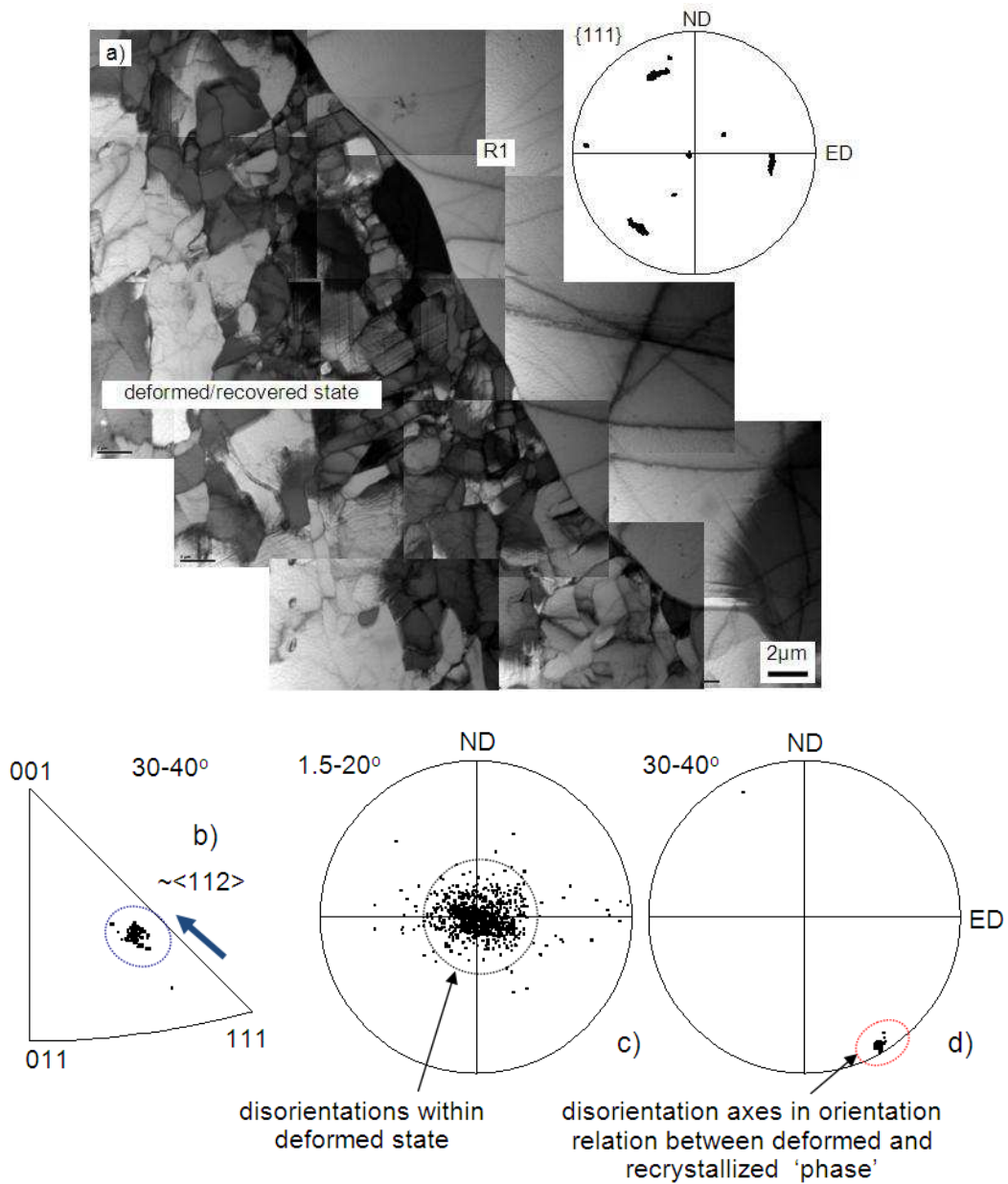


Fig. 6.22. Recrystallization grain growth during in-situ recrystallization in TEM (case 4). (a) TEM microstructure observed in the ND-TD section of Al-1%Mn sample with (110)[1-1-2] orientation and corresponding the {111} pole figure. (b) Standard triangle showing disorientation axes distribution in relation across recrystallization front (within the angles range of 35-45°). Disorientation axes projections showing the disorientation axes distribution between neighbouring points of (c) the deformed state and (d) across recrystallization front. Sample deformation 0.92.

6.1.7. *Recrystallization twinning in high SFE metals*

The orientation maps made for pure aluminium (Fig. 6.23) and Al-1%Mn alloy for both orientations occasionally indicate recrystallization twinning but its frequency is very low as discussed by Cahn [Cahn (1954)].

Annealing twins are frequently observed in fcc metals of medium-low SFE. Little significance was attached to annealing twins in Al until the publication of results in Göttingen based on the application of high voltage TEM to recrystallization [Berger and Wilbrandt (1988)] produced evidence of extensive twin formation during the early stages of recrystallization of several fcc metals including Al. However, there are several problems with the interpretation of results obtained on thin foils, mainly due to small sample thickness. Similar problems were encountered during SEM in-situ annealing experiments.

Humphreys and Ferry [Humphreys and Ferry (1996)] have shown that annealing twins are more frequently formed on a free surface than in the specimen interior, and that the twins formed on the surface during primary recrystallization may not be stable. The experimental results on the annealing of pure copper obtained by Field et al [Field *et al.* (2007)] showed that when a grain appeared to stagnate in growth (for any reason) it would often twin and rapid growth would be resumed. They observed that the lower the recrystallization temperature, the larger the fraction of twin-related grain boundaries.

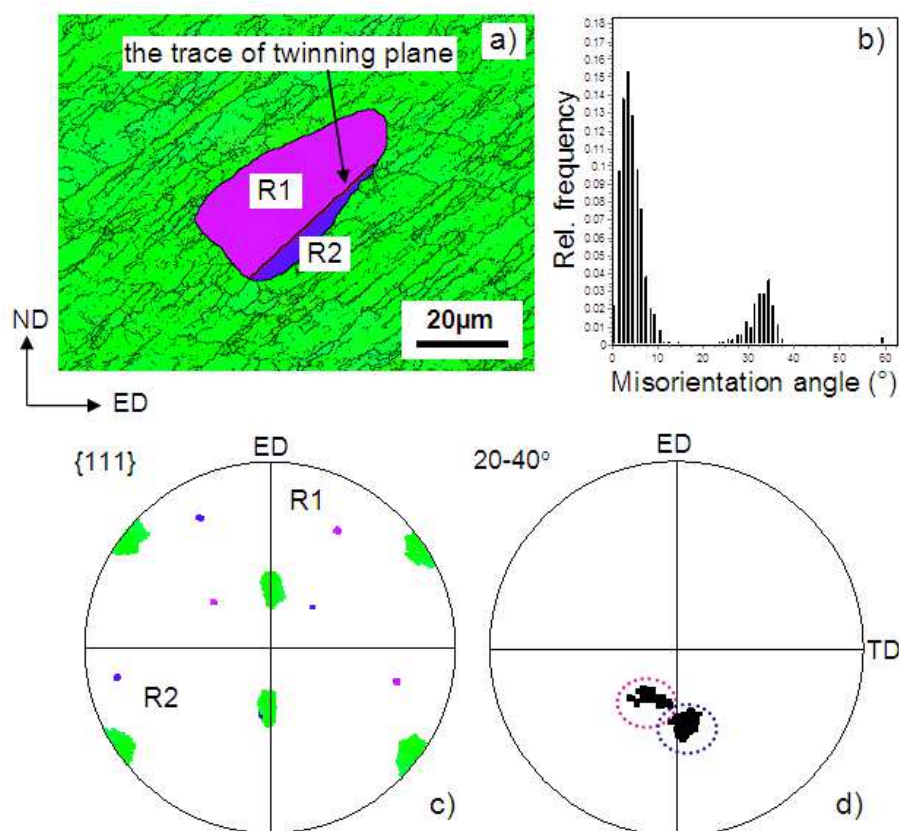
The results of Berger *et al.* (1988) and Humphreys and Ferry (1996) suggest that observations of intensive twinning in high SFE metals and alloys during either SEM or TEM in-situ annealing experiments are not representative of the behaviour in the interior of a sample. But the crystallographic aspects of this twinning in high SFE metals are probably the same.

At the moment, the details of the mechanism by which annealing twins are formed in fcc metals are still not entirely clear. However, it is likely that twins are formed at moving grain boundaries by the initiation of growth faults on {111} planes. In both cases of pure aluminium and Al-1%Mn, regardless of the grain orientation, only first generation twins were observed.

The appearance of recrystallization twins can be linked to growth stoppage of the 'primary nucleus'. That is, if for some reason the nucleus growth is blocked, a recrystallized grain may continue to grow by the formation of a twinned orientation. If we consider growth of a recrystallized grain as a thermally-activated rearrangement of dislocations towards the migrating recrystallization front, growth suppression may be related to reducing the options of

dislocation movement within the current 'system'. The most common case of twinning (although not the only one) was on the plane characterized by the pole lying in the immediate vicinity of the rotation axis (from the disorientation between the initial nucleus/grain and the surrounding group of deformed orientations). The pole defining the twinning face plane approaches, but does not coincide with, the disorientation axis between the deformed and recrystallized areas. For the situation shown in Fig. 6.23 the formation of the R1 orientation can be explained as a composition of rotations around two axes $[2-11]$ and $[-121]$ by an angle of about $30-35^\circ$. These rotations may result from the displacement of dislocations on the (111) plane. If, in the neighbouring region (R2), two rotations of opposite sense about the same axes and by the same angle occur, they lead to the formation of a twinning relationship between these regions. The latter rotation may result from the migration of dislocation groups in opposite directions (with respect to those described before).

If twinning takes place on a plane other than that determined by the disorientation axis between the deformed and recrystallized regions, the process may be interpreted as the tendency of the structure to displace other dislocation systems, which otherwise could not be displaced during the initial nucleus formation and its subsequent growth.



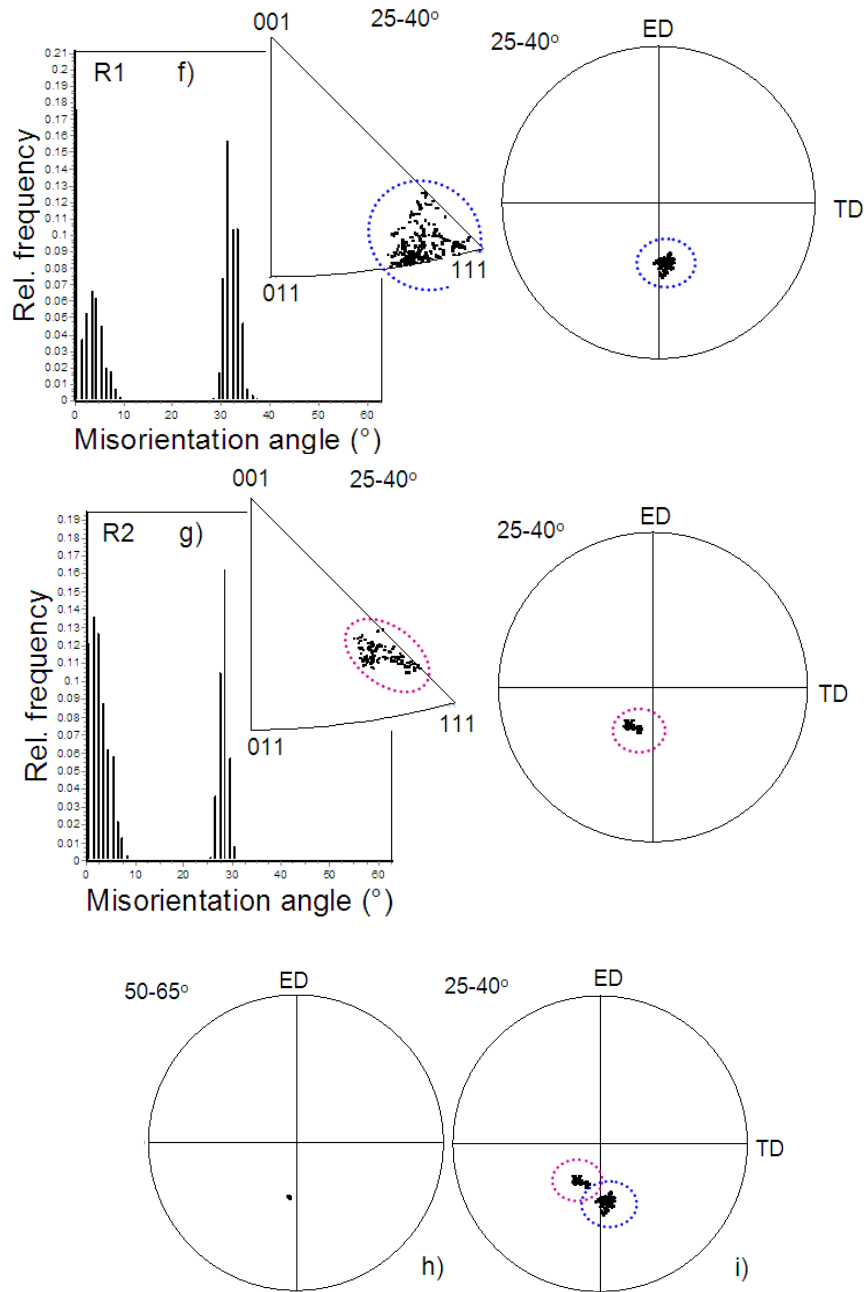


Fig. 6.23. Recrystallization twinning in pure aluminium. (a) SEM/EBSD orientation map (IPF colour $\parallel Y$ was applied) and (b) corresponding disorientation angle distribution and (c) the $\{111\}$ pole figure. (d) Disorientation axis distribution across the recrystallization front, i.e. between neighbouring pixels of the deformed and recrystallized grains. Stereographic projection on (110) plane showing situation of the disorientation axes. Disorientation angle and axis distribution for (f) and (g) R1 and R2 areas, respectively. Disorientation axis projections showing the difference of the position: (h) twinning plane normal o and (i) the disorientation axes between deformed and recrystallized grains. Goss (110)[00-1] oriented sample strained 0.51 and then recrystallized at 618K for 25s.

6.2. Early stages of recrystallization in medium and low SFE fcc metals

The other group of metals are single crystals of Ni, Cu and Cu-2%Al alloy and their common feature during recrystallization is strongly determined by the intensive formation of recrystallization twins. However, in the following only the disorientation relations between recrystallized and deformed 'phases' were analysed. The twin-related orientation relationships between the adjacent regions of recrystallized grains (and/or twins) have been ignored (Figs. 6.24-6.29). This follows from the fact that after the formation of the primary nucleus, further 'evolution' of the recrystallization texture may take place only through twinning on all four {111} planes and up to the third generation of twins as shown in an earlier study on Ag single crystals of {112}<111> initial orientation [Paul *et al.* (2007)].

6.2.1. Large area analysis

In the case of metals with medium and low SFE (i.e. containing annealing twins), grains of uniform orientation completely surrounded by deformed regions are only rarely seen (Fig. 6.25 and 6.28). Consequently, the number of cases of disorientation relationship between the regions of recrystallized grains and their deformed neighbourhood is rather small. However, certain preferences in the formation of 'primary' grain orientations could be recognized, analogous to those observed in high SFE metals (Fig. 6.24 g), 6.25 g), 6.26 g), 6.27 g), 6.28 g)). The appearance of recrystallization twins causes the initial orientation relations to 'disappear' quickly.

The disorientation relations across the recrystallization front for the entire set of orientation maps (between recrystallized and deformed grains - twinned and non-twinned) shows that the maximum value of the disorientation angle is close to 30° . It is usually accompanied by another maximum near $45-55^\circ$ (Fig. 6.24 b)). *A local minimum was noted for the disorientation angle densities close to 40° in practically all six cases.* Another general rule, common to all three metals (and two orientations), was that the <111> poles of the deformed/recovered grains, do not coincide with the <111> poles of the recrystallized grains or more precisely overlapping of the <111> rotation axes was observed only rarely.

Basically, the majority of the disorientation axes across the recrystallization front are concentrated around (but not coincide with) the <111> poles of the two slip planes during deformation. A 'grouping' of rotation axes near the two remaining poles could, however, be

detected but was clearly weaker. Very occasionally other disorientation axes were observed, but their presence did not significantly change the predominance of axes near the (111) and (11-1) poles of the active slip planes.

Similarly to the high SFE metals (virtually non-twinned in recrystallized grains) the disorientation axes are slightly deviated from the normals of the {111} planes and 'occupy' a wide range near the $\langle 112 \rangle$, $\langle 012 \rangle$ and $\langle 122 \rangle$ directions (Fig. 6.25 g), 6.26 g), 6.27 g), 6.28 g), 6.29 g)). Another observable rule, applying to both the (110)[00-1] and (110)[1-1-2] orientations, was that the maximum disorientation axis density (between individual pixels of the orientation map for the deformed/recovered state) did not coincide with the density maxima of disorientation axes evaluated between the deformed and recrystallized grains.

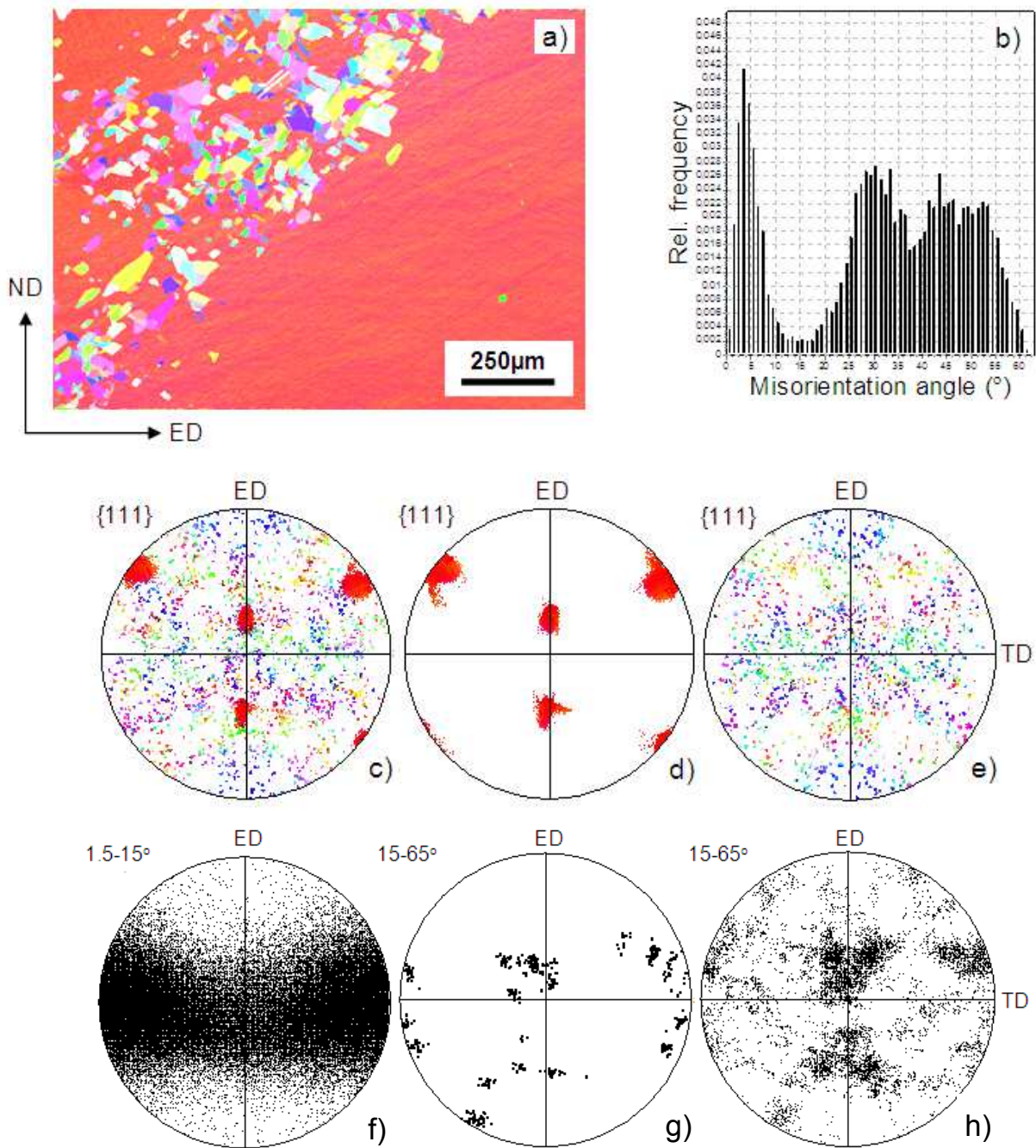


Fig. 6.24. Early stages of recrystallization in Ni single crystal of (110)[00-1] orientation. (a) Orientation map, (b) disorientation angle distribution for the entire orientation map, (c) - (e) the {111} pole figures showing orientations of: (c) deformed state, (d) recrystallized grains and (e) single isolated grains of uniform orientation. The disorientation axis distributions : (f) between pixels of the deformed state, (g) between recrystallized grains and the deformed state and (h) between single isolated recrystallized grains and the deformed state. Sample strained 0.51 and recrystallized at 863K for 25s.

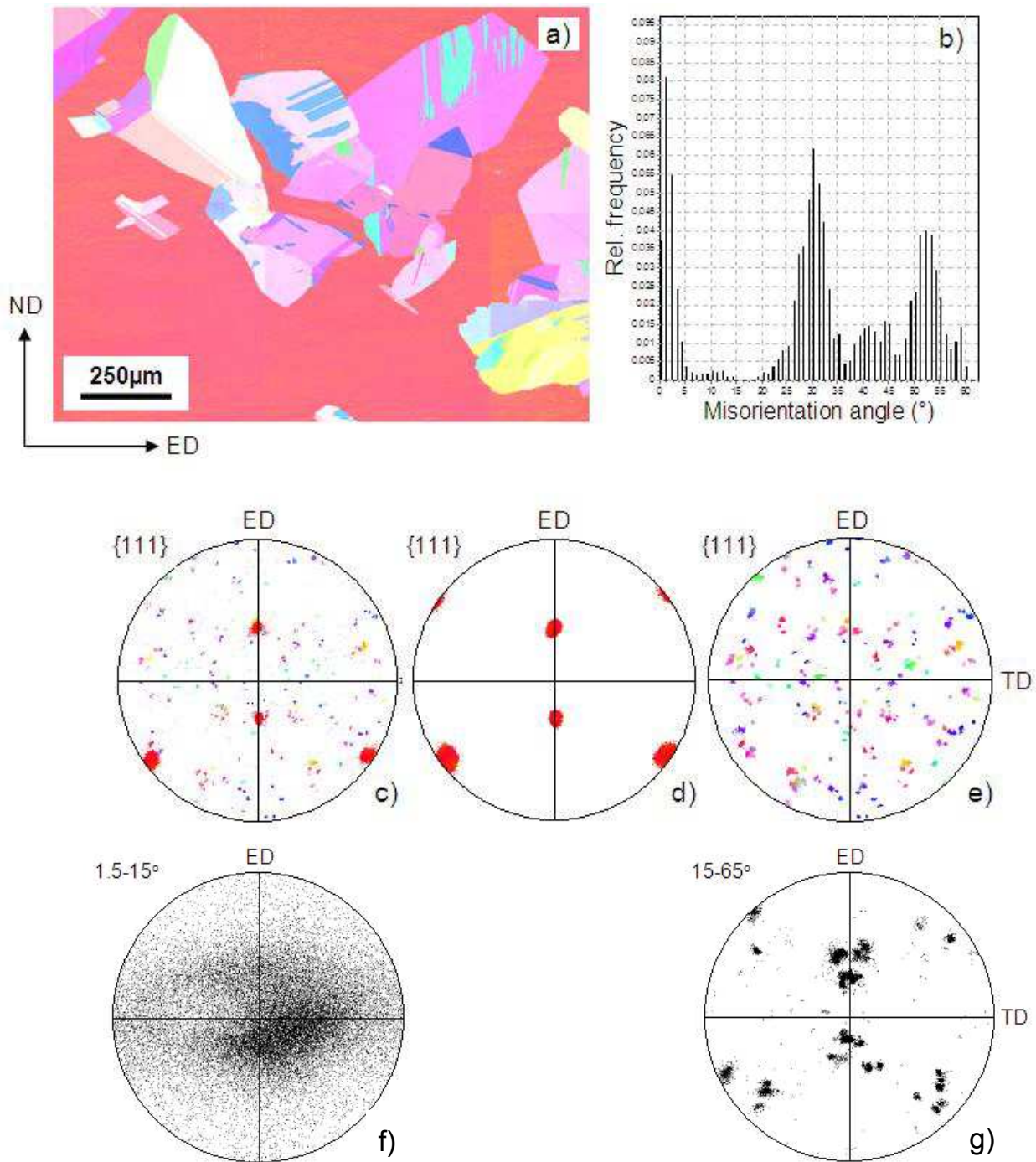


Fig. 6.25. Early stages of recrystallization in Cu single crystal of (110)[00-1] orientation. (a) Orientation map, (b) disorientation angles distribution for whole orientation map, (c) and (d) the {111} pole figures showing orientations of: (c) only deformed state, (d) only recrystallized grains and (e) the distribution of disorientation axes between recrystallized grains and the deformed state. Sample deformed 0.51 and then recrystallized at 608K for 40s.

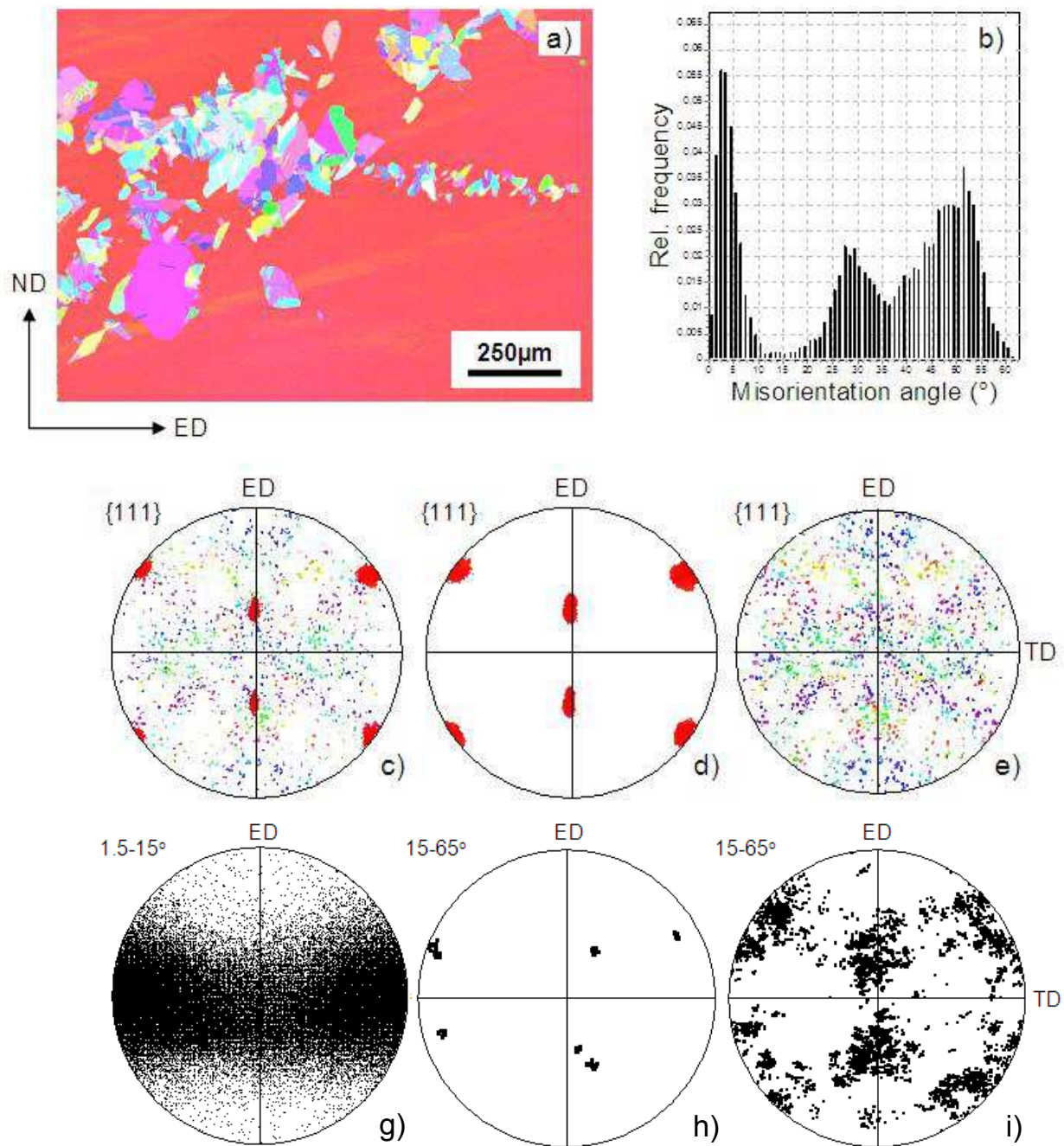


Fig. 6.26. Early stages of recrystallization in Cu-2%Al single crystal of (110)[00-1] orientation. (a) Orientation map, (b) disorientation angles distribution for whole orientation map, (c) - (e) the {111} pole figures showing orientations of: (c) only deformed state, (d) all recrystallized grains and (e) only single isolated grains of uniform orientation. The distribution of disorientation axes: (f) only between pixels of the deformed state, (g) between recrystallized grains and the deformed state and (h) between single isolated grains of uniform orientation and the deformed state. Sample deformed 0.51 then recrystallized at 843K for 30s.

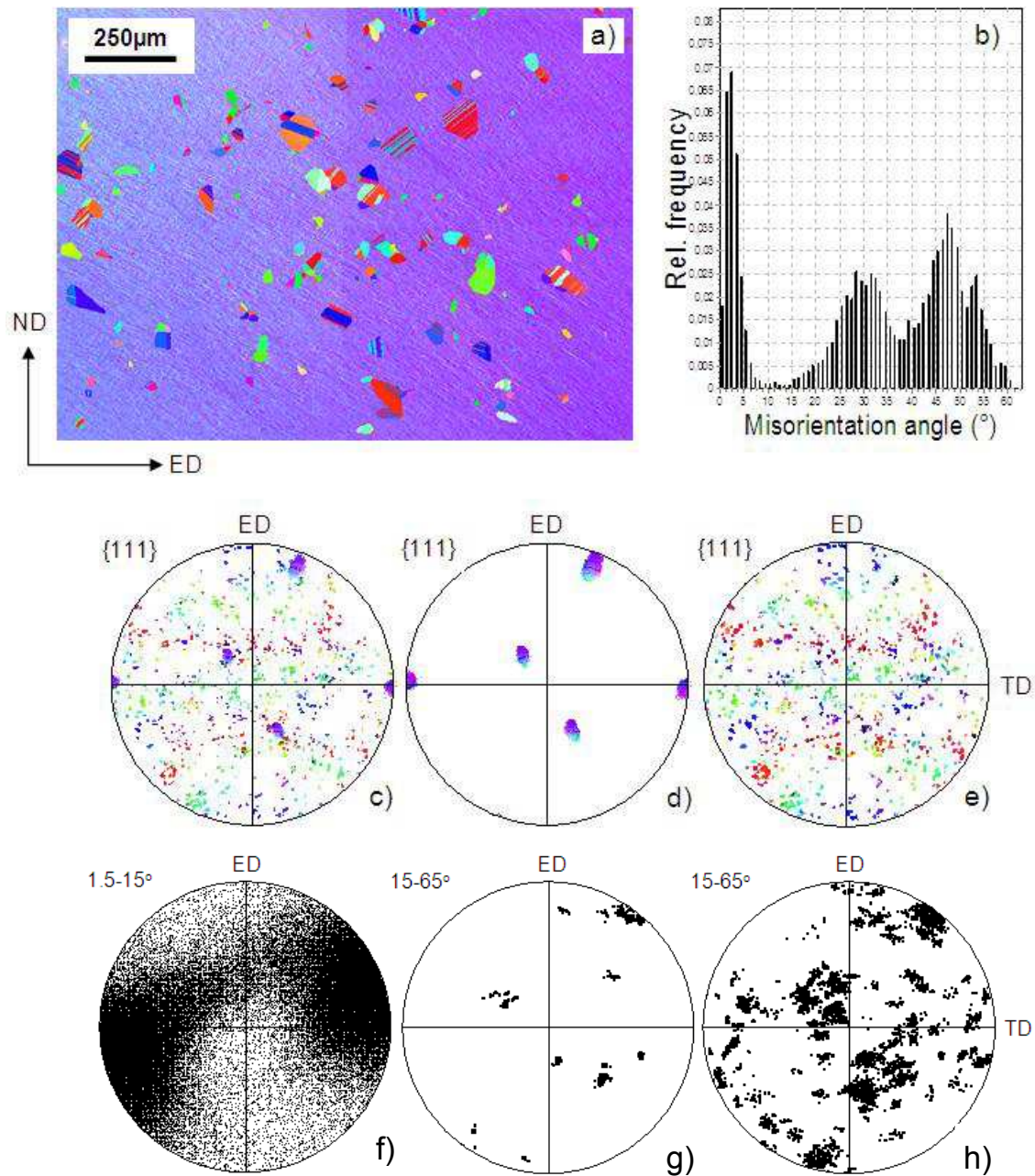


Fig. 6.27. Early stages of recrystallization in Ni single crystal of (110)[1-1-2] orientation. (a) Orientation map, (b) disorientation angles distribution for whole orientation map, (c) - (e) the {111} pole figures showing orientations of: (c) only deformed state, (d) all recrystallized grains and (e) only single isolated grains of uniform orientation. The distribution of disorientation axes: (f) only between pixels of the deformed state, (g) between recrystallized grains and the deformed state and (h) between single isolated grains of the recrystallized phase and the deformed state. Sample deformed 0.51 and then recrystallized at 913K for 30s.

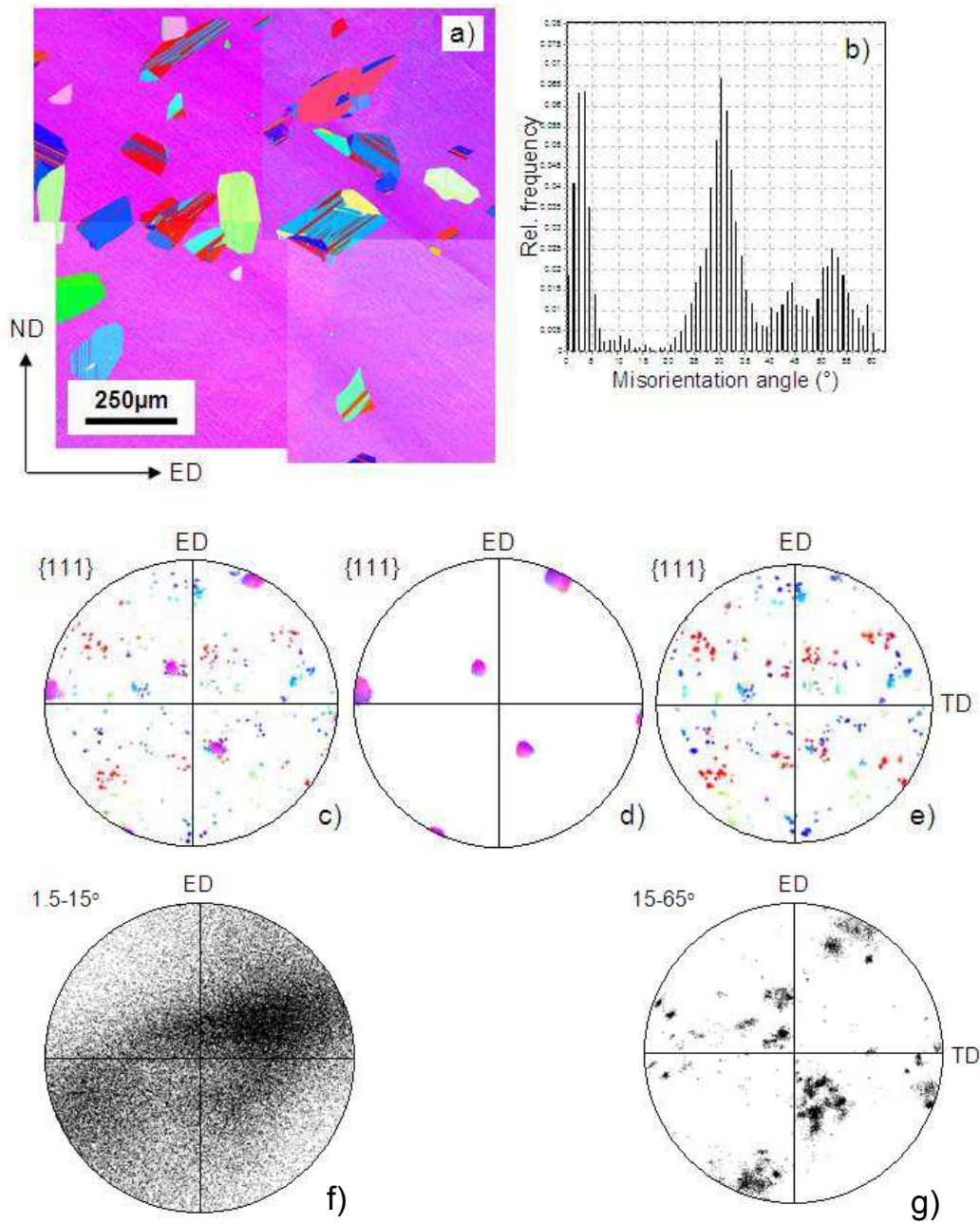


Fig. 6.28. Early stages of recrystallization in Cu single crystal of (110)[1-1-2] orientation. (a) Orientation map, (b) disorientation angles distribution for whole orientation map, (c) and (d) the {111} pole figures showing orientations of: (c) only deformed state, (d) only recrystallized grains and (e) the distribution of disorientation axes between recrystallized grains and the deformed state. Sample deformed 0.51 and then recrystallized at 608K for 70s.

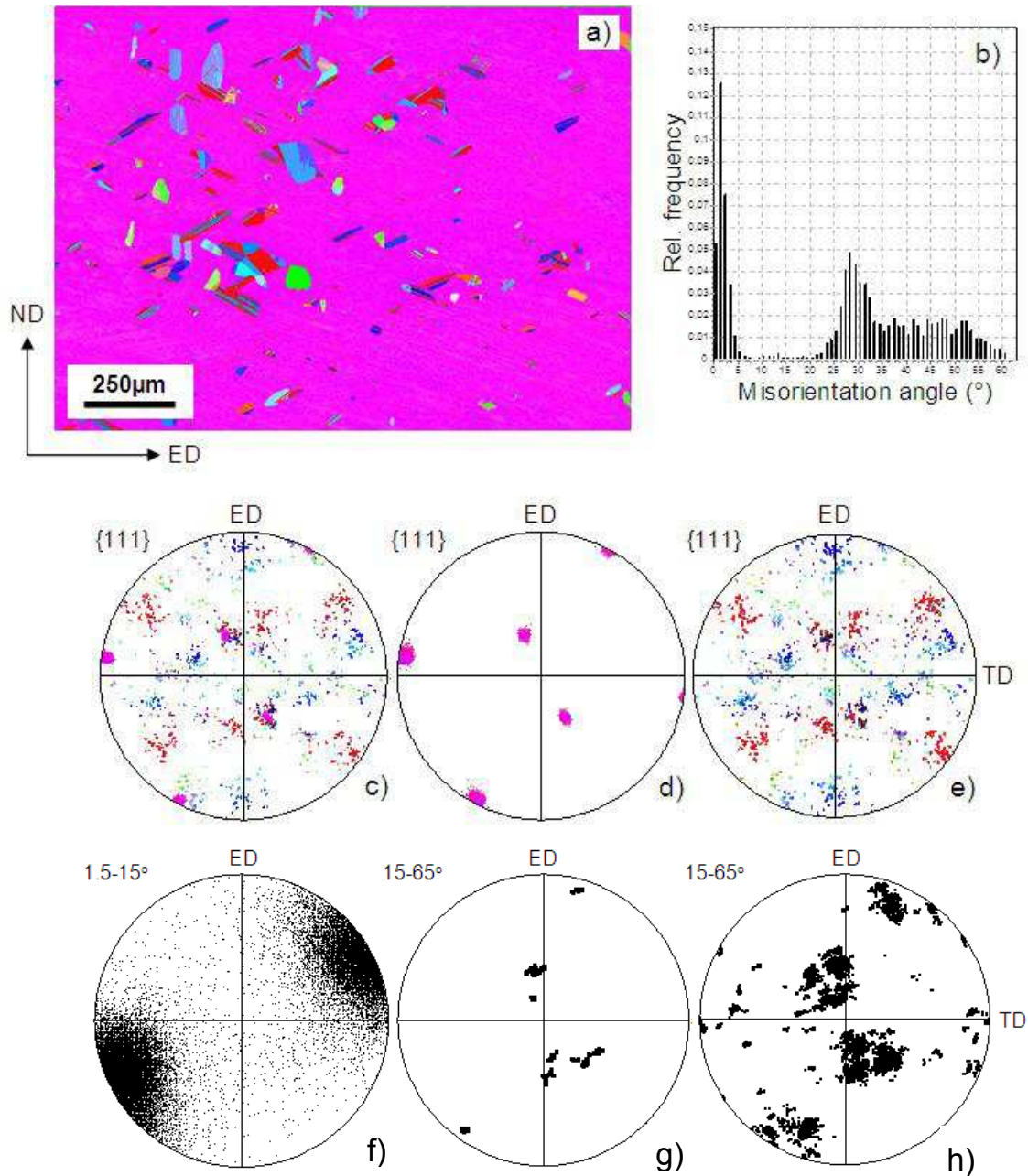


Fig. 6.29. Early stages of recrystallization in Cu-2%Al single crystal of $(110)[1-1-2]$ orientation. (a) Orientation map, (b) disorientation angles distribution for whole orientation map, (c) - (e) the $\{111\}$ pole figures showing orientations of: (c) only deformed state, (d) all recrystallized grains and (e) only single isolated grains of uniform orientation. The distribution of disorientation axes: (f) only between pixels of the deformed state, (g) between recrystallized grains and the deformed state and (h) between single isolated grains of uniform orientation and the deformed state. Sample deformed 0.51 then recrystallized at 843K for 45s.

6.2.2. Statistical analysis of the disorientation angle and axis distributions in medium-low SFE metals

In contrast to the above analyses dealing with high SFE metals (Fig. 6.1-6.4), this part analyzes the disorientation relations between each region of recrystallized, twinned and non-twinned phases, and the as-deformed orientations. As before (i.e. for high SFE metals), statistical results obtained for various annealing conditions (function of the metal and orientation) are interpreted in terms of the disorientation angle/axes distributions. The samples were strained to 0.51, and between a few tens and a few thousand disorientations measured.

The calculated frequencies of particular disorientation axes are shown in Tables 6.3 and 6.4. Similarly to the high SFE metals it can be concluded that the axes around the $\langle 111 \rangle$ directions are less heavily populated than some others. Axes near $\langle 122 \rangle$ or $\langle 112 \rangle$ and, to a lesser degree $\langle 123 \rangle$, are equally (often even more strongly) represented. There is, however, a significantly lower frequency of $\langle 012 \rangle$ axes than in the case of high SFE metals.

The 'frequency' distributions of the disorientation angles between recrystallized and deformed (recovered) regions are presented in Figs. 6.30 and 6.31. The range of potential disorientation angles was binned into intervals of 1.25° into which the number of disorientations across the recrystallization front corresponding to a given angular interval was counted. Figs. 6.30 and 6.31 show that the prevalent range of angles across the migrating recrystallization front was within a wide range between 25° and 55° and was not identical for all cases. As expected [Paul *et al.* (2007)], two maxima of disorientation angle are observed. One maximum occurred near an angle $\sim 30^\circ$ and the other near $50-55^\circ$. According to the preceding results on high SFE metals, the first maximum can be associated with disorientations between the primary nucleus and the deformed matrix, whereas the other between twinned regions and the deformed matrix. However, as shown in the following chapter, it may happen that both the 'original region' and the region of the first generation twin may exhibit the same type of orientation relationship with respect to the deformed neighbourhood. This case occurs when the disorientation axis of the 'original region' is close to the normal of a twinning plane.

Ni (110)[00-1]						
Classification of 5295 axes						
Classes	Counts	[%]	Rand1 [%]	Rand2[%]	Distrib1	Distrib2
0 0 1	131	2.47	10.0	6.3	0.25	0.39
0 1 1	387	7.31	8.7	10.8	0.84	0.68
0 1 2	569	10.75	25.2	19.5	0.43	0.55
1 1 1	565	10.67	5.0	7.1	2.13	1.51
1 1 2	779	14.71	15.5	15.1	0.95	0.98
1 2 2	1512	28.56	11.4	16.3	2.50	1.75
1 2 3	1352	25.53	24.2	25.0	1.06	1.02

Cu (110)[00-1]						
Classification of 1644 axes						
Classes	Counts	[%]	Rand1 [%]	Rand2[%]	Distrib1	Distrib2
0 0 1	16	0.97	10.0	6.3	0.10	0.15
0 1 1	5	0.30	8.7	10.8	0.03	0.03
0 1 2	48	2.92	25.2	19.5	0.12	0.15
1 1 1	205	12.47	5.0	7.1	2.49	1.77
1 1 2	317	19.28	15.5	15.1	1.25	1.28
1 2 2	744	45.26	11.4	16.3	3.97	2.78
1 2 3	309	18.80	24.2	25.0	0.78	0.75

Cu-2%Al (110)[00-1]						
Classification of 3714 axes						
Classes	Counts	[%]	Rand1 [%]	Rand2[%]	Distrib1	Distrib2
0 0 1	89	2.40	10.0	6.3	0.24	0.38
0 1 1	156	4.20	8.7	10.8	0.48	0.39
0 1 2	157	4.23	25.2	19.5	0.17	0.22
1 1 1	560	15.08	5.0	7.1	3.01	2.14
1 1 2	545	14.67	15.5	15.1	0.95	0.97
1 2 2	1177	31.69	11.4	16.3	2.78	1.94
1 2 3	1030	27.73	24.2	25.0	1.15	1.11

1 - in relation to random directions on the unit sphere.

2 - in relation to DISorientation axes of random MISorientations.

Tab. 6.3. Fractional classes of disorientation axes calculated for Ni, Cu and Cu-2%Al single crystals of (110)[00-1] orientation. Samples strained 0.51 and then lightly annealed.

Ni (110)[1-1-2]						
Classification of 1975 axes						
Classes	Counts	[%]	Rand1 [%]	Rand2[%]	Distrib1	Distrib2
0 0 1	30	1.52	10.0	6.3	0.15	0.24
0 1 1	35	1.77	8.7	10.8	0.20	0.16
0 1 2	153	7.75	25.2	19.5	0.31	0.40
1 1 1	116	5.87	5.0	7.1	1.17	0.83
1 1 2	314	15.90	15.5	15.1	1.03	1.06
1 2 2	817	41.37	11.4	16.3	3.63	2.54
1 2 3	510	25.82	24.2	25.0	1.07	1.03

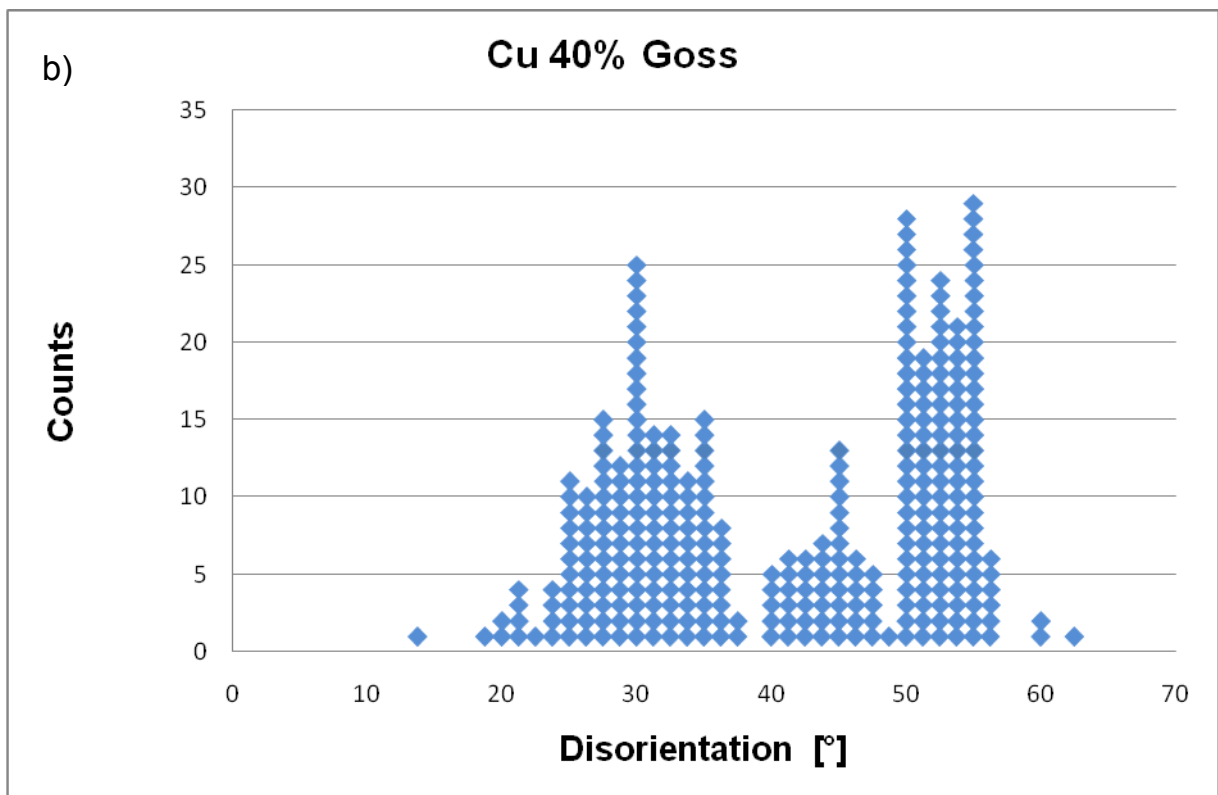
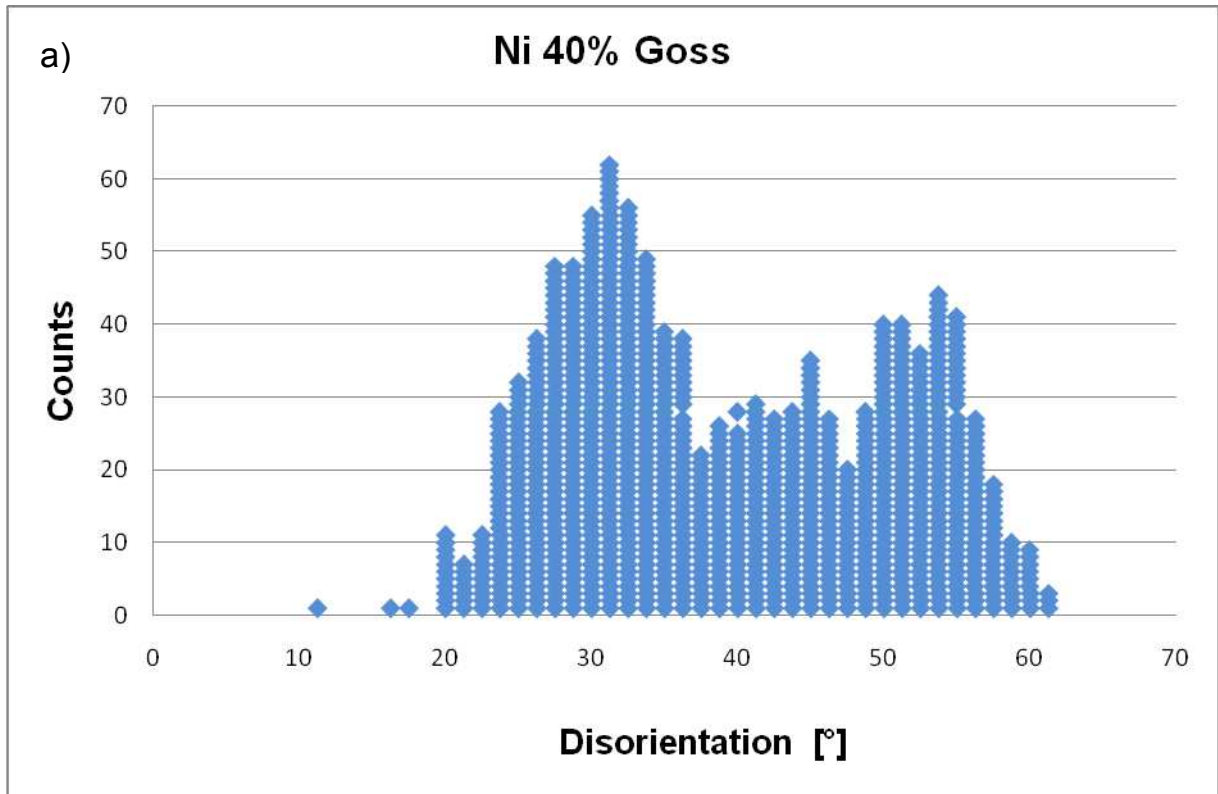
Cu (110)[1-1-2]						
Classification of 970 axes						
Classes	Counts	[%]	Rand1 [%]	Rand2[%]	Distrib1	Distrib2
0 0 1	0	0.00	10.0	6.3	0.00	0.00
0 1 1	4	0.32	8.7	10.8	0.04	0.03
0 1 2	15	1.20	25.2	19.5	0.05	0.06
1 1 1	168	13.39	5.0	7.1	2.67	1.90
1 1 2	154	12.27	15.5	15.1	0.79	0.81
1 2 2	592	47.17	11.4	16.3	4.14	2.89
1 2 3	322	25.66	24.2	25.0	1.06	1.03

Cu-2%Al (110)[1-1-2]						
Classification of 2005 axes						
Classes	Counts	[%]	Rand1 [%]	Rand2[%]	Distrib1	Distrib2
0 0 1	17	0.85	10.0	6.3	0.08	0.13
0 1 1	51	2.54	8.7	10.8	0.29	0.24
0 1 2	39	1.95	25.2	19.5	0.08	0.10
1 1 1	293	14.61	5.0	7.1	2.92	2.07
1 1 2	335	16.71	15.5	15.1	1.08	1.11
1 2 2	901	44.94	11.4	16.3	3.94	2.76
1 2 3	369	18.40	24.2	25.0	0.76	0.74

1 - in relation to random directions on the unit sphere.

2 - in relation to DISorientation axes of random MISorientations.

Tab. 6.4. Fractional classes of disorientation axes calculated for Ni, Cu and Cu-2%Al single crystals of (110)[1-1-2] orientation. Samples deformed 0.51 and then lightly annealed



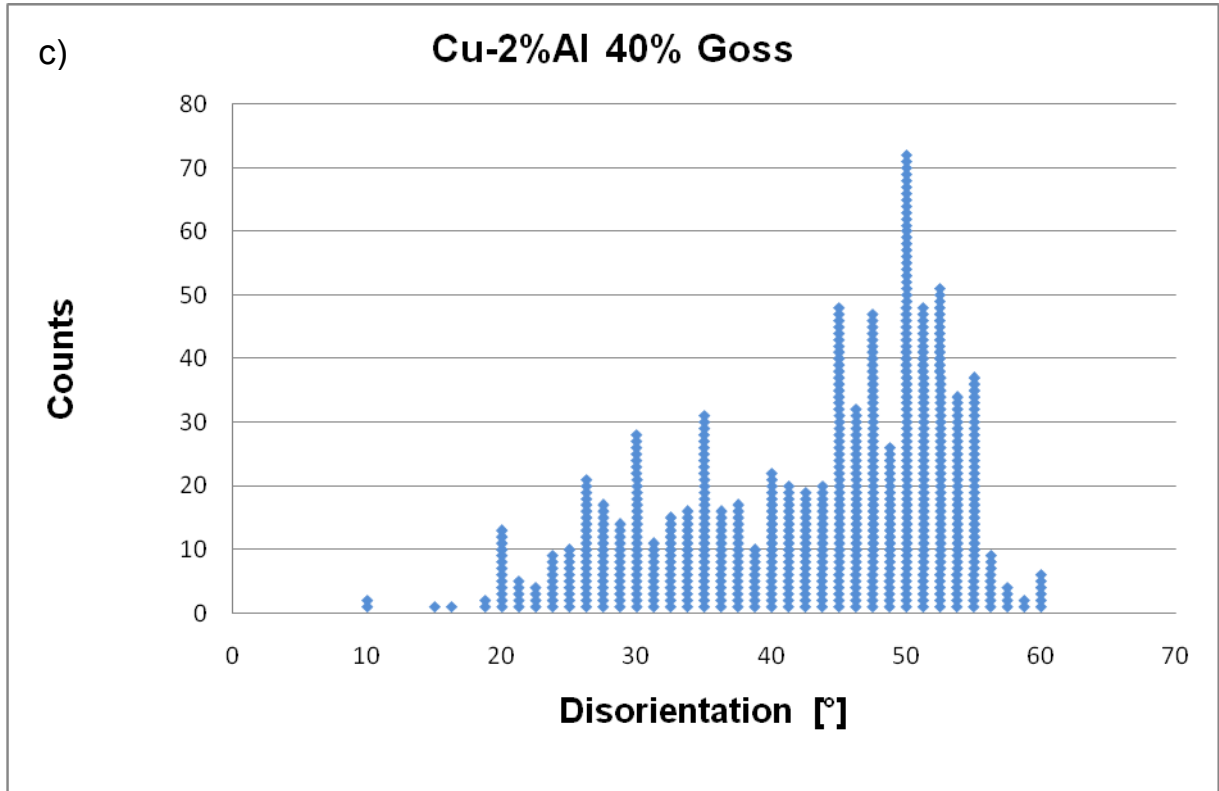
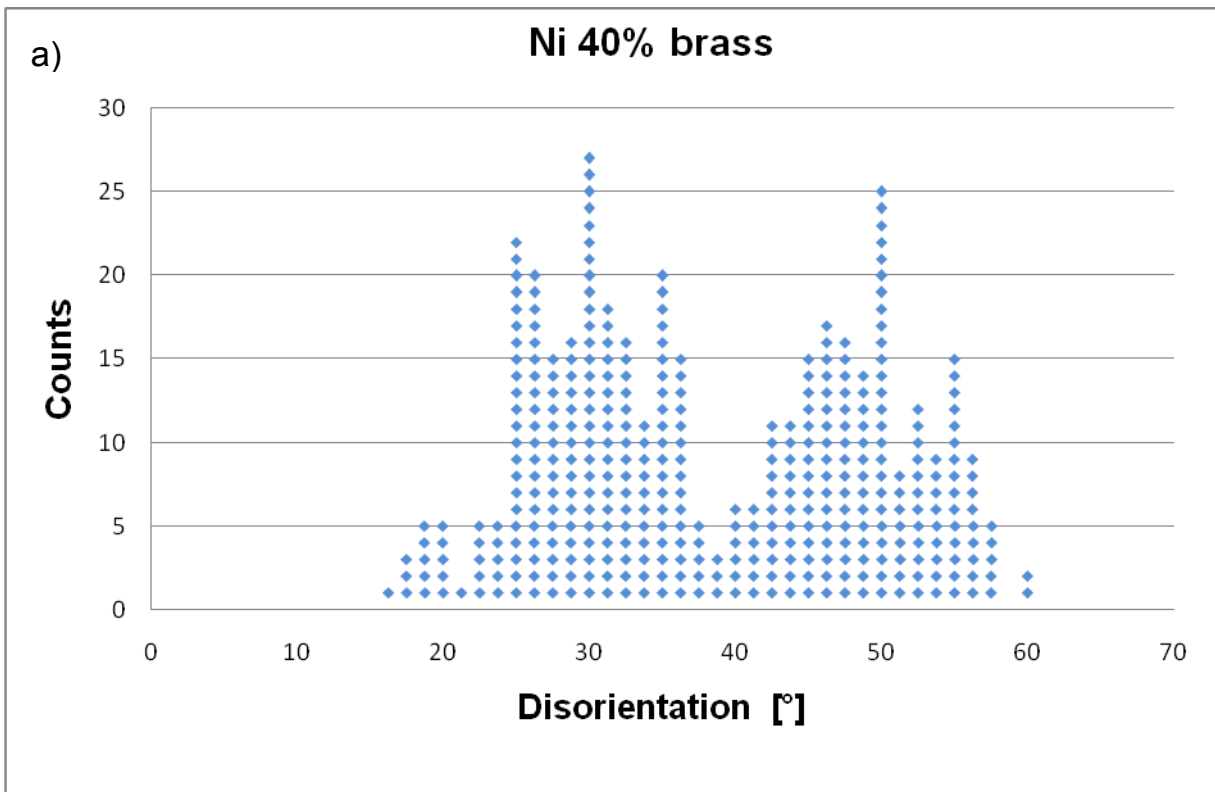


Fig. 6.30. Distribution of disorientation angles for: (a) Ni, (b) Cu and (c) Cu-2%Al with (110)[00-1] orientation. Disorientation relation between recrystallized area and nearest as-deformed neighbourhood.



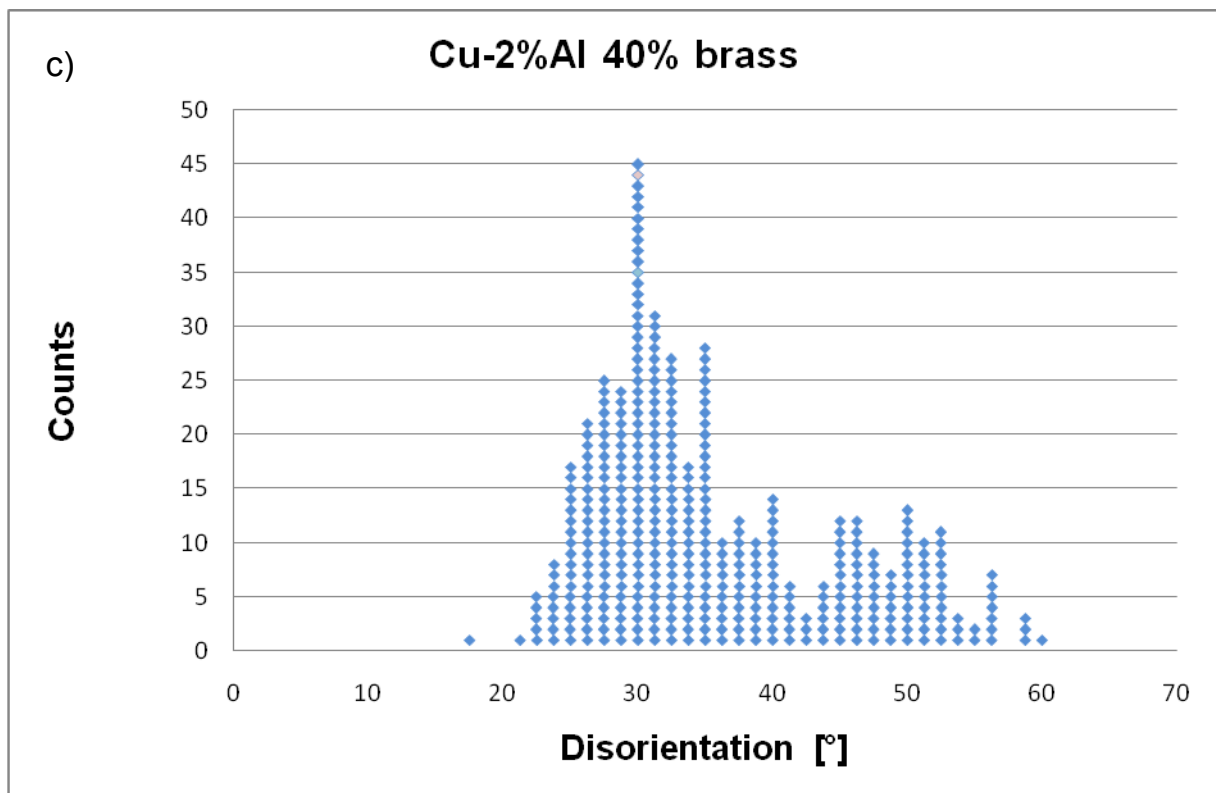
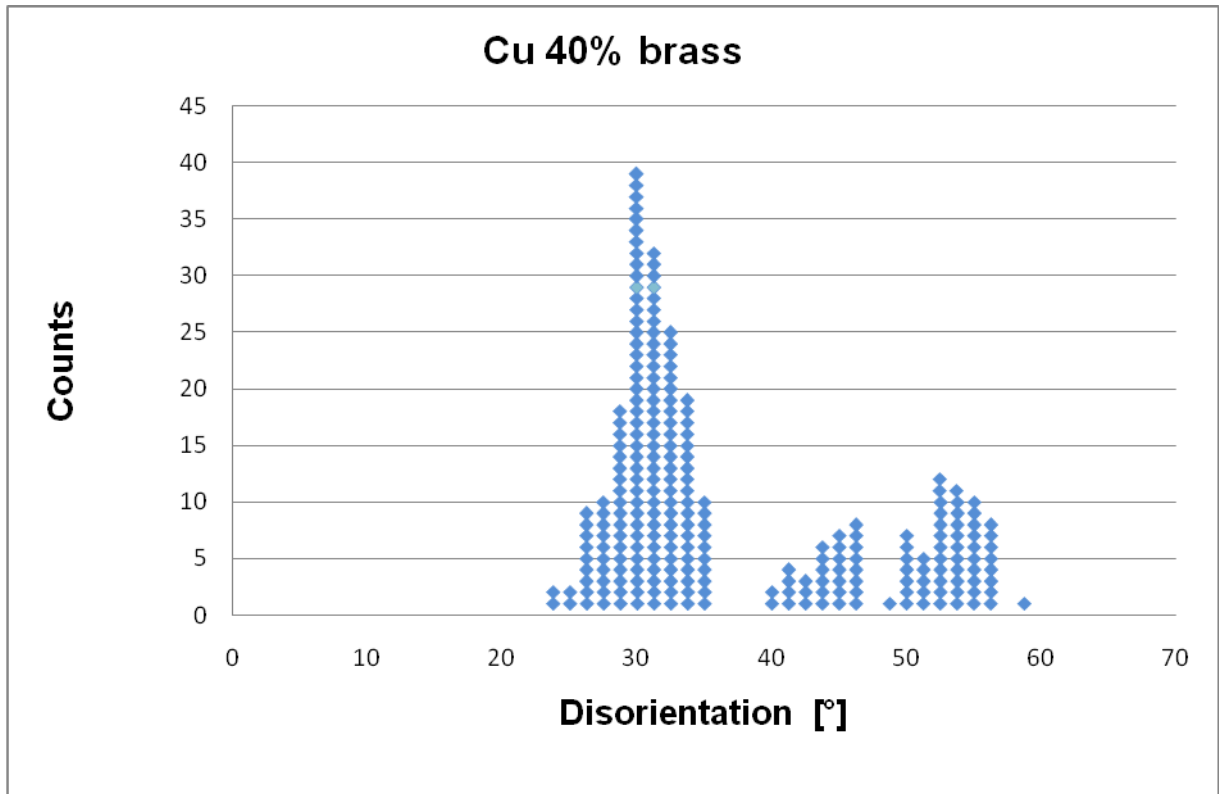


Fig. 6.31. Distribution of disorientation angles for: (a) Ni, (b) Cu and (c) Cu-2%Al with (110)[1-1-2] orientation. Disorientation relation between recrystallized area and nearest as-deformed neighbourhood.

6.2.3. *Single grains of uniform orientation and first recrystallization twins*

Annealing twins play an important role during the recrystallization process. When a grain appears to have stagnated in growth, it would often twin and rapid growth would resume. For this group of metals, the appearance of a 'primary nucleus' of homogeneous orientation is linked to the rotation around an axis located near the pole of one of the four $\{111\}$ planes. Once a nucleus appears, it transforms very quickly through the formation of a first generation twin. The most frequent situation occurs when the twinning plane normal is situated near the rotation axis. In this situation the normals of the twinning planes are close to the poles of all the four $\{111\}$ planes, i.e. both the (111) and (11-1) slip plane poles, and the (1-1-1) and (-11-1) poles which are less preferred for slip during straining.

It may be assumed that the formation of the primary nucleus of homogeneous orientation, growing into the deformed crystal, is subject to the same rules that apply to high SFE metals. The difference concerns the next step during recrystallization. Grain growth by the thermally activated movement of dislocation systems that caused the formation of the primary nucleus is blocked very early. This is probably a consequence of the fact that in medium and low SFE metals dislocation climb is strongly restricted (due to the wide splitting of the partial dislocation in low SFE materials). The present study proposes the thesis that, *after exhausting the options of dislocation migration of systems that led to nucleus formation, a change of the migrating dislocation systems ensues*. The transformation of the dislocation systems that migrate to the recrystallization front occurs in such a way that it is energetically favourable for a new, dislocation-free region to appear, with a twinning relation with respect to the original region. However, it seems to be extremely difficult to prove this hypothesis experimentally.

The occurrence of single isolated grains in the copper single crystals of (110)[00-1] orientation is presented in Figs. 6.32 and 6.33, whereas the first generation recrystallization twins in this crystallite are presented in Figs. 6.34 and 6.35. The orientation map shown in Fig. 6.34a well illustrates the morphological aspect of the 'directionality' of grain growth. As discussed for metals of high SFE, the formation of new orientations show some symmetry characteristics, i.e. the texture image of the first recrystallized grains with twins is quite symmetrical with respect to the external coordinate directions. It is clearly visible that if a grain is formed by a positive or negative rotation around a certain axis in a given region, the neighbouring twinned areas represent orientations rotated in the opposite manner with respect

to the 'primary' region. In this group of grains the disorientation axes are very close to the normals of the twinning plane.

The relation between the rotation axes and the normals of the $\{111\}$ planes of the deformed state is shown in Figs. 6.35a-m. The longest (twinned) grain direction runs along the traces of (111) and (11-1) planes, i.e. the most active planes during strain, and which are symmetrically located with respect to the ND-TD plane. The rotation axes are situated near the poles of (111) and (11-1) planes. Although the rotation axes approach the normal vector of the preferred slip planes they do not coincide with the exact location of the $\langle 111 \rangle$ directions. This may suggest a mechanism for the formation of a new grain by thermally activated movement of dislocation families, 'travelling' in pairs on one of the above-mentioned planes, as discussed above for high SFE metals.

The occurrence of single isolated grains in the copper single crystal of (110)[1-1-2] orientation is presented in Figs. 6.36 and 6.37. The orientations of new grains can be rotated around axes lying close to the normals of both highly and less active (in deformation) planes, as presented in Figs. 6.36 and 6.37, respectively. For this case of the 'brass' orientation the occurrence of first recrystallization twins is illustrated in Figs. 6.38 and 6.39. The orientation maps shown in Figs. 6.38a and 6.39a represent two different cases of recrystallization twinning. In the first case (Figs. 6.38) the rotation axis which coincides with twinning plane normal lies near the pole of the less active (during straining) $\{111\}$ planes. In the second case (Figs. 6.39) the rotation axis and twinning plane normal lie close to the pole of the highly active $\{111\}$ plane.

Crystallographically, annealing and deformation twins are identical, and consist of stacking faults on consecutive $\{111\}$ planes. These faults are produced by the glide of Shockley partials. It is easy to visualize the formation of these partials during deformation [Christian and Mahajan (1995)]. However, in the absence of an external stress the movement of partials is difficult to comprehend.

Several models have attempted to address this issue. Dash and Brown [Dash and Brown (1963)] showed for the first time that annealing twin nuclei consist of stacking faults. Based on these experimental data, Meyers and Murr [Meyers and Murr (1978)] suggested that the faults pop out from ledges present on grain boundaries. But the mechanistic details of this model were missing. In the model presented by Pande et al [Pande *et al.* (1990)], the authors assumed that the formation of twins is caused by grain boundary migration and their density

depends on the driving force for migration. More recently, a microscopic model for the formation of annealing twins in fcc metals was proposed by Mahajan *et al.* [Mahajan *et al.* (1997)]. The authors argued that Shockley partial loops nucleate on consecutive $\{111\}$ planes by growth accidents occurring at propagating $\{111\}$ steps which are associated with a moving grain boundary. They also stated that the higher the velocity of the boundary, the higher the probability of growth accidents. However, this latter statement was not confirmed by the experimental results of Field *et al.* [Field *et al.* (2007)] who showed that the slower grain growth, the higher the fraction of twin boundaries.

A lot of effort was made in earlier work [Paul *et al.* (2002c) and (2007)] to prove the thesis that after the formation of primary nucleus of homogeneous orientation, further orientation changes during recrystallization may be effected only by recrystallization twinning. In metals of medium and low SFE, the repeated appearance of recrystallization twins (on different twinning planes and various generations of twins) leads to a strong scattering of the texture 'image'. This scattering is so profuse, that the appearance of third generation twins (at a given fraction of primary nucleus orientations) virtually leads to an entirely scattered texture image [Paul *et al.* (2007)]. Nevertheless, it is not clear at the moment if the appearance of specific variations of recrystallization may be related to dislocation mechanisms, analogous to those involved in the formation of primary nuclei.

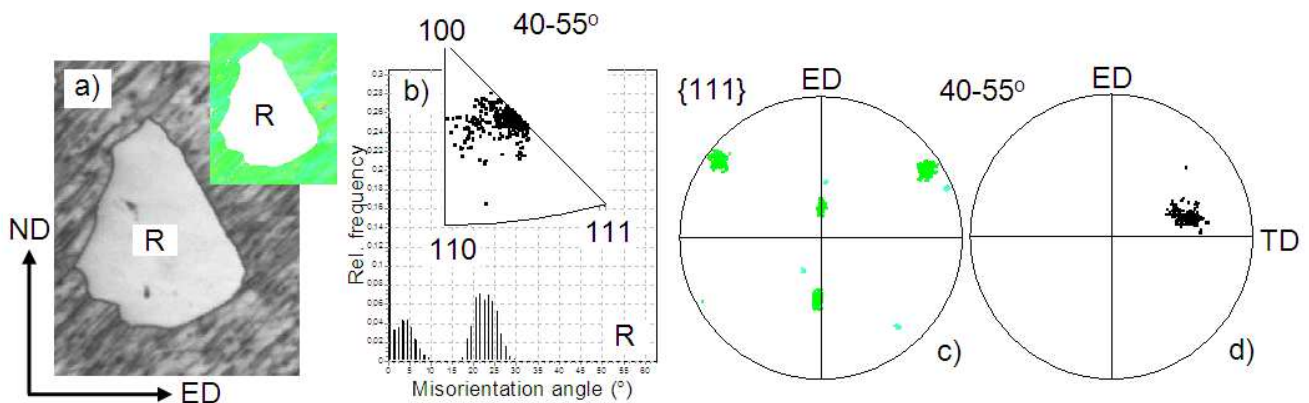


Fig. 6.32. (a) SEM/EBSD orientation maps showing an isolated nuclei of uniform orientation growing in $(110)[00-1]$ oriented copper samples deformed up to 0.51. (b) Disorientation angles and axes (in crystallite co-ordinate) distributions. (c) The $\{111\}$ pole figure and (d) disorientation axes distribution presented in sample co-ordinates. SEM/EBSD local orientation measurements with 200nm step size. Sample recrystallized at 350K for 25s. Orientation maps presented as 'function' of band contrast (larger) and IPF||Y (smaller).

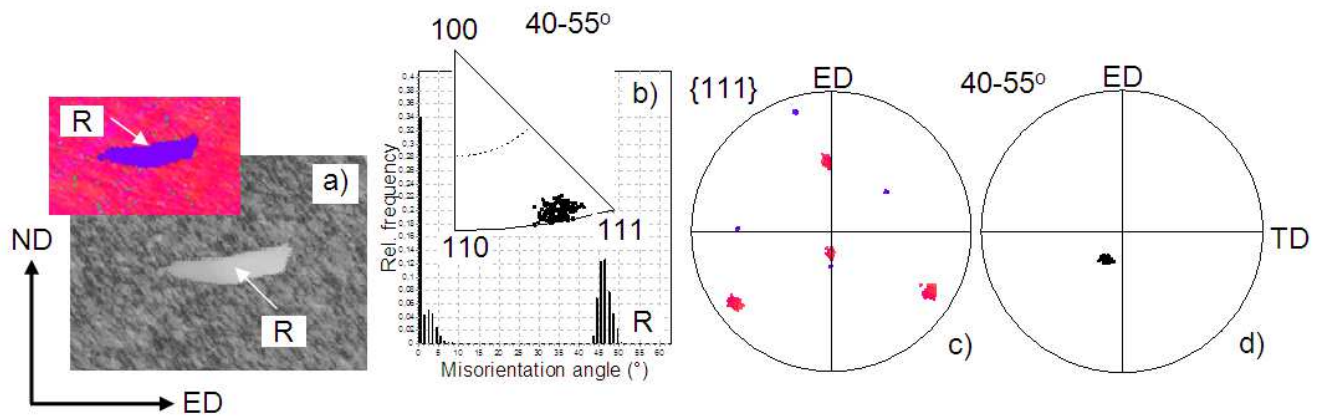


Fig. 6.33. (a) SEM/EBSD orientation maps showing an isolated nuclei of uniform orientation growing in (110)[00-1] oriented copper samples deformed up to 0.51. (b) Disorientation angles and axes (in crystallite co-ordinate) distributions. (c) The {111} pole figure and (d) disorientation axes distribution presented in sample co-ordinates. SEM/EBSD local orientation measurements with 200nm step size. Sample recrystallized at 346K for 30s. Orientation maps presented as 'function' of band contrast (larger) and IPF||X (smaller).

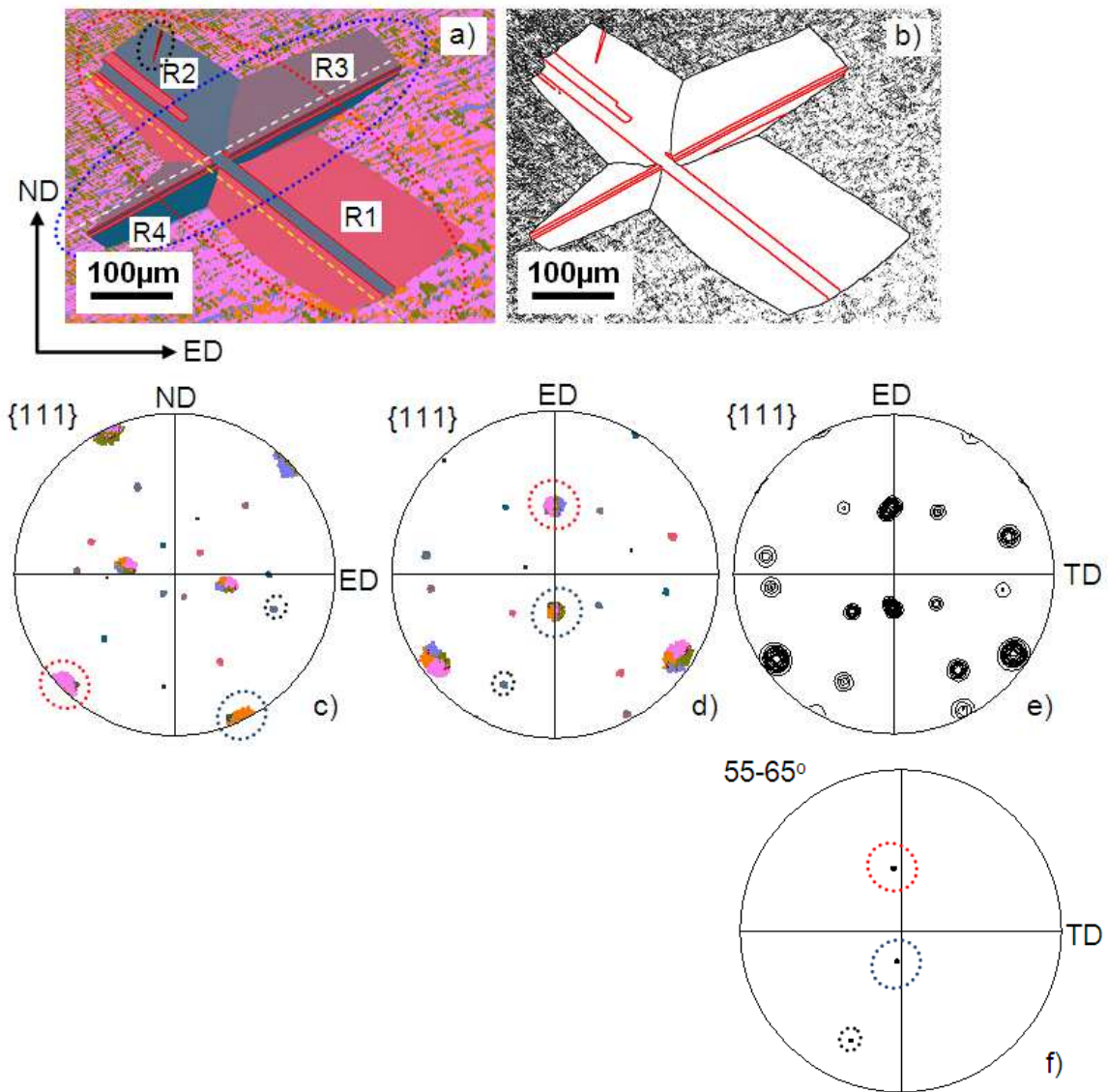


Fig. 6.34. Directionality of grain growth observed in Cu with (110)[00-1] orientation deformed up to 0.51 and then recrystallized at 355K for 40s for. SEM/EBSD orientation maps presented as 'function' of: (a) 'all Euler' colour code (b) grain boundaries >15deg, (c) and (d) the {111} pole figures presented on ND-ED and ED-TD plane, respectively. (e) Continuous form of the {111} pole figure on ED-TD plane. (f) Disorientation axes distribution showing positions of the twinning planes.

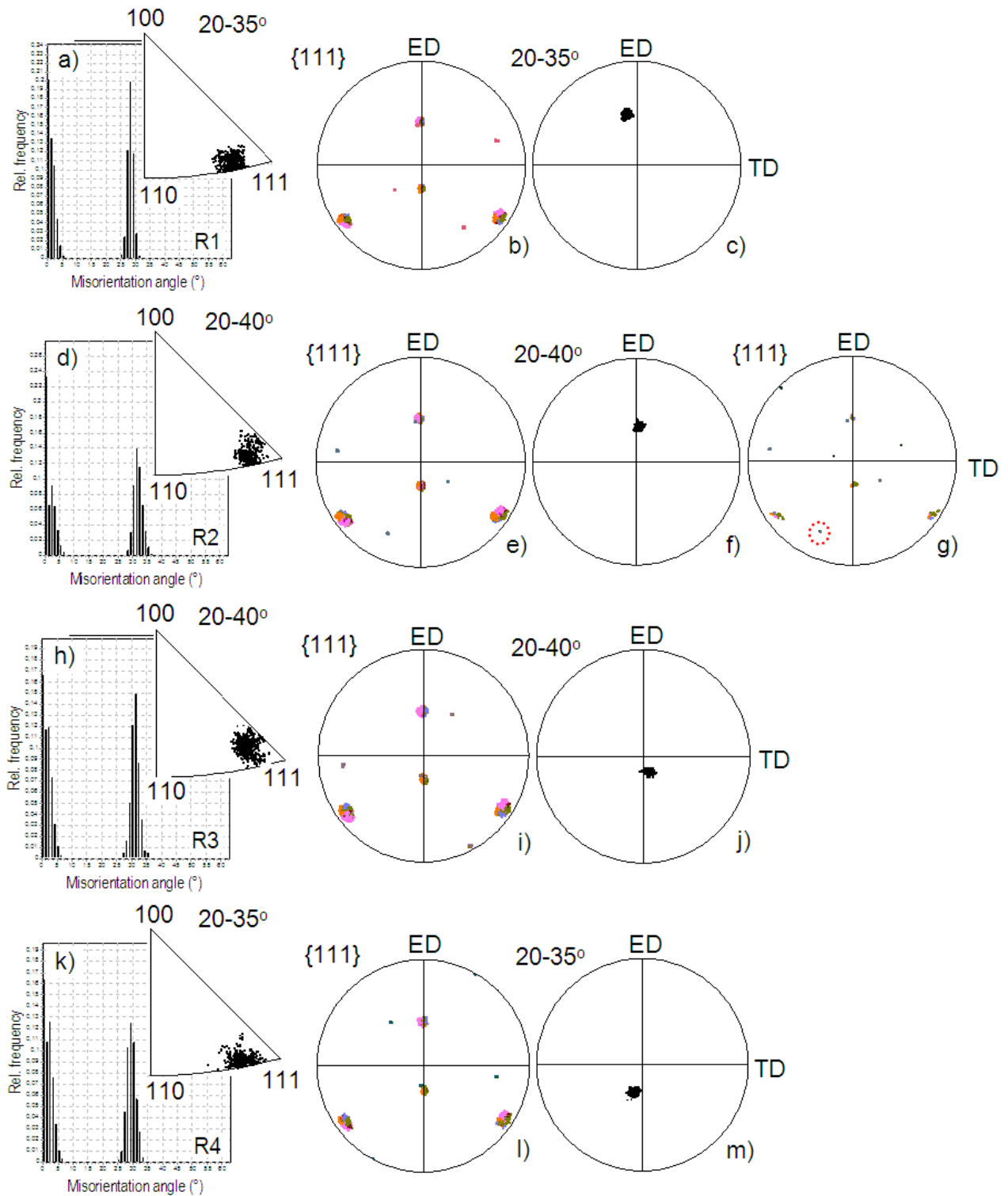


Fig. 6.35. Crystallographic aspect of grain growth in Cu with (110)[00-1] orientation deformed up to 0.51 and then recrystallized at 355K for 40s. (a), (d), (h) and (k) Disorientation angles and axes distributions. (b), (e), (g), (j) and (l) The {111} pole figures showing the orientations of recrystallized areas and nearest deformed neighbourhood. (c), (f), (j) and (m) Disorientation axes projections in sample coordinates.

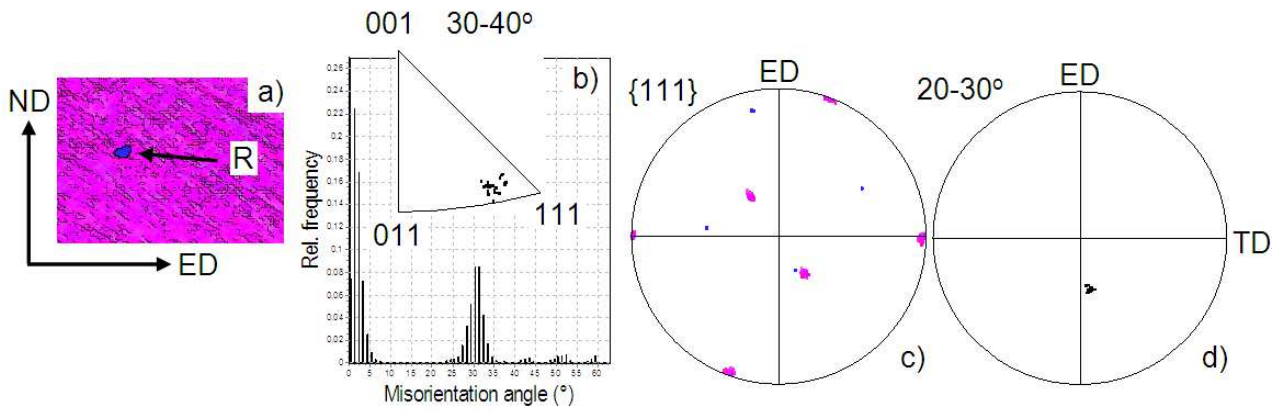


Fig. 6.36. (a) SEM/EBSD orientation maps showing an isolated nuclei of uniform orientation growing in (110)[1-1-2] oriented copper samples deformed up to 0.51. (b) Disorientation angles and axes (in crystallite co-ordinate) distributions. (c) The {111} pole figure and (d) disorientation axes distribution presented in sample co-ordinates. SEM/EBSD local orientation measurements with 200nm step size. Sample recrystallized at 628K for 70s. Orientation maps presented as 'function' of IPF||Y color code. Case of rotation around poles of highly active (during deformation) planes.

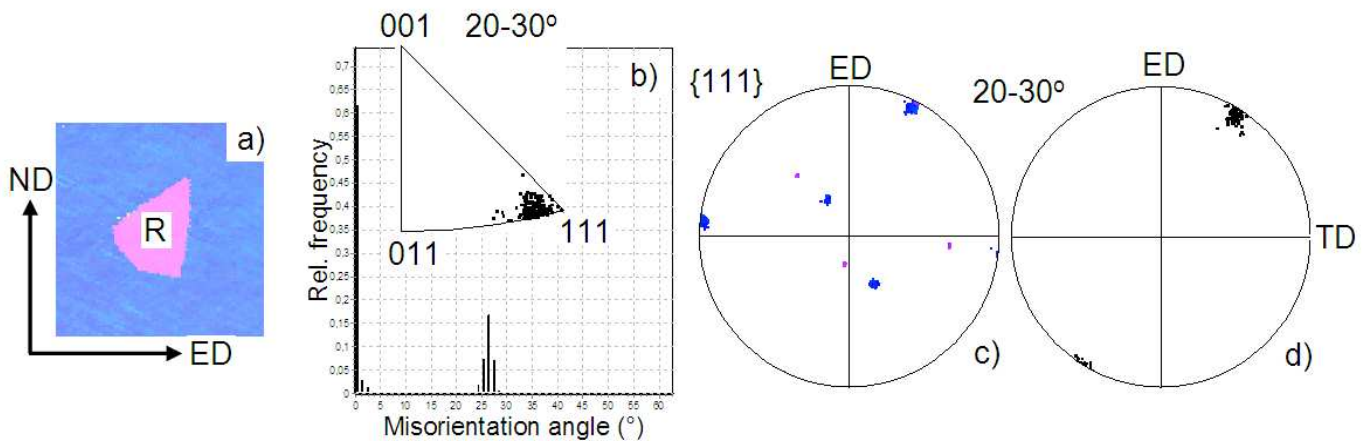


Fig. 6.37. (a) SEM/EBSD orientation maps showing an isolated nuclei of uniform orientation growing in (110)[1-1-2] oriented copper samples deformed up to 0.51. (b) Disorientation angles and axes (in crystallite co-ordinate) distributions. (c) The {111} pole figure and (d) disorientation axes distribution presented in sample co-ordinates. SEM/EBSD local orientation measurements with 200nm step size. Sample recrystallized at 623K for 65s. Orientation maps presented as 'function' of IPF||Y color code. Case of rotation around poles of less active (during deformation) planes.

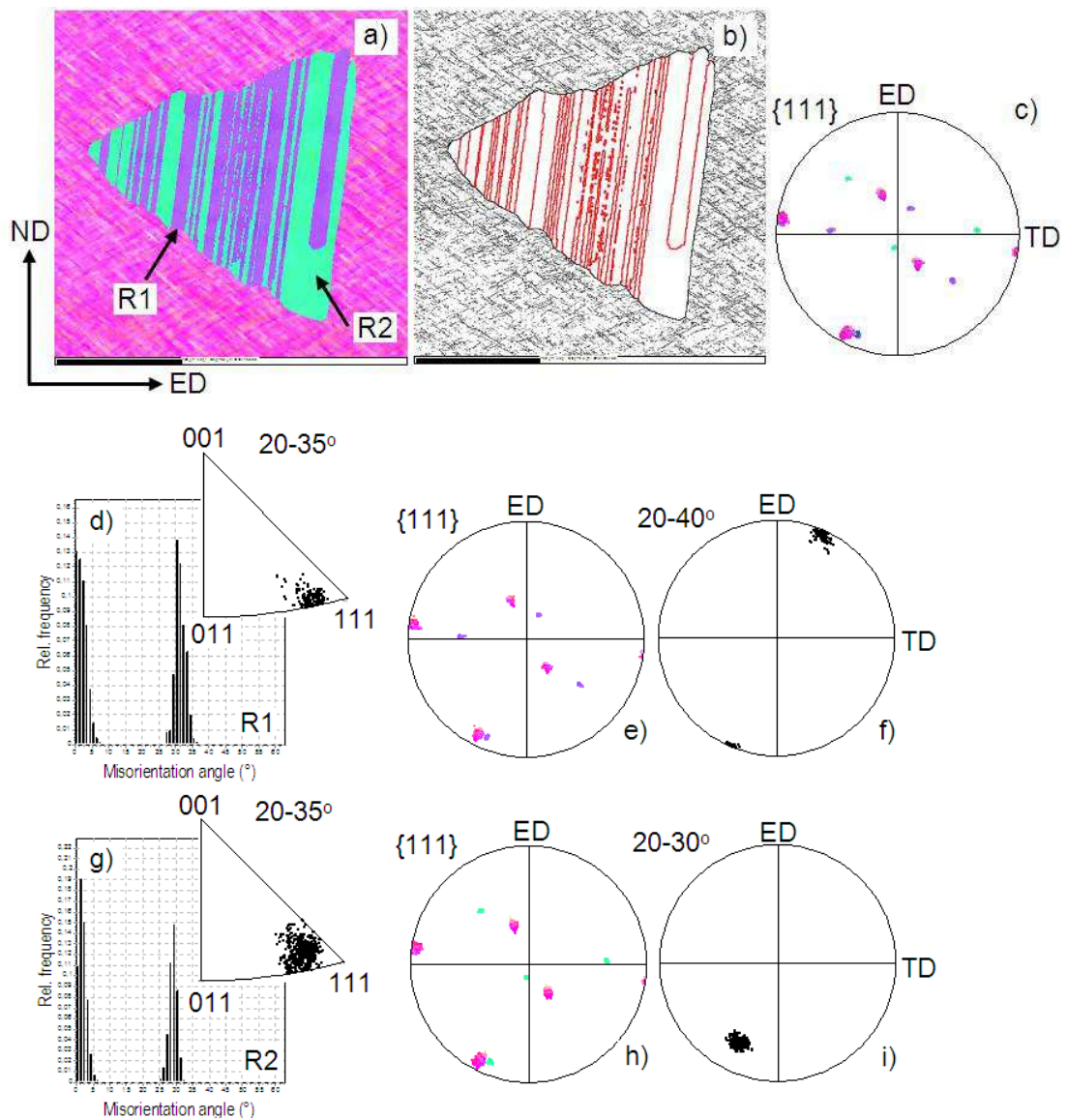


Fig. 6.38. First recrystallization twins observed in Cu of (110)[1-1-2] initial orientation deformed up to strain of 0.51 and recrystallized at 628K for 70s. (a) and (b) orientation maps and (c) corresponding {111} pole figure. (d) and (g) Disorientation angles and axes (in crystallite co-ordinate) distributions. (e) and (h) The {111} pole figures showing orientations of recrystallized areas and nearest deformed neighbourhood. (f) and (j) Disorientation axes projections in sample coordinates. Case 1 - the twinning plane normal is situated near the pole of less active (during deformation) plane.

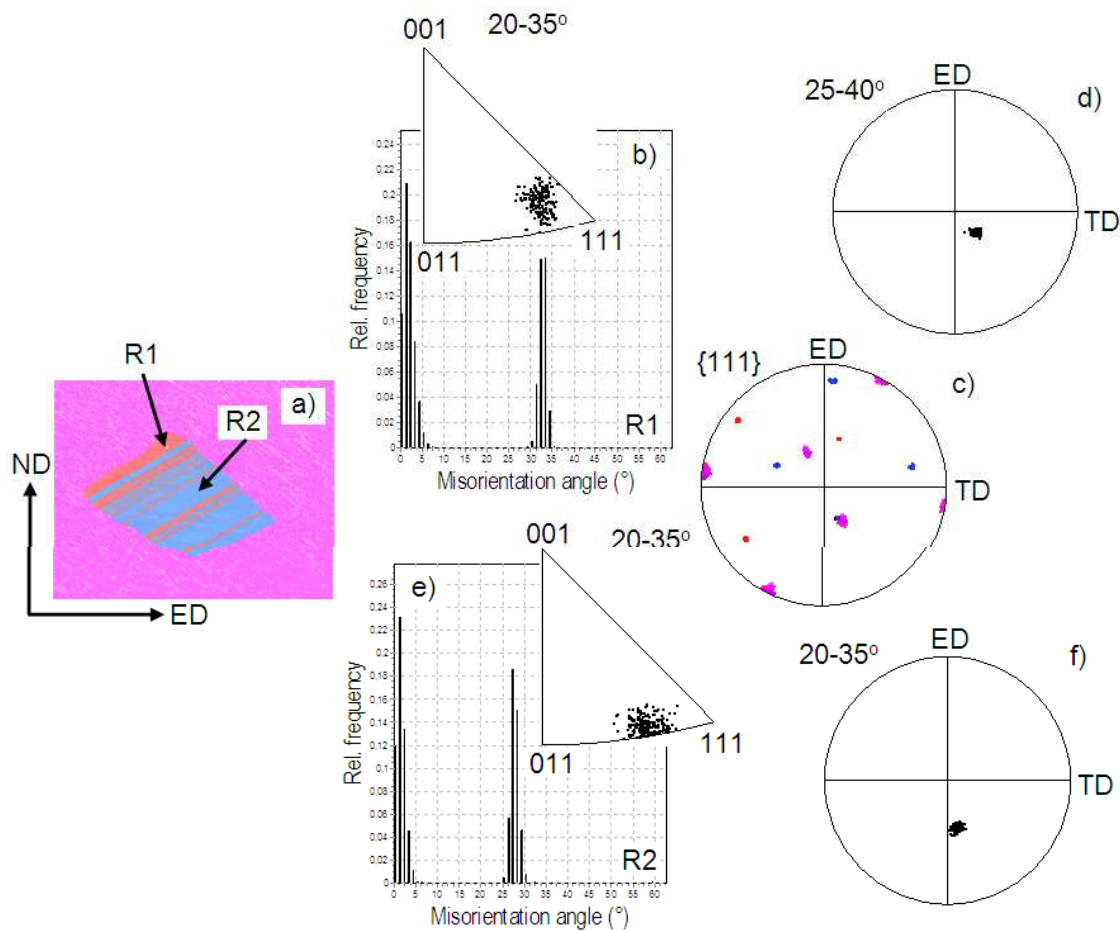


Fig. 6.39. First recrystallization twins observed in Cu of (110)[1-1-2] initial orientation deformed up to strain of 0.51 and recrystallized at 632K for 63s. (a) and (b) orientation maps and (c) corresponding {111} pole figure. (d) and (g) (b) Disorientation angles and axes (in crystallite co-ordinate) distributions. (e) and (h) The {111} pole figures showing orientations of recrystallized areas and nearest deformed neighbourhood. (f) and (j) Disorientation axes projections in sample coordinates. Case 2 - the twinning plane normal is situated near the pole of less active (during deformation) plane.

6.2.4. *The crystallography of recrystallization growth*

In this section the different stages of recrystallization nucleation and growth are characterized by EBSD orientation maps. They can be described as [Paul *et al.* (2007)]:

1. the formation of single isolated nuclei of uniform orientation,
2. the early stages of recrystallization growth and the first recrystallization twins,
3. the formation of grains with different twinning variants leading to successive twin generations, and
4. the formation of chains of different nuclei by recrystallization twinning.

This sequence of events is generally observed in all three metals (and both orientations) included in group II.

The single grains of uniform orientation. All orientation maps are presented as IPF maps. Analysis of different cases of single isolated nuclei in Ni, Cu and the Cu-2%Al alloy leads to the conclusion that the same types of orientation relations between deformed and recrystallized grains occurs, as previously observed in aluminium and the Al-1%Mn alloy. Figures 6.32 and 6.33 illustrate a single isolated nuclei that appears in the copper single (110)[00-1] crystal, whereas Figs. 6.36 and 6.37 show new grains in the copper (110)[1-1-2] single crystal after 0.51 deformation. The deformation structure is composed of two sets of microbands. The {111} pole figures show the orientations of the grain and the adjacent as-deformed areas. A detailed analysis of all the disorientations in different directions across the recrystallization front clearly shows the occurrence of $\alpha\langle uvw \rangle$ orientation relation. The disorientation axes lie close to the normal of (111) plane but not coincide with them. In the case of Figs. 6.33 and 6.36 the new grains are disoriented with respect to deformed state by rotation around axes lying close to the normal of the highly active (during deformation) {111} planes, whereas in the situation presented in Fig. 6.37 around less active ones. In both cases, the distribution of angles across the recrystallization front has mostly a maximum close to 25-35°.

In the above cases, the orientation relationship across the recrystallization front may be quite precisely described as a relation close to $\sim(25-35^\circ)\langle uvw \rangle$, with disorientation axes lying close

to $\langle 111 \rangle$ (but coincidence is observed very rarely)².

For the case presented in Fig. 6.34 and 6.35), the orientation relation between the recrystallized grains and their nearest deformed regions can, to a first approximation, be specified as a relation of type $\sim 25\text{-}35^\circ \langle 111 \rangle$. However, such a description is not precise. Namely, the rotation around an axis situated near the $[111]$ direction can be presented as a composition of two rotations (by about $35\text{-}40^\circ$) around the $[-121]$ and $[211]$ axes, resulting from the thermally activated movement of two dislocation families on the $(1-11)$ plane. The final result would be comparable in both cases. It is impossible to decide if the crucial role in the formation of new orientations is played by the poles of either the (111) or $(11-1)$ planes, or if the rotation occurs around the pole situated near $[111]$, or even if this is the 'final result' of a more complicated rotation around two axes related by dislocation mechanisms. *The resolution of this matter is difficult and the results of in-situ annealing TEM experiments should be considered unsuccessful.*

The occurrence of the first recrystallization twins. In medium-low SFE metals, growth occurs by both boundary migration and twinning (from the initial nucleus orientation) on different $\{111\}$ twinning planes followed by growth of the twinned areas. In most cases the normal of the twinning plane lies very close to the rotation axis. (It is important to note that in the case of the first recrystallization twins it is very difficult to know which of the two areas is the primary nucleus). However, it is important to note that first generation recrystallization twinning can result from twinning on a plane with a normal near that of inactive (e.g. Fig. 6.32) or active slip planes (e.g. Fig. 6.33). Examples of microstructures with first generation recrystallization twins are shown in Figs. 6.34-6.35 and 6.38-6.39 for the Goss and brass orientations, respectively.

The chains of primary nuclei with recrystallization twins. For even the most complicated chains of twinned, recrystallized grains, it is always possible to identify, within the set of recrystallized orientations, the original area (or areas) which exhibits the above type of disorientation with respect to the deformed crystal. Identification of the 'original' area is simple in principle, except for the cases when the rotation axis is close to the normal of the twinning plane. In these cases it cannot be unequivocally determined which area is the

² However, it should be emphasized that this 'simple' explanation of the observed disorientations may result from an 'illusion'. We assume that the grain with uniform orientation is completely surrounded by deformed regions, whereas in fact it should be the twin.

original region 'growing out of' the deformed state and which is its twin.

Figs. 6.34 and 6.35 show a system of two groups of grains with recrystallization twins, growing into the deformed structure with a planar front. The orientation relation between the recrystallized and deformed grains, including all segments of the recrystallization front, is defined by disorientation angles within the range of 25-35°, whereas the disorientation axes are close (but do not coincide) to the $\langle 111 \rangle$ directions. Large recrystallization twins of the first generation appear as the result of twinning on planes whose normals lie in the immediate proximity of the rotation axis of the 'primary' area. As in earlier examples of elongated grains observed in high SFE metals, in this case (Cu (110)[00-1] orientation), the interfaces lie along the traces of the $\{111\}$ planes whose normals are situated near the rotation axis for the grain to deformed/recovered matrix relation.

Growth of the recrystallized grains and multiple twinning. For the most complicated chains of recrystallized grains it is always possible to identify, within the set of twin related orientations, the original area characterized by near 25-35°($\langle uvw \rangle$) type disorientation, with respect to the deformation components [Paul et al (2002c, 2007)]. But which of the different possible recrystallization twinning systems will be successful during growth appears too complicated to be explained.

Wilbrandt [Wilbrandt (1989)] has shown that multiple twinning can lead to an almost 'grey' texture after six generations if the twinning systems operated at random. (In this study only third generation twins were observed). However, the formation of annealing twins on a particular system from a single isolated grain orientation does not occur at random. This result has major consequences for the interpretation of annealing texture formation. Non-random twinning limits the number of orientations which can occur in the recrystallized structure. This is also confirmed by the present observations. Despite the fact that all 4 $\{111\}$ planes can play an important role in the creation of new nuclei orientation, the normals of the most active slip planes are preferred in this process. Subsequently, the initial nucleus can change the orientation by twinning. In this context, recrystallization twinning can only be regarded as a secondary mechanism.

Multiple twinning can re-orientate the grain into twin relations with respect to the components of the as-deformed state. However, an exact twin relation between isolated, recrystallized grains, of uniform orientation has never been observed in this work. This is contrary to some earlier experimental data. A twin relationship between the deformed and recrystallized grains

(forming compact chains of grains) was found, e.g. by Berger *et al.* (1988) in the context of their detailed local orientation measurements by TEM and also by Gottstein (1984) where the twin related components were derived from ODFs and pole figures.

The mechanisms responsible for the texture transformations observed at the very early stages of recrystallization are schematically summarized in Figure 2.1, as proposed earlier by Paul *et al.* [Paul et al (2007)].

7. SUMMARY AND CONCLUSIONS

This thesis has systematically analysed the initial stages of recrystallization in a series of fcc metals possessing a wide range of SFEs. Although recrystallization nucleation has been studied for several decades, it can be stated that we are still a long way from a full description of the mechanisms controlling the structural changes during this exceptional transformation. This is particularly true for the description of morphological and textural changes. In the current research project, and to reduce the number of variables that control the process, the experiments were performed on single crystal samples of stable orientations, deformed in plane strain compression. This choice avoids ambiguities in interpretation caused by the pronounced role of high-angle boundaries from other deformed structures, during the formation of a new grain in annealing.

This study focuses on an explanation of the mechanism leading to the formation of primary nucleus/grain during recrystallization, and particularly on the possible relation of this process to dislocation mechanisms. The interest in the above topic originated in the fact that current theories to describe the processes of texture transformation are inconsistent. The most conspicuous case regards the 'classical' disorientation relation of $40^\circ\langle 111 \rangle$ type across the migrating recrystallization front. From the perspective of operative dislocation mechanisms there is no physical justification for these values of angle or disorientation axis.

The recrystallization process is closely related to the preceding straining process during which numerous crystal defects are generated. Therefore, intuitively one expects that the nucleation stages of recrystallization, when the deformed structure is transformed into a new recrystallized grain, must be connected with the removal of defects. Thermally activated displacement of dislocations inside the dislocation cells and the migration of dislocation small-angle boundaries imply a change of orientation of the area where these processes occur.

Based on local orientation measurement techniques by SEM and TEM, the orientation relations which appear at the initial stages of recrystallization between a new grain and the as-deformed orientations have therefore been systematically analysed. Our research allows us to draw the following conclusions:

- The classical orientation relation for fcc metals between the deformed matrix and the recrystallized grain, described as $40^\circ\langle 111 \rangle$, was only rarely found. In most cases, it was

replaced by other orientation relations, in which disorientation axes were close to $\langle 122 \rangle$, $\langle 012 \rangle$ and $\langle 112 \rangle$.

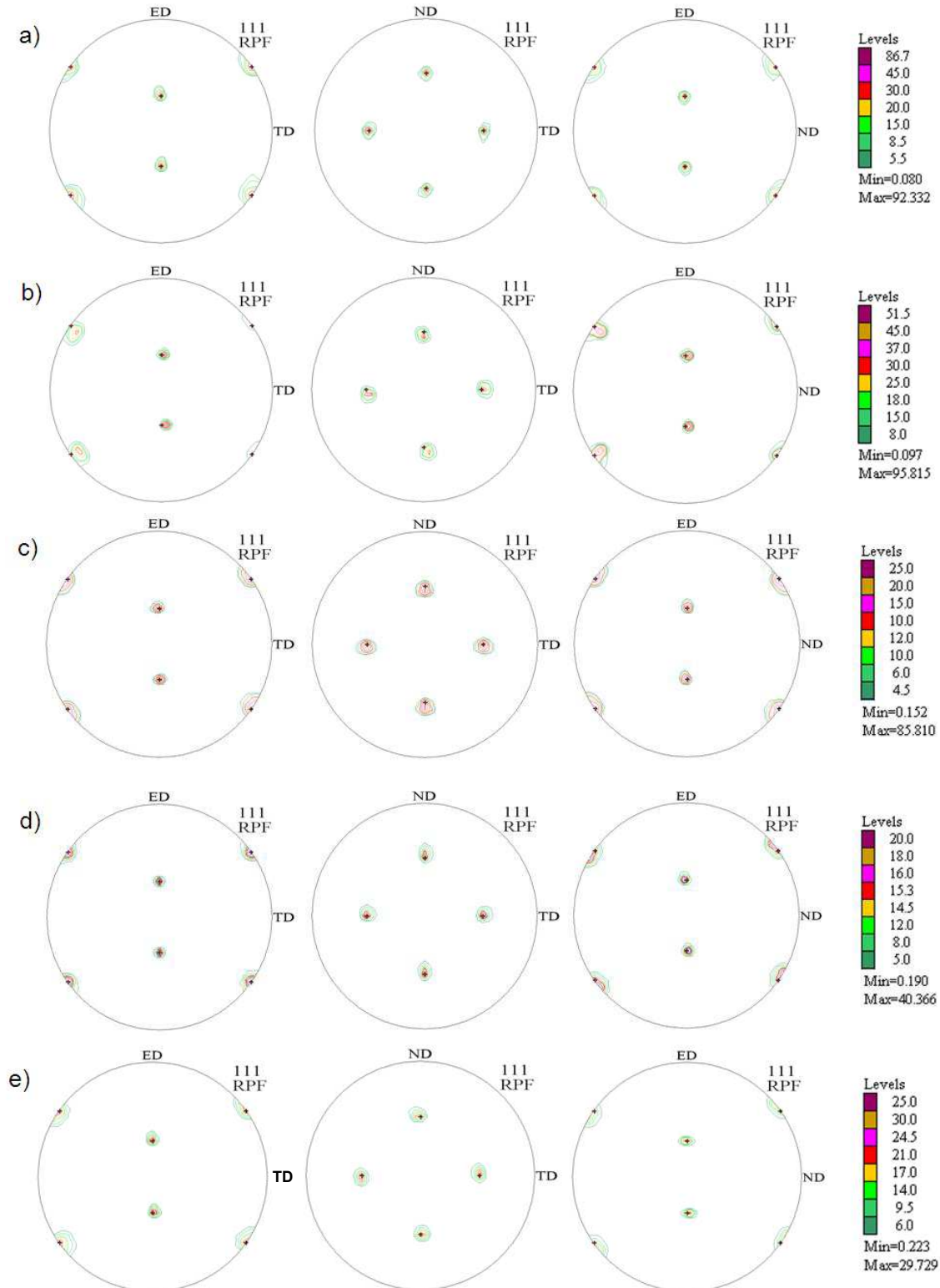
- The present experiments show that the migration of newly formed grain boundaries and the 'consumption' of the deformed regions occur as a result of mechanisms related to the crystal lattice rotations in the deformed state.
- Regardless of the initial crystal orientation, there is a strong relation of the as-deformed orientations with the orientations of new grains at the initial stages of recrystallization. For the metals studied here and both initial orientations at the initial stages of recrystallization, the appearance of a specific number of new orientation groups of new grains was demonstrated. The orientation relation across the recrystallization front 'defines' the final rotation by angles in the range $25-45^\circ$ around axes mostly grouped about the $\langle 122 \rangle$, $\langle 012 \rangle$, $\langle 112 \rangle$ and $\langle 111 \rangle$ directions. In the case of high SFE metals, the decisive role is played by axes close to the poles of the most active $\{111\}$ planes during deformation. In the case of metals with medium and low SFE (i.e. undergoing twinning in recrystallized grains) these were the axes grouped around the normals of all four $\{111\}$ planes. But also in this case, one clearly observes a grouping of disorientation axes around the poles of the most active planes during deformation.
- The variations of disorientation axes tend to follow the orientation variations in the deformed state. This facilitates 'the orientation stability' of a new grain growing into the as-deformed structure.
- In the case of metals of medium-low SFE, the orientation of the growing new grain quickly transforms through the formation of a first generation twin. The most frequent situation occurs when the normal of the twinning face plane is situated near the rotation axis, around which the crystal lattice of the 'primary nuclei' rotates. This configuration means that the normals to the twinning planes are close to the poles of all the four planes $\{111\}$, i.e. of both the active (111) and $(11-1)$ planes as well as the latent $(1-1-1)$ and $(-11-1)$ slip planes.
- A large fraction of new grains, regardless of the metal, are characterised by a strongly elongated shape. For both initial orientations, preferred grain growth occurred along the (111) and $(11-1)$ planes, i.e. the most active planes during strain, which are located symmetrically to the ND-TD plane. The orientations of the elongated grains were directly related to those of the group of as-deformed orientations. The crystal lattice of each grain

group undergoes rotations (positive or negative) around diverse groups of disorientation axes. Since the rotation axes are situated near the poles of the (111) and (11-1) planes, this may 'define' the mechanism responsible for the formation of the new grain orientation. It probably results from the thermally activated movement of dislocation families, travelling in pairs on one of the above-mentioned planes. Although the rotation axes approach the normal vector of the active slip planes during deformation, they only rarely coincide with the exact location of the $\langle 111 \rangle$ direction.

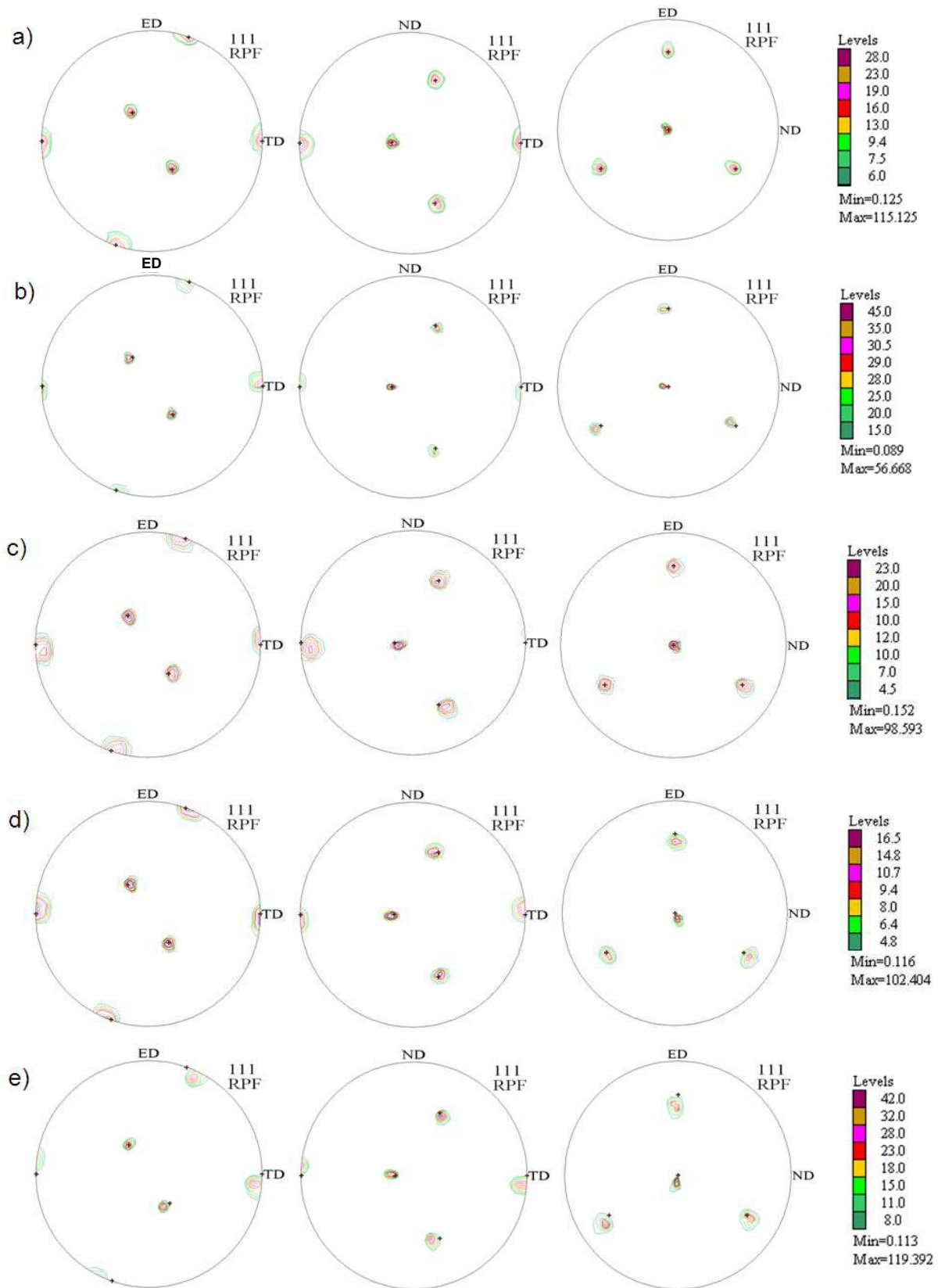
- The crystal lattice rotation of elongated grains takes place around the axes situated near the $\langle 111 \rangle$ pole, which determines the particular {111} plane, across which preferred grain growth occurs. The crystal lattice of the grains elongated along the (111) plane undergoes a general rotation around an axis near [111]. By analogy, the crystal lattice of the grains elongated along the (11-1) plane undergoes a general rotation around an axis near [11-1].
- The local rotation tendencies (during the formation of the primary nucleus) can be explained by the thermally activated, coordinated movement of dislocation families. If the rotation axis coincides with the [111] direction, it can be assumed that the dislocation movement takes place on the (11-1) plane. Then, rotations by $25-45^\circ$, resulting from the movement of two dislocation families on that plane, induce an 'overall' rotation around an axis near the pole of the (111) plane. The movement of dislocation families on the (111) plane, inducing rotation around axes close to the [11-1] pole can be similarly assumed. A change in the direction of movement of dislocation families explains the opposing tendency of the crystal lattice rotation of recrystallized grain. The spread in the value of the lattice rotation angle of individual grains (of a given category) may result from the 'uneven' contribution of two dislocation families (systems) grouped on one plane.
- An additional 'contribution' to the rotation of a grain crystal lattice is possible, resulting from the thermally activated movement of dislocations concentrated in another system, less preferred during deformation, or the occurrence of a different combination (compared with the deformation) of dislocation family movements. In each of these cases, dislocation motion must lead to a slight variation of the disorientation axes. These cases seem to predominate during the transformation of the texture 'image' at the initial stages of recrystallization.

- The observed disorientation axes across the recrystallization front are very different from the ones observed in the deformed state, i.e. between individual pixels of the orientation map of the deformed (recovered) state.

ANNEXE 1

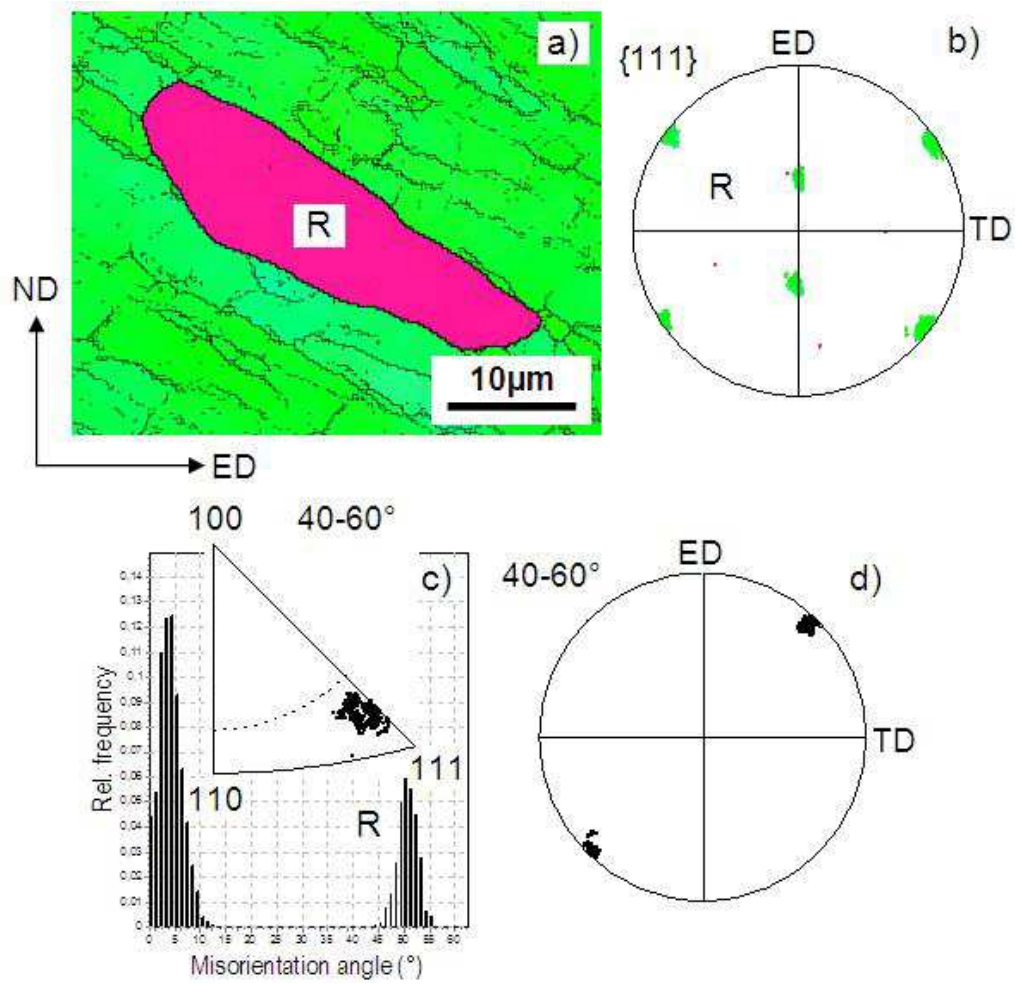


A. 1.1. Global texture measurements by X-ray diffraction. The {111} pole figures measured on ED-TD, ND-TD and ED-ND planes for: (a) Al, (b) Al-1%Mn, (c) Ni, (d) Cu and (e) Cu-2%Al. Single crystals of (110)[00-1] orientations.

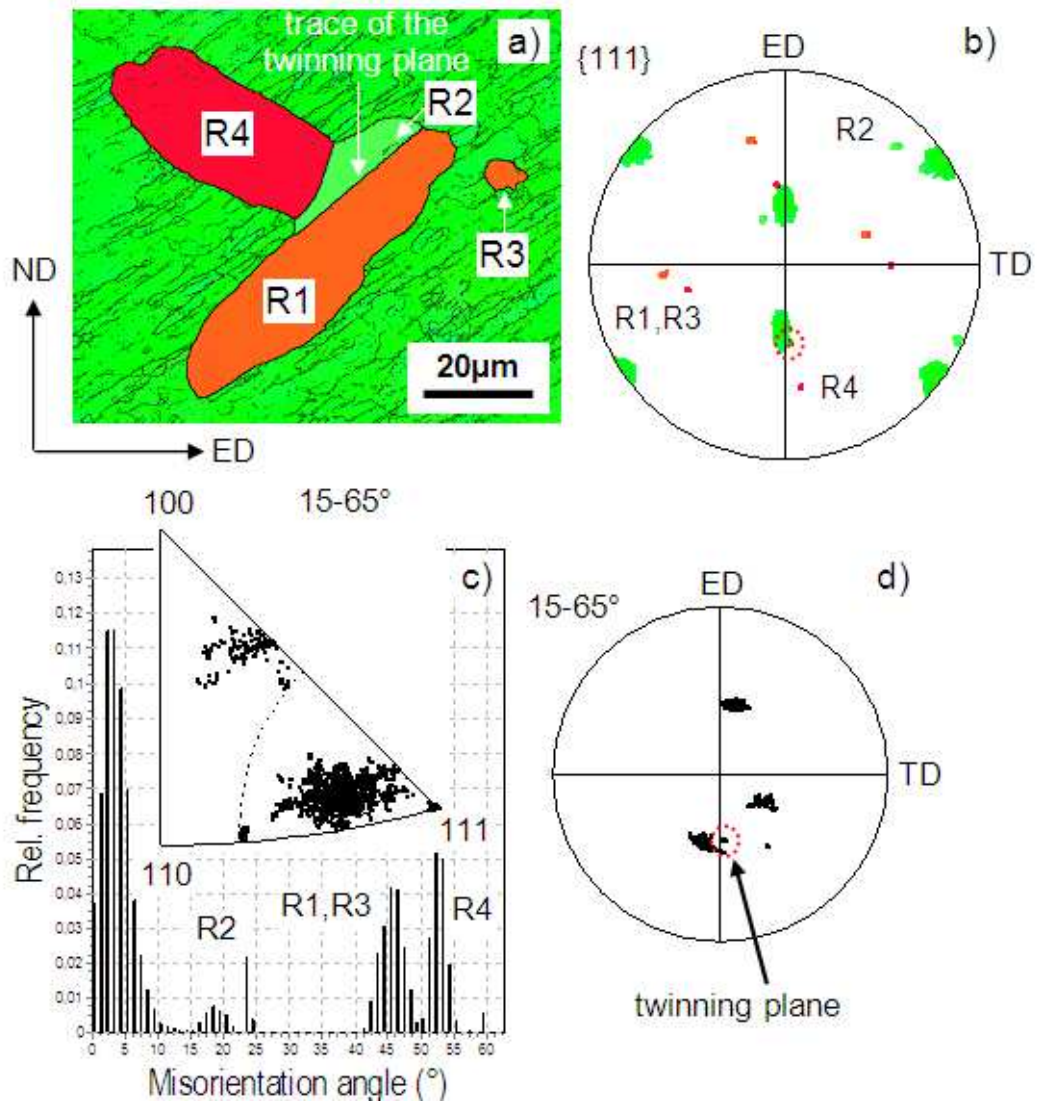


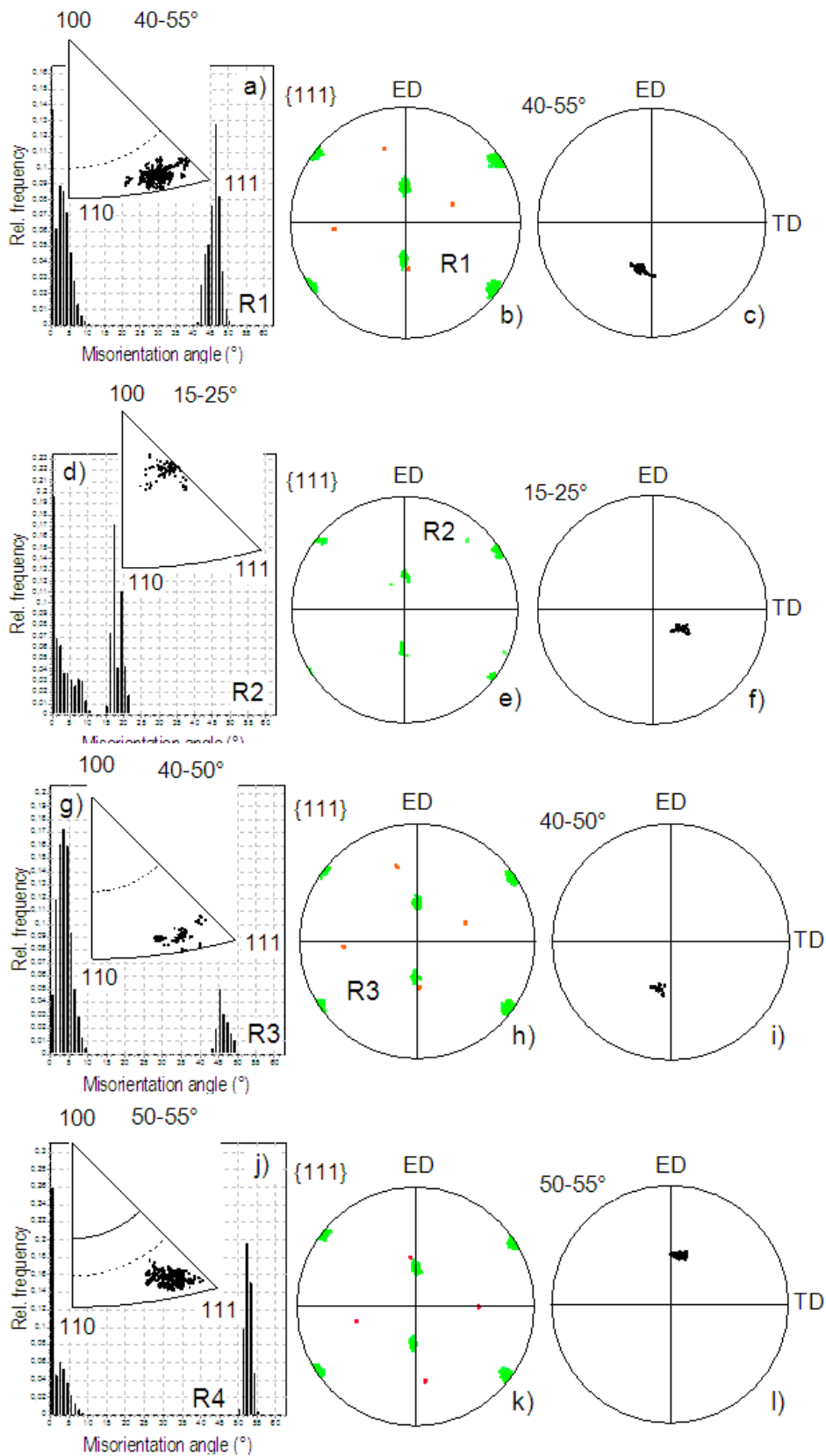
A. 1.2. Global texture measurements by X-ray diffraction. The {111} pole figures measured on ED-TD, ND-TD and ED-ND planes for: (a) Al, (b) Al-1%Mn, (c) Ni, (d) Cu and (e) Cu-2%Al. Single crystals of (110)[1-1-2] orientations.

ANNEXE 2

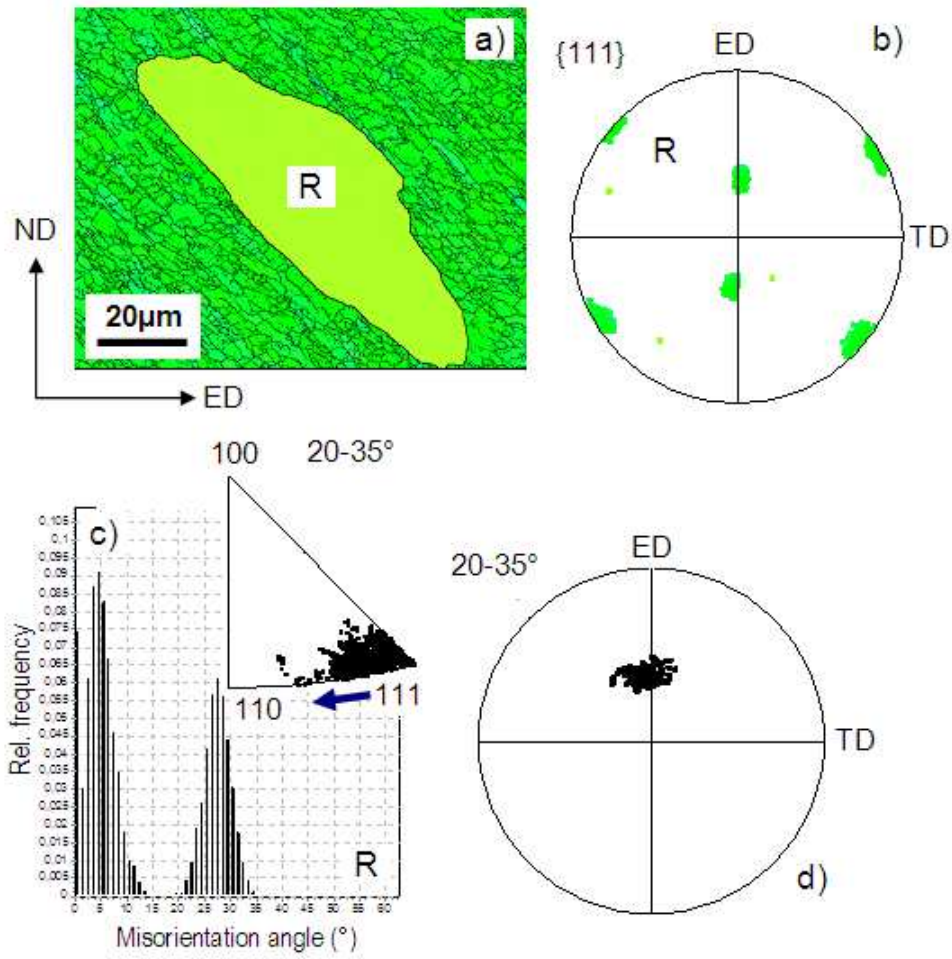


Case A. 2.1. Single isolated grain of uniform orientation. Disorientation relation of $\alpha\langle 111 \rangle$ -type. Al - (110)[00-1] orientation, $\epsilon=0.51$, $R=618K/25s$.

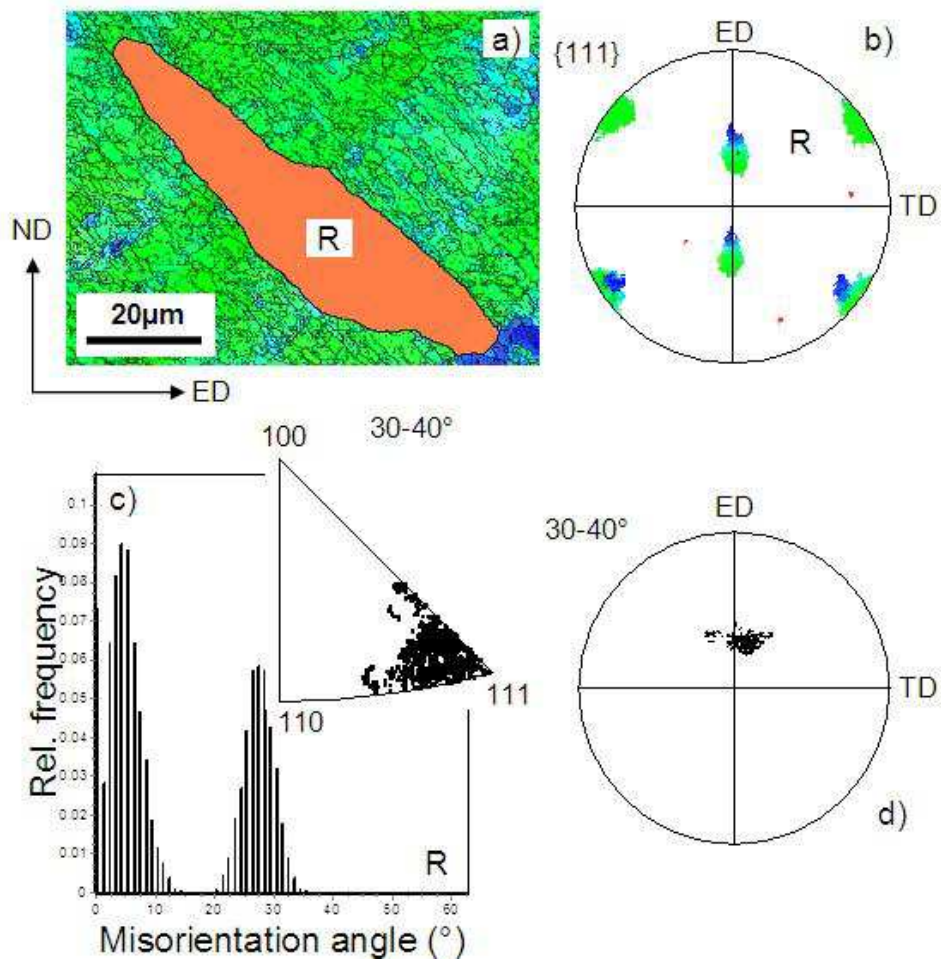




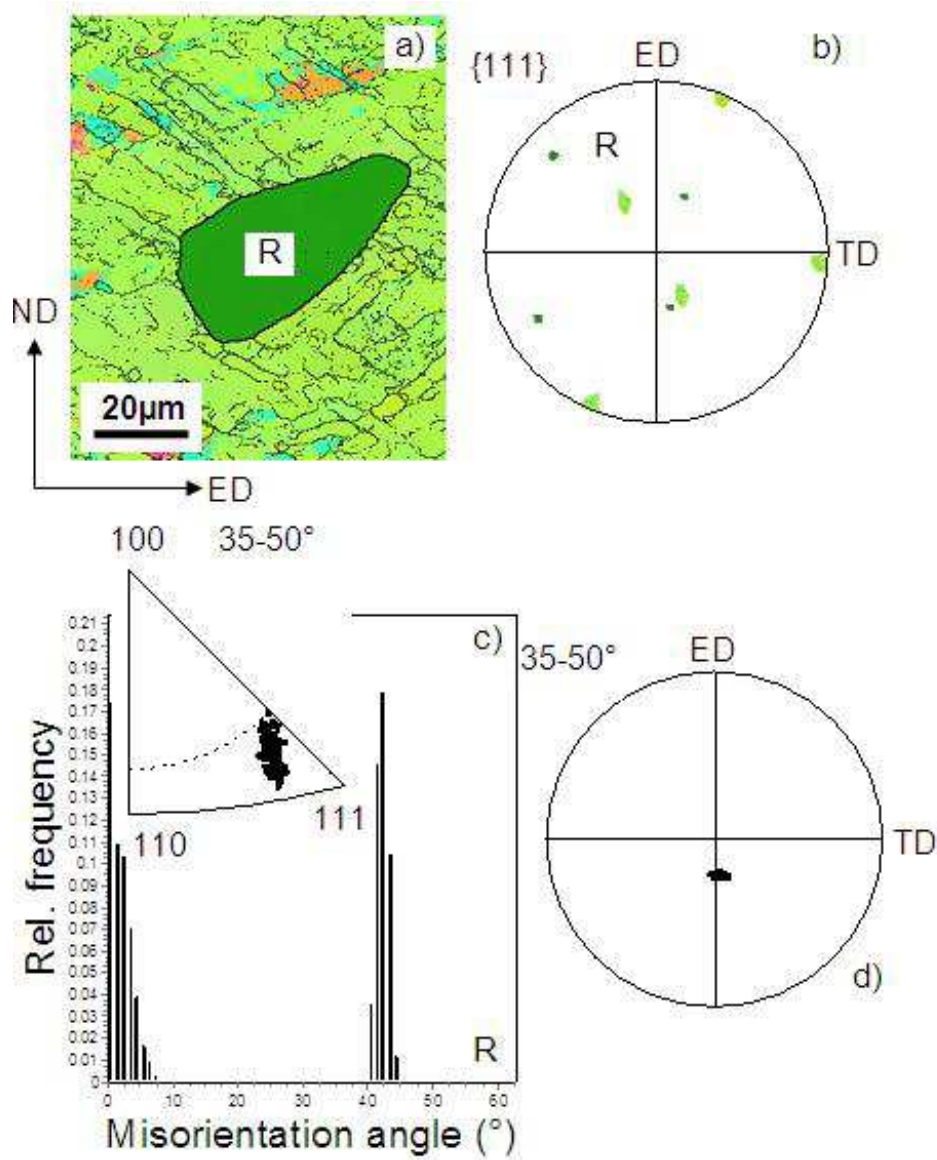
Case A. 2.2. Cluster of recrystallized grains. Al - (110)[00-1] orientation, $\varepsilon=0.51$,
R=618K/25s.



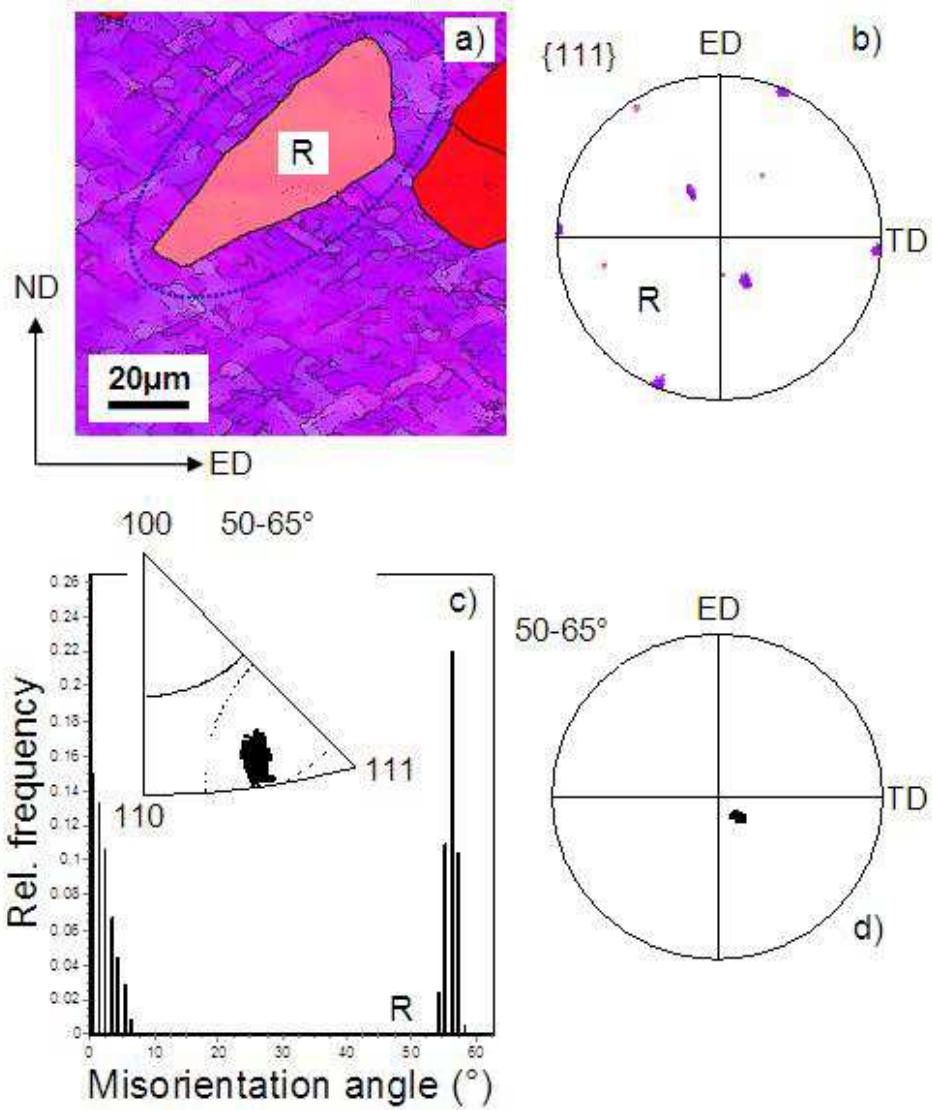
Case A. 2.3. Single isolated nuclei of uniform orientation. Disorientation relation of $\alpha<111>$ -type. Al - (110)[00-1] orientation, $\epsilon=0.92$, R=603K/20s.



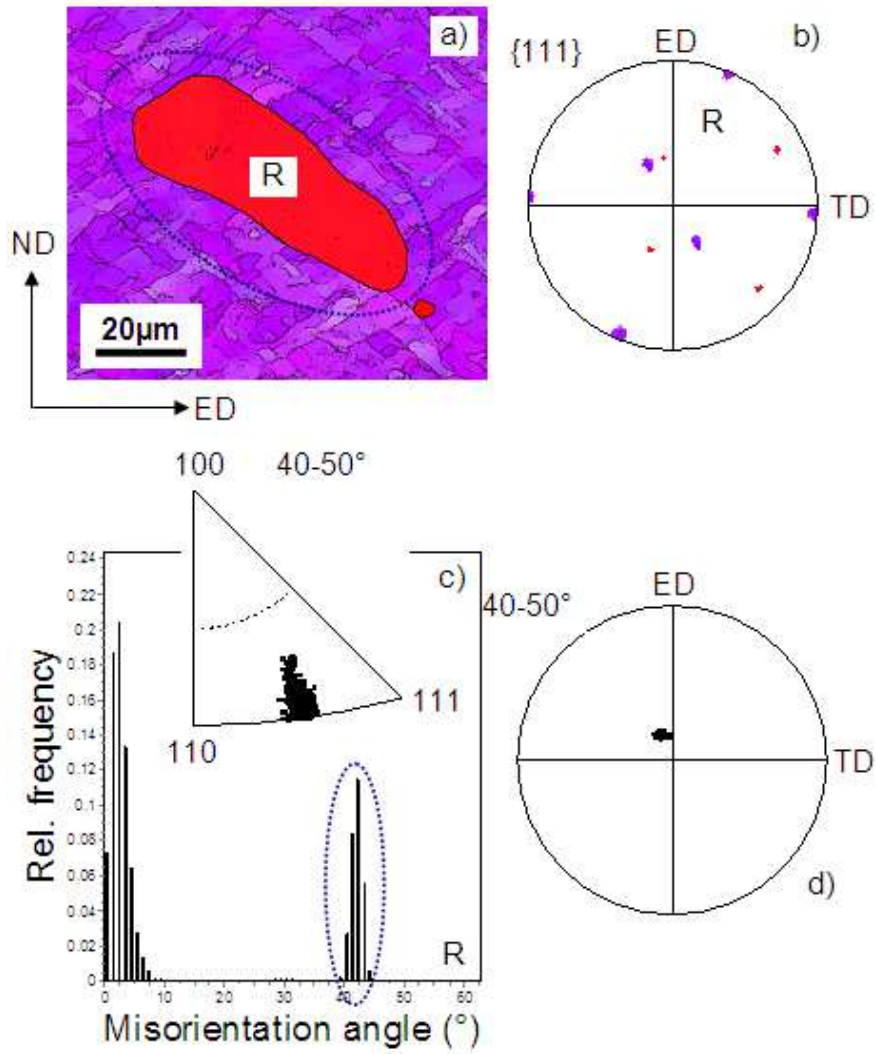
Case A. 2.4. Single isolated grain of uniform orientation. Disorientation relation of $\alpha <111>$ -type. Al - (110)[00-1] orientation, $\epsilon=0.92$, R=603K/20s.



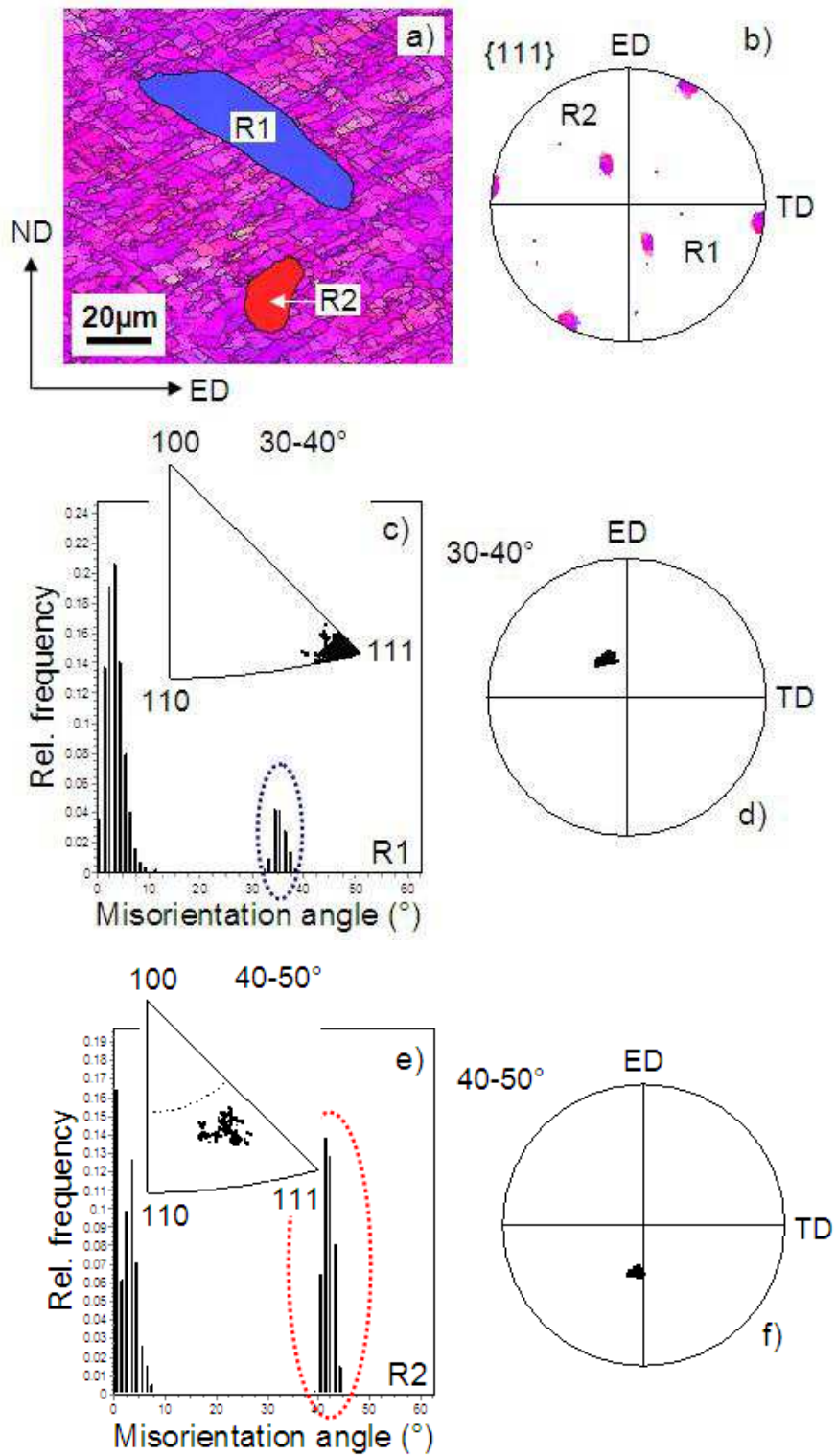
Case A. 2.5. Single isolated grain of uniform orientation. Disorientation relation of $\alpha(\langle 112 \rangle - \langle 221 \rangle)$ -type. Al - (110)[1-1-2] orientation, $\epsilon=0.51$, $R=723\text{K}/25\text{s}$.



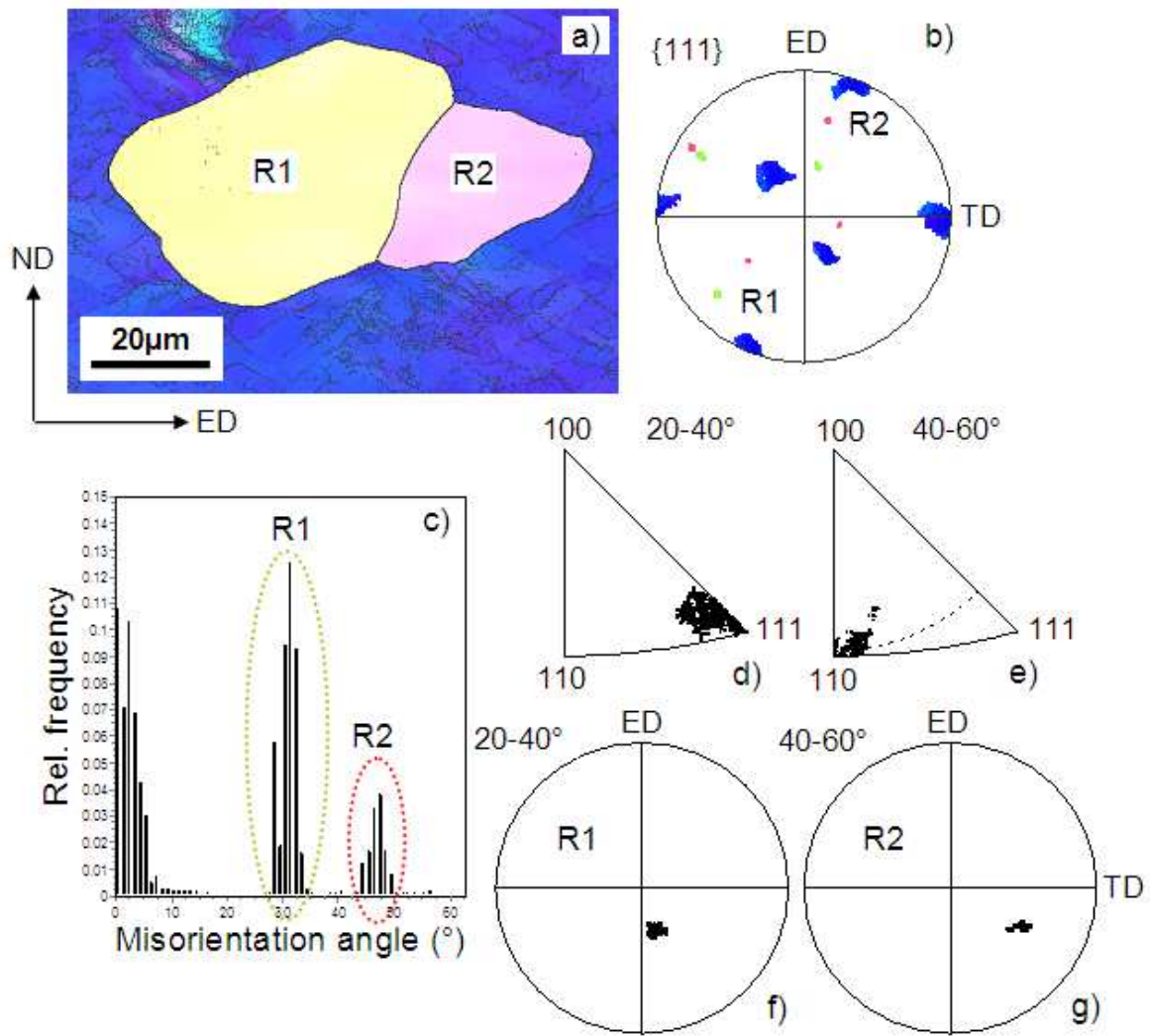
Case A. 2.6. Single isolated grain of uniform orientation. Disorientation relation of $\alpha<221>$ -type. Al - (110)[1-1-2] orientation, $\epsilon=0.51$, R=723K/25s.



Case A. 2.7. Single isolated grain of uniform orientation. Disorientation relation of $\alpha\langle 221 \rangle$ -type. Al - (110)[1-1-2] orientation, $\epsilon=0.51$, $R=723\text{K}/25\text{s}$.

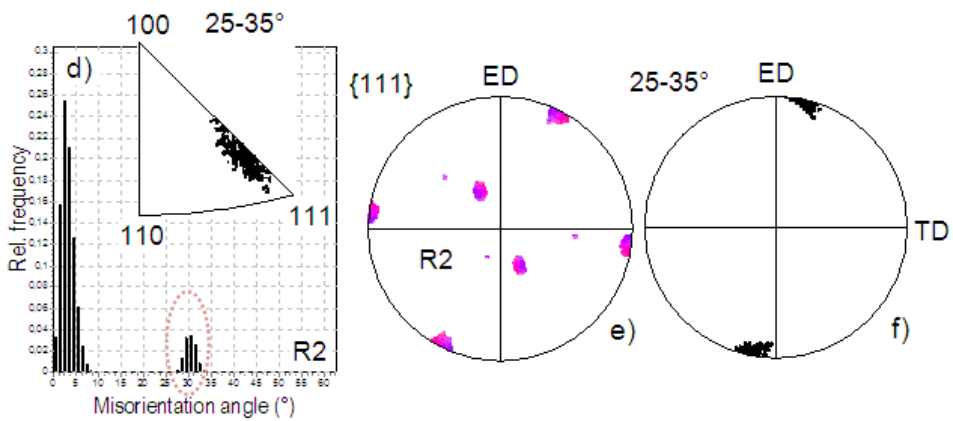
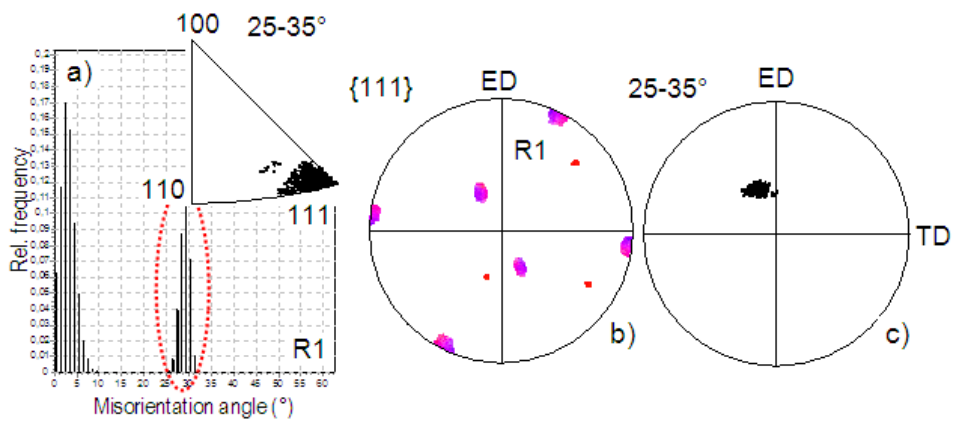
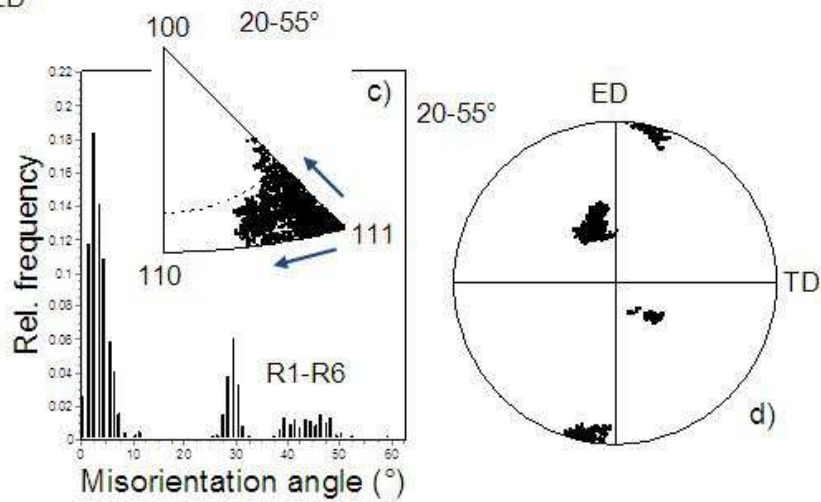
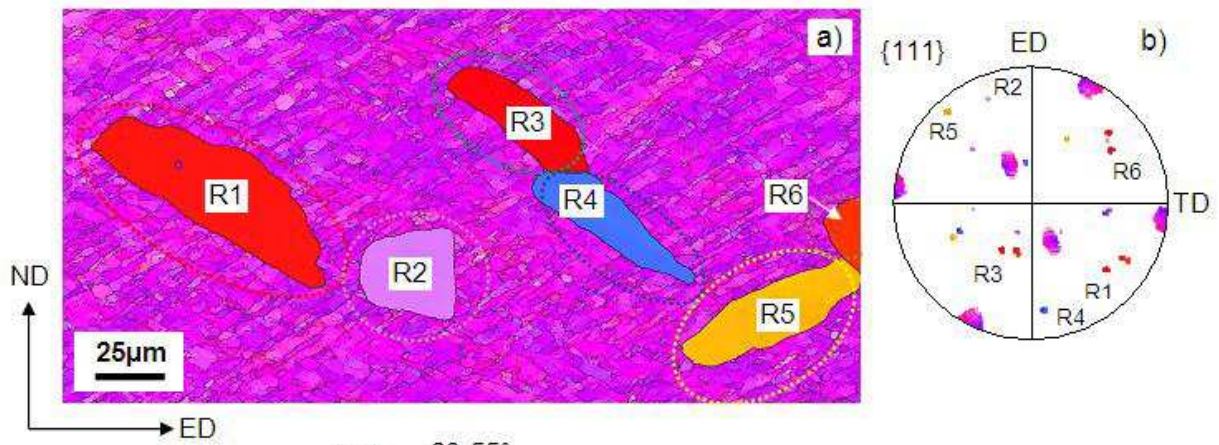


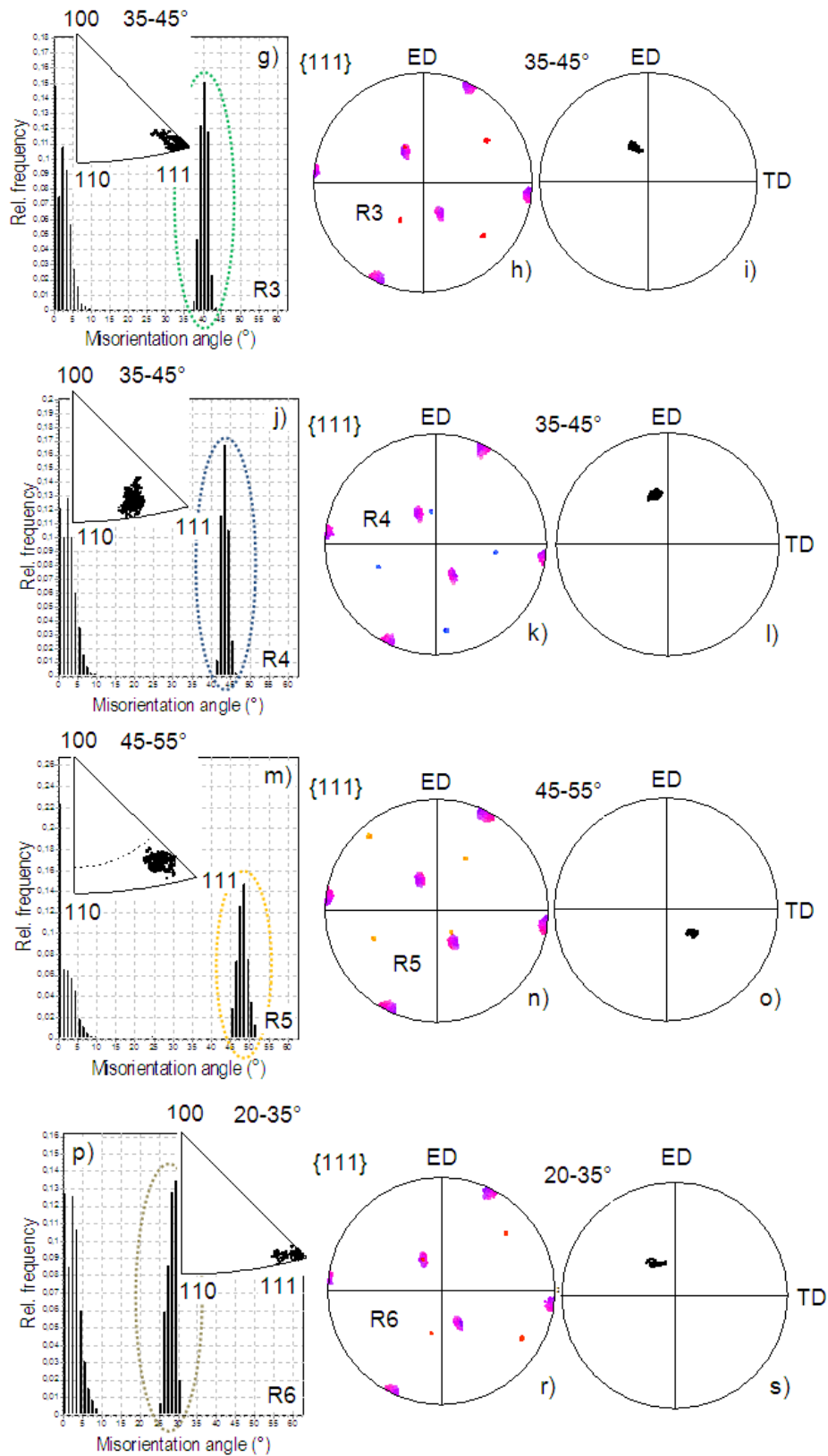
Case A. 2.8. Single isolated grain of uniform orientation. Disorientation relation of $\alpha\langle 111 \rangle$ and $\alpha\langle 123 \rangle$ type. Al - (110)[1-1-2] orientation, $\epsilon=0.92$, $R=703K/25s$.



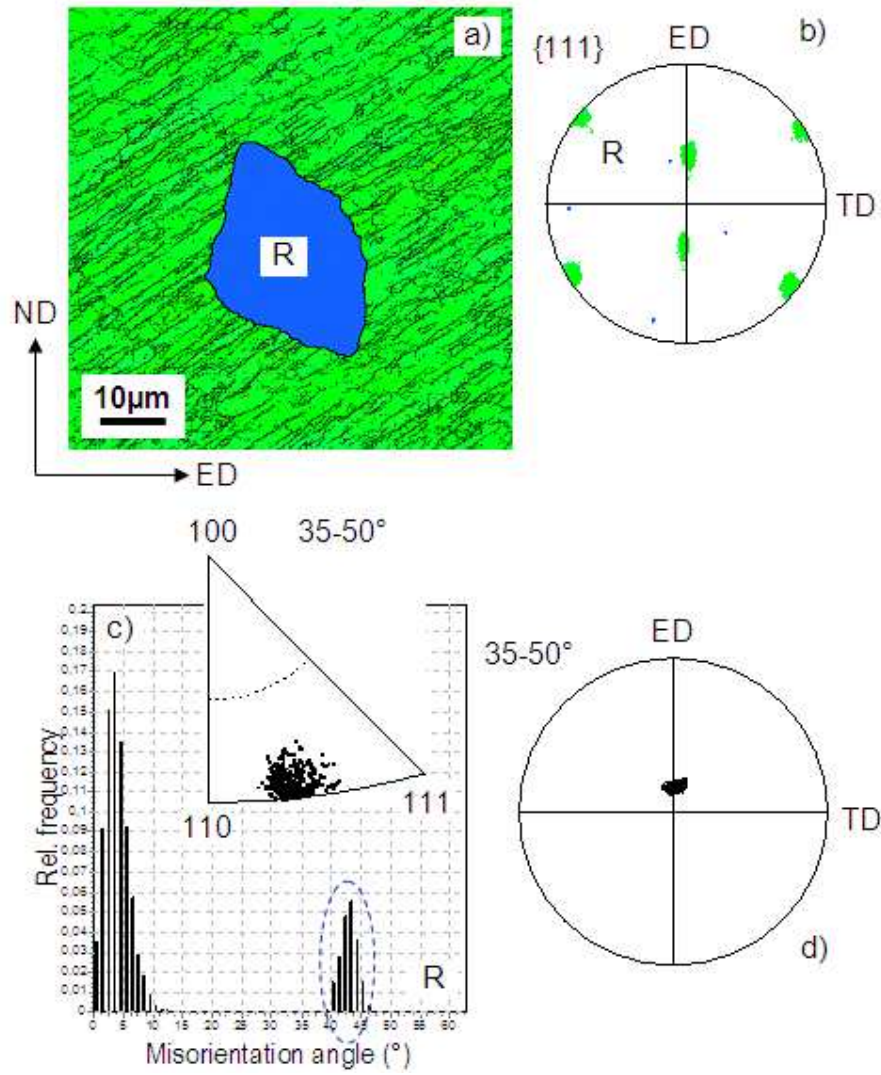
Case A. 2.9. Group of grains. Disorientation relation of α - $\langle 111 \rangle$ and α - $\langle 110 \rangle$ type.

Al - (110)[1-1-2] orientation, $\epsilon=0.51$, R=723K/25s.

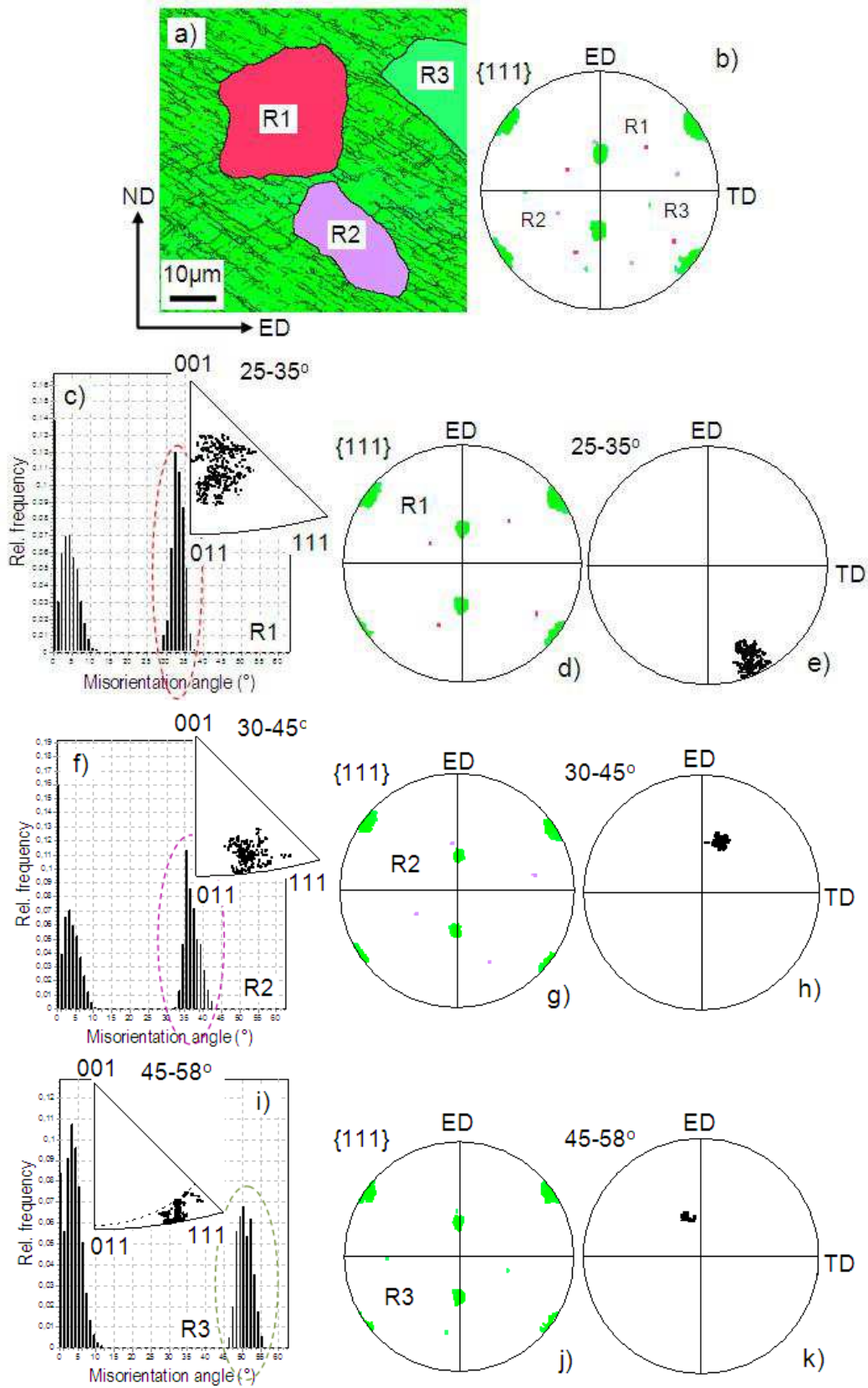




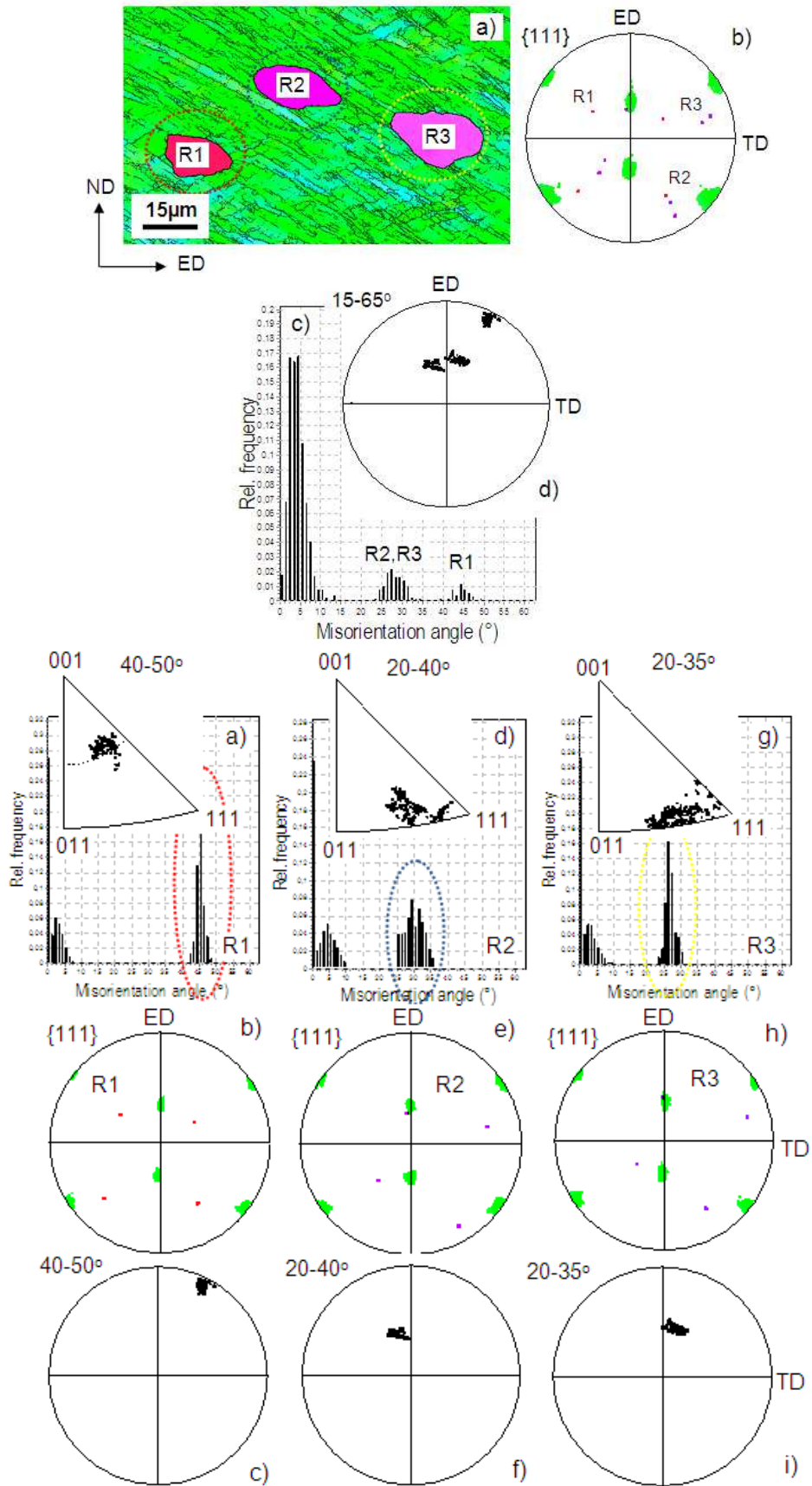
Case A. 2.10. Single isolated grains of uniform orientation. Disorientation relation of $\alpha\langle 111 \rangle$, $\alpha\langle 112 \rangle$, $\alpha\langle 221 \rangle$ and $\alpha\langle 123 \rangle$ type. Al - (110)[1-1-2] orientation, $\varepsilon=0.92$, R=703K/25s (see page 167 and 168).



Case A. 2.11. Single isolated grain of uniform orientation. Disorientation relation of $\alpha<221>$ type. Al-1%Mn of (110)[00-1] orientation, $\epsilon=0.51$, R=686K/25s.

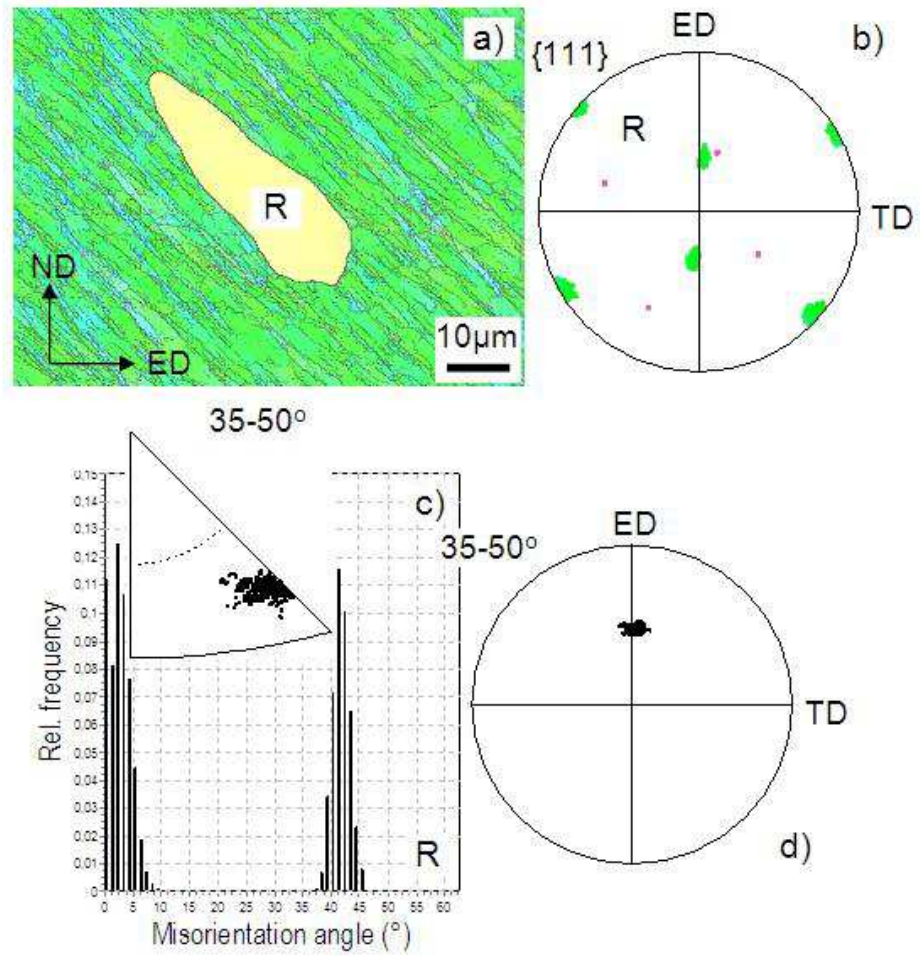


Case A. 2.12. Group of grains. Disorientation relation of $\alpha\langle 123 \rangle$ and $\alpha\langle 221 \rangle$ type. Al-1%Mn of (110)[00-1] orientation, $\epsilon=0.51$, $R=686K/25s$.

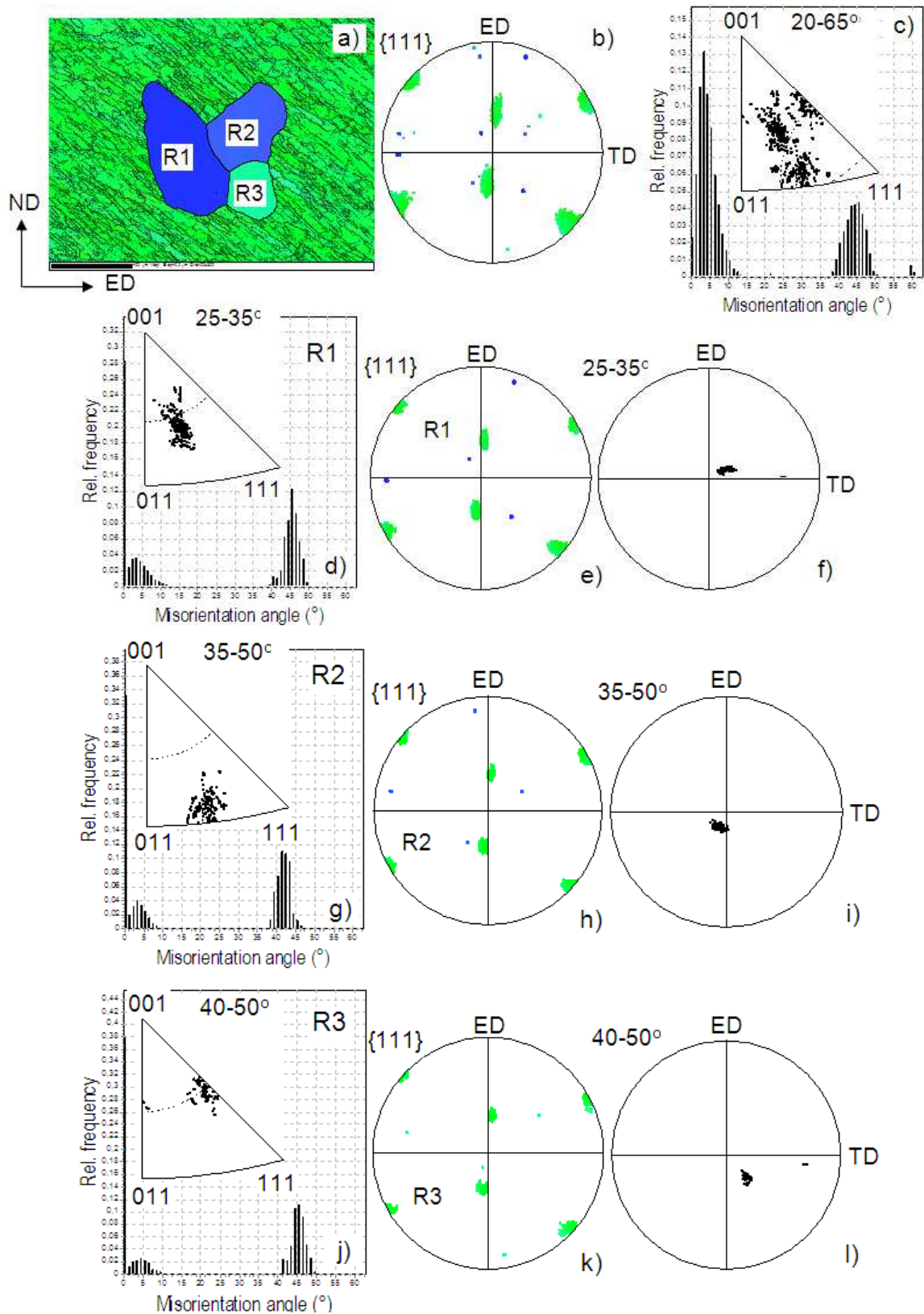


Case A. 2.13. Group of grains. Disorientation relation of $\alpha\langle 221 \rangle$ and $\alpha\langle 123 \rangle$ type.

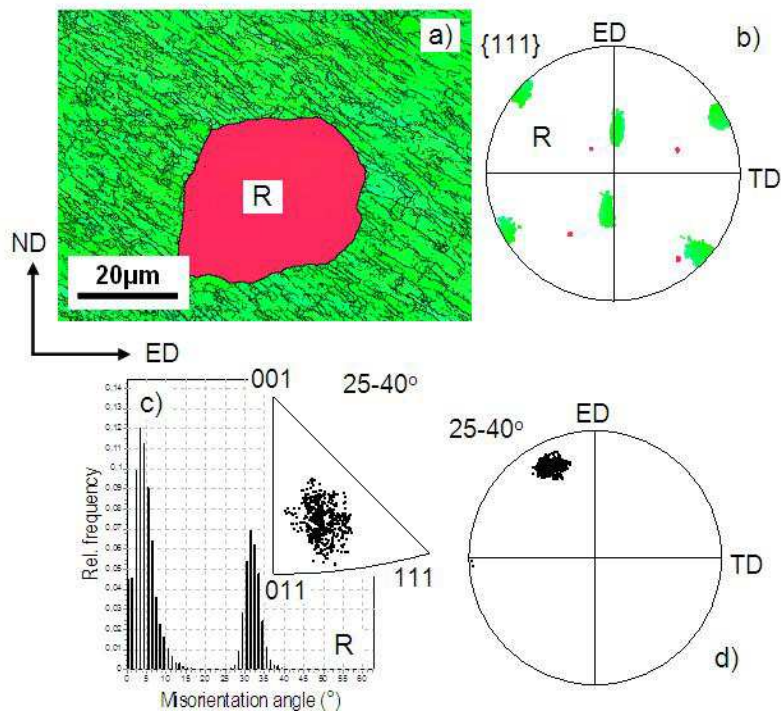
Al-1%Mn of (110)[00-1] orientation, $\epsilon=0.51$, $R=686\text{K}/25\text{s}$.



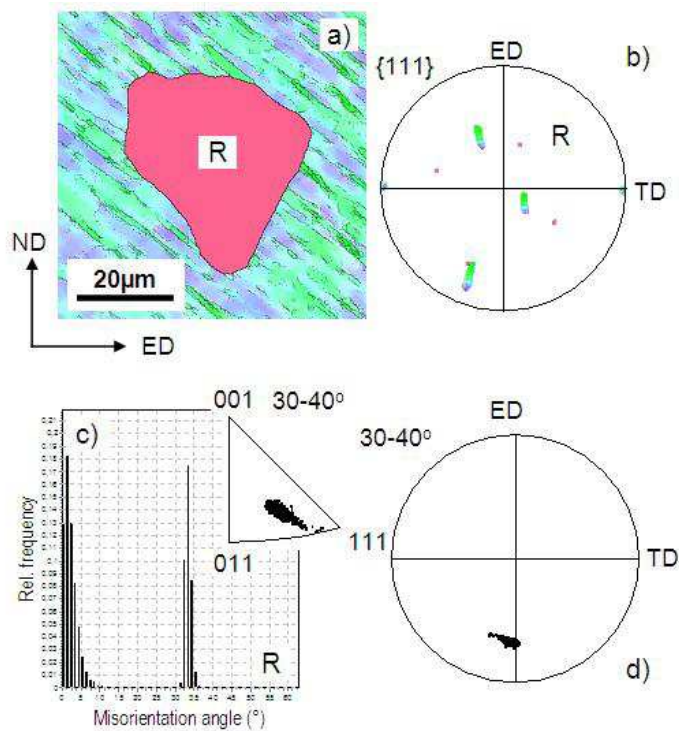
Case A. 2.14. Single isolated grain of uniform orientation. Disorientation relation of $\alpha<112>$ type. Al-1%Mn of (110)[00-1] orientation, $\epsilon=0.92$, R=676K/20s.



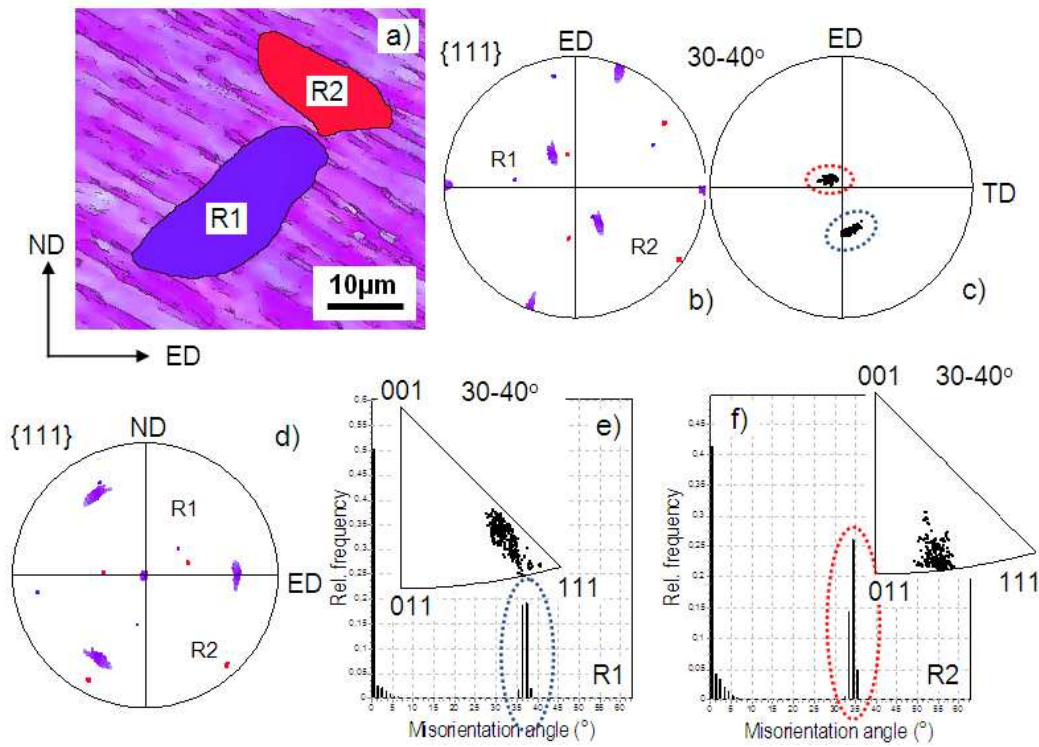
Case A. 2.15. Group of grains. Disorientation relation of $\alpha\langle 112 \rangle$, $\alpha\langle 221 \rangle$ and $\alpha\langle 123 \rangle$ type. Al-1%Mn of (110)[00-1] orientation, $\epsilon=0.92$, R=676K/20s.



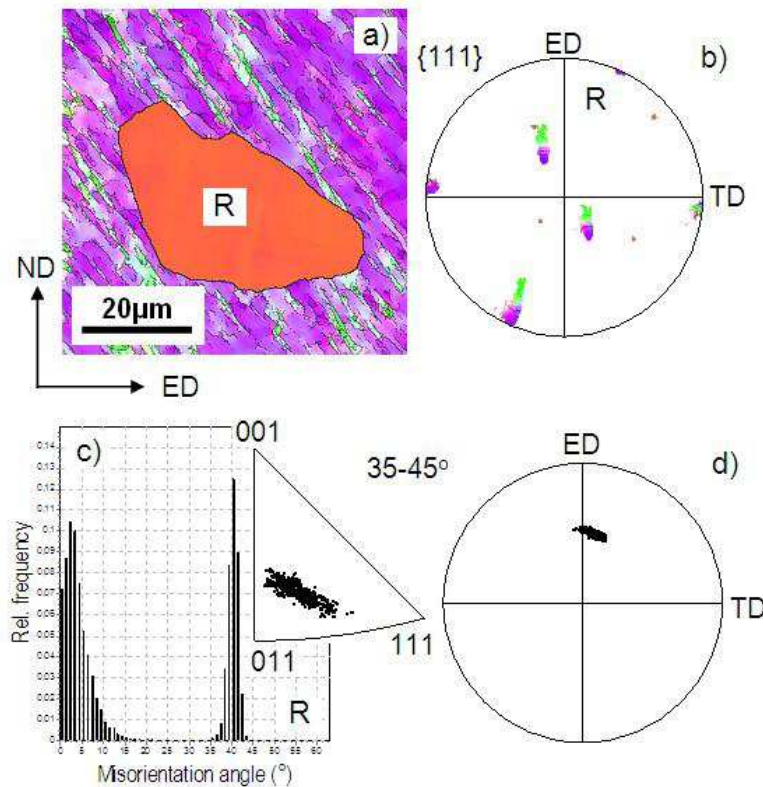
Case A. 2.16. Single isolated grain of uniform orientation. Disorientation relation of $\alpha<123>$ type. Al-1%Mn of (110)[00-1] orientation, $\epsilon=0.92$, R=676K/20s.



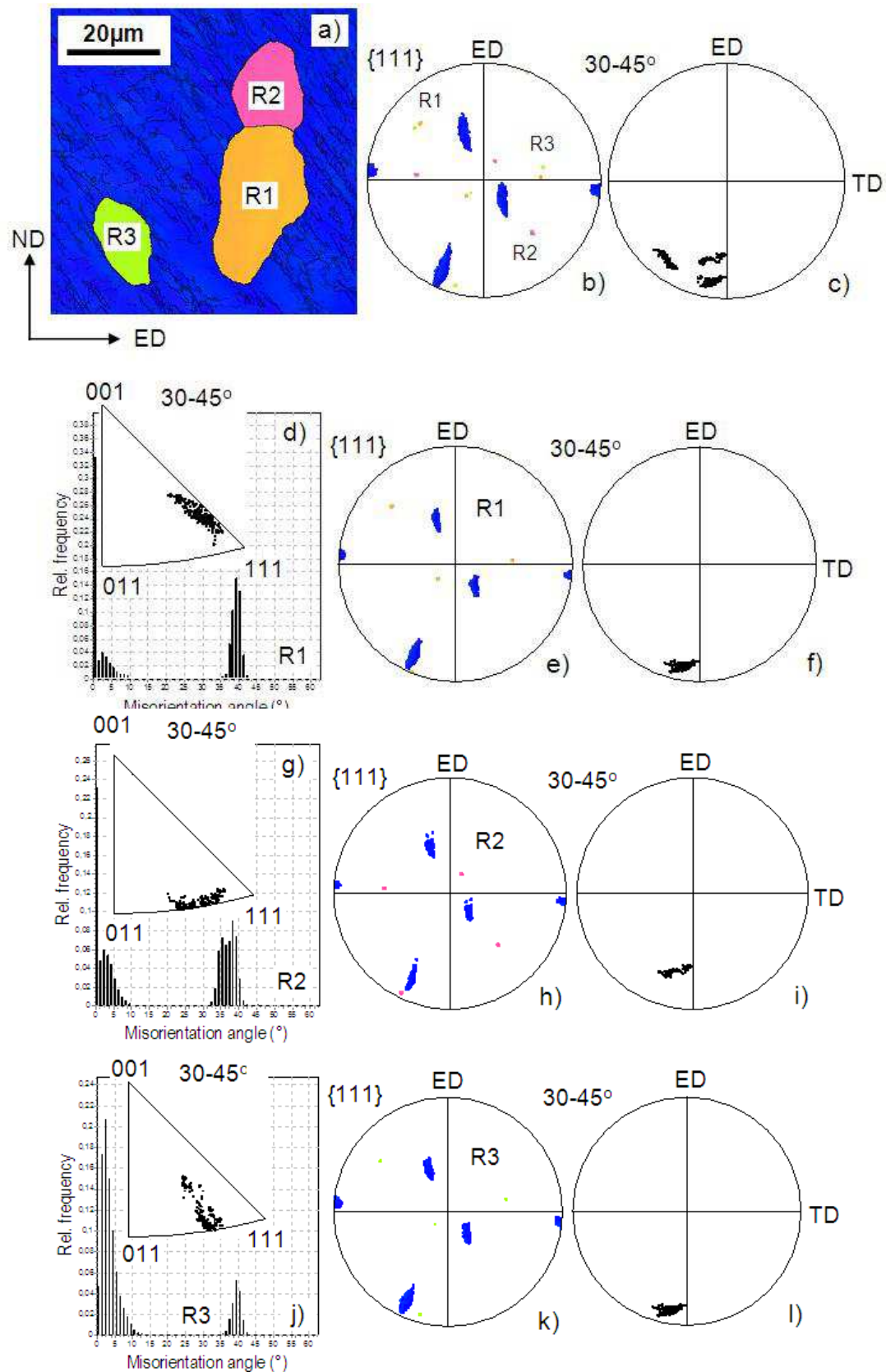
Case A. 2.17. Single isolated grain of uniform orientation. Disorientation relation of $\alpha(<221>-<123>)$ type. Al-1%Mn of (110)[1-1-2] orientation, $\epsilon=0.51$, R=696K/30s.



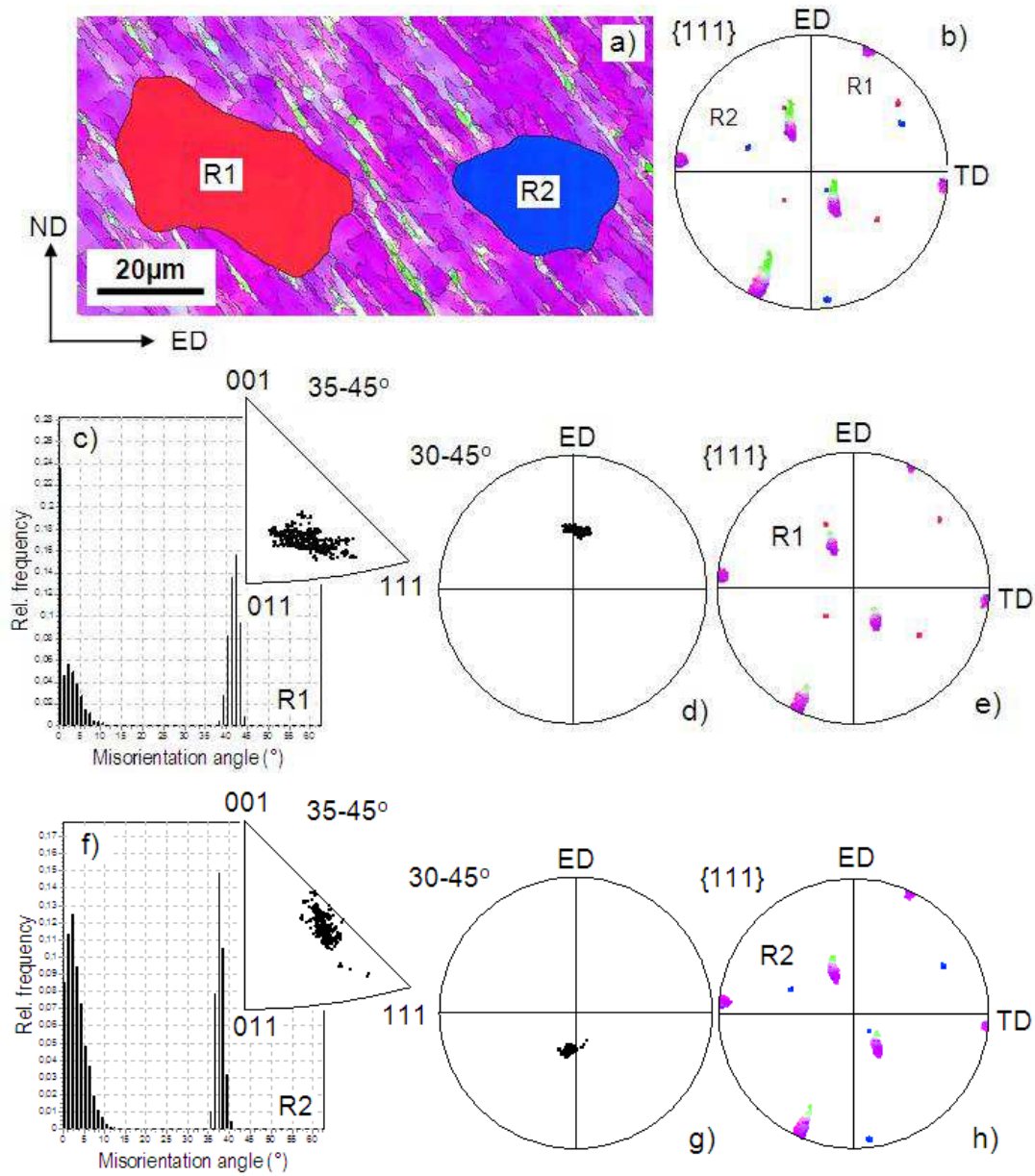
Case A. 2.18. Group of grains. Disorientation relation of $\alpha\langle 221 \rangle$ and $\alpha\langle 112 \rangle$ type. Al-1%Mn of (110)[1-1-2] orientation, $\epsilon=0.51$, $R=696\text{K}/30\text{s}$.



Case A. 2.19. Single isolated grain of uniform orientation. Disorientation relation of $\alpha\langle 221 \rangle$ and $\alpha\langle 012 \rangle$ type. Al-1%Mn of (110)[1-1-2] orientation, $\epsilon=0.92$, $R=658\text{K}/30\text{s}$.



Case A. 2.20. Group of grains. Disorientation relation of $\alpha\langle 112 \rangle$, $\alpha\langle 221 \rangle$ and $\alpha\langle 123 \rangle$ type. Al-1%Mn of (110)[1-1-2] orientation, $\epsilon=0.92$, $R=658K/30s$.



Case A. 2.21. Group of two grains. Disorientation relation of $\alpha\langle 112 \rangle$, $\alpha\langle 221 \rangle - \langle 123 \rangle - \langle 012 \rangle$ type. Al-1%Mn of (110)[1-1-2] orientation, $\epsilon=0.92$, $R=658K/30s$.

REFERENCES:

- [Afrin *et al.* (2011)]; Afrin N., Quadir M. Z., Bassman L., Driver J. H., Albou A., Ferry M.: The three-dimensional nature of microbands in a channel die compressed Goss-oriented Ni single crystal, *Scripta Materialia*, Vol. 64/3, (2011), 221-224.
- [Akef and Driver (1991)]; Akef A., Driver J. H.: Orientation splitting of cube-oriented face-centred cubic crystals in plane strain compression, *Materials Science and Engineering A*, Vol. 132, (1991), 245-255.
- [Albou *et al.* (2010a)]; Albou A., Driver J. H., Maurice C.: Microband evolution during large plastic strains of stable {110}<112> Al and Al-Mn crystals, *Acta Materialia*, Vol. 58, (2010a), 3022-3034.
- [Albou *et al.* (2010b)]; Albou A., Raveendra S., Karajagikar P., Samajdar I., Maurice C., Driver J. H.: Direct correlation of deformation microstructures and cube recrystallization nucleation in aluminium, *Scripta Materialia*, Vol. 62/7, (2010b), 469-472.
- [Ardakani and Humphreys (1994)]; Ardakani M. G., Humphreys F. J.: The annealing behavior of deformed particle-containing aluminium single crystals, *Acta Metallurgica et Materialia*, Vol. 42/3, (1994), 763-780.
- [Bailey (1963)]; Bailey J. E.: Electron microscopy and strength of crystals. In: "Electron Microscope observations on recovery and recrystallization process in cold worked metals", ed. Thomas G., Washburn J., New York, Interscience, (1963), 535-564.
- [Barrett (1940)]; Barrett C. S.: Recrystallization texture of aluminium after compression, *Transaction Metallurgical Society AIME*, Vol. 137, (1940), 128-149.
- [Bate *et al.* (2005)]; Bate P. S., Knutsen R. D., Brough I., Humphreys F. J.: The characterization of low-angle boundaries by EBSD, *Journal of Microscopy*, Vol. 220, (2005), 36-46.
- [Bauer *et al.* (1977)]; Bauer R. E., Mecking H., Lücke K.: Texture of copper single crystals after rolling at room temperature, *Materials Science and Engineering*, Vol. 27, (1977), 163-180.
- [Beck and Sperry (1950)]; Beck P. A., Sperry P. R.: Strain inducted boundary migration in high purity aluminium, *Journal of Applied Physics*, Vol. 21/02, (1950), 150-152.
- [Beck (1953)]; Beck P. A.: Notes on the theory of annealing textures, *Acta Metallurgica*, (1953), 230-234.
- [Berger *et al.* (1988)]; Berger A., Wilbrandt P. J., Ernst F., Klement U., Haasen P.: On the generation of new orientations during recrystallization: Recent Results on the

- Recrystallization of Tensile-Deformed fcc Single Crystals, Progress in Material Science, Vol. 32, (1988), 1-95.
- [Bijak (2008)]; Bijak M.: Zależności orientacji w procesie rekrytalizacji odkształconych monokryształów stopu Al-Mn, PhD thesis, Kraków (2008), (in polish).
- [Bishop and Hill (1951)]; Bishop J. F. W., Hill R.: A theory of the plastic distortion of a polycrystalline aggregate under combined stresses, Philosophical Magazine, Vol. 42, (1951), 414-427.
- [Blicharski and Gorczyca (1978)]; Blicharski M., Gorczyca S.: Structural inhomogeneity of deformed austenitic stainless steel, Metal Science, (1978), 303-312.
- [Blicharski *et al.* (1995)]; Blicharski M., Dymek S., Wróbel M.: Inhomogeneities of microstructure evolved in metals under plastic deformation, Journal of Materials Processing Technology, Vol. 53, (1995), 75-84.
- [Blum *et al.* (1995)]; Blum W., Schlögl C., Meier M.: Subgrain formation and subgrain boundary migration in Al-5Mg during high temperature deformation in the range of class – A behavior in comparison with pure aluminium, Zeitschrift für Metallkunde, Vol. 86/9, (1995), 631-637.
- [Borbély *et al.* (2007)]; Borbély A., Maurice C., Piot D., Driver J. H.: Spatial characterization of the orientation distributions in a stable plane strain-compressed Cu crystal: A statistical analysis, Acta Materialia, Vol. 55, (2007), 487-496.
- [Burgers and Louwse (1931)]; Burgers W.G., Louwse P.C.: Über den Zusammenhang zwischen Deformationsvorgang und Rekristallisationstextur bei Aluminium. (Rekristallisation von Aluminiumeinkristallen III), Zeitschrift für Physik, Vol. 67, (1931), 605–678.
- [Cahn (1949)]; Cahn R.W.: Recrystallization of single crystals after plastic bending, Journal of the Institute of Metals, Vol. 76, (1949), 121-143.
- [Cahn (1950)]; Cahn R.W.: A New Theory of Recrystallization Nuclei, Proceeding Physic Society A, Vol. 63, (1950), 323-336.
- [Cahn (1955)]; Cahn R. W.: Twinned crystals, Advances in Physics, Vol.3/12, (1954), 363-445.
- [Christian and Mahajan (1995)]; Christian J. W., Mahajan S.: Deformation twinning, Progress in Materials Science, Vol. 39/1-2, (1995), 1- 157.
- [Cottrell and Mould (1976)]; Cottrell P., Mould P. R.: Recrystalliation and grain growth in metals, London, Surrey University, (1976), 85.

- [Dash and Brown (1963)]; Dash S., Brown N.: An investigation of the origin and growth of annealing twins, *Acta Metallurgica*, Vol. 11/9, (1963), 1067-1075.
- [Doherty (1978)]; Doherty R. D.: *Recrystallization of Metallic Materials*, ed. F. Haessner, Dr. Rieder Verlag, Berlin, Vol. 23, (1978).
- [Doherty and Szpunar (1984)]; Doherty R. D., Szpunar J. A.: Kinetics of subgrain coalescence-a reconsideration of the theory, *Acta Metallurgica*, Vol. 32/10, (1984), 1789-1798.
- [Doherty (1997a)]; Doherty R. D.: *Recrystallization and texture*, *Progress in Materials Science*, Vol. 42, (1997a), 39-58.
- [Doherty (1997b)]; Doherty R. D., Hughes D. A., Humphreys F. J., Jonas J. J., Juul Jensen D., Kassner M. E., King W. E., McNelly T. R., McQueen H. J., Rollet A. D.: Current issues in recrystallization: a review, *Material Science and Engineering A*, Vol. 238, (1997b), 219-274.
- [Driver *et al.* (1994)]; Driver J. H., Juul Jensen D., Hansen N.: Large strain deformation structures in aluminium crystals with rolling texture orientations, *Acta Metallurgica et Materialia*, Vol. 42/9, (1994), 3105-3114.
- [Driver *et al.* (2000)]; Driver J. H., Paul H., Glez J. C., Maurice C.: Relations between deformation substructure and nucleation in fcc crystals, In "Recrystallization – fundamental aspects and relations to deformation microstructure", ed. N. Hansen et al, Roskilde, Proc. of the 21st RISØ International Symposium on Materials Science, Denmark, (2000), 35-48.
- [Duggan *et al.* (1990)]; Duggan B. J., Sindel M., Köhlhoff G. D., Lücke K.: Oriented nucleation, oriented growth and twinning in cube texture formation, *Acta Metallurgica et Materialia*, Vol. 38/1, (1990), 103-111.
- [Duggan *et al.* (1993)]; Duggan B. J., Lücke K., Köhlhoff G. D., Lee C. S.: On the origin of cube texture in copper, *Acta Metallurgica et Materialia*, Vol. 41/6, (1993), 1921-1927.
- [Dymek and Wróbel (2003)]; Dymek S., Wróbel M.: Pholytypism in copper single crystals deformed at room temperature, *Materials Chemistry and Physics*, Vol. 81/2-3, (2003), 552-554.
- [Engler *et al.* (1996)]; Engler O., Yang P., Kong X. W.: On the formation of recrystallization textures in binary Al-1,3%Mn investigated by means of local texture analysis, *Acta Materialia*, Vol. 44/8, (1996), 3349-3369.

- [Engler *et al.* (1997)]; Engler O., Kong X. W., Yang P.: Influence of particle stimulated nucleation on the recrystallization textures in cold deformed Al-alloys. Part I – experimental observations, *Scripta Materialia*, Vol. 37/11, (1997), 1665-1674.
- [Engler *et al.* (2001)]; Engler O., Kong X. W., Lücke K.: Recrystallization textures of particle-containing Al-Cu and Al-Mn single crystals, *Acta Materialia*, Vol. 49, (2001), 1701-1715.
- [Ferry and Humphreys (1996)]; Ferry M., Humphreys F. J.: The deformation and recrystallization of particle-containing $\{011\}\langle 100\rangle$ aluminium crystals, *Acta Materialia*, Vol. 44, (1996), 3089-3103.
- [Field *et al.* (2007)]; Field D. P., Bradford L. T., Nowell M. M., Lillo T. M.: The role of annealing twins during recrystallization of Cu, *Acta Materialia*, Vol. 55, (2007), 4233-4241.
- [Fujita *et al.* (1967)]; Fujita H., Kawasaki Y., Furubayashi E., Kajiwara S., Taoka T.: A new slow electron diffraction apparatus, *Japan Journal of Applied Physics*, Vol. 6, (1967), 214-230.
- [Funderberger *et al.* (2002)]; Funderberger J. J., Bouzy E., Morawiec A., Lecomte J. S.: Orientation maps on TEM, *Materials Science Forum*, Vol. 408-412, (2002), 209-214.
- [Funderberger *et al.* (2003)]; Funderberger J. J., Morawiec A., Bouzy E., Lecomte J. S.: System for creating orientation maps using TEM, *Materials Chemistry and Physics*, Vol. 81, (2003), 535-537.
- [Glez and Driver (2003)]; Glez, J. C., Driver J. H.: Substructure development in hot plane compressed Al-1%Mn crystals, *Acta Materialia*, Vol. 51/10, (2003), 2989-3003.
- [Godfrey *et al.* (1998)]; Godfrey A., Juul Jensen D., Hansen N.: Slip pattern, microstructure and local crystallography in an aluminium single crystal of brass orientation $\{110\}\langle 112\rangle$, *Acta Materialia*, Vol. 46, (1998), 823-833.
- [Godfrey *et al.* (2001)]; Godfrey A., Juul Jensen D., Hansen N.: Recrystallization of channel-die deformed single crystals of typical rolling orientations, *Acta Materialia*, Vol. 49, (2001), 2429-2440.
- [Gottstein (1984)]; Gottstein G.: Annealing texture development by multiple twinning in fcc crystals, *Acta Metallurgica*, Vol. 32, (1984), 1117-1138.
- [Gottstein and Shvindlerman (1992)]; Gottstein G., Shvindlerman L. S.: On the orientation dependence of grain boundary migration, *Scripta Metallurgica Materialia*, Vol. 27, (1992), 1515-1520.

- [Gottstein and Shvindlerman (1999)]; Gottstein G., Shvindlerman L. S.: Grain boundary migration in metals, CRC Press, Boca Raton (FL), (1999).
- [Gottstein *et al.* (2002)]; Gottstein G., Winning M., Shvindlerman L. S.: On the mechanics of grain boundary migration. Grain boundary migration: X-ray diffraction (XRD), *Acta Materialia*, Vol. 50, (2002), 353-363.
- [Guiglionda *et al.* (2004)]; Guiglionda G., Borbély A., Driver J. H.: Orientation-dependent stored energies in hot deformed Al-2.5%Mg and their influence on recrystallization, *Acta Materialia*, Vol. 52/12, (2004), 3413-3423.
- [Haessner (1978)]; Haessner F.: Systematic survey and basic problems of recrystallization. Recrystallization of metallic materials, Stuttgart: Dr. Rieder Verlag, (1978), 159-194.
- [Heidenreich (1949)]; Heidenreich R. D.: Electron microscope and diffraction study of metal crystal textures by means of thin sections, *Journal of Applied Physics*, Vol. 20, (1949), 993-1010.
- [Hejelen *et al.* (1991)]; Hjelen J., Ørsund R., Nes E.: On the origin of recrystallization textures in aluminium, *Acta Metallurgica*, Vol. 39, (1991), 1377-1404.
- [Hornbogen and Köster (1878)]; Hornbogen E., Köster U.: Recrystallization of two-phase alloys. Recrystallization of metallic materials, Stuttgart: Dr. Riederer Verlag, ed. Haessner F., (1878), 159-194.
- [Hu (1962)]; Hu H.: Direct observations on the annealing of Si-Fe crystals in the electron microscope, *Transactions of the Metallurgical Society of AIME*, Vol. 224/1, (1962), 75-84.
- [Hu (1963)]; Hu H.: Recrystallization by subgrain coalescence in electron microscopy and strength of crystals, ed. Thomas G., Washbuer J., New York, Interscience, (1963), 564-573.
- [Humphreys (1977)]; Humphreys F. J.: The nucleation of recrystallization at second phase particles in deformed aluminium, *Acta Metallurgica*, Vol. 25/11, (1977), 1323-1344.
- [Humphreys and Chan (1996a)]; Humphreys F. J., Chan H. M.: Discontinuous and continuous annealing phenomena in aluminium – nickel alloy, *Materials Science and Technology*, Vol. 12/2, (1996a), 143-148.
- [Humphreys and Ferry (1996b)]; Humphreys F. J., Ferry M.: On the role of twinning in the recrystallization of aluminium, *Scripta Materialia*, Vol. 35, (1996b), 99-105.
- [Humphreys and Hatherly (2004a)]; Humphreys F. J., Hatherly M.: Recrystallization and related annealing phenomena, Pergamon, 2nd Edition, (2004a).

- [Humphreys (2004b)]; Humphreys F. J.: Nucleation in recrystallization, in Proc. 2nd Joint Int. Conf. Rex & GG 2, ed. B. Bacroix et al, Annecy, France, (2004b), 107-116.
- [Humphreys and Bate (2006)]; Humphreys F. J., Bate P. S.: Measuring the ailment of low-angle boundaries formed during deformation, *Acta Materialia*, Vol. 54, (2006), 817-829.
- [Hurley *et al.* (2003)]; Hurley P. J., Bate P. S., Humphreys F. J.: An objective study of substructural boundary ailment in aluminium, *Acta Materialia*, Vol. 51, (2003), 4737-4750.
- [Hutchinson and Ray (1973)]; Hutchinson W. B., Ray R. K: On the feasibility of in situ observations of recrystallization in the high voltage microscope, *Philosophical Magazine*, Vol. 28, (1973), 953-959.
- [Ibe and Lücke (1966)]; Ibe G., Lücke K.: Growth selection during recrystallization of single crystals, In: “Recrystallization, Grain Growth and Textures”, ed. H. Margolin, American Society Metals, Metals Park, OH, (1966), 434-453.
- [Inoko and Kashihara (1993)]; Inoko F., Kashihara K.: Formation of recrystallized grains along deformation bands single crystals, *Materials Science Forum*, Vol. 113-115, (1993), 139-144.
- [Inoko *et al.* (2010)]; Inoko F., Kashihara K., Tagami M., Okada T.: Relationship between $\langle 111 \rangle$ rotation recrystallization mechanism and slip bands with compressive strain during tensile deformation in aluminium single crystals, *Material Transactions*, Vol. 51/4, (2010), 597-606.
- [Jazaeri and Humphreys (2004a)]; Jazaeri H., Humphreys F. J.: The transition from discontinuous to continuous recrystallization in some aluminium alloys I – the deformed state, *Acta Materialia*, Vol. 52, (2004a), 3239-3250.
- [Jazaeri and Humphreys (2004b)]; Jazaeri H., Humphreys F. J.: The transition from discontinuous to continuous recrystallization in some aluminium alloys II – annealing behavior, *Acta Materialia*, Vol. 52, (2004b), 3251-3262.
- [Jones *et al.* (1979a)]; Jones A. R., Ralph B., Hansen N.: Subgrain coalescence and the nucleation of recrystallization at grain boundaries in aluminium, *Proceedings of the Royal Society of London (A)*, Vol. 368, (1979a), 345-357.
- [Jones *et al.* (1979b)]; Jones A. R., Ralph B., Hansen N.: Nucleation of recrystallization in aluminium containing dispersions of alumina, *Metal Science*, Vol. 13, (1979b), 149-154.

- [Jones (1980)]; Jones A.R.: Grain boundary phenomena during the nucleation of recrystallization, In: "Grain boundary structure and kinetics", Ohio: ASM, Metals Park, (1980), 379-425.
- [Juul Jensen (1995)]; Juul Jensen D.: Growth rates and misorientation relationships between growing nuclei/grains and the surrounding deformed matrix during recrystallization, *Acta Metallurgica et Materialia*, Vol. 43/11, (1995), 4117-4129.
- [Kreisler and Doherty (1978)]; Kreisler A., Doherty R. D.: Structure of well defined deformation bands and formation of recrystallization nuclei in aluminium, *Metal Science*, Vol. 12, (1978), 551-560.
- [Li (1962)]; Li J. C. M.: Possibility of subgrain rotation during recrystallization, *Journal of Applied Physics*, Vol. 33/10, (1962), 2958-2965.
- [Liebmann *et al.* (1956)]; Liebmann B, Lücke K, Masing G.: Untersuchungen über die Orientierungsabhängigkeit der Wachstumsgeschwindigkeit bei der primären Rekristallisation von Aluminium-Einkristallen, *Zeitschrift für Metallkunde*, Vol. 47, (1956), 57-63.
- [Liu and Hibbard (1955)]; Liu Y. C., Hibbard W. R. Jr.: On the relationship of texture changes of cold-rolled face-centered-cubic metals during recrystallization, *Transaction AIME*, 203, (1955), 381-384.
- [Liu *et al.* (1995)]; Liu Y. L., Hu H., Hansen N.: Deformation and recrystallization of a channel die compressed aluminium bicrystal with $(112)[11\bar{1}]/(123)[41\bar{2}]$ orientation, *Acta Metallurgica et Materialia*, Vol. 43/6, (1995), 2395-2405.
- [Lücke (1974)]; Lücke K.: The orientation dependence of grain boundary motion and the formation of recrystallization textures, *Canadian Metallurgical Quarterly*, Vol. 13, (1974), 261-272.
- [Mackenzie and Thomson (1957)]; Mackenzie J. K., Thomson M. J.: Some statistics associated with the random disorientation of cubes, *Biometrika*, Vol. 44, (1957), 205-210.
- [Mackenzie (1964)]; Mackenzie J. K.: The distribution of rotation axes in a random aggregate of cubic crystals, *Acta Metallurgica*, Vol. 12, (1964), 223-225.
- [Mahajan *et al.* (1997)]; Mahajan S., Pande C. S., Imam M. A., Rath B. B.: Formation of annealing twins in f.c.c. crystals, *Acta Materialia*, Vol. 45/6, (1997), 2633-2638.
- [McQueen and Jones (1975)]; McQueen H. J., Jones J. J.: Recovery and recrystallization during high temperature deformation. In: "Treatises on Materials Science and Technology (Plastic Deformation of Materials)", Vol. 6, (1975), 393-493.

- [Meyers and Murr (1978)]; Meyers M. A., Murr L. A.: A model for the formation of annealing twins in fcc metals and alloys, *Acta Metallurgica*, Vol. 26, (1978), 951-962.
- [Miszczyk *et al.* (2011)]; Miszczyk M., Paul H., Driver J. H., Maurice C.: Microstructure and texture evolution during annealing of plane strain compressed Al and Al-1%Mn alloy single crystals, *Archives of Metallurgy and Materials*, Vol. 56, (2011), 933-938.
- [Mizera and Driver (1999)]; Mizera J., Driver J. H.: Microtexture analysis of a hot deformed Al-2.3wt%Li-0.1wt%Zr alloy, *Materials Science and Engineering A*, Vol. 271/1-2, (1999), 334-343.
- [Molodov (1984)]; Molodov D. A., Straumal B. B., Shvindlerman L. S.: The effect of pressure on migration of $\langle 001 \rangle$ tilt grain boundaries in tin bicrystals, *Scripta Metallurgica*, Vol. 18/3, (1984), 207-211.
- [Molodov *et al.* (1995)]; Molodov D. A., Czubayko U., Gottstein G., Shvindlerman L. S.: Mobility of $\langle 111 \rangle$ tilt grain boundaries in the vicinity of the special misorientation Sigma 7 in bicrystals of pure aluminium, *Scripta Metallurgica Materialia*, Vol. 32, (1995), 529-534.
- [Morawiec (1999)]; Morawiec A.: Automatic orientation determination from Kikuchi patterns, *Journal of Applied Crystallography*, Vol. 32, (1999), 788-798.
- [Morawiec (2004)]; Morawiec A.: *Orientations and Rotations: Computations in Crystallographic Textures*, Springer, Berlin, 2004.
- [Morniroli, (1998)]; Morniroli J. P.: *Diffraction électronique en faisceau convergent à grand angle: LACBED*, ed. Société Française des Microscopies, (1998).
- [Murr (1975)]; Murr L. E.: *Interfacial phenomena in metal and alloys*, Addison-Wesley, UK, (1975).
- [Pande *et al.* (1990)]; Pande C. S., Imam M. A., Rath B. B.: Study of annealing twins in fcc metals and alloys, *Metallurgical Transactions A*, Vol. 21/11, (1990), 2891 – 2896.
- [Parthasarathi and Beck (1961)]; Parthasarathi M. N., Beck P. A.: The oriented growth mechanism of the formation of recrystallization textures in aluminium, *Transactions of the Metallurgical Society of AIME*, Vol. 221, (1961), 831-838.
- [Paul *et al.* (2000)]; Paul H., Driver J. H., Jasiński Z.: Early stages of recrystallization in (112)[11-1] oriented single crystals of Cu and Cu-2%Al, *Proc. of the 21st RISØ International Symposium on Materials Science*, ed. Hansen N. et al, Roskilde, Denmark, (2000), 505-512.

- [Paul *et al.* (2002a)]; Paul H., Driver J. H., Jasieński Z.: Shear banding and nucleation of recrystallization in a Cu-2%Al alloy single crystal, *Acta Materialia*, Vol. 50, (2002a), 815-830.
- [Paul *et al.* (2002b)]; Paul H., Darrieulat M., Piątkowski A.: Nucleation process in aluminium single crystals deformed at 77K, *Proceed. of the 3rd Japanes-Polish Join Seminar of Materials Analysis*, Zakopane 16-19 July, (2002b), 37-40.
- [Paul *et al.* (2002c)]; Paul H., Driver J. H., Maurice C., Jasieński Z.: Crystallographic aspects of the early stages of recrystallisation in brass-type shear bands, *Acta Materialia*, Vol. 50, (2002c), 4339-4355.
- [Paul (2003)]; Paul H.: Nucleation of recrystallization in channel-die compressed aluminium single crystals, *Materials Chemistry and Physics*, Vol. 81/2-3, (2003), 531-534.
- [Paul and Driver (2005)]; Paul H., Driver J. H.: Deformation behavior of channel-die compressed Al bicrystals with $\{100\}\langle 001\rangle/\{110\}\langle 011\rangle$ orientation, *Archives of Metallurgy and Materials*, Vol. 50, (2005), 209-218.
- [Paul *et al.* (2007)]; Paul H., Driver J. H., Maurice C., Piątkowski A.: Recrystallization mechanisms of low stacking fault energy metals as characterized on model silver single crystals, *Acta Materialia*, Vol. 55, (2007), 833-847.
- [Paul *et al.* (2008a)]; Paul H., Driver J. H., Wajda W.: Strain hardening and microstructure evolution of channel-die compressed aluminium bicrystals, *Materials Science and Engineering A*, Vol. 477/1-2, (2008a), 282-294.
- [Paul (2009)]; Paul H.: *Pasma ścinania w metalach o sieci regularnej ściennie centrowanej*, (2009), Kraków.
- [Paul *et al.* (2008b)]; Paul H., Driver J. H., Maurice C.: 3D microstructures and textures of a plane strain compressed $\{110\}\langle 112\rangle$ Al-0.3%Mn single crystal, *Ceramic Transactions*, (2008b), 181-189.
- [Paul *et al.* (2010a)]; Paul H., Maurice C., Driver J. H.: Microstructure and microtexture evolution during strain path changes of an initially stable Cu single crystal, *Acta Materialia*, Vol. 58, (2010a), 2799-2813.
- [Paul *et al.* (2010b)]; Paul H., Maurice C., Driver J. H., Miszczyk M.: Application of orientation imaging to the study of substructural development in cold deformed Al-0.3Mn single crystal of $\{110\}\langle 112\rangle$ orientation, *Materials Science and Engineering*, Vol. 7, (2010b), 1-10.
- [Paul *et al.* (2012)]; Paul H., Morawiec A., Baudin T.: Early stages of recrystallization in Equal-Channel Angular Pressing (ECAP)-deformed AA3014 alloy investigated using

- Scanning Electron Microscopy (SEM) and Transmission Electron Microscopy (TEM) orientation mappings, *Metallurgical and Materials Transactions A*, Vol. 43/12, (2012), 4777-4793.
- [Ray *et al.* (1975)]; Ray R. K., Hutchinson W. B., Duggan B. J.: A study of the nucleation of recrystallization using HVEM, *Acta Metallurgica*, Vol. 23/7, (1975), 831-840.
- [Ridha and Hutchinson (1984)]; Ridha A. A., Hutchinson W. B.: Recrystallization mechanisms and the origin of cube texture in copper, *Acta Metallurgica*, Vol. 30, (1984), 1929-1939.
- [Rios and Sandim (2005)]; Rios P. R., Jr. F. S., Sandim H. R. Z.: Nucleation and growth during recrystallization, *Materials Research*, Vol. 8/3, (2005), 225-238.
- [Roberts and Lehtinen (1974)]; Roberts W., Lehtinen B.: The feasibility of in situ observations of recrystallization in the high voltage electron microscope, *Philosophical Magazine*, Vol. 29, (1974), 1431-1433.
- [Sabin *et al.* (2003)]; Sabin T. J., Winther G., Jensen D. J.: Orientation relationships between recrystallization nuclei at triple junctions and deformed structures, *Acta Materialia*, Vol. 51, (2003), 3999-4011.
- [Sandström *et al.* (1978)]; Sandström R., Lehtinen B., Hedman E., Groza I., Karlsson S.: Subgrain in Al and Al-1%Mn during annealing, *Journal of Materials Science*, Vol. 13/6, (1978), 1229-1242.
- [Skalli *et al.* (1983)]; Skalli A., Driver J. H., Wintenberger M.: Etude théorique et expérimentale de la plasticité de cristaux d'aluminium, 2ème partie: Compression plane partiellement imposée, *Memoires Scientifiques de la Revue Métallurgie*, V. 80, (1983), 293-302.
- [Smith (1947/48)]; Smith C. S.: Discussion on paper by Mr. J. S. Bowles and Dr. W. Boas.: The effect of crystal arrangements on secondary recrystallization in metals, *Journal of the Institute of Metals*, Vol. 74, (1947/48), 742-758.
- [Steeds and Morniroli (1992)]; Steeds J. W., Morniroli J. P.: Selected Area Electron Diffraction (SAED) and Convergent Beam Electron Diffraction in Minerals and Reactions at Atomic Scale TEM, ed. Buseck P., *Reviews in Mineralogy* 27, (1992), 37-87.
- [Sztwiertnia and Haessner (1995)]; Sztwiertnia K., Haessner F.: Compromise and noncompromise orientations in recrystallization texture formation, In: "Microstructural and Crystallographic Aspects of Recrystallization", ed. N. Hansen et al, Roskilde,

- Proceedings of 16th RISØ International Symposium on Materials Science, Denmark (1995) 565-571.
- [Taylor (1938)]; Taylor G. I.: Plastic strains in metals, *Journal of the Institute of Metals*, Vol. 62, (1938), 307-324.
- [Tucker (1961)]; Tucker G. E. G.: Texture and earning in deep drawing of aluminium, *Acta Metallurgica*, Vol. 9, (1961), 275-286.
- [Varma and Willitis (1984)]; Varma K., Willitis B. L.: Subgrain growth in aluminium during static annealing. *Metallurgical Transactions A*, Vol. 15, (1984), 1502-1053.
- [Verlinden *et al.* (2007)]; Verlinden B., Driver J., Samajdar I., Doherty R. D.: Thermo-mechanical processing of metallic materials, *Pergamon Materials Series*, Vol. 11, (2007).
- [Walter and Koch (1963)]; Walter J. L., Koch E. F.: Substructures and recrystallization of deformed (100)[001]-oriented crystals of high purity silicon-iron, *Acta Metallurgica*, Vol. 11/8, (1963), 923-938.
- [Wilbrandt (1989)]; Wilbrandt P. J., The limits of a reliable interpretation of recrystallization texture in terms of multiple twinning, *Physica Status Solidi (a)*, Vol. 61, (1989), 411-418.
- [Wilbrandt and Haasen (1980)]; Wilbrandt P. J., Haasen P.: HVEM of the recrystallization of tensile deformed $\langle 110 \rangle$ - oriented copper single crystals, *Zeitschrift für Metallkunde*, Vol. 71, (1980), 385-395.
- [Winning *et al.* (2002)]; Winning M., Gottstein G., Shvindlerman L. S.: On the mechanisms of the grain boundary migration, *Acta Materialia*, Vol. 50, (2002), 353-563.
- [Winther *et al.* (2000)]; Winther G., Huang X., Hansen N.: Crystallographic and macroscopic orientation of planar dislocation boundaries-correlation with grain orientation, *Acta Materialia*, Vol. 48, (2000), 2187-2198.
- [Winther (2003)]; Winther G.: Slip patterns and preferred dislocation boundary plane, *Acta Materialia*, Vol. 51, (2003), 417-429.
- [Winther *et al.* (2004)]; Winther G., Huang X., Godfrey A., Hansen N.: Critical comparison of dislocation boundary ailment studied by TEM and EBSD: technical issues an theoretical consequences, *Acta Materialia*, Vol. 52, (2004), 4437-4446.
- [Winther (2009)]; Winther G.: Slip system, dislocation boundaries and lattice rotations in deformed metals, *RISO*, (2009).

- [Wróbel *et al.* (1995)]; Wróbel M., Dymek S., Blicharski M., Driver J.: Microstructural changes due to rolling of austenitic stainless steel single crystals with initial orientation (110)[001] and (110)[110], *Scripta Metallurgica et Materialia*, Vol. 32/12, (1995), 1985-1991.
- [Wróbel *et al.* (1996)]; Wróbel M., Dymek S., Blicharski M.: The effect of strain path on microstructure and texture development in copper single crystals with (110)[001] and (110)[110] initial orientations, *Scripta Materialia*, Vol. 35, (1996), 417-422.
- [Wróbel *et al.* (2003)]; Wróbel M., Moskalewicz T., Krawczyk J., Blicharski M., Dymek S.: Development of microstructure and texture during recrystallization of a Cu-Al single crystal with (100)[011] orientation, *Materials Chemistry and Physics*, Vol. 81/2-3, (2003), 534-527.
- [Zaefferer (2000)]; Zaefferer S.: New developments of computer-aided crystallographic analysis in transmission electron microscopy, *Journal of Applied Crystal*, Vol. 33, (2000), 10-25.